TIME VARIATION OF COSMIC RAY INTENSITY

THESIS FOR PH. D. DEGREE

BY

A. G. ANANTH

OCTOBER 1975

PHYSICAL RESEARCH LABORATORY

AHMEDABAD 380 009

INDIA

TIME VARIATION OF COSMIC RAY INTENSITY

THESIS

PRESENTED BY

A. G. ANANTH

(ALEVOOR GOPALAKRISHNACHAR ANANTH)

TO

THE GUJARAT UNIVERSITY, AHMEDABAD

FOR

THE DEGREE OF

DOCTOR OF PHILOSOPHY

OCTOBER 1975

PHYSICAL RESEARCH LABORATORY

AHMEDABAD - 380009

INDIA.

D E D I C A T E D

TO

MY PARENTS

ACKNOWLEDGEMENT

I am extremely grateful to my guiding teacher Prof. U.R. Rao for his inspiring guidance and constant encouragement throughout the course of the present investigation. I am deeply indebted to him for his supervision and valuable suggestions during the preparation of this thesis.

I express my sincere gratitude to my co-worker Dr. S.P. Agrawal for his fruitful collaboration and Dr. R.P. Kane, Dr. G. Subramanian, and Mr. B.L. Agrawal for their valuable suggestions during the course of this work.

I am very much thankful to Miss Hansa Shah, Mr. K. J. Shah and Mr. V.R. Choksi for computational assistance and Mr. D. Stephen for his excellent typing of the thesis. The author is also thankful to Miss B.R. Vidya, Miss Vasumathi, Mr. M.V. Joseph and Mr. Panduranga of Indian Scientific Satellite Project, Bangalore, for their help during the preparation of this thesis.

The author expresses his indebtedness to the world data centres and to all the investigators who have supplied the neutron monitor data and in particular to Dr. C.P. Sonnet, and Dr. N.F. Ness for providing the interplanetary magnetic field observations.

The author is indebted to the P.R.L. Computing Centre, Electronics Laboratory, Drafting Section and Photography Section for their cooperation throughout the present investigation.

I greatly appreciate the cooperation shown by my wife and my parents throughout the work and I am thankful to all those who encouraged and helped me during my thesis work.

A.G. Ananth

(A.G. ANANTH).

LIST OF PUBLICATIONS

1. Effect of non-uniform solar wind velocity on inter-planetary medium and on cosmic radiation
   by Ananth, A.G. and Agrawal, S.P.
   Ind. J. Pure & Applied Phys. (1971)
   9, 498-500.

2. Diurnal variation of cosmic radiation in the energy range 1-100 GeV, on a day to day basis
   by Ananth, A.G., Agrawal, S.P., and Rao, U.R.
   Proc. 12th Int. Conf. Cosmic Rays, Hobart (1971)
   2, 651-656.

3. Diurnal variation characteristics on a day to day basis
   by Ananth, A.G., Agrawal, S.P., and Rao, U.R.
   Proc. 13th Int. Conf. Cosmic Rays, Denver (1973)
   2, 999-1004.

4. Study of cosmic ray diurnal variation on a day to day basis
   by Ananth, A.G., Agrawal, S.P., and Rao, U.R.
   Pramana, (1974), 3, 74-88.

5. Characteristics of quiet as well as enhanced diurnal anisotropy of cosmic radiation
   by Rao, U.R., Ananth, A.G., and Agrawal, S.P.
   Planet. Space Sci. (1972)
   20, 1799-1816.

6. Comparison of long term variation of diurnal anisotropy derived between meson and neutron monitors during the period 1965-1969
   by Agrawal, S.P., Ananth, A.G., and Rao, U.R.
   Proc. 12th Int. Conf. Cosmic Rays, Hobart (1971)
   2, 646-650.

7. Characteristics of cosmic ray diurnal variation from Deep River neutron and meson data and temperature effects
by Agrawal, S.P., Ananth, A.G., and Rao, U.R.
Can. J. Phys. (1972)
50, 1323-1331.

8. Average characteristics of cosmic ray diurnal anisotropy at relativistic energies
by Agrawal, S.P. and Ananth, A.G.
Proc. 13th Int. Conf. Cosmic Rays, Denver (1973)
2, 1005-1010.

9. High energy cosmic ray intensity increases of non solar origin and the unusual Forbush decrease of August 1972
by Agrawal, S.P., Ananth, A.G., Bemalkhedkar, M.M., Kargathra, L.V., Rao, U.R., and Razdan, H.
J. Geophys. Res. (1974)
79, 2269-2280.

.....

C E R T I F I C A T E

I hereby declare that the work presented in this thesis is original and has not formed the basis for the award of any degree or diploma by any University or Institution.

A G Ananth

A.G. ANANTH
(Author)

Certified by,

U.R. RAO
(Professor-in-charge)

S T A T E M E N T

Even though the galactic cosmic radiation as observed within the solar system is largely isotropic, the presence of a significant diurnal variation with an amplitude $\sim$1% has been known for the last 2 to 3 decades. Realising that the observed diurnal variation is the result of the modulation by the solar system magnetic fields, the earth based observations have been successfully used for inferring the electromagnetic state of the interplanetary medium. Since unlike the 'in situ' space-craft observations which refer to the condition only at a particular point in space, the cosmic ray particles have in their memory the electromagnetic condition along the entire region of space through which they have traversed, the study of cosmic ray variations assumes a considerable importance in the understanding of the interplanetary physics.

The time averaged characteristics of the diurnal anisotropy of cosmic radiation have been well established by a number of experimental workers using observations from a large number of neutron and meson monitors. Theoretical interpretation of the same has also been attempted by a number of workers in terms of electric and magnetic fields in the interplanetary medium. Whereas the experimental observations on a day to day basis showed significant departures from the average characteristics, the theoretical interpretation of the diurnal anisotropy in terms of the cosmic ray particles corotating with the sun has not been able to account for the large variability observed on a day to day basis.

The poor statistics, particularly in the earlier observations have further complicated this problem.

The author was in-charge of the neutron monitoring cosmic ray station at Ahmedabad, India, during 1970-74. The data collected from this equatorial monitoring station have been analysed by the author along with the data available from the world wide net-work of neutron monitoring stations to establish the time averaged as well as the day to day characteristics of diurnal variation for the entire period 1965-72. Extending the theoretical interpretation of the observed low energy solar induced cosmic ray anisotropy measurements to the relativistic particle observations, the author has proposed an unified concept based on radial convection and field aligned diffusion to explain the cosmic ray flux distribution in the interplanetary medium. The present thesis describes in detail, the above concept and attempts to explain the ground based observations in the light of this concept.

A complete theoretical formulation of the cosmic ray streaming in the interplanetary medium can be described in terms of contribution from four major components namely (1) radial convection (2) field aligned diffusion (3) transverse diffusion (4) transverse gradient currents. Assuming that the transverse diffusion and transverse gradient currents are negligible, it is clear that the observed anisotropy is completely described in terms of radial convection current and field aligned diffusion current. The successful explanation of the observed anisotropy of solar cosmic ray

particles at low energies ($\sim$10 MeV) in terms of convection and diffusion shows that the perpendicular diffusion component is in fact negligible most of the times. Natural extension of this concept to relativistic energies would essentially mean that the diurnal anisotropy results when the particles are convected out with the full solar wind velocity. On an average condition, a balance between convection and diffusion currents exists which results in a 1800 hours corotational diurnal vector of the right magnitude. On a day to day basis such a balance need not exist due to the varying conditions of both solar plasma and interplanetary magnetic field which should yield a resultant diurnal variation having a maximum either earlier or later than 1800 hours.

In order to verify the applicability of this concept it is necessary to calculate the convection current using the observed solar wind velocity values. The diffusion current is then derived by subtracting the convection current from the observed diurnal anisotropy vector. It is then only necessary to compare the azimuth of the diffusion vector with the observed interplanetary field azimuth derived from 'in situ' observations, in order to establish the correctness of the above physical concept.

Using the data from a large number of ground based neutron monitoring stations, the author has first examined the time averaged diurnal anisotropy characteristics. The results clearly indicate that the yearly average as well as 27-day average diurnal anisotropy during the period 1965-72 is consistent with

the above physical concept and the estimate of the radial gradient $\sim$ 5%/AU obtained from the observations is in good agreement with the presently accepted measurements. The author has extended the analysis to the explanation of the observed diurnal variation on a day to day basis and has shown that in spite of the large variability in diurnal anisotropy observed in both amplitude and time of maximum on a day to day basis, the observed anisotropy on more than 80% of the days are explainable in terms of simple radial convection and field aligned diffusion.

The solar terrestrial relationship on nearly 20% of days on which the above concept does not fully explain the observations have been critically examined. Such days on which there is a significant contribution due to transverse diffusion currents are shown to be associated with interplanetary field irregularities with scale sizes ranging from 4 hours to 1 day.

The thesis is divided into four main chapters. The first chapter gives a brief survey of the subject of cosmic ray time variations. The second chapter deals with the neutron monitor set up at Ahmedabad and a brief account of the methodology adopted for the processing and analysis of the data. In the third chapter the proposed convection-diffusion physical concept and its applicability for understanding the time averaged diurnal variation is described. In chapter four, the analysis is extended for a critical understanding of the observed diurnal anisotropy on a day to day basis. The important results that emerge from these studies are

briefly summarized below.

(1) The yearly mean and 27-day mean diurnal anisotropy observed during the period 1965-72 can be completely understood in terms of an equilibrium established between a radial convection current and a field aligned diffusion current in the interplanetary medium. The radial density gradient derived ($\sim$5%/AU) from the observations at these energies are quite consistent with other observations.

(2) On an average basis diffusion perpendicular to the magnetic field and gradient currents are negligible ($K_\perp \sim 0, (\frac{\partial u}{\partial r})_\perp \sim 0$).

(3) The enhanced diurnal variation observed on a day to day basis can be described as a resultant of radial convection and an enhanced field aligned diffusion current in the interplanetary medium. The enhanced field aligned diffusion is caused by a significantly enhanced radial gradient ($\sim$ 10%/AU) established in the interplanetary medium due to the presence of either a "sink" of cosmic ray particles in the garden-hose hemisphere or a "source" of cosmic ray flux from the anti-garden-hose hemisphere.

(4) On a day to day basis on $\sim$ 80% of the days the large variability observed in the amplitude and time of maximum of the diurnal anisotropy can be explained as a consequence of variable convection and field aligned diffusion current in the interplanetary medium.

(5) Nearly 20% of the days which show departure from the proposed convection-diffusion concept are found to be associated with magnetic field irregularities of scale size >4 hours indicating the presence of significant transverse diffusion current in the interplanetary medium ($\frac{K_\perp}{K_\parallel} \sim 1$).

In addition the author has also examined the complex Forbush decreases which were observed during August 1972. The author in association with his colleagues has proposed a qualitative model to explain all the observed complex features associated with the above Forbush decrease event. Since this does not form the main body of the thesis a reprint giving the results of the above study is attested at the end of the thesis.

A.G. Ananth

A.G. ANANTH
(Author)

U.R. RAO
(Professor -in-charge)

C O N T E N T S

.....

C H A P T E R - I

INTRODUCTION

1.1 General survey:

Since their discovery in 1914, cosmic rays have served as an unique tool for investigating a large variety of problems in High energy physics, Elementary particle physics, Astronomy, Astrophysics, Cosmology, Geophysics and Heliophysics. The scales over which cosmic rays serve as an effective space probe varies from atoms to the environs of our planets and even beyond. The spectacular progress in the last two decades have contributed enormously to our understanding of the earth's immediate environment and the properties of the interplanetary medium through a large number of ' in situ ' space-craft observations. Whereas the direct measurements provide point observations, it is only through cosmic ray studies that we can infer the electromagnetic state of the interplanetary medium as a whole. The ' in situ ' observations however provide the boundary conditions within which the complex propagation scheme of cosmic ray particles in the interplanetary medium can be constructed.

It is now known that the solar system magnetic fields extend over very large regions in space ($\sim$ 100 AU) and have high energy density ($\geq$10 times) compared to galactic magnetic fields. Consequently the cosmic ray propagation in the interplanetary space is dictated by the characteristics of solar system magnetic fields, the large scale properties of which

are now known to be consistent with their being stretched in the form of an Archimedean spiral by the radially blowing solar wind. Superimposed on this uniform field are present large and small scale magnetic field irregularities which act as effective scattering centres for cosmic ray particles of different energies. Using extensive cosmic ray observations from a chain of ground based monitors well distributed in longitude and latitude and the large amount of 'in situ' space-craft observations of the interplanetary plasma and magnetic field parameters, it is possible to gain a complete understanding of the electromagnetic processes which operate in the interplanetary medium.

The most spectacular cosmic ray variation is the enhancement of cosmic ray intensity observed in association with large solar flares. During the solar flares sun produces a large number of cosmic ray particles of low energies ($\leq$ 100 MeV), sometimes extending even to higher energies ($\geq$1 GeV) which can be recorded by a ground based detector. In fact the first inference on the Archimedean spiral character of the interplanetary fields was actually obtained from a detailed study of the cosmic ray particle anisotropies observed at ground based neutron monitors. (McCracken, 1962). Direct 'in situ' observations of cosmic ray anisotropies carried out onboard Pioneer and IMP space-crafts (Ness et al, 1964; McCracken and Ness, 1966) have conclusively established the spiral nature

of the interplanetary magnetic fields, superimposed upon which exist the small scale irregularities. A comprehensive review on the low energy cosmic ray phenomena has been recently published by McCracken and Rao (1970).

Even though there are a large number of space-crafts continuously monitoring the behaviour of particles and fields in the interplanetary medium, the ground based detectors play an unique role in the investigation of the characteristics of the interplanetary medium as these are sensitive to only high energy galactic cosmic ray particles ($\geqslant$ 1 GeV). The cosmic ray time variation studies by ground based monitors not only provide information on the long term characteristics of the interplanetary medium but also on the electromagnetic conditions of the 'inaccessible' regions away from the plane of the ecliptic as well as at large distances away from the orbit of the earth. Detailed comprehensive reviews on the various aspects of cosmic ray time variations are available in the literature to-day. (Lockwood, 1971; Pomerantz and Duggal, 1971; Rao, 1972).

1.2 Atmospheric effects on relativistic cosmic ray particles:

Before interpreting the ground based cosmic ray observations in terms of primary cosmic ray variations in the interplanetary medium, it is very essential to have a clear understanding of the effect of earth's atmosphere and the earth's magnetic field on the incident primary particles. The primary

cosmic ray particles interacts with atmospheric nuclei and produces various secondary particles depending on the energy of the incident particle. An understanding of the effect of the earth's atmosphere essentially implies a complete understanding of the generic relations between cosmic ray primaries and secondaries. The evaluation of the effect of earth's magnetic field on the incident primary cosmic ray particles involves a complete knowledge of the motion of charged particles in the extended geomagnetic field.

A number of attempts have been made using theoretical calculations (Dorman, 1957 and reference therein; Wainio et al, 1968; Debrunner and Fluckiger, 1971) to relate the secondary cosmic ray intensity with the primary cosmic ray intensity at the top of the atmosphere. Following Dorman (1957) the cosmic ray variation observed at any ground based detector can be expressed as,

$$\frac{\partial N_\lambda^i}{N_\lambda^i} = -\delta E_\lambda^c W_\lambda^i (E_\lambda^c, h) + \int_{E_\lambda^c}^{\infty} \frac{\delta m^i(E, h)}{m^i(E, h)} W_\lambda^i (E, h)\, dE + \int_{E_\lambda^c}^{\infty} \frac{\delta D(E)}{D(E)} W_\lambda^i (E, h)\, dE \qquad (1.1)$$

where N_λ^i is the intensity of the secondary component 'i' observed at a latitude ' λ ' and atmospheric depth 'h' having a cut-off energy E_λ^c . D(E) is the differential energy spectrum which can be expressed in a simple form as $AE^{-\gamma}$, where A is a constant and γ is the spectral exponent. m^i (E, h) is defined as the multiplicity and W_λ^i (E, h) as the coupling constant or the differential response function can be

obtained from latitude surveys. The first term of the equation 1.1 represents the variation due to the changes in cut-off energy, which is usually negligible except for few days which are associated with large magnetic storms. The second term shows the variation caused by the atmospheric (meteorological) parameters such as pressure and temperature, which can be easily corrected for and the third term essentially includes the variation caused by the changes in the primary energy spectrum and is of interest in all studies of cosmic ray variations. Further it was observed that deriving a multiplicity or specific yield function from observed latitude effects was found very useful in interpreting the cosmic ray secondary variations in terms of the primary cosmic ray variations at the top of the atmosphere. A number of authors (Neher, 1952; Treiman, 1952; Simpson et al, 1953; Dorman, 1957; Webber and Quenby, 1959; Lockwood and Webber, 1967) have obtained appropriate multiplicity functions for both sea level and mountain stations which are applicable to cosmic ray variation studies.

The geomagnetic field acts as a spectrum analyser to the incoming particles and at any location 'λ', only particles above a minimum energy (cut-off) E_λ^c are allowed to reach the detector. The latitude effect observed in the cosmic ray intensity clearly indicated that the cut-off energy (E_λ^c) is maximum at the equator and minimum at the poles. Though there are extensive calculations on cosmic ray particle trajectories

in the geomagnetic field are available (Stormer, 1955; Schwartz, 1959; Vallarta, 1961; Bland, 1962; Hedgecock, 1963), the concept of 'Asymptotic directions' and 'Asymptotic cone of acceptance' developed by Rao et al (1963) was found extremely useful for deriving particle trajectories prior to their entry into the earth's magnetic field and for applying them to the study of cosmic ray variations observed at a ground based monitor.

The 'Asymptotic cone of acceptance' of a detector is defined as the cone which includes all those asymptotic directions which makes a significant contribution to the count rate of a detector. As the earth spins on its axis, the asymptotic cone of acceptance of a given detector scans the entire celestial sky in the course of a day. Since the cosmic ray detectors have essentially a narrow asymptotic cone of acceptance, with a suitable choice of detectors widely distributed in longitude, it is possible to separate the cosmic ray anisotropic (spatial) variations from isotropic (time) variations and thus understand the various physical mechanisms responsible for the redistribution of cosmic ray particles in the interplanetary medium.

In order to understand the cosmic ray time variations, it is necessary to know the average electromagnetic condition that exists in the interplanetary medium. It must however be remembered that all measurements done so far essentially relate

to the conditions as the tubes of force corotate with the sun. On the other hand what is important is to understand the cosmic ray effects in the field configuration along the line of force extending upto the sun. Nevertheless the 'in situ' observations can be considered as broad boundary conditions, which should be taken into consideration in drawing any inference from ground based cosmic ray observations.

1.3 Solar wind:

Since the early measurement of the solar wind made by Gringauz et al (1960) and Snyder et al (1963) establishing the continuous emission of the solar wind plasma radially away from the sun, a large number of observations have been made with a number of space-crafts and deep space-probes. With the availability of a large amount of data on solar wind parameters at different helio longitudes and distances, it is now possible to infer the large scale as well as small scale properties of the solar wind plasma and also to study the spatial and temporal variations of solar wind parameters in the interplanetary medium.

Table 1.1 summarizes some of the bulk properties of the solar wind plasma and their variability. The average properties of the solar wind at the orbit of the earth (1 AU) indicates that the solar wind plasma on an average is characterized by a velocity $\sim$ 400 kms/sec and density $\sim$ 8 particles/cm^3 is in good agreement with the theoretical

Table 1.1

Sr. No.	Solar wind plasma parameters	Average characteristics	Variability
1.	Velocity	400 kms/sec	275 to 800 kms/sec
2.	Flow direction	1.6^{o}E of the Sun-Earth line	8^{o}E to 8^{o}W of the Sun-Earth line
3.	Proton and Electron density	8 particles/cm^3	1 to 50 particles/cm^3
4.	Proton temperature	4×10^4 ^{o}K	3×10^4 to 5×10^5 ^{o}K
5.	Electron temperature	1×10^5 ^{o}K	1 to 2×10^5 ^{o}K
6.	Ratio of Helium to Hydrogen (n_α / n_p)	0.05	0.01 to 0.20
7.	Magnetic field	5 γ	2 to 12 γ

Table 1.1 - The observed average solar wind plasma parameters and its variability at the orbit of the earth (1 AU).

predictions. A large variability in the solar wind parameters such as velocity, density and temperature (Snyder et al, 1963; Hundhausen, 1970) has been well established from a large number of space-craft observations such as Luna, Vela, Mariner, Explorer and Pioneer space-crafts. Recent Pioneer-10 and Pioneer-11 space-craft observations indicate that the solar wind at the orbit of the Jupiter (4.3 AU) has a velocity $\sim$420 kms/sec, density$\sim$ 0.5 particles/cm^3 and a proton temperature$\sim$ 5 x 10^4 ^oK are in good agreement with the steady state (theoretical) model of the solar wind. Both the theoretical aspects and experimental observations are extensively reviewed in the literature (Dessler, 1967; Axford, 1968; Hundhausen, 1968, 1970; Parker, 1969; Burlaga, 1971).

The solar wind properties show significant correlations with solar activity. Many investigators (Snyder et al, 1963; Pai et al, 1967; Bame et al, 1967) have demonstrated excellent correlations between solar wind velocity and ΣK_p index, the index of geomagnetic disturbance. Similarly the 27-day recurrence tendency in the enhanced solar wind velocity and their association with M-region magnetic storms are also well established (Snyder et al, 1963). Though large variations in the solar wind properties exists on a day to day basis, on a long term basis contrary to the theoretical predictions the observations show that the solar wind as well as interplanetary magnetic field parameters remain practically invariant with the solar

cycle. (Gosling et al, 1971; Mathews et al, 1971; Hedgecock et al, 1972).

The solar wind flow though largely radial, occasionally shows a significant component ($\pm 5^{\circ}$) perpendicular to the ecliptic plane (Wolfe et al, 1966; Strong et al, 1967). For a clear understanding of the observed solar wind properties, Burlaga and Ness (1968) introduced the concept of scale length (time). They have pointed out that the Macro and Meso-scale properties ($f \sim 3 \times 10^{-4}$ to 3×10^{-8} sec^{-1}) of the solar wind are important to the study of high energy cosmic rays (≥ 2 GeV) in a field of $\sim 5\gamma$, whereas only Micro-scale properties (3×10^{-2} to 3×10^{-4} sec^{-1}) are most relevant to the study of low energy cosmic rays (≤ 1 GeV).

1.4 Interplanetary magnetic field (IPMF):

Since the particle energy density in the solar wind is much larger than the magnetic energy density of the solar dipole field, the solar wind plasma freely expands in the interplanetary space. Due to the large conductivity, the field lines are frozen into the solar wind plasma and they are constrained to move along with the solar wind (Alfven, 1950). Under these conditions, the radially blowing solar wind transports the magnetic fields from the base of the corona to very large distances from the sun ($\sim$ 100 AU). Due to the uniform rotation of the sun, the field lines which are firmly anchored to the solar wind plasma are twisted in the form of an

Archimedean spiral (Parker, 1958 a,b; Ahluwalia and Dessler, 1962). The garden-hose angle (ψ) between the Archimedean spiral interplanetary magnetic field and the radius vector can be derived using the simple relation

$$\tan\psi = \frac{V_p}{\Omega r} \qquad (1.2)$$

For a normal solar wind velocity $V_p \sim 400$ kms/sec the garden-hose angle (ψ) at the orbit of the earth ($r \sim 1$ AU) turns out to be of $\sim 45^\circ$. Direct observations of the interplanetary magnetic field (IPMF) from a number of space-crafts have conclusively shown that the large scale properties of the IPMF are in good agreement with the predicted Archimedean spiral configuration (Ness and Wilcox, 1966). The recent measurements obtained with instrumentation onboard Pioneer-10 and Pioneer-11 space-crafts at the orbit of the Jupiter have also confirmed the Archimedean spiral configuration of the field even at as large a distance as 4.3 AU, where the garden-hose angle changes from 45° to 67°. The ordering of the interplanetary field in the form of well defined structures is now established, alternate sectors showing field lines oppositely directed to each other, one directed away from the sun (positive) and the next directed towards the sun (negative). These sectors which corotate with the sun are found to exist throughout the solar cycle (Wilcox and Ness, 1965; Wilcox and Colburn, 1972). Correlating the polarity of the mean photospheric field and the IPMF near the earth, the solar origin of the IPMF

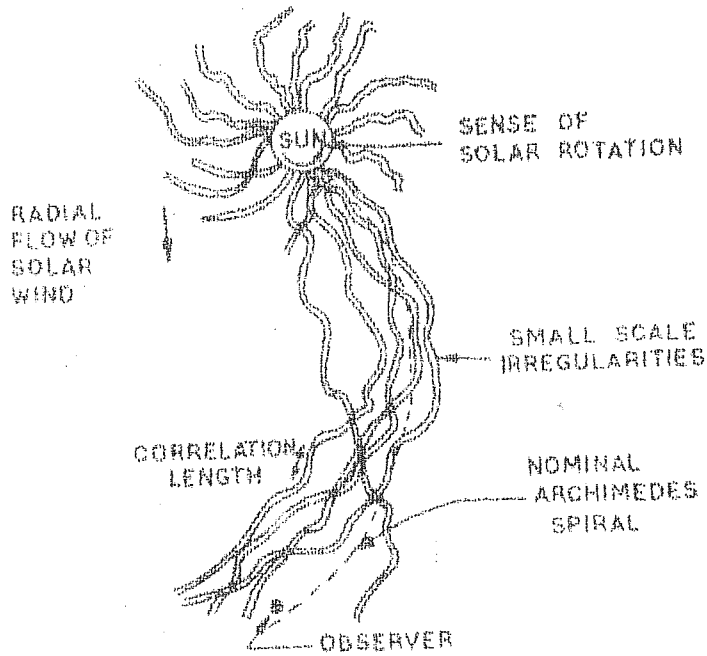

Figure 1.1 - A schematic diagram of the Interplanetary magnetic field (IPMF) configuration illustrating the random walk of field lines as a result of large scale inhomogeneities in the solar wind. The uniform Archimedean spiral magnetic field is shown by dotted lines.

has also been established (Severney et al, 1970). Though the average IPMF does not show significant variations in magnitude or in direction, the frequency of number of days with high amplitude magnetic fields does show an increase with solar activity and the IPMF observed on a day to day basis shows significant departures from their average characteristics.

1.5 Irregularities in the interplanetary magnetic field:

It was found that the IPMF when observed with time scales < 1 day, showed considerable departures from their average behaviour due to a continuous distribution of irregularities. The origin of these irregularities of different scale sizes was attributed (Michel, 1967; Jokipii and Parker, 1969) to the motion of prominent photospheric features such as granulations ($\sim 10^3$ km in diameter) and super-granulations ($\sim 10^4$ km in diameter) on the photosphere. In addition to the small scale irregularities, the turbulent motion of the solar plasma makes the field lines stochastic resulting in a random walk of the field lines, which is generally attributed to the horizontal displacement of the feet of the lines of force, resulting from the motion of granules and supergranules in the photosphere.

The propagation of cosmic ray particles in the interplanetary space is considerably affected by the distribution of irregularities, their scale sizes, and the mean distance between the irregularities which produces a considerable deviation

in the large scale magnetic field. Since the Alfven velocity is small compared to the solar wind velocity, both the regular and irregular magnetic fields which are frozen into the solar plasma are convected out along with the solar wind and the observed time dependence of the IPMF at any given point can be transformed into spatial variations. Cosmic ray particles diffuse through the irregularities against the outward blowing solar plasma before reaching the earth. The scattering due to the irregularities (field) is maximum for particles whose gyro-radius is comparable to the scale size of the irregularities. In other words the scattering of particles of rigidity R GV depends mainly on the power $P_{xx}(f)$ in the transverse component of the field in the vicinity of the resonant frequency 'f' given by

$$f(R) = 10^{-4} R^{-1} Hz \qquad (1.3)$$

and $P_{xx}(f)$, the frequency power spectrum can be expressed by a power law in frequency as $P_{xx}(f) \propto f^{-\alpha}$. From a detailed power spectrum analysis of the observed IPMF (discussed in chapter II) a number of workers (Coleman Jr., 1966; Jokipii and Coleman, 1968; Siscoe et al, 1968; Sari and Ness, 1969) have estimated the diffusion coefficients both parallel ($K_{\parallel}$) and perpendicular to the magnetic field ($K_{\perp}$), and have found that the perpendicular diffusion ($K_{\perp}$) is essentially caused by (a) random walk of the field lines ($K'_{\perp}$) and (b) resonant scattering due to the field fluctuations expressed in the form,

$$K_{\perp} = K'_{\perp} + \frac{R_c^2}{\lambda^2} K_{\parallel} \qquad (1.4)$$

Where R_c is the particle gyro-radius (cyclotron radius) and $K_{\parallel}$ the parallel diffusion coefficient can be easily computed using the simple relations

$$K_{\parallel} = \begin{cases} A \beta R^{2-\alpha} \text{ for } R_u > R > R_1 \\ \frac{1}{3} CD\beta \text{ for } R < R_1 \end{cases} \qquad (1.5)$$

Where A is a constant, R_u is the rigidity at which the cyclotron radius R_c of the particle is comparable to scattering mean free-path λ given by $\lambda = 3 K_{\parallel} / C\beta$ and R_1 is the particle rigidity for which the mean free-path λ becomes smaller and approach D. At low energies $\sim$ 10 MeV, $K'_{\perp} \approx K_{\parallel}$ and hence $K_{\perp} \approx K_{\parallel}$ leads to an isotropic diffusion and at high energies $\geq$ 1 GeV, $K_{\perp} << K_{\parallel}$ will essentially lead to anisotropic diffusion. Recently Owens and Jokipii (1973, 1974) have shown that the cosmic ray scintillations observed at high energies ($\geq$ 1 GeV) and at low frequencies ($\leq 5 \times 10^{-5}$ Hz) are caused mainly by the fluctuating component of the IPMF due to the strong interaction of the high energy cosmic ray particles with the magnetic field irregularities during their propagation in the interplanetary medium.

1.6 Cosmic ray variations:

Even though the continuous monitoring of cosmic ray data started in 1936 with the establishment of a net-work of

ionization chambers by Carnegie Institute of Washington, a systematic observation and interpretation of cosmic ray variations in terms of propagation of cosmic rays in the interplanetary space became possible, only after the establishment of a world wide net-work of neutron and meson monitors during IGY. The encouraging results obtained from the data collected during IGY period, finally led to the establishment of high counting rate super neutron monitors and large area scintillation telescopes (meson monitors) during IQSY. With the high statistical accuracy of the data obtained from ground based monitoring instruments, it is now possible to study the short term variations such as diurnal and semi-diurnal variation on a day to day basis.

The cosmic ray variations observed at ground based monitors can be broadly divided into two classes (1) Isotropic variations such as 11-year variation, 27-day variation and Forbush decrease and (2) Anisotropic variations such as diurnal and semi-diurnal variation.

ISOTROPIC VARIATION

1.7 The long term 11-year solar modulation of cosmic ray intensity and the convection-diffusion theory:

The inverse correlation between the galactic cosmic ray intensity and the solar activity has been known for a long time (Forbush, 1958). The intensity variations observed

which is approximately of $\sim$ 20% at neutron monitors and of $\sim$ 5% at meson monitors from solar minimum to solar maximum is found to be strongly energy dependent. The convection-diffusion theory proposed by Morrison (1956) and Parker (1958a) which was later modified (Gleeson and Axford, 1967, 1968a, 1968b; Fisk and Axford, 1968, 1969; Jokipii, 1967; Jokipii and Parker, 1967, 1968a; Skadron, 1967) on the basis of pioneering work done by Parker (1965, 1966) taking energy losses and adiabatic deceleration into consideration was found successful in explaining the experimental observations for particles $\geq$ 100 MeV. The basic mechanism of 11-year modulation involves convective removal of cosmic ray particles radially away from the sun by the solar wind, establishes a positive radial density gradient. Due to the positive density gradient, cosmic ray particles always diffuse into the solar system through the solar system magnetic fields and attain a steady state when the outward convection of particles is balanced by the inward diffusion. For a symmetrically expanding solar wind carrying with it magnetic field irregularities of uniform statistical distribution, the number density of cosmic ray particles of energy 'E' in a steady state at any radial distance 'r' from the sun is given by

$$U(r,E) = U_o(E) \exp\left\{ - \int_r^R \frac{V_p}{K} dr \right\} \qquad (1.6)$$

where $U_o(E)$ is the number density at a radial distance R from the sun beyond the modulating region, V_p is the solar

wind velocity and K is the isotropic diffusion coefficient. This model has been further improved by a number of workers taking into account of various other factors such as,

(1) The adiabatic energy changes due to the non-zero divergence of the solar wind velocity (Parker, 1965; Gleeson and Axford, 1967; Singer et al, 1962).

(2) Anisotropic diffusion due to the non-fluctuating (average) component of the IPMF (Parker, 1965; Axford, 1965b).

(3) Relationship between diffusion tensor and the magnetic field power spectrum (Jokipii, 1966, 1967; Hasselmann and Wibberentz, 1968; Roelof, 1968).

1.8 Long term modulation:

From the modified convection-diffusion equation, the radial density gradient of cosmic ray particles estimated was found to be $\sim 9\%/AU$ (for $K \sim 9.3 \times 10^{21}$ cm^2/sec at 5 GeV). Recently the results on the radial density gradients at various energies have been summarized by Rao (1972) and O'Gallagher (1972). The experimental observations on radial density gradients are still unfortunately not clear and they are not able to provide strong support to the existence of a radial density gradient. A large amount of data concerning the rigidity dependence of the long term modulation and its relationship with other solar and terrestrial parameters are now available to examine the theoretical predictions. The

results indicate that the modulation is maximum at low energies and there exists a residual modulation even during solar minimum.

The observed time lag between the minimum solar activity and maximum cosmic ray intensity (peak) has been utilized to estimate the size of the modulating region. The observed time lag of $\sim$9 - 12 months (Forbush, 1958) corresponds to R $\sim$ 100 AU was found to be higher compared to other independent estimates obtained for the size of the modulating region. Using ΣK_p index and coronal green line intensity (λ-5303), it was shown that (Simpson and Wang, 1967; Hatton et al, 1968; Pathak and Sarabhai, 1970) the time lag between cosmic ray intensity and solar activity is of $\sim$ 1 month corresponds to R $\sim$ 7 AU. The size of the modulating region inferred from density gradient measurements obtained from both space-craft and ground based detectors are in agreement with above estimates of R. Comprehensive reviews dealing with both experimental observations and theoretical interpretation of long term modulation of cosmic ray intensity are available in the literature to-day. (Webber, 1967; Gleeson, 1971 ; Rao, 1972).

1.9 Forbush decrease and 27-day variation :

Forbush (1938) first noted the occurrence of a sudden decrease of cosmic ray intensity at ground based monitors almost simultaneously with geomagnetic storms following a day or two after a large solar flare occurring on the sun. Simpson (1954) suggested that these world wide decreases are caused by

a sudden and drastic change in the electromagnetic condition of the interplanetary medium due to the flare occurring on the sun. The intensity variations observed which is typically of $\sim$ 5 - 15% in ground based neutron monitors is found to be energy dependent.

Forbush decreases are normally characterized by a sudden decrease of cosmic ray intensity simultaneously from all the directions followed by a slow recovery which extends over few days. Various models has been suggested by Alfven (1954) and Dorman (1957), who attributed the Forbush decrease to the energy losses produced by the electric field associated with the solar plasma beam. The two most important successful models are one due to Gold (1960), who introduced the concept of "magnetic bottle" inside of which cosmic ray intensity would be reduced. As the magnetic bottle expands and engulfs the earth the Forbush decrease sets in. The second model due to Parker (1963) attributes the Forbush decrease to the reduction of cosmic ray intensity occurring behind the magnetic shock front (Blast wave) produced by a sudden outward explosion in the solar corona following a solar flare. The effect of the blast wave on cosmic rays has been calculated (Parker, 1963; Quenby, 1967) and the result is found to be in agreement with many of the experimental observations.

In addition to flare initiated Forbush decreases, corotating Forbush decreases showing a strong 27-day recurrence

tendency has been detected. McCracken et al (1966b) and Bukata et al (1968) suggested that the corotating Forbush decreases observed at low energies ($\sim$ 10 MeV) can manifest themselves as enhanced diurnal wave trains at high energies ($\geq$ 1 GeV). Detailed reviews are available in the literature on the subject (Webber, 1962; Lockwood, 1971) and since this does not form the main part of the thesis, we have only touched upon the subject.

ANISOTROPIC VARIATION

1.10 The diurnal variation:

As the earth spins on its axis with a period of 24 hours (1 day), a ground based detector on earth scans the entire celestial sky and any anisotropy of galactic cosmic radiation in the interplanetary medium will be observed as a daily variation of cosmic ray intensity. Brunberg and Dattner (1954) were the first to attribute the diurnal variation observed at ground based detectors to an excess of cosmic ray particles arriving from the asymptotic direction 1800 hours local time. They also proposed that the galactic cosmic rays in the vicinity of the sun corotates with the sun, and gives rise to a higher cosmic ray intensity in a direction opposite to earth's orbital motion.

1.11 Characteristics of diurnal variation and experimental observations:

From an extensive and systematic analysis of ground based neutron monitor data obtained from a large number of stations during 1954-65, Rao et al (1963) and McCracken and Rao (1965) clearly demonstrated that the average diurnal variation observed at relativistic energies ($\geq$ 1 GeV) can be expressed in the form

$$\frac{\delta J(E)}{J(E)} = AE^{-\beta} \cos(\psi - \psi_o) \cos\lambda \text{ , for } E \leq E_{max}$$
$$= 0 \text{ , for } E > E_{max} \qquad (1.7)$$

where A is a constant found to be $\sim (0.38 \pm 0.02) \times 10^{-2}$, $\beta = 0$ and $\psi_o = 89^\circ \pm 1.6^\circ$ east of the sun-earth line. λ is the declination and E_{max} is the upper energy limit (cut-off) for corotation. They summarized that the average diurnal anisotropy has following characteristics.

(1) An average amplitude $\sim 0.38 \pm 0.02\%$

(2) A time of maximum around $89^\circ \pm 1.6^\circ$ east of the sun-earth line, that is 1800 hours local time.

(3) Energy independent upto an energy $E_{max} \sim 100$ GeV, and

(4) Varies as the cosine of declination.

The observations of many other investigators (Bercovitch, 1963; Pomerantz et al, 1962; Kane, 1964; Faller and Marsden, 1965; Willetts et al, 1970) are found to be in good agreement with

these findings. The yearly mean diurnal amplitude and diurnal phase remained practically constant over the solar cycle, except for a small decrease in the amplitude during solar minimum (Duggal et al, 1967). The decrease in the diurnal amplitude during solar minimum was attributed to the significant reduction of the upper cut-off energy E_{max}. The change of E_{max} has been investigated by a large number of workers (Rao et al, 1963; Jacklyn and Humble, 1965). Using the ratio of diurnal vectors observed at neutron and underground meson telescopes at Hobart E_{max} estimated to be $\sim$ 100 GeV. Later using similar methods a number of authors (Peacock, 1970; Summer and Thompson 1970; Jacklyn et al, 1970; Ahluwalia and Ericksen, 1970; Agrawal et al, 1972) have concluded that $E_{max} \leq 100$ GeV and varies with solar cycle, attains a lowest value of $\sim$ 40 - 50 GeV during solar minimum and a highest value of $\sim$ 100 GeV during solar maximum.

Even though neutron monitors did not indicate any long term variation in the diurnal variation during 1957-70, the observations from other detectors such as meson monitors and underground detectors indicated a significant long term variation of diurnal variation (Duggal et al, 1970). From an rigorous analysis of ion-chamber and meson monitor data, Forbush (1967, 1969) showed that the average diurnal variation is composed of two distinct components W and V. the component W has its maximum or minimum in the direction 128° east of the

sun-earth line, which is roughly the average IPMF direction and varies sinusoidally with a periodicity of 20 years and passes through its zero amplitude when the sun's polar magnetic field is reversed (Forbush, 1973). The other component V has its maximum along 90° east of the sun-earth line and varies with solar activity, shows a solar cycle dependence.

1.12 Theoretical models:

Based on the concept of solar wind and the spiral structure of the interplanetary magnetic field developed by Parker (1960), Ahluwalia and Dessler (1962) suggested that the corotation of the IPMF lines with the sun produces an electric field and in turn an electric drift ($\bar{E} \times \bar{B}/B^2$) cause the diurnal variation of cosmic rays. The model predicted that,

(1) The source of the diurnal variation lies in the plane of the sun's equator.

(2) The amplitude of the anisotropy depends on the solar wind velocity and is maximum in the direction perpendicular to the magnetic field.

(3) The existence of an upper energy cut-off $E_{max} \sim 100$ GeV for cosmic ray particles which takes part in corotation and cause diurnal variation and

(4) The anisotropy is energy independent ($\gamma = 0$) below the upper cut-off energy $E_{max} \leq 100$ GeV.

Though some of the predictions were found to be in good agreement with the experimental observations of the average diurnal variation (Bercovitch, 1963; Rao et al, 1963; Snyder et al, 1963), the observed amplitude and direction was not found to be in agreement with theoretical predictions. At the same time Stern (1964) pointed out that in a highly conducting plasma an electric field $\bar{E} = - \bar{V} \times \bar{B}$ can exist. For a magnetic field which is axisymmetric around the axis, $\nabla \times \bar{E} = - \partial \bar{B} / \partial t \approx 0$, and the electric field will be conservative. According to Liouville's theorem, the cosmic ray density is preserved in any conservative system (Lemaitre and Vallarta, 1933; Fermi and Rossi, 1933; Swann, 1933), thus if the cosmic ray intensity is same in all the directions at any point outside the solar system then it must be so at any accessible point inside the solar system. The electric field $\bar{E}$ in turn produces a density gradient and the streaming produced by this density gradient will exactly cancel the streaming produced by the electric drift and no time independent magnetic field can produce an anisotropy such as diurnal anisotropy in the solar system. Later Parker (1964) suggested that the assumption of fields in the interplanetary space being conservative is not completely correct, that is $\partial \bar{B} / \partial t \neq 0$ and in reality one can expect a large number of small scale irregularities to be present in the magnetic field which is convected out along with the solar wind. Then in such a case

the irregularities present in the magnetic field will wipe out most of the cosmic ray density gradient produced by the electric field ($\bar{E} = -\bar{V} \times \bar{B}$) and the density gradient does not cancel the electric drift proposed by Ahluwalia and Dessler (1962), resulting in a net streaming of cosmic ray particles in the interplanetary medium. While Parker (1964) assumed the presence of irregularities beyond the orbit of the earth, Axford (1965a) assuming the presence of scattering centres over the entire modulating region arrived at the same conclusion. The basic assumptions are,

(1) The IPMF is quite regular across the orbit of the earth, so that the particles are constrained to move along the lines of force of the general spiral field, that is the diffusion perpendicular to the field lines is negligible ($K_{\parallel} \gg K_{\perp}$).

(2) There are sufficient irregularities in the magnetic field beyond the orbit of the earth to wipe out most of the density gradient produced in the incoming particles by the electric field ($-\bar{V} \times \bar{B}$), that is there is no density gradient perpendicular to the ecliptic plane ($(\frac{\partial U}{\partial r})_{\perp} \approx 0$) and

(3) There is no net radial streaming of cosmic ray particles in the solar system.

Under these conditions the cosmic ray particles undergo a rigid corotation with the sun and will give rise to a net streaming in the azimuthal direction and this rigid corotation of cosmic ray particles in the interplanetary medium is the origin of diurnal variation. The amplitude of the

anisotropy produced by the rigid corotation of cosmic ray particles at any distance 'r' from the sun is given by (Compton and Getting, 1935)

$$\xi_{\odot}(r) = 3\,CV\,(r)/v \qquad (1.8)$$

Where V(r) is the velocity of rigid corotation of the spiral magnetic field with the sun and v is the particle velocity and C is related to the Compton-Getting factor. At the orbit of the earth ($r \sim 1$ AU), the diurnal anisotropy observed at a ground based monitor due to the rigid corotation of cosmic ray particles in the interplanetary medium is given by

$$\xi_{co} = \frac{3CV_{co}}{v} \qquad (1.9)$$

Where $C = (2 + \alpha\gamma)/3$, $V_{co} = \Omega r$ is the corotation velocity at 1 AU. For a $\gamma \sim 2.65$ and $V_{co} \sim 400$ kms/sec the diurnal anisotropy (ξ_{co}) observed for cosmic ray particles of energy ≥ 1 GeV is of $\sim 0.6\%$. The theory predicted an energy independent anisotropy at relativistic energies and a time of maximum around ~ 1800 hours local time, that is along 90^{o} east of the sun-earth line.

Though the theoretical predictions were found to be in good agreement with the experimentally observed average diurnal variation characteristics (Rao et al, 1963; McCracken and Rao, 1965), the observed average diurnal amplitude $\sim 0.4\%$ was found less by $\sim$ 44% during solar minimum ($\gamma = 2.65$) and $\sim$ 30% during solar maximum ($\gamma = 2.25$) compared to the

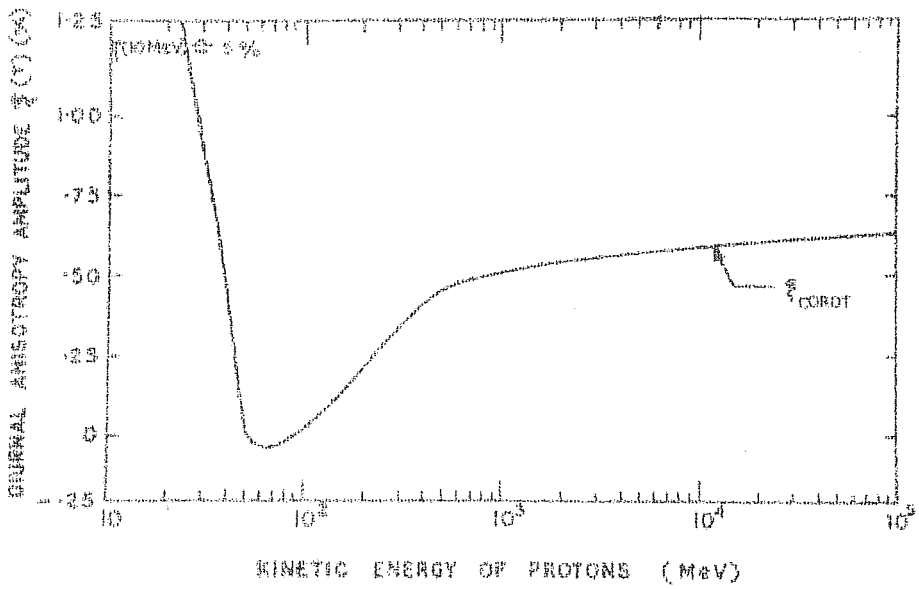

Figure 1.2 - Theoretically expected (maximum) amplitude of the corotational diurnal anisotropy as a function of kinetic energy.

theoretically predicted amplitude. Parker (1967) and Jokipii and Parker (1967) suggested that the discrepancy in the observed and calculated diurnal amplitude can be attributed to a finite diffusion coefficient perpendicular to the magnetic field ($K_\perp \neq 0$). A reduction in the diurnal amplitude can be produced when (a) $K_\perp$ is small beyond the orbit of the earth and (b) $K_\perp$ is large at the orbit of the earth.

When $K_\perp$ is small beyond the orbit of the earth, that is when the magnetic field is very smooth through out the modulating region, the cosmic ray density gradients perpendicular to the ecliptic plane are not completely wiped off and the partial neutralization of cosmic ray gradients perpendicular to the ecliptic will cause a reduction in the diurnal amplitude (Parker, 1967). The diurnal amplitude will reach the theoretical limit of $\sim$ 0.6%, when $K_\perp$ is large beyond the orbit of the earth and to explain the observed reduction in the diurnal amplitude it was found necessary to assume the ratio $K_\perp / K_{||}$ is of $\sim 10^{-2}$.

An alternate way to explain the reduction is to assume a significant diffusion perpendicular to the magnetic field ($K_\perp$) at the orbit of the earth. (Jokipii and Parker, 1967). When $K_\perp$ is very large at the orbit of the earth, the cosmic ray particles are not constrained to move along the corotating magnetic fields and the diurnal amplitude is reduced. The expected corotational anisotropy with a finite $K_\perp / K_{||}$ ratio

at the orbit of the earth was given by (Krymskiy, 1964; Parker, 1967; Forman and Gleeson, 1970)

$$\lambda_\psi = \lambda_{\psi_{co}} \left\{ \frac{(1 - K_\perp / K_{11}) \tan\psi}{1 + (K_\perp / K_{11}) \tan^2\psi} \right\} \qquad (1.10)$$

Where $\lambda_{\psi_{co}}$ is the corotational diurnal amplitude given by equation 1.9 and ψ is the angle between the average IPMF and the radius vector. The two limiting cases follows from the equation (1.10)

when $K_\perp / K_{11} \simeq 0$, then $\lambda_\psi = \lambda_{\psi_{co}} \sim 0.6\%$, leads to maximum corotation.

$K_\perp / K_{11} \simeq 1$, then $\lambda_\psi = 0$, leads to zero corotation. (1.11)

$K_\perp / K_{11} \simeq 0.15$, then $\lambda_\psi = \frac{2}{3} \lambda_{\psi_{co}} \sim 0.4\%$, gives the observed diurnal amplitude.

At relativistic energies the observed diurnal amplitude can be understood in terms of a finite $K_\perp / K_{11}$ and is estimated to be ~ 0.15 is in good agreement with experimental observations (Jokipii and Coleman, 1968). At low energies $\sim$ 10 MeV (Rao et al, 1967) $K_\perp / K_{11} \simeq 1$ leads to an isotropic diffusion due to the random walk or meandering of field lines (Jokipii and Parker, 1969) and the azimuthal streaming at these energies was found to be almost zero.

1.13 Modified theory of diurnal variation:

Recently Subramanian (1971) from a critical analysis of the neutron monitor data of Deep River suggested that the discrepancy between the observed and predicted diurnal amplitude

can be very well explained if due allowance is made for the four cumulative effects of extra atmospheric origin. Using a variable spectral exponent γ = 1.5 to 2.5 for the modulated part of the spectrum corresponding to particle energies 2 to 15 GeV, using a $E_{max} \sim$ 90 GeV and normalizing the variational coefficients by considering a significant contribution from particles of rigidity $>$ 500 GeV, showed that during solar maximum the observed average diurnal amplitude is in good agreement with the theoretically predicted amplitude and the assumption of a significant transverse diffusion ($K_\perp / K_\parallel \sim 0.2$) at relativistic energies near the orbit of the earth ($\geq$ 1 GeV) is not necessary to explain the observed reduction in the amplitude of diurnal variation. Such a conclusion is in good agreement with low energy flare particle observations of McCracken et al (1968, 1971).

Following Gleeson and Axford (1967) and Gleeson (1969), for a spherically symmetric configuration, we can write the equations governing the differential current density S and differential number density U of cosmic ray particles in the presence of magnetic field $\bar{B}$ and electric field $\bar{E}$, as,

$$S = UV = \Phi_\parallel + \frac{1}{1+\eta^2} \Phi_\perp + \frac{\eta}{1+\eta^2} \left(\Phi_\perp \times \frac{\bar{B}}{B} \right) \qquad (1.12)$$

where $\Phi = C(r,E)\, UV - K \left(\frac{\partial U}{\partial r}\right) + C(r, E) \frac{\eta\, U\bar{E}}{B}$ (1.13)

$\eta = \omega\tau$, $\omega = eB/m$ is the proton gyro-frequency

τ is the collision time and $K = v^2\tau/3$ is the isotropic

diffusion coefficient, v is the particle velocity and $C(r, E)$ is related to Compton-Getting factor given by $C(r, E) = (2 + \gamma)/3$ and in the presence of a magnetic field, K has components $K_{\parallel} = K$ and $K_{\perp} = K/(1 + \eta^2)$.

In the interplanetary space the solar wind plasma with a velocity V_p, due to its high electrical conductivity convects out the magnetic field $\bar{B}$ induces an electric field $\bar{E} = -V_p \times \bar{B}$. Rewriting the equation 1.12 in terms of $V_{\parallel}$ and $\bar{E}$ we have

$$S = CUV_{\parallel} - K\left(\frac{\partial U}{\partial r}\right)_{\parallel} - \frac{K}{1+\eta^2}\left(\frac{\partial U}{\partial r}\right)_{\perp} - \frac{\eta K}{1+\eta^2}\left(\frac{\partial U}{\partial r} \times \frac{\bar{B}}{B}\right) + CU\left(\frac{\bar{E} \times \bar{B}}{B^2}\right) \qquad (1.14)$$

Recently Forman and Gleeson (1970, 1974) showed that in the interplanetary medium, the electric field drift and convection parallel to the magnetic field can easily combine into a simple convective flow of particles with the solar wind. That is the first and last term of the equation 1.14 combines to yield a single convective term CUV_p, then the above equation reduces to the form

$$S = CUV_p - K\left(\frac{\partial U}{\partial r}\right)_{\parallel} - \frac{K}{1+\eta^2}\left(\frac{\partial U}{\partial r}\right)_{\perp} - \frac{\eta K}{1+\eta^2}\left(\frac{\partial U}{\partial r} \times \frac{\bar{B}}{B}\right) \qquad (1.15)$$

Including the effects of random walk of the field lines on the cosmic ray particles (Jokipii and Parker, 1969) the modified equation for the net cosmic ray streaming in the interplanetary medium is given by,

$$S = S_c - K_{\parallel}\left(\frac{\partial U}{\partial r}\right)_{\parallel} - K_{\perp}\left(\frac{\partial U}{\partial r}\right)_{\perp} - A\left(\frac{\partial U}{\partial r} \times \frac{\bar{B}}{B}\right) \qquad (1.16)$$

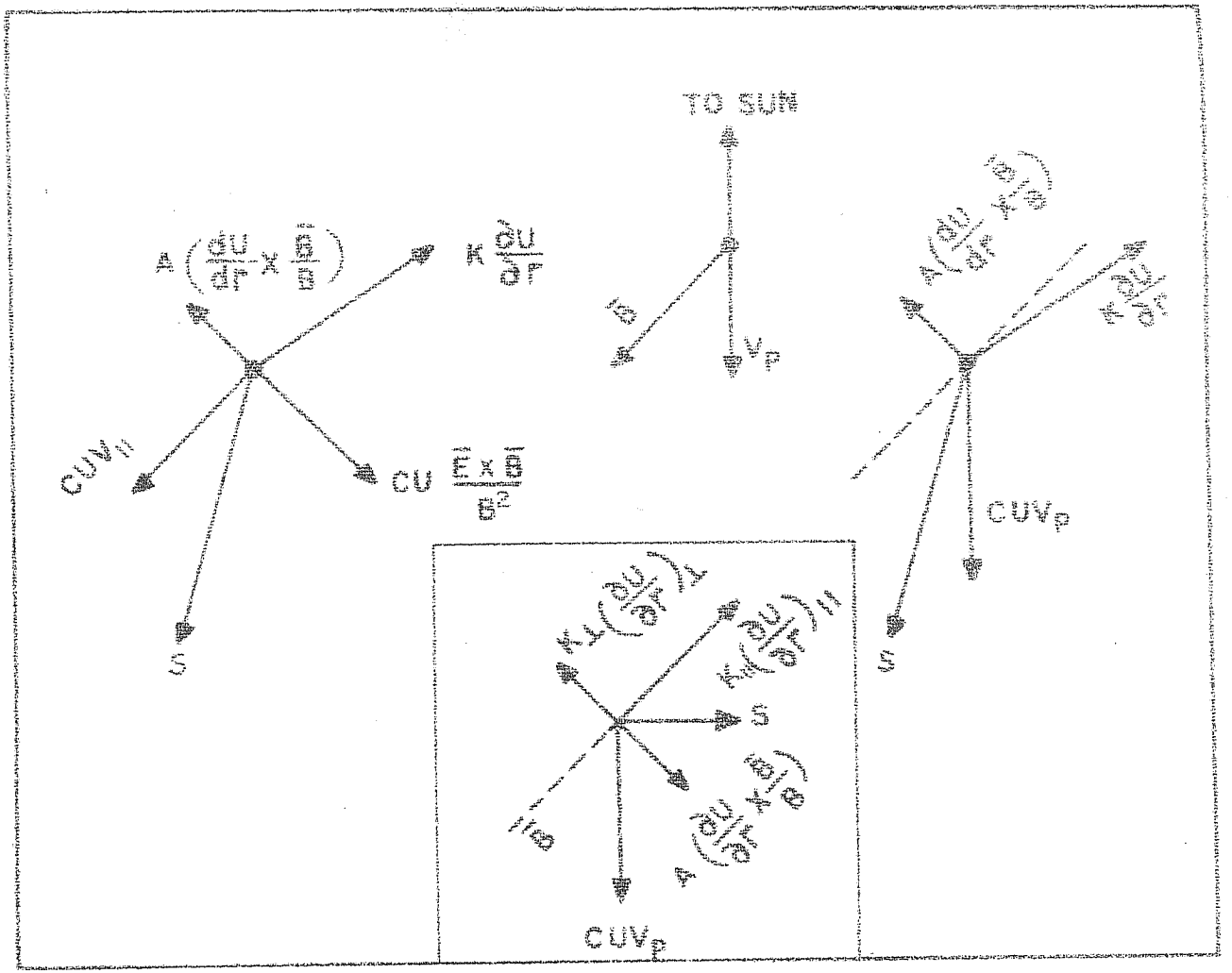

Figure 1.3 - The net differential cosmic ray current density described in terms of (a) Electric field (b) Convection component (wind velocity) (c) All the four components given in equation (1.16).

Where $S_c = CUV_p$ is the convection current density, V_p is the solar wind velocity and

$$K_\perp = K'_\perp(\bar{B}, r, t) + \frac{K_{||}}{1+\eta^2}, \quad K\left(\frac{\partial U}{\partial r}\right) = K_{||}\left(\frac{\partial U}{\partial r}\right)_{||} + K_\perp\left(\frac{\partial U}{\partial r}\right)_\perp \tag{1.17}$$

$$A = v^2 \eta^2 / 3\omega(1+\eta^2)$$

Interpreted in terms of physical mechanisms, the net streaming of cosmic ray particles in the interplanetary space is essentially governed by (equation 1.16)

1. The convection of particles radially away from the sun.

2. The diffusion of particles parallel to the magnetic field.

3. The diffusion of particles perpendicular to the magnetic field.

4. The streaming produced by the density gradient perpendicular to the ecliptic plane.

The observed diurnal variation follows from the above equation (1.16) with the following assumption that,

(a) The radial component is zero ($S_r = 0$).

(b) The diffusion coefficient perpendicular to the

magnetic field is negligible $K_{\perp} \sim 0$ and

(c) The transverse gradient current is zero $(\frac{\partial U}{\partial r} \times \frac{\bar{B}}{B}) \approx 0$.

Under these conditions the radial convective component $S_c = CUV_p$ is balanced by the inward diffusive component $K_{\parallel} (\frac{\partial U}{\partial r})_{\parallel}$ and since the field lines are inclined to the radial direction by an angle ψ (garden-hose angle) results in a net azimuthal streaming given by $CUV_p \tan\psi$, which corresponds to the particles corotating with a velocity $V_{co} = V_p \tan\psi$ and give rise to a diurnal anisotropy given by

$$\xi_{\varphi}(r) = \frac{3CV_{co}}{v} = \frac{3\ CV_p \tan\psi}{v} \qquad (1.18)$$

At relativistic energies ($v \sim c$) the amplitude of diurnal anisotropy is $\xi_{\varphi}(r) \sim 0.6\%$ for a $V_p \sim 400$ kms/sec and $\psi \sim 45^{\circ}$.

A detailed study of the low energy solar cosmic rays from widely spaced Pioneer space-craft observations (McCracken et al, 1968, 1971; Rao et al, 1971; Allum et al, 1974) showed that the low energy cosmic ray anisotropies observed during both initial phase as well as late in the solar flare event can be completely explained in terms of simple convection and field aligned diffusion mechanism. Extending these arguments to relativistic energies, Rao et al (1972) and Hashim et al (1972) showed independently that the diurnal variation observed at relativistic energies (≥ 1 GeV) can also be explained in terms of convection and diffusion concept. They clearly demonstrated that on an average basis under equilibrium conditions, the radial convective flow will exactly balance the

inward field aligned diffusive flow resulting in the observed corotational diurnal variation. Extending the unified convection-diffusion theory, the author in this thesis has made a detailed examination of the diurnal anisotropy characteristics on an average basis using cosmic ray intensity observations from a large number of neutron monitoring stations during the period 1965-72 ($\sim$ 8 years). Further using the 'in situ' spacecraft observations of the solar wind and IPMF parameters and deriving appropriate convection and magnetic field vectors, he has demonstrated that (chapter III), the yearly as well as the 27-day average diurnal anisotropy characteristics observed during 1965-72 can be understood in terms of simple convection and field aligned diffusion of particles in the interplanetary medium and the assumption of a significant transverse diffusion current ($K_\perp / K_\parallel \simeq .2$) at the orbit of the earth is not necessary to explain the observed average diurnal variation.

1.14 Short term variation of diurnal anisotropy:

Though the average behaviour of the diurnal variation is well understood, understanding of the short term variations of the diurnal anisotropy and the large variability observed on a day to day basis which is essentially caused by significant variations in the electromagnetic properties of the interplanetary medium is considerably less. Several investigators (Rao and Sarabhai, 1961, 1964; Patel et al, 1968; Pomerantz and Duggal, 1971; Rao, 1972) have pointed out that the observed

variability in the diurnal amplitude and the diurnal time of maximum on a day to day basis is significantly more than that expected from a statistical behaviour. Applying the method of variational coefficients, Patel et al (1968) determined the energy spectrum of diurnal and semi-diurnal variation on a day to day basis using a large number of stations and showed that a large variability in the energy spectrum exists on a day to day basis even during relatively quiet period. During geomagnetic storms however the diurnal time of maximum seems to shift towards earlier hours (Dorman, 1957; Tanskanen, 1968; Ostman and Awadalla, 1970).

Occurrence of trains of days having abnormally high diurnal amplitude ($> 0.6\%$) has been reported by a number of workers during quiet as well as disturbed periods. Mathews et al (1969) and Hashim and Thambyahpillai (1969) showed that, these are caused by a depletion of cosmic ray intensity along the garden-hose direction. The possible existence of sinks in the garden-hose direction was inferred much earlier by Rao and Sarabhai (1964) from the study of the distribution of diurnal time of maximum. The large amplitude diurnal wave trains studied by Duggal and Pomerantz (1962) showed a systematic anti-clockwise shift in the diurnal anisotropy for ~ 8 days. The diurnal phase shift towards later hours (~ 21 hours) caused by enhanced radial gradients was studied by Rao et al (1972).

The present thesis deals with the extension of convection-diffusion theory and the applicability in successfully explaining not only the average characteristics of diurnal variation but also the characteristics of diurnal variation observed on a day to day basis. The relationship with the other solar terrestrial parameters such as plasma and interplanetary magnetic field, which are responsible for the occurrence of significant deviations in the observed diurnal variation from the average behaviour are examined to understand the electromagnetic processes that operate in the interplanetary medium.

....

C H A P T E R - II

INSTRUMENTATION

2.1 Super neutron monitor:

Regular monitoring of primary cosmic radiation through the measurement of secondary components such as neutrons and muons which occur as daughter products during the interaction of the incident primary cosmic ray particles with atmospheric nuclei, has been extensively carried out in the past two decades. The comparatively large magnitude of the latitude effect observed on the secondary neutron component, which is suggestive of their association with the lower energy part of the spectrum of cosmic radiation makes the monitoring of primary cosmic ray variations through nucleonic component very attractive (Simpson, 1948, 1949). However, it is only in 1952 that, an effective neutron monitor developed by Simpson and his co-workers become available which after a few minor changes was adopted as a standard cosmic ray monitoring equipment for IGY during 1957-58. In spite of vary reliable results obtained from the data from a world wide net-work of about 50 IGY type of monitors, it was quite apparent that the counting rates obtained from these monitors were too low to permit an unambiguous interpretation of many aspects of cosmic ray time variations. Whereas the IGY monitors were quite adequate to study the large cosmic ray enhancements of solar origin and through them the interplanetary field configuration (McCracken, 1962), these monitors offered poor statistics for the study of

short term variations such as diurnal and semi-diurnal variation on a day to day basis. This led to the design of super neutron monitors (18-NM-64), which employ a total of 18 large size BF_3 counters giving a counting rate of $\sim 10^6$ counts / hour at a typical sea level station having a cut-off rigidity ≤ 2 GV (Carmichael, 1964).

Even though more than ~ 30 (18-NM-64) super neutron monitors are operating at various parts of the world, conspicuous gaps in the longitude range 25° E to 180° E and an almost complete absence of equatorial monitors are still noticeable. The establishment of a super neutron monitor (NM-64) at Ahmedabad during 1968, a sea level station located at geographic latitude 23.01 $^{\circ}$N and geographic longitude 72.61 $^{\circ}$E having an upper cut-off rigidity $\sim$ 15.94 GV has to some extent been responsible to fill this big gap in the longitude range 25 $^{\circ}$E to 130 $^{\circ}$E and provide an extremely valuable input to the world data coverage.

2.2 Description of the super neutron monitor at Ahmedabad:

The basic design of the super neutron monitor (18-NM-64) at Ahmedabad (India) essentially follows the standard design recommended by Carmichael (1964) during IQSY period. The neutron pile consists of 18 large size BF_3 gas filled copper proportional counters enclosed in a cylinder of paraffin wax moderator. Each counter along with its moderator cylinder is surrounded by 18 lead rings of purity

greater than 99.9%, cast in the form of cylinders each of length of $\sim$ 11.5 cm, weighing about $\sim$ 89.3 $\pm$ 0.6 Kg ($\sim$ 200 pounds). The 18 counters are distributed in three identical arrays of 6 counters each, with the three individual arrays being completely shielded by a rectangular box of low density paraffin wax of thickness $\sim$ 7.5 cm, which acts as a reflector and establishes a full albedo of neutrons inside the monitor. In addition the paraffin wax also diminishes the proportion of low energy neutrons arriving at the detector from outside the monitor, thus making it less susceptible to the variable environmental flux of thermal neutrons which can be often as high as $\sim$ 5%. Fig. 2.1 shows one such array which forms a part of the neutron monitor assembly at Ahmedabad. The output of each counter after amplification and discrimination is fed to a mixer-amplifier. The output of the mixer-amplifier from each of the three sections (arrays) are separately counted and recorded.

2.3 The principles of neutron counter:

The proportional counters filled with Boron trifluoride (BF_3) gas enriched with Boron isotope B^{10} are the most efficient detectors for detecting thermal neutrons. The large size counters used in the neutron monitor are filled with pure BF_3 gas enriched with 96% B^{10} isotope at a pressure of $\sim$ 20 cm of Hg at 22 ^{o}C, when operated in the proportional region with a high voltage of about $\sim$ 2800 V, the counters are found to have

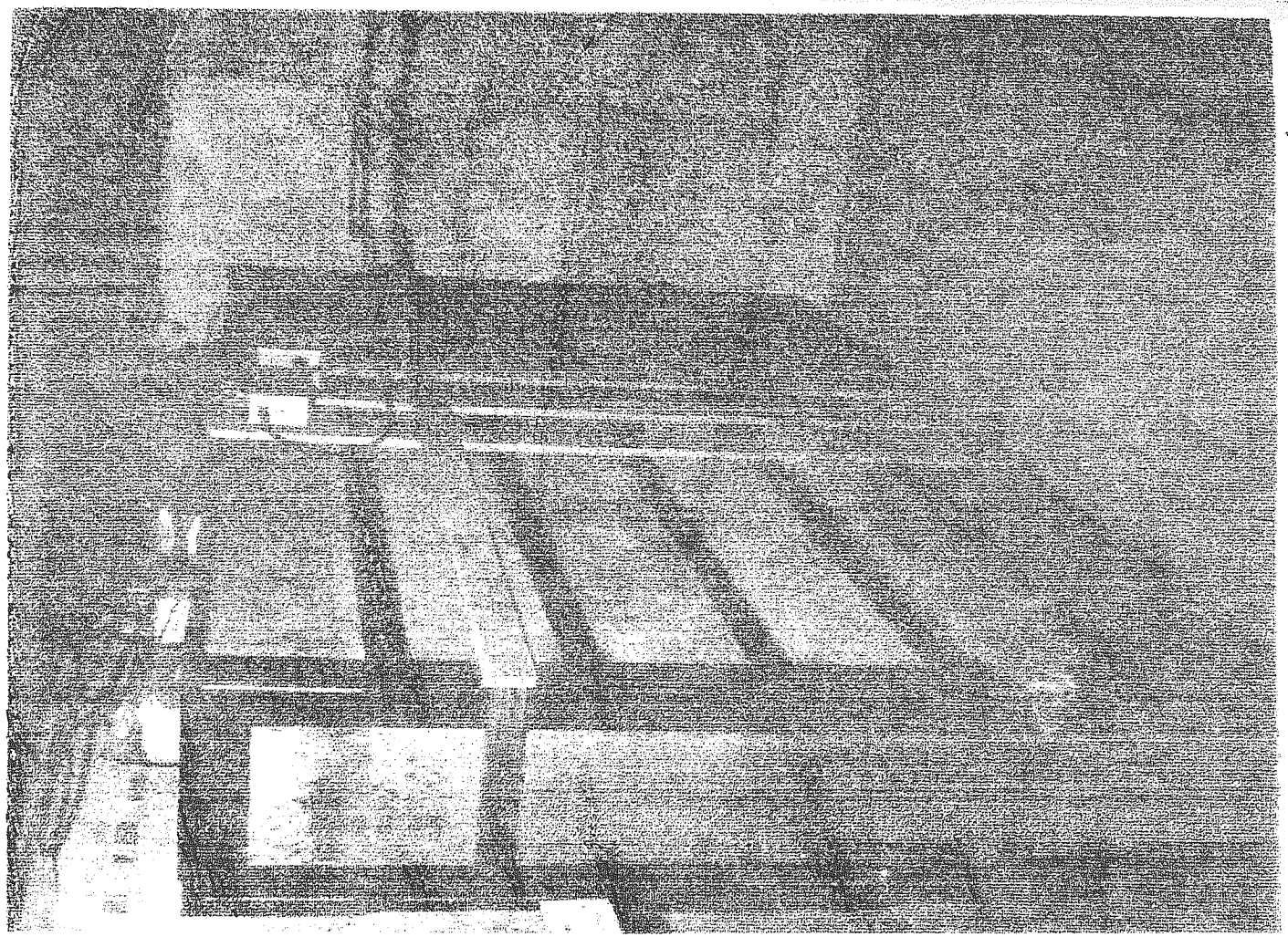

Figure 2.1 - A section of the neutron pile of 18-NM-64 neutron monitor at Ahmedabad. The boxes projecting out of the proportional counters contain pre-amplifier and amplifier-discriminator assembly. The amplifier-mixer box and the box containing high voltage distribution points can be seen on the top of the neutron pile.

a gas multiplication ~ 35. These counters exhibit a plateau over a range of ~ 400 V with a slope $\sim$ 1%/100 V in the proportional region. A resonant exothermic reaction occurs when a thermal neutron collide with Boron (B^{10}) nucleus producing Lithium and Helium following the reaction,

$$ {}_5B^{10} + {}_0n^1 \longrightarrow {}_3Li^7 + {}_2He^4 + 2.78 \text{ MeV} \qquad (2.1) $$

The cross-section of this reaction is inversly proportional to the velocity V of the captured neutron ($\frac{1}{V}$ dependence) is found to be of ~ 3820 barns for thermal neutrons of energies (1/40 eV). In 94% of the reaction ${}_3Li^7$ nucleus is left in an excited state (~ 0.48 MeV) and the remaining 2.30 MeV energy is shared between ${}_3Li^7$ and ${}_2He^4$ nuclei. In the remaining 6% of the reaction , ${}_3Li^7$ nucleus is left in the ground state and ${}_3li^7$ and ${}_2He^4$ nuclei have a total kinetic energy of ~ 2.78 MeV. The output pulse of about $\sim$ 1 milli-volt due to the neutrons captured can be suitably amplified and discriminated from the relatively small pulses produced by muons, electrons and γ -rays passing through the counter.

A high energy incident secondary neutron interacts with lead and produces a large number of evaporation neutrons, the number being proportional to the energy of the incident interacting particle. Typically a parent secondary nuclei of energy of $\sim$ 200 - 300 MeV produces on an average 10 evaporation neutrons. In the neutron monitor a spectrum of excitation

energies of the lead nuclei results because (a) the incident nucleons have a wide range of energies and (b) the nucleons with a given energy produces a range of excitation energies due to the statistical nature of the intranuclear cascade process. The evaporation neutrons produced are decelerated due to collisions in the moderator and give rise to slow or thermal neutrons, which are easily captured by B^{10} isotope present in the counter gas. The absorption losses of thermal neutrons in the moderator and the counter walls is almost negligible and the detection efficiency of the evaporation neutrons in the NM-64 neutron monitor is found to be of $\sim$ 6% (Hatton and Carmichael, 1964).

2.4 Neutron production by nucleons:

The nucleon-nucleus interaction is found to develop in two stages. In the first "cascade phase" the pions and the knock on nucleons are emitted with a broad energy spectrum with an angular distribution peaked along the direction of motion of the incident nucleon. The residual nucleon at the end of the first phase are left in an excited state and further emission of particles that is the production of evaporation neutrons follow during the second "de-excitation" or evaporation phase. It has been shown theoretically (Shen, 1968) and experimentally (Hughes et al, 1964) that the production of evaporation neutrons increases with the energy of the incident particle and also with the increase of the producer thickness.

The stochastic nature of the processes leading to the production of the evaporation neutrons which results in a broad and exponential neutron production spectrum, essentially limits the use of neutron monitor as a energy spectrometer.

2.5 Data recording system:

Fig. 2.2 shows the data recording system of the super neutron monitor at Ahmedabad. A block diagram shown in Fig. 2.3 gives complete details of the data recording system. The $\sim$ 1 millivolt pulses produced due to the passage of thermal neutrons in the counter are fed to a pre-amplifier followed by a three stage amplifier and a simple tunnel diode discriminator which will reject the small pulses produced by other secondary particles such as muons, electrons and γ -rays. The counting rate of each counter at Ahmedabad is of $\sim$ 10,000 counts/hour. The discriminator output from the six counters in each section are separately amplified and suitably mixed in the mixer-amplifier and the combined output from each section is accumulated in intervals of 4 minutes duration. At the end of each 4 minute interval, the accumulated counts are transferred to a temporary discrete memory system which introduces a known dead time of $\sim$ 6 μs during which period the decades are reset and kept ready for continuing the accumulation for the next interval of time. The data from the buffer memory of all the three sections, together with the exact time information from a crystal clock and the atmospheric pressure data from a digital

Figure 2.2 - The automatic data recording system of the super neutron monitor at Ahmedabad. The first rack from the left contains all the high and low voltage power supplies, the middle one all the decades, memory storage systems and the serial converter and the third rack contains the electronic typewriter and punchers used for recording the data.

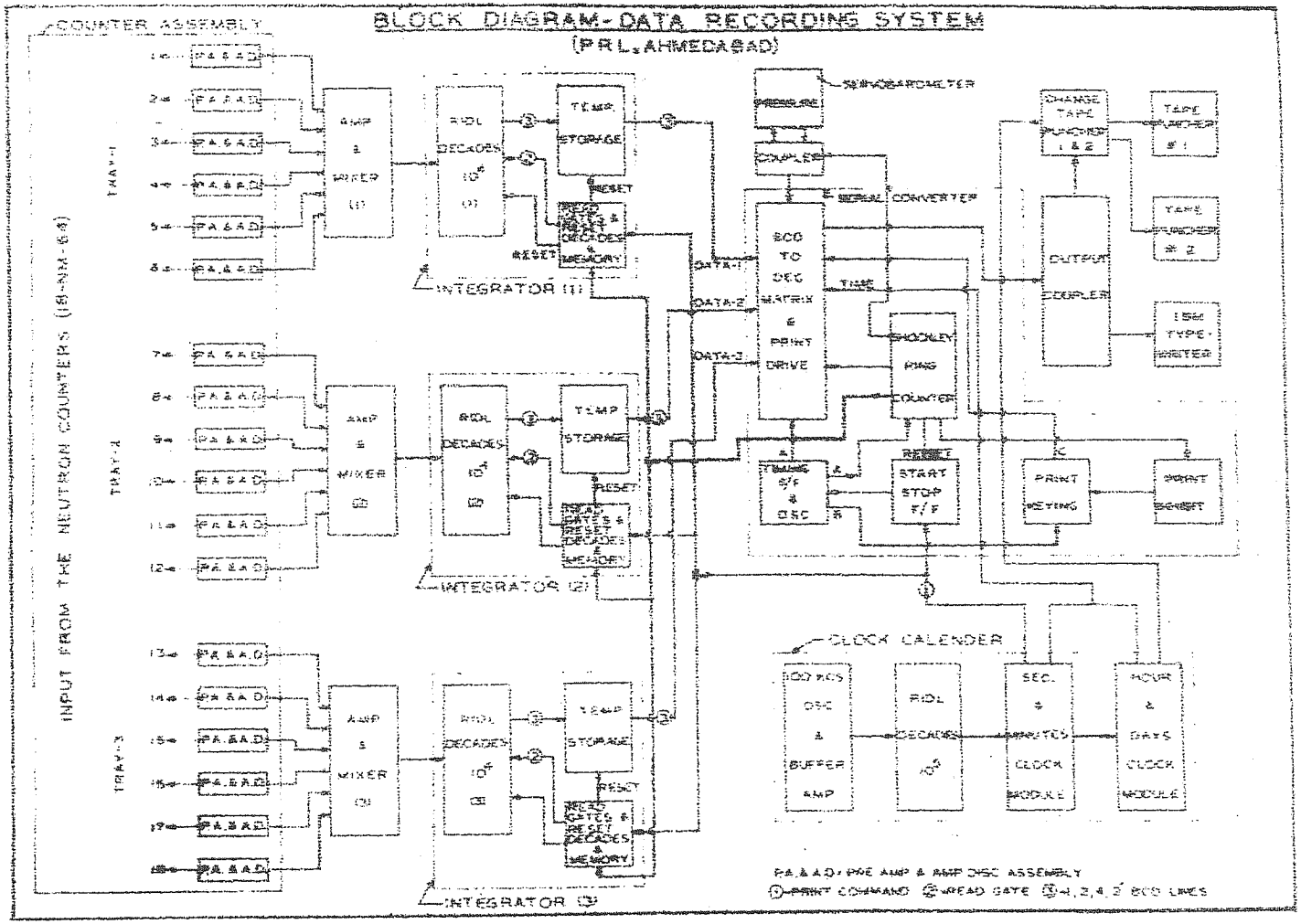

Figure 2.3 - A block diagram of the data recording system at Ahmedabad. The 18- counters and the pre-amplifier and amplifier-discriminator assembly are also shown.

servo-barometer with an accuracy of $\sim$ 0.1 mm are then serially transferred in BCD form on to a paper tape punch recorder and in digital form on to a electronic typewriter. The entire recording operation is controlled by a crystal clock which produces command pulses at the end of each 4 minute interval. The hourly and daily mean cosmic ray intensity at Ahmedabad is derived from this 4 minute basic data.

2.6 Zenith angle dependence of a neutron monitor:

The relative contribution of the secondary nucleon incident at a zenith angle varying between θ and $\theta + d\theta$ to the counting rate of a detector is given by

$$N(\theta)\, d\theta \propto J(\theta).S(\theta).\sin\theta.d\theta \qquad (2.2)$$

Where $J(\theta)$ is the zenith angle distribution of the nucleonic component and $S(\theta)$ is the sensitivity of the detector to this component is a function of zenith angle. $S(\theta)$ is found to be approximately a constant indicating that the neutron monitor essentially behaves as an omni-directional detector. Phillips and Parsons (1962) using a mobile IGY monitor showed that the zenith angle distribution of the nucleonic component can be expressed as $J(\theta) \propto \cos^5\theta$ over a range of θ, varying between 0 - 40° and at larger angles $\theta > 40^\circ$ the function decreases very slowly. The largest contribution to the counting rate of a neutron monitor is from zenith angle $\sim 25^\circ$ and less than 7% of the counting rate being accounted for by neutrons arriving at large zenith angles $\theta > 60^\circ$ (Carmichael et al, 1969).

2.7 Plateau and pulse height characteristics:

The proportional region of a neutron counter can be determined by a typical plot of the variation of the counting rate with applied voltage. It is found that in the proportional region the pulses due to various secondary particles such as muons, electrons and γ -rays (noise pulses) are relatively smaller compared to the pulses due to thermal neutrons, thus making it possible to discriminate between the two. A number of authors have investigated the relative contributions made by various secondary components to the counting rate of both IGY and NM-64 monitors. (Simpson et al, 1953; Hughes and Marsden, 1966; Harman and Hatton, 1968; Hatton, 1971). Table 2.1 gives the relative contribution by different secondary cosmic ray components to the counting rate of a typical IGY and NM-64 monitor. The proportional region of a NM-64 neutron counter typically extends from 2700 to 3200 Volts with a plateau of $\sim$400 - 500 V and a slope of $\sim$ 1%/100 V. McCracken et al (1966a)pointed out that a periodical examination of the pulse height characteristics of a neutron counter can be effectively used to detect a slowly deteriorating counter. Since then, this method of monitoring the health of a neutron monitor has been well accepted as a general practice. The pulse height analysis of each counter using a 400 channel analyser has been regularly carried out and the resolution of each counter is periodically measured. The typical full-width

Table 2.1

Sr. No.	Components	Percentage contribution IGY Monitor	Percentage contribution NM-64 Monitor
1.	Neutrons	83.6 ± 2.0	85.2 ± 2.0
2.	Protons	7.4 ± 1.0	7.2 ± 1.0
3.	Pions	1.2 ± 0.3	1.0 ± 0.3
4.	Stopping muons	4.4 ± 0.8	3.6 ± 0.7
5.	Interacting muons	2.4 ± 0.4	2.0 ± 0.4
6.	Background	1.0	1.0

Table 2.1 - The relative contributions (percent) made by various secondary cosmic ray components to the counting rate of an IGY and NM-64 monitor

at half-maximum of a good NM-64 counter is found to be of $\sim$ 11% at the operating voltage and varies from 9 to 20% for all the 18 counters used in Ahmedabad neutron monitor.

2.8 Data processing:

The ratio's of the counting rates obtained by three independent sections of the neutron monitor both on an hourly as well as on a daily basis is regularly monitored and used to determine the self consistency of the data. Since both the cosmic ray primaries and secondaries show a random distribution in time, they can be assumed to obey Poisson distribution. The statistical error associated with the 4 minute count rate N is given by

$$\sigma = M/ (N)^{\frac{1}{2}} \qquad (2.3)$$

Where M is the multiplicity which is of $\sim$ 1.4 for Ahmedabad monitor. The error associated with the ratio can be written as

$$\sigma_r = \sigma (2)^{\frac{1}{2}} \qquad (2.4)$$

Knowing the count rate obtained by the individual sections, the errors associated with any two sections can be calculated. Using a 4σ limit as the minimal acceptable level for both the ratio's and the actual count rate difference between any two sections, the pressure corrected data is then computed from which the hourly mean and daily mean pressure corrected cosmic ray intensity at Ahmedabad has been obtained. The

total counts over each day is also computed for each individual section and is used to compute the daily ratio's between different sections and these ratio's are used for checking the long term stability of the monitor.

2.9 Pressure correction of neutron monitor data:

Before using Ahmedabad neutron data for any further analysis it is very essential to correct the data for meteorological variations, as most of the secondary neutrons are produced during the interaction of primary cosmic ray particles with the atmospheric nuclei. Earlier observations clearly indicated that the neutron intensity at the ground is significantly affected by pressure variations, whereas the temperature corrections for neutron component is almost negligible. The neutron intensity N at any atmospheric pressure P can be expressed as,

$$N(P) = \exp(-P/L) \qquad (2.5)$$

Where L is the absorption mean free-path of the neutron component, which depends on the mean energy of the recorded neutron component. Differentiating equation (2.5) with respect to P it can be shown that

$$\alpha = -\frac{1}{N}\frac{dN}{dP} \qquad (2.6)$$

Where $\alpha = \frac{1}{L}$ is known as the barometric attenuation coefficient. Extensive investigations have shown that the

attenuation coefficient (α) of a neutron monitor is a function of both latitude and altitude (Bachelet et al, 1965, 1972; Carmichael et al, 1968) and varies with solar cycle having a maximum value during solar minimum. The attenuation coefficients obtained for various sea level neutron monitoring stations having different cut-off rigidities for the period 1964-1965 (Bachelet et al, 1972) and those obtained for 1965 by Carmichael and Bercovitch (1969) from latitude surveys show that there is a good agreement in the values of the attenuation coefficient derived for low latitude stations having cut-off rigidities $\geq$ 8 GV. Following well established methods, the attenuation coefficient (α) for Ahmedabad NM-64 neutron monitor has been estimated by performing a complex regression analysis of successive differences (Lapointe and Rose, 1962) of the logarithm of the daily mean intensity (N) and the daily mean pressure (P) using equations

$$\mathrm{Ln}(N_2) - \mathrm{Ln}(N_1) = -\alpha (P_2 - P_1) \qquad (2.7)$$

Using the data of Ahmedabad neutron monitor during the period 1968-73, after adequately correcting for the changes in the efficiency of the monitor with time, the attenuation coefficient appropriate to Ahmedabad monitor ($P_c \sim 15.9$ GV) has been derived is found to be $\sim 0.84 \pm 0.02\%$/mm Hg is in good agreement with the results reported by Forman (1968) and Bachelet et al (1972). Since the solar cycle variation of α at

stations with $P_c \geq 15.9$ GV is quite negligible, we have used the same attenuation coefficient for correcting Ahmedabad neutron monitor data for the entire period 1968-73. The pressure corrected neutron intensity N has been derived using the relationship

$$N = N_o \exp\{\alpha(P - P_o)\} \qquad (2.8)$$

Where N_o is the observed neutron intensity at pressure P and $(P - P_o)$ is the difference between the observed pressure (P) and the standard pressure (P_o) which is basically chosen as the yearly mean pressure at a particular station. The yearly mean pressure (P_o) at Ahmedabad is found to be of $\sim$ 750.08 mm (1000 mb), and the attenuation coefficient is $\sim$ 0.84%/mm Hg. The pressure corrected hourly neutron data at Ahmedabad has been used for all further analysis.

2.10 Determination of solar daily variation:

Even though the solar daily variation can be studied using different methods (Rao and Sarabhai, 1964; Kane, 1966) most of the qualitative information on the daily variation obtained so far has been through the study of the diurnal (I harmonic) and the semi-diurnal (II harmonic) components derived from a Fourier analysis (Chapman and Bartels, 1940) of the cosmic ray intensity observed over a period of 24-hours (1 day). The amplitude and time of maximum of the diurnal and semi-diurnal anisotropy vectors derived from the harmonic

coefficients implicitly assumes that the anisotropy remains constant over a period of 24 hours. Therefore whenever large world wide variations and short term variations (< 24 hours) occur, the harmonic coefficients and the diurnal and semi-diurnal vectors derived from above method have to be viewed with caution. In order to derive the 12 hour and 24 hour periodic components, it is customary to employ the well known 24-hour moving average method (Dorman, 1957) to remove the effects of slowly varying components (>24 hours). The data obtained after removing the slowly varying components are then subjected to Fourier analysis.

2.11 Harmonic analysis:

Any periodic function Y (t), over a finite interval t = 0 to t = 2π, with 24 equidistant points within the interval, can be expressed in the simple form of a Fourier's series as,

$$Y(t) = A_o + \sum_{n=1}^{24} (A_n \cos nt + B_n \sin nt) \qquad (2.9)$$

where A_o is the mean value of Y(t) in the interval 0 to 2π and A_n, B_n are coefficients of the n^{th} harmonic given by

$$A_o = \frac{1}{24} \sum_{i=1}^{24} R_i, \quad A_n = \frac{1}{12} \sum_{i=1}^{24} R_i \cos nt_i$$

$$B_n = \frac{1}{12} \sum_{i=1}^{24} R_i \sin nt_i \qquad (2.10)$$

The amplitude R_n and phase Θ_n of the n^{th} harmonic can be obtained from the equation

$$R_n \cos (nt - \Theta_n) = A_n \cos nt + B_n \sin nt \qquad (2.11)$$

Where

$$R_n = (A_n^2 + B_n^2)^{\frac{1}{2}} \quad \text{and} \quad \Theta_n = \text{Arc tan } (B_n/A_n) \qquad (2.12)$$

Assuming that the hourly counts follow a standard Gaussian distribution, the standard error in the determination of various harmonics is given by

$$\sigma A_n^2 = \sigma B_n^2 = \sigma R_n^2 = \sigma^2/12 \quad \text{and}$$
$$\sigma \Theta_n = \sigma R_n / R_n \qquad (2.13)$$

Where σ is the standard error associated with the hourly count rate of the observed cosmic ray intensity.

2.12 Corrections for geomagnetic field:

Before interpreting the secondary cosmic ray variations observed at a ground based monitor in terms of primary cosmic ray variations in the interplanetary space, it is very essential to correct the observations for the effects of geomagnetic field. A number of investigators (McCracken et al, 1962, 1965; Rao et al, 1963; Shea et al, 1965, 1968) using a six degree simulation for the earth's magnetic field, have numerically computed the 'asymptotic directions' (the direction before entering the earth's magnetic field) of primary

cosmic ray particles having different rigidities varying from 1 - 500 GV, which are incident at different zenith and azimuth angles at the top of the atmosphere. The concept of "asymptotic cone of acceptance" of a detector developed by them has been found extremely useful in interpreting most of the secondary cosmic ray variations observed at a ground based monitor. From an extensive study of ground based neutron monitor observations Rao et al 1963 and McCracken and Rao (1965) further showed that the cosmic ray variations observed at a ground based detector corrected for the width and declination of the asymptotic cone of acceptance of the detector and geomagnetic bending at each station can be effectively used for deriving the characteristics of cosmic ray anisotropies in the interplanetary medium. A brief discussion of the variational coefficients and their application to diurnal variation are presented.

2.13 The concept of variational coefficients:

If J_o is the isotropic cosmic ray intensity from all directions, then the anisotropic cosmic ray intensity from within the solid angle Ω_i can be represented in a simple form $J_o(1+A_i R^{+\beta})$, where A_i is a function of asymptotic directions, R is the rigidity (in BV) and β is the spectral exponent. This anisotropy will essentially produce a fractional change in the counting rate of a ground based

detector given by (Rao et al, 1963; McCracken et al, 1965)

$$\frac{\Delta N}{N} = v(\Omega_i, \beta) A_i \qquad (2.14)$$

Where N is the counting rate observed, when the cosmic ray intensity is J_o from all the directions and $v(\Omega_i, \beta)$ is defined as the variational coefficients corresponding to a solid angle Ω_i and spectral exponent β. The variational coefficients however can be expressed in a simple form as

$$v(\Omega_i, \beta) = \int W(R)\, R^{+\beta}\, Y(\Omega_i, R) / Y(4\pi, R)\, dR \qquad (2.15)$$

Where W(R) is the coupling coefficient (Dorman, 1957) or differential response function of a detector (Lockwood and Webber, 1967) and $Y(\Omega_i, R)$ is the fraction of hemisphere above the detector which is accessible from asymptotic directions within the solid angle Ω_i.

2.14 Evaluation of variational coefficients:

Using spherical harmonics upto and including 6^{th} degree simulation of the earth's magnetic field (McCracken et al, 1962, 1965; Shea et al, 1965, 1968) and defining the elementary solid angle Ω_i by planes of constant geographic longitude at 0, 5 and 10 degrees and by surfaces of constant geographic latitude spaced every 5 degrees on either side of the equator, it is possible to determine the fraction of the hemisphere above the detector which is accessible from asymptotic directions included within Ω_i, if the asymptotic directions corresponding to all directions (θ, ϕ)

and for all rigidities (R_k) are known. For evaluating the variational coefficients, cosmic ray particles of various rigidities arriving from nine specific directions namely vertical, geomagnetic north, south, east and west and at zenith angles 0, 16 and 32 degrees are used. Further it is assumed that for K^{th} rigidity (R_k), if a direction (θ_o, ϕ_o) is accessible from some elementary solid angle Ω_i, then for $\theta_o \neq 0$ all directions within the solid angle $\theta_o \pm 8^o$ and $\phi_o \pm 45^o$ are accessible from Ω_i for rigidities in the range $\frac{R_{k-1} + R_k}{2}$ to $\frac{R_k + R_{k+1}}{2}$. An acceptable estimate of $Y(\Omega_i, R)$ is the number of above nine directions (θ_o, ϕ_o) which are accessible from infinity. The variational coefficients then simplify to

$$v(\Omega_i, \beta) = \sum_k W(R_k) \cdot R_k^{+\beta} \cdot \frac{Y(\Omega_i, R_k)}{Y(4\pi, R_k)} \cdot \frac{(R_{k+1} - R_{k-1})}{2} \qquad (2.16)$$

Where the summation extends from near cut-off rigidity to a value $R_{max} \sim$ 500 GV.

Expressing the anisotropy as a power law in rigidity, we have

$$\frac{\Delta J_i(R)}{J_o(R)} = AR^{+\beta} = f(\psi) R^{+\beta} \cos\Lambda \qquad (2.17)$$

Where A is the amplitude of the anisotropy which is a separable function of the asymptotic latitude Λ and longitude ψ and varies as the cosine of declination. The fractional change in the counting rate produced by the radiation from Ω_i can be written as,

$$\frac{dN(\Omega_i)}{N} = f(\psi) \cdot V(\Omega_i, \beta) \cos\Lambda \qquad (2.18)$$

and summing over all Ω_i, equation 2.18 gives

$$\frac{dN(\psi_j)}{N} = f(\psi_j) \sum V(\Omega_i, \beta) \cos\Lambda$$
$$= f(\psi_j) \cdot V(\psi_j, \beta) \qquad (2.19)$$

Where $dN(\psi_j)$ is the solid angle defined between two meridional planes 2.5 degrees on either side of the meridional plane at geographic longitude ψ_j. Using the above expression (2.19) the variational coefficients $V(\psi_j, \beta)$ for different asymptotic longitudes and for a wide range of spectral exponents (β) ranging from 1.0 to -1.2 have been evaluated for a large number of stations (McCracken et al, 1965; Shea et al, 1968) are available in the literature (IQSY Instruction Manual No.10).

2.15 Application to diurnal variation:

From a detailed knowledge of the variational coefficients and cosmic ray observations at various stations, the amplitude and phase of the cosmic ray anisotropy in space can be easily predicted. Any anisotropy can be expanded as a function of 'η' in the form of a Fourier's series as

$$f(\eta) = J_o(R) \sum_{m=1}^{\infty} \alpha_m \cdot \cos\{m(\eta - C_m)\} \qquad (2.20)$$

Where α_m and C_m are the arbitrary amplitude and phase constants and C_m is also the direction from which a maximum of the m^{th} harmonic is seen. Referring to figure 2.4 the intensity from

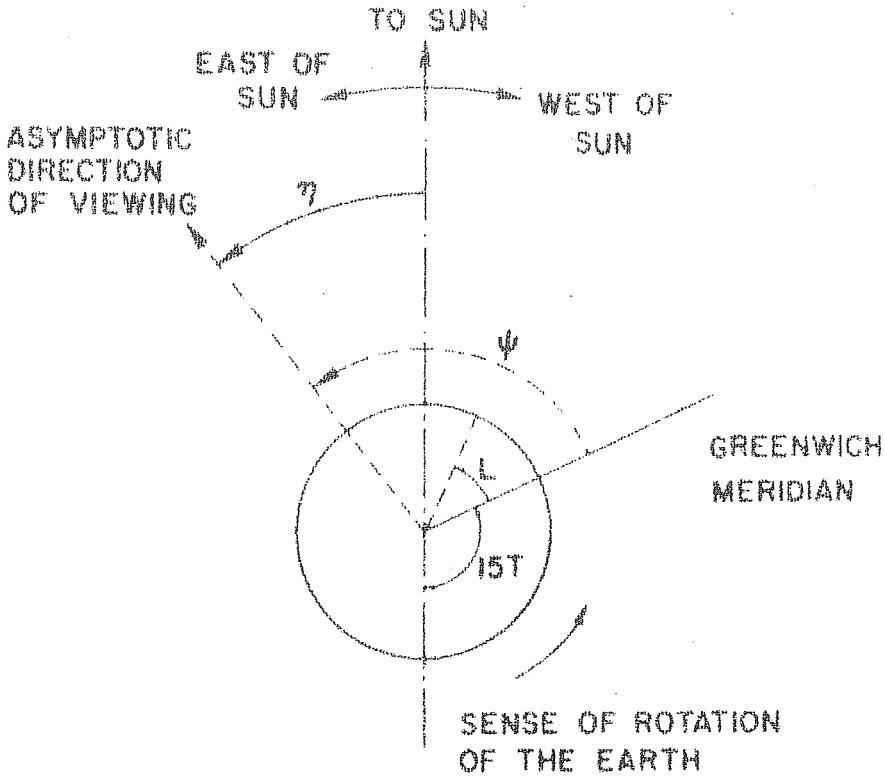

Figure 2.4 - Defines the angles employed to specify the asymptotic direction of viewing of an arbitrary station.

the asymptotic longitude ψ can be written as

$$f(\psi) = J_o(R) \sum_{m=1}^{\infty} \alpha_m \cos\left\{ m\,(\psi + 15T - 180 - C_m)\right\} \qquad (2.21)$$

Where the asymptotic longitude $\psi = (5i + 2.5)^o$ is the mean longitude of all the particles arriving from solid angles lying between $\psi = 5i^o$ and $\psi = 5(i+1)^o$. Inserting this value of $f(\psi)$ and summing over ' i ' the deviation of the counting rate of a detector at time T from the mean value is given by,

$$\frac{\Delta N(T)}{N} = \sum_{i=0}^{71} V(\psi_j, \beta) \sum_{m=1}^{\infty} \alpha_m \cos\left\{ m(5i+2.5+15T-C_m-180)\right\} \qquad (2.22)$$

$$= \sum_{m=1}^{\infty} \alpha_m B_m \cos\left\{ m\,(15T - 180 - C_m) + \gamma_m \right\} \qquad (2.23)$$

where

$$B_m^2 = \left[\sum_{i=0}^{71} V(\psi_j, \beta) \sin\left\{ m\,(5i + 2.5)\right\} \right]^2 + \left[\sum_{i=0}^{71} V(\psi_j, \beta) \cos\left\{ m\,(5i + 2.5)\right\} \right]^2 \qquad (2.24)$$

and

$$\tan \gamma_m = \frac{\sum_{i=0}^{71} V(\psi_j, \beta) \sin\left\{ m\,(5i + 2.5)\right\}}{\sum_{i=0}^{71} V(\psi_j, \beta) \cos\left\{ m\,(5i + 2.5)\right\}} \qquad (2.25)$$

Where $\alpha_m B_m$ and $(-mC_m + \gamma_m)$ represents the amplitude and phase constants of the m^{th} harmonic. The local time of maximum intensity at a station whose geographic longitude L is given by

$$T_m = \frac{180m + mC_m - \gamma_m}{15m} \quad \text{hours} \qquad (2.26)$$

The terms $(\gamma_m - mL)/15m$ makes due allowance for the deflection suffered by cosmic ray particles in their passage through the geomagnetic field. The amplitude and phase of the diurnal variation observed at each neutron monitoring station are corrected both on an average as well as on a day to day basis using the amplitude and phase constants of the I^{st} harmonic assuming an energy independent spectrum ($\gamma = 0$) to derive the diurnal anisotropy vectors in the interplanetary space during the period 1965-72.

2.16 Space-time diagrams:

As the earth spins on its axis, a ground based neutron monitor which looks into a narrow region in space, will effectively scan the entire celestial sky in a period of one day (24 hours). By using a large number of high latitude neutron monitoring stations ($P_c \leq 2$ GV) well distributed in longitude and having a narrow asymptotic cone of acceptance, it is always possible to separate the cosmic ray spatial variations (anisotropic) from time variations (isotropic) and

to monitor continuously along each asymptotic direction the cosmic ray intensity variations as a function of time. A space-time diagram essentially represents the cosmic ray intensity variations observed in different asymptotic directions at any instant of time. The space-time contour diagrams essentially provide an integrated three dimensional view of the cosmic ray intensity profile in space and hence can be effectively utilized to derive the space and time evolution of cosmic ray anisotropies in the interplanetary medium. The method of constructing three dimensional space-time diagrams developed by a number of workers (Fenton et al, 1959; Ables et al, 1967; Mercer and Wilson, 1968; Carmichael and Steljes, 1969) is ideally suited for studying rapidly evolving cosmic ray anisotropies, for distinguishing the presence of sinks and sources of cosmic ray particles and also to understand the physical processes which leads to redistribution of cosmic ray particles in the interplanetary medium.

In this thesis, we have used this technique to understand particularly the trains of days having enhanced diurnal amplitude. The average daily mean cosmic ray intensity observed three days prior to the commencement of the enhanced diurnal variation event are used for normalization purposes. In order to derive the three dimensional cosmic ray intensity profile in space, the space is divided into 8 equal sectors, each covering a longitude of width $\sim 45^{\circ}$ (3 hours). After

correcting the observed cosmic ray intensity at each station for the width and declination of the asymptotic cone of acceptance and geomagnetic bending, the 3 hourly average cosmic ray intensity deviation in each sector are then computed for a number of selected high latitude neutron monitoring stations ($P_c \leq 2$ GV). Combining similar informations from a large number of neutron monitoring stations well distributed in longitude, the average intensity deviation in each sector is then derived for each day. The average intensity deviation observed in all the 8 sectors covering the entire space are used to construct three-dimensional space-time diagrams on a day to day basis during enhanced diurnal amplitude days. The results are discussed in chapter III.

2.17 Power spectrum analysis:

Though most of the cosmic ray time variations observed at ground based monitors can be understood in terms of the cosmic ray particle propagation in the large scale (Archimedean spiral) magnetic fields present in the solar system, when one deals with the short term cosmic ray variations of periodicity $\leq$ 1 day, it is very essential to have a detailed description of the magnetic fields present in the interplanetary medium. As the field fluctuations ($\leq$ 1 day) are frozen into the solar wind plasma, the observed time variation of the magnetic field at any point in space can be easily transformed into spatial variations. From a detailed power spectrum

analysis of the magnetic field obtained from direct space-craft measurements a number of authors (Jokipii, 1966, 1967; Coleman Jr., 1966; Jokipii and Coleman, 1968; Siscoe et al, 1968; Sari and Ness, 1969) have clearly demonstrated that the large scale interplanetary magnetic fields are associated with irregularities of all scale sizes and these irregularities manifest themselves as deviations in the observed IPMF. These irregularities act as scattering centres for cosmic ray particles make them isotropic and also cause significant transverse diffusion in the interplanetary medium.

The observed fluctuations in time at a fixed point in space can be regarded as a pattern which is stationary in the frame of the solar wind, which is convected past the point of observation. Any variable B(t) as a function of time, generated by a random (or stochastic) process is one of an ensemble of random function which might be generated by the process. The value of the function at any particular point in time is thus a random variable with the probability distribution induced by the ensemble. If we assume that the random process is Gaussian, then for every n, t_1, t_2 .....t_n, the joint probability distribution of $B(t_1)$, $B(t_2)$ .....$B(t_n)$, is an n-dimensional Gaussian or normal distribution. The ensemble average is then given by

$$\bar{B}(t_i) = \text{ave}\left\{B(t_i)\right\} \qquad (2.27)$$

and the covariance $C_{ij} = \text{ave}\left\{B(t_i) \times B(t_j)\right\}$ (2.28)

The random process is stationary and it is not affected by translation of origin in time, the covariance C_{ij} depends only on the separation $(t_i - t_j)$ such that

$$C_{ij} = C(t_i - t_j) \qquad (2.29)$$

The covariance at any time lag τ in single function terms is given by

$$C(\tau) = \text{ave}\left\{ B(t) \times B(t + \tau) \right\} \qquad (2.30)$$

Where $C(\tau)$ is called the auto correlation function. If the averages of all random process are assumed to be zero, then $C(\tau)$ is called as the auto-covariance function. The auto-covariance function can be reduced to the form

$$C(\tau) = \int_{-\infty}^{\infty} P(f)\, e^{2\pi i f \tau}\, df \qquad (2.31)$$

Where $P(f)$ is the power spectrum of the stationary random process as a function of frequency. $P(f)$ is also called spectral density or power spectral density. The power spectrum can also be expressed as a Fourier transform of the auto-covariance function given by

$$P(f) = 2 \int_{0}^{\infty} C(\tau) \cos 2\pi f \tau \; d\tau \qquad (2.32)$$

Using the radial component of the hourly average IPMF vectors obtained from 'in situ' space-craft observations for nearly 5 days, the power spectral density at each frequency was obtained using a Nyquist frequency of $\sim 4.6 \times 10^{-6}$ Hz

($\sim$60 hours) and applying Blackman and Tukey window in equation 2.32. The power density distribution as a function of frequency is studied for a number of non-field aligned trains of days as well as for a number of completely field aligned trains of days. The results are discussed in chapter IV.

.....

C H A P T E R - III

AVERAGE DIURNAL VARIATION

3.1 Introduction:

The neutron monitor at Ahmedabad has been in continuous operation since 1968. The data from this equatorial monitor which forms an important link in the world wide net-work of neutron monitoring stations has been regularly processed and presented to the world data centre. In this chapter, we first present the results obtained from Ahmedabad neutron monitor for the period 1968-73 and then use this data together with the observations from other world wide neutron monitoring stations (table 3.3) to establish the average characteristics of diurnal variation and its long term variability. We also propose a new unified convection-diffusion model to explain the diurnal anisotropy of cosmic radiation and then critically examine the observed diurnal variation both on a long term as well as on a day to day basis in the light of this theory.

3.2 The neutron monitor observations at Ahmedabad:

Before using Ahmedabad neutron monitor observations for deriving any information on the diurnal anisotropy, it is very essential to compare the observations with other neutron monitoring stations to ensure that the intensity variations observed are world wide and not of a local origin. The pressure corrected cosmic ray data from Ahmedabad neutron monitor (18-NM-64) is compared with similar data obtained

from other neutron monitoring stations both on a long term as well as on a day to day basis to identify and remove the intensity variations of local origin. As a typical example, Fig. 3.1 shows a comparison of the normalized monthly mean intensity of neutrons observed at Ahmedabad (15.9 GV), Dallas (4.4 GV) and Kiel (2.3 GV) plotted for the period 1968-73. The figure clearly shows that the cosmic ray intensity observed at all the stations reached a minimum intensity level in June 1969 and then gradually recovered. The intensity variations at Ahmedabad are of lesser magnitude as compared to the observations at Dallas and Kiel is essentially due to the high geomagnetic cut-off rigidity at Ahmedabad ($\sim$15.9 GV). Further it may be seen that, whereas the intensity at Kiel increased by $\sim$ 10% from Jun. 1969 - Dec. 1973, the corresponding increase at Ahmedabad is only of $\sim$ 3%, which is in reasonable agreement with theoretical predictions. Fig. 3.2 shows a detailed comparison between the normalized daily mean intensity of neutrons recorded at Ahmedabad and at Kiel during the year 1973. It is seen that the world wide isotropic long term variations as well as the transient Forbush decreases are clearly observed at both the places, even though the observed amplitude of these variations at Ahmedabad is of lesser magnitude is consistent with their being energy dependent.

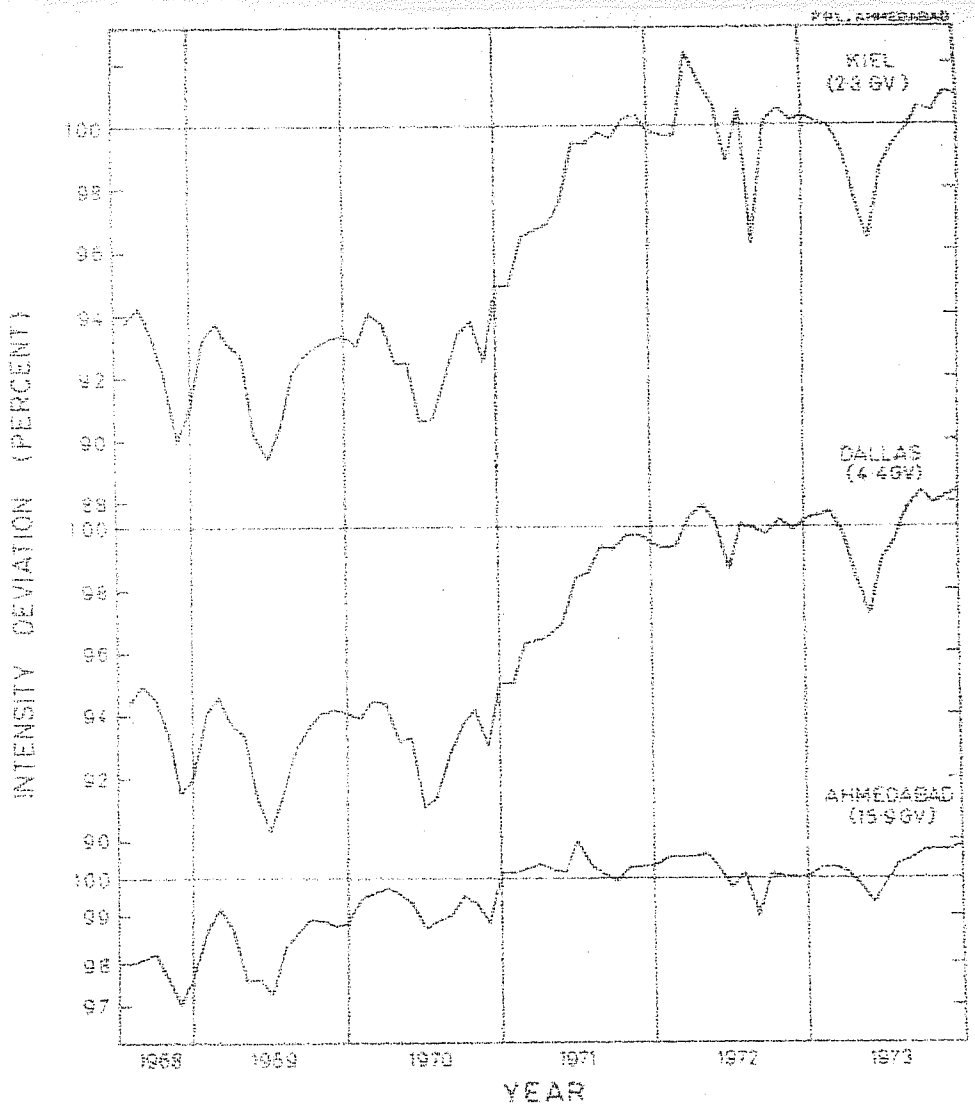

Figure 3.1 - The monthly mean cosmic ray intensity deviations observed at Ahmedabad and other stations during the period 1968-73.

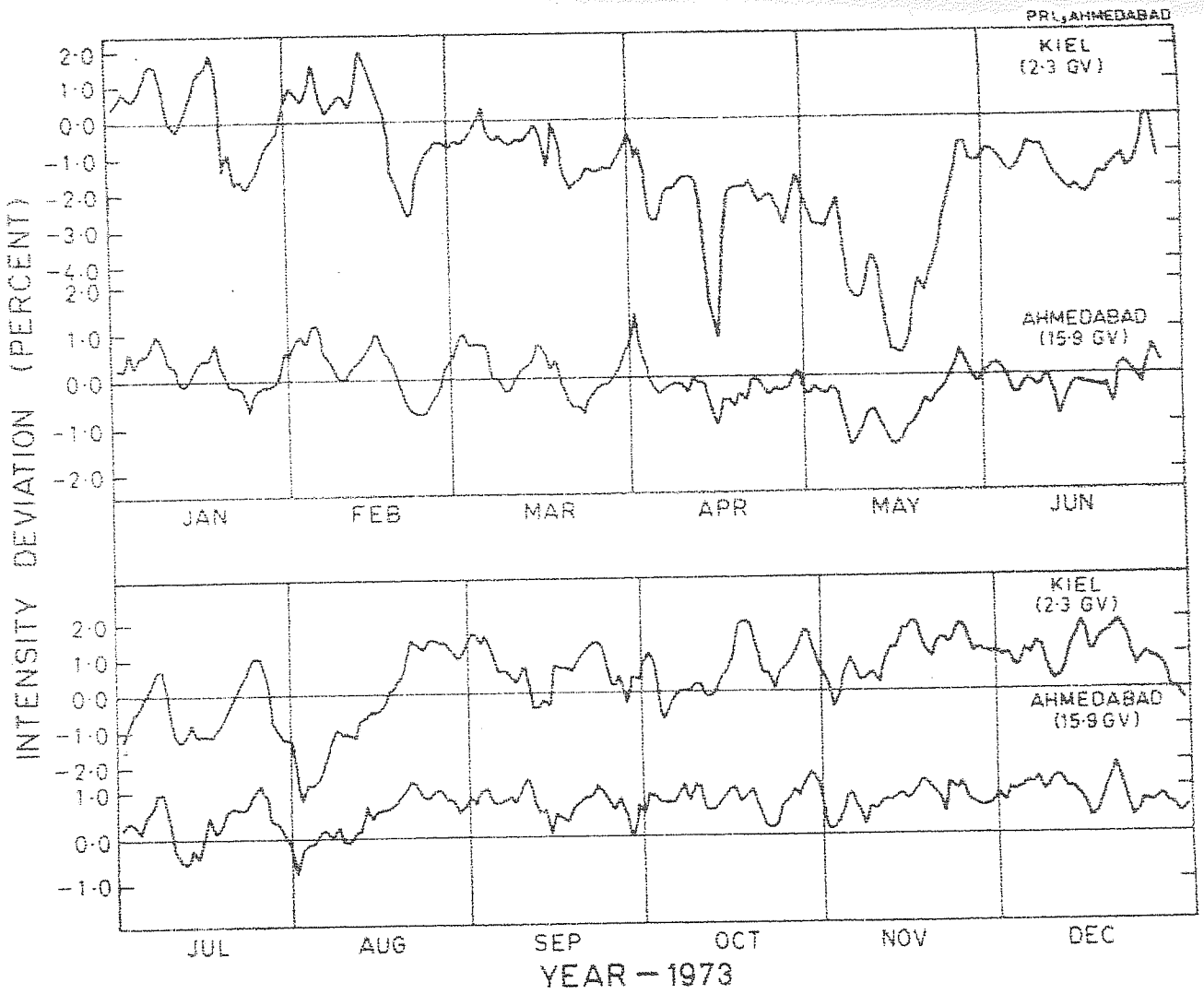

Figure 3.2 - The daily mean cosmic ray intensity deviations observed at Ahmedabad (15.9 GV) and Kiel (2.3 GV) during the year 1973.

3.3 The diurnal and semi-diurnal variation at Ahmedabad:

After correcting for long term variations, the pressure corrected hourly neutron data at Ahmedabad is subjected to harmonic analysis (chapter II) to derive the amplitude and phase of the diurnal and semi-diurnal variation on each day during the period 1968-73. Using the day to day observations, the yearly mean diurnal and semi-diurnal variation are then obtained. Table 3.1 lists the amplitude and phase of the yearly mean diurnal variation (3.1a) and also the yearly mean semi-diurnal variation (3.1b) observed at Ahmedabad during 1968-73 along with the standard errors associated with each observation. For purposes of comparison, the yearly mean diurnal and semi-diurnal variations obtained at few other stations such as Dallas and Kiel are also given in the same table. The table clearly shows that, within the errors of observation, there is a one to one correspondence between the amplitude and phase of the yearly mean diurnal and semi-diurnal variations observed at Ahmedabad and other stations. It may also be noted that the yearly mean diurnal and semi-diurnal variation observed are consistent with their being time invariant during 1968-73 (Rao et al, 1963; McCracken and Rao, 1965; Rao and Agrawal, 1970).

3.4 The average diurnal anisotropy at Ahmedabad:

The amplitude and phase of the yearly mean diurnal variation (Table 3.1a) observed at Ahmedabad are then suitably corrected for the width and declination of the asymptotic cone

Table 3.1

(a) DIURNAL VARIATION

Year	AHMEDABAD		DALLAS		KIEL	
	Amplitude (%)	Phase (Deg)	Amplitude (%)	Phase (Deg)	Amplitude (%)	Phase (Deg)
1968	0.28 ± .02	219 ± 2	0.24 ± .02	228 ± 3	0.24 ± .02	212 ± 3
1969	0.24 ± .02	216 ± 2	0.28 ± .02	229 ± 2	0.29 ± .02	218 ± 2
1970	0.19 ± .02	196 ± 2	0.27 ± .02	222 ± 2	0.28 ± .02	213 ± 2
1971	0.16 ± .01	172 ± 2	0.24 ± .02	207 ± 2	0.31 ± .02	200 ± 2
1972	0.13 ± .01	178 ± 3	0.21 ± .03	210 ± 3	0.25 ± .02	202 ± 2
1973	0.14 ± .01	163 ± 3	0.19 ± .02	191 ± 3	0.25 ± .01	196 ± 2

(b) SEMI-DIURNAL VARIATION

Year	AHMEDABAD		DALLAS		KIEL	
	Amplitude (%)	Phase (Deg)	Amplitude (%)	Phase (Deg)	Amplitude (%)	Phase (Deg)
1968	0.15 ± .01	51 ± 2	0.12 ± .01	77 ± 3	0.12 ± .01	76 ± 3
1969	0.15 ± .01	51 ± 2	0.12 ± .01	74 ± 3	0.10 ± .01	78 ± 3
1970	0.12 ± .01	69 ± 3	0.11 ± .01	80 ± 3	0.11 ± .01	80 ± 3
1971	0.10 ± .01	69 ± 3	0.10 ± .01	69 ± 3	0.10 ± .01	79 ± 3
1972	0.11 ± .01	72 ± 3	0.11 ± .01	72 ± 3	0.10 ± .01	85 ± 3
1973	0.10 ± .01	66 ± 3	0.12 ± .01	63 ± 3	0.08 ± .01	77 ± 3

Table 3.1- The amplitude and phase of the yearly average (a) diurnal and (b) semi-diurnal variation vectors observed at Ahmedabad (15.9 GV), Dallas (4.4 GV) and Kiel (2.3 GV) during 1968 - 73.

of acceptance of the detector and for the geomagnetic bending using variational coefficient techniques (described in chapter II) to derive the amplitude and phase of the average diurnal anisotropy vectors in space for each year during 1968-73. In table 3.2 the average diurnal anisotropy vectors observed at Ahmedabad are compared with other stations such as Dallas and Kiel. It is clearly evident that the diurnal anisotropy vectors observed at Ahmedabad are quite consistent with other observations and do not show significant departures from the average diurnal anisotropy characteristics established by Rao et al (1963) and McCracken and Rao (1965). The systematic variation observed in the diurnal amplitude during 1968-73 could be however explainable in terms of the change of E_{max} with solar activity (Peacock, 1970; Summer and Thompson, 1970; Jacklyn et al, 1970; Ahluwalia and Ericksen, 1970; Agrawal et al, 1972). An interesting point to be noted is that the diurnal time of maximum which remained constant ($\sim$1800 hours) during 1968-69 (McCracken and Rao, 1965) started shifting towards early hours ($\sim$1500 hours) during 1970-73, the phase shift observed is being maximum at Ahmedabad, which has the maximum energy of response.

3.5 Day to day diurnal and semi-diurnal variation at Ahmedabad:

Fig. 3.3 shows the frequency distribution of the amplitude and phase of the diurnal (3.3a) and the semi-diurnal variation (3.3b) observed on a day to day basis at Ahmedabad plotted in the form of a histogram for each year, during the observational

Table 3.2

Year	AHMEDABAD		DALLAS		KIEL	
	Amplitude (%)	Phase (Deg)	Amplitude (%)	Phase (Deg)	Amplitude (%)	Phase (Deg)
1968	0.47 ± .02	273 ± 2	0.34 ± .02	280 ± 3	0.33 ± .02	265 ± 3
1969	0.40 ± .02	270 ± 2	0.41 ± .02	281 ± 2	0.38 ± .02	271 ± 2
1970	0.31 ± .02	250 ± 2	0.39 ± .02	274 ± 2	0.37 ± .02	266 ± 2
1971	0.27 ± .01	226 ± 2	0.35 ± .02	259 ± 2	0.41 ± .02	253 ± 2
1972	0.22 ± .01	232 ± 3	0.30 ± .03	262 ± 3	0.33 ± .02	255 ± 2
1973	0.23 ± .01	217 ± 3	0.28 ± .02	243 ± 3	0.33 ± .01	249 ± 2
Mean (1968-73)	0.35 ± .01	250 ± 2	0.40 ± .01	268 ± 2	0.43 ± .01	261 ± 2

Table 3.2 - The amplitude and phase of the yearly average diurnal anisotropy vectors observed at Ahmedabad, Dallas and Kiel during 1968-73.

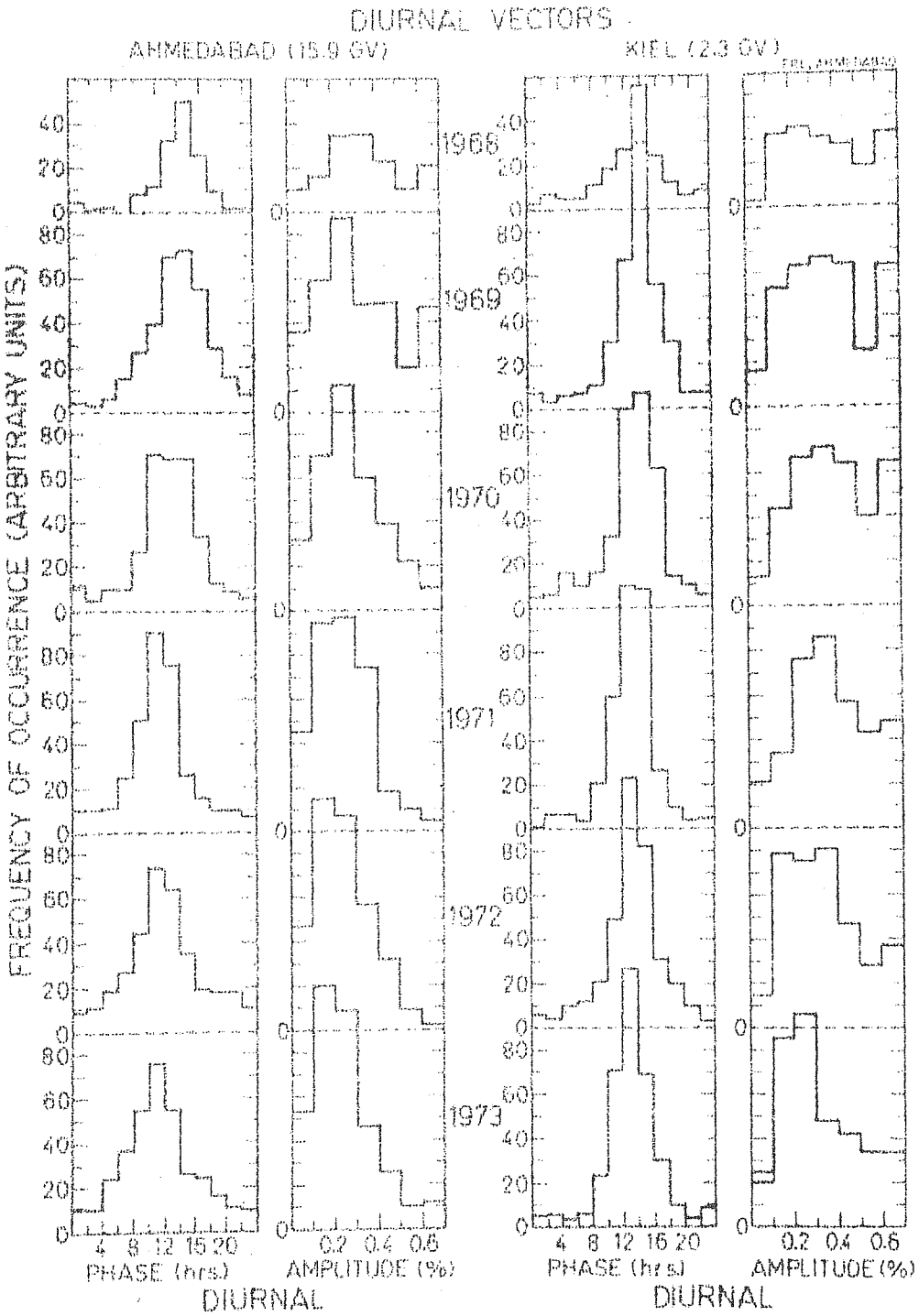

Figure 3.3a - The frequency of occurrence of diurnal phase and diurnal amplitude observed at Ahmedabad and Kiel are plotted in the form of a histogram and shown for each year during 1968-73.

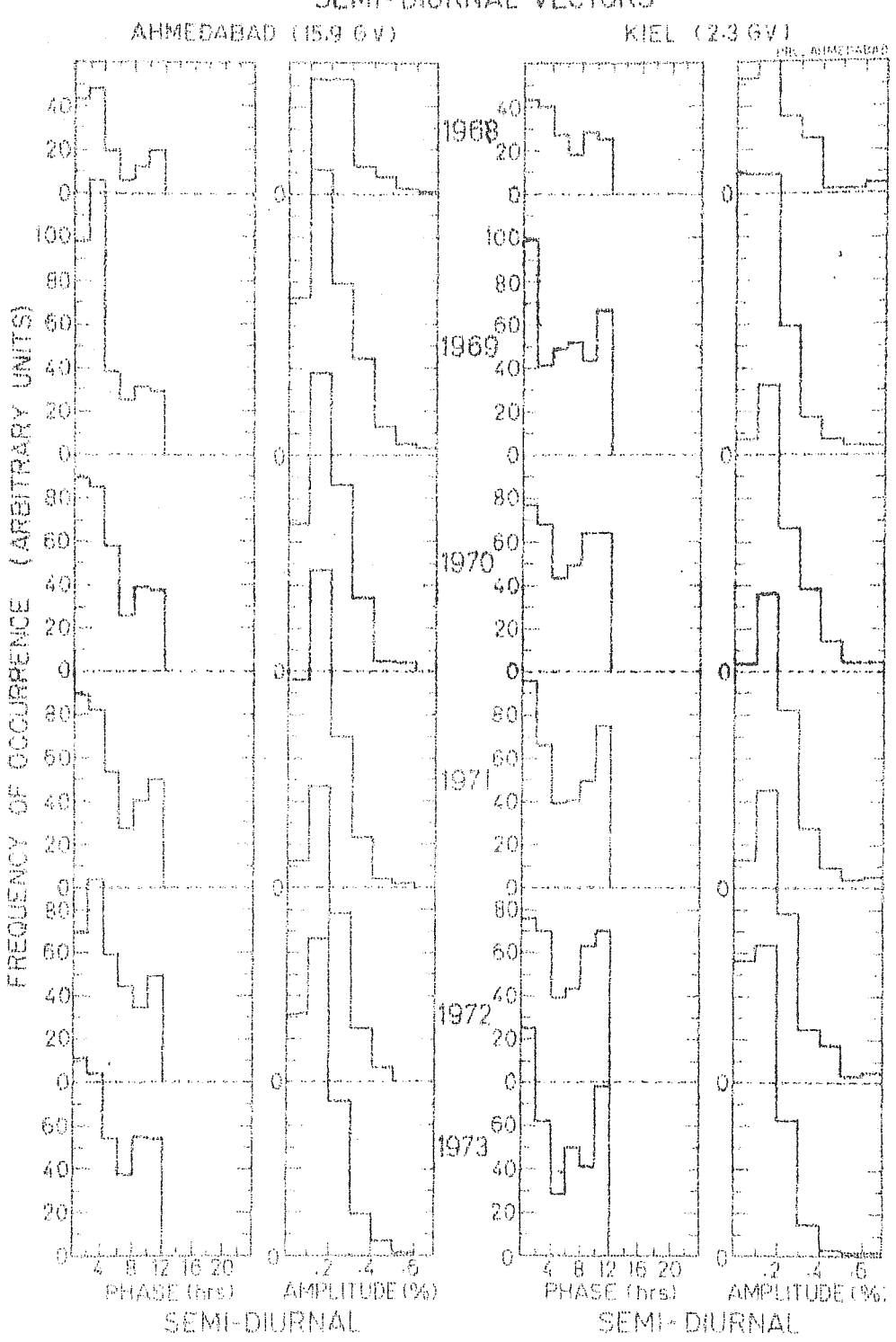

Figure 3.3b - The frequency of occurrence of the phase and amplitude of semi-diurnal variation observed at Ahmedabad and Kiel plotted in the form of a histogram for each year during 1968-73.

period 1968-73. In the same figure the corresponding frequency distribution observed at Kiel are also shown for purposes of comparison. Though the diurnal amplitude distribution shows a peak around 0.1 - 0.3% and the diurnal phase around 12 - 16 hrs. (Fig. 3.3a) which is consistent with the characteristics of yearly mean diurnal variation (Table 3.1a), a large dispersion in the distribution of both diurnal amplitude and diurnal phase from day to day is clearly evident from the histograms. A large variability in the characteristics of diurnal variation on a day to day basis has also been reported by other workers (Rao and Sarabhai, 1964; Patel et al, 1968; Pomerantz and Duggal, 1971; Rao, 1972). The histograms of the amplitude and phase of the semi-diurnal variation observed during 1968-73 (Fig. 3.3b) also shows a large variability on a day to day basis is consistent with other observations.

3.6 Determination of diurnal anisotropy vectors using a number of stations:

In spite of applying adequate corrections to minimize the contamination due to short term variations on the derived diurnal variation, the qualitative evaluation of diurnal anisotropy in space based on the observations from a single station is not always reliable. The large intensity gradients developed during world wide variations and Forbush decreases will considerably affect the determination of diurnal

anisotropy vectors on a day to day basis. In order to examine the diurnal anisotropy vectors on an average as well as on a day to day basis in a statistically meaningful way, we have combined the data from a large number of neutron monitoring stations well distributed in longitude and having a narrow asymptotic cone of acceptance. Table 3.3 lists all the stations used in the analysis along with their geographic and asymptotic coordinates. The pressure corrected hourly neutron data at each station after removing the long term variation, is harmonically analysed (chapter II) to derive the amplitude and phase of diurnal variation on each day during the entire period 1965-72 ($\sim$ 8 years). The observed diurnal variation at each station is then corrected for the width and declination of the asymptotic cone of acceptance of the detector and also for geomagnetic bending (Rao et al, 1963; McCracken and Rao, 1965) assuming an energy independent spectrum ($\gamma = 0$) to derive the amplitude and phase of the diurnal anisotropy in space. The diurnal anisotropy vectors thus obtained from various individual stations are then combined to derive the average diurnal anisotropy vectors on an yearly basis and on 27-day basis during 1965-72. Similar exercises are carried out for deriving these vectors on a day to day basis for the period 1967-68. For deriving diurnal anisotropy vectors on a day to day basis, an additional criteria namely that there should be a good inter-station agreement ($\bar{\sigma}_{Amp} < 0.1\%$ and $\bar{\sigma}_{Pha} \leq 30^{\circ}$) between diurnal anisotropy vectors observed at

Table 3.3

Sr. No.	Station	Geographic coordinates		Mean asymptotic coordinates		Cut-off rigidity
		Lat. (Deg)	Long. (Deg)	Lat. (Deg)	Long. (Deg)	(GV)
1.	Ahmedabad	23.0	72.6	19	125	15.94
2.	Alert	82.5	297.7	77	331	<0.05
3.	Alma-Ata	43.2	76.9	25	143	6.69
4.	Calgary	51.1	245.9	28	269	1.09
5.	Churchill	58.8	265.9	40	286	0.21
6.	Dallas	32.8	263.2	25	316	4.35
7.	Deep River	46.1	282.5	27	319	1.02
8.	Durham	43.1	289.2	25	332	1.41
9.	Goose Bay	53.3	299.6	35	339	0.52
10.	Hermanus	-34.4	19.2	-24	67	4.90
11.	Inuvik	68.4	226.3	47	233	<0.18
12.	Kiel	54.3	10.1	31	63	2.29
13.	Lindau	51.6	10.1	29	67	3.00
14.	Mawson	-67.6	62.9	-42	55	0.22
15.	Mt. Norikura	36.1	137.6	26	195	11.39
16.	Mt. Washington	44.3	288.7	25	331	1.24
17.	Mt. Wellington	-42.9	147.2	-25	193	1.89
18.	Pic-du-Midi	42.9	0.3	26	73	5.36
19.	Sulphur Mt.	51.2	244.4	27	270	1.14
20.	Wilkes	-66.4	110.5	-56	107	<0.05

Table 3.3 - The geographic and asymptotic coordinates of the selected neutron monitor stations whose data has been used in this thesis.

different stations has been imposed before deriving the mean diurnal anisotropy vectors on each day during 1967-68.

Before studying the characteristics of diurnal variation on an average basis it is educative to compare the diurnal anisotropy vectors determined using a number of neutron monitoring stations with the diurnal anisotropy vectors observed at a single station. Fig. 3.4 shows the comparison between the frequency distribution of 27-day mean diurnal phase and diurnal amplitude plotted in the form of a histogram for the period 1965-72 determined from the data from a number of stations (solid lines) and the corresponding vectors obtained for Deep River (dashed lines). The one to one correspondence between the two histograms on an average basis in the diurnal amplitudes as well as in the diurnal phase clearly suggests that the diurnal anisotropy vectors determined from a number of stations represent the true anisotropy in space. This method of determining the diurnal anisotropy vectors using a number of stations well distributed in longitude not only eliminates the data from faulty stations but also assures the constancy of diurnal anisotropy for atleast a period of 24 hrs. Table 3.5 lists the yearly mean diurnal anisotropy vectors determined using a number of neutron monitoring stations. Fig. 3.5 shows a plot of the amplitude and phase of the yearly mean diurnal anisotropy vectors observed during 1965-72. For a comparison the amplitude and phase of the yearly mean diurnal anisotropy

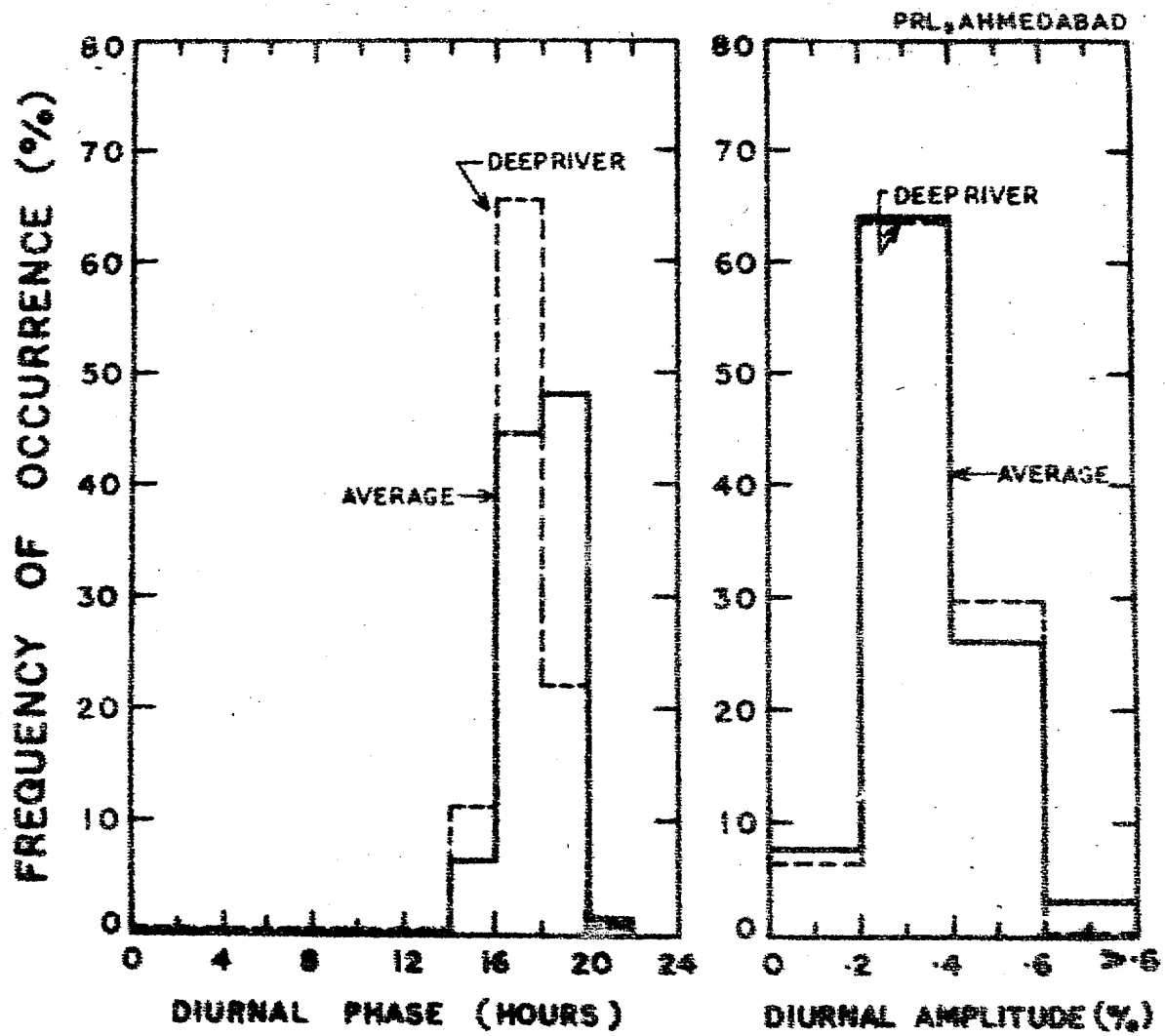

Figure 3.4 - The histograms showing the frequency of occurrence of the phase and amplitude of 27-day average diurnal anisotropy vectors derived using a number of stations (solid lines) and observed at Deep River (dashed lines) during 1965-72.

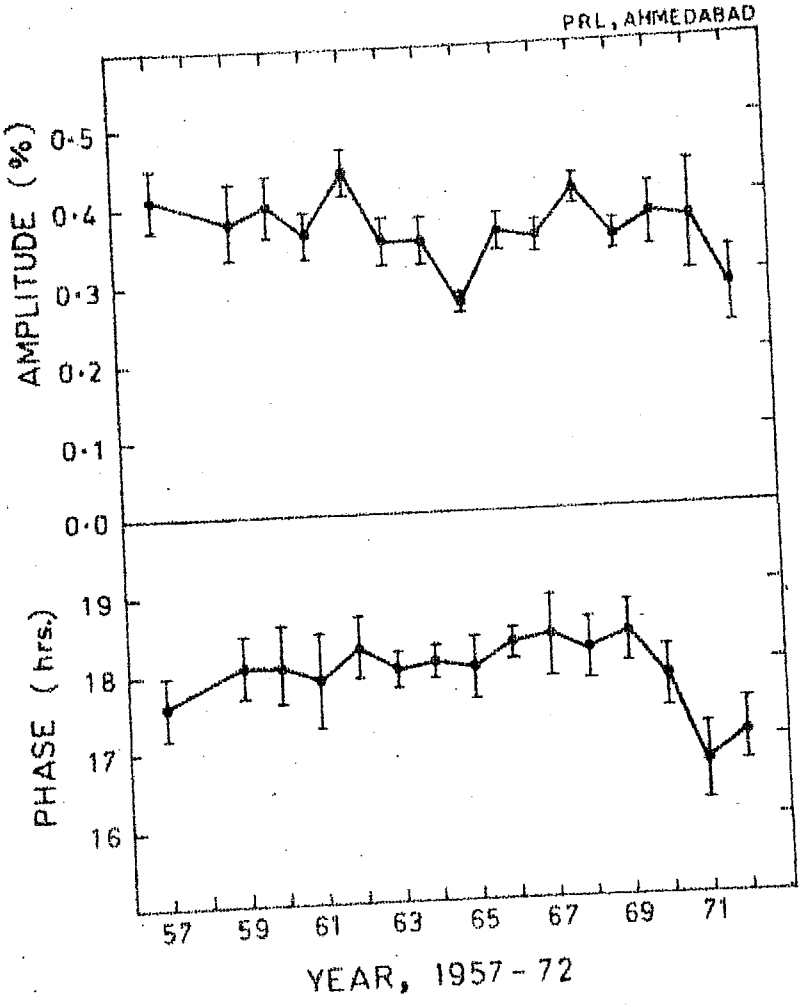

Figure 3.5 - The amplitude and the time of maximum of the yearly mean diurnal anisotropy vectors observed during the entire period 1957-72. Note the shifting of diurnal time of maximum to earlier hours during 1970-72.

vectors for the earlier period namely 1954-65 derived by McCracken and Rao (1965) are also plotted in the same figure along with the errors of observation. It is clearly evident from the figure that even though the amplitude and phase of the anisotropy are almost constant, significant deviations from year to year do exist. For example, the diurnal amplitude observed during 1965 and 1972 are significantly lower than the average diurnal amplitude observed during rest of the years. Similarly the diurnal phase which remained constant upto 1970, shows a significant shift to earlier hours during 1971-72 as compared to the average diurnal phase observed during 1965-70.

3.7 The average diurnal variation:

From a detailed analysis of the neutron monitor data from a world wide net-work of neutron monitoring stations during the period 1954-65, Rao et al (1963) and McCracken and Rao (1965) for the first time experimentally established the characteristics of average diurnal variation. They clearly demonstrated that the observed diurnal variation can be expressed in a simple form as,

$$\frac{\partial J(E)}{J(E)} = AE^{-\beta} \cos(\psi - \psi_0) \cos\Lambda, \text{ for } E \leq E_{max}$$

$$= 0, \text{ for } E > E_{max} \qquad (3.1)$$

Where γ is the spectral index, Λ being the declination and E_{max} is the upper energy limit for corotation. The characteristic features of the average diurnal anisotropy can be summarized as follows:

1. The yearly mean diurnal amplitude is of$\sim$ 0.38 $\pm$ 0.02%.

2. The time of maximum is along the asymptotic direction 1800 hours local time, that is 90° east of the sun-earth line.

3. The anisotropy is energy independent upto an energy $E_{max} \leq$ 100 GeV. and

4. The anisotropy varies as the cosine of the declination.

Using the concept of solar wind and a spiral configuration for the interplanetary magnetic field developed by Parker (1960), Ahluwalia and Dessler (1962) suggested that the $(\bar{E} \times \bar{B}/B^2)$ electric drift of cosmic ray particles in the interplanetary medium causes diurnal variation. Though some of the predictions of the theory were in good agreement with the observations, Stern (1964) pointed out that in conservative fields, Liouville's theorm does not permit any streaming of cosmic ray particles in the interplanetary medium, that is, the streaming produced by the electric drift is completely cancelled by an equal and opposite streaming caused by a density gradient perpendicular to the ecliptic plane established by the $(-\bar{V} \times \bar{B})$ electric field. This objection was overcome by Parker (1964, 1965)

and Axford (1965a) who postulated the presence of magnetic field irregularities in the Archimedean spiral magnetic field which essentially cancel the perpendicular density gradient established by the $(-\overline{V} \times \overline{B})$ electric field. A large amount of data on the propagation of low energy solar particles accumulated since then has shown that the perpendicular diffusion of particles at the orbit of the earth is almost negligible, that is $K_{\perp} \approx 0$ (McCracken et al, 1968, 1971), thus confirming the correctness of the theory. Further the presence of small scale irregularities throughout the modulating region which is now well established by a number of 'in situ' space-craft measurements of the IPMF (Jokipii and Coleman, 1968) essentially reduces the perpendicular density gradients and leads to the earlier picture of the diurnal variation resulting from a simple corotation of cosmic ray particles with the Archimedean spiral magnetic fields present in the solar system. The amplitude of the energy independent corotational diurnal anisotropy is given by, $\xi_{co} = (2+\gamma)V_{co}/v$. Assuming a spectral index $\gamma = 2.65$ and a corotation velocity $V_{co} \approx 400$ kms/sec at the orbit of the earth for relativistic particles ($v \sim c$), the expression yields a value $\xi_{co} \sim 0.6\%$ for the corotational diurnal anisotropy with a time of maximum along 90^{o} east of the sun-earth line (1800 hours local time).

A simple comparison with the experimental observations of the yearly average diurnal variation presented earlier (Table 3.5) shows that the gross characteristics of the

observations are consistent with the corotation theory. However a few discrepancies are still noticeable. For example, the observed average diurnal amplitude of $\sim$ 0.4% (McCracken and Rao, 1965) is considerably less than that predicted by corotation theory. Even though Subramanian (1971) pointed out that the application of few corrections and making due allowance for the maximum energy (E_{max}) beyond which corotation ceases, narrows the difference between the observed and predicted amplitude, the variation of the average diurnal amplitude from year to year still remained. Though the long term variability of the average diurnal variation for monitors having higher energy response such as underground meson monitors (Thambyahpillai and Elliot, 1953; Forbush, 1973; Duggal et al, 1967; Sarabhai et al, 1954) was more spectacular and could be explained as due to the change in the upper cut-off rigidity from 40-100 GV from solar minimum to solar maximum, the large variabilities observed on a day to day basis still remains to be clearly understood. The only way to reconcile with this apparent discrepancy, as suggested by Jokipii and Parker (1967) is to invoke a random walk of the field lines in the interplanetary medium, which could substantially contribute to the perpendicular diffusion of cosmic ray particles at the orbit of the earth, thus reducing the observed diurnal amplitude. In other words one could explain the observed reduction of the diurnal amplitude by a substantial increase in the ratio $K_\perp / K_\parallel \sim 0.15$ (Jokipii and Coleman, 1968).

From a detailed study of the anisotropies of low energy solar cosmic ray particles McCracken et al (1968, 1971) showed that their propagation in the interplanetary medium is essentially governed by convection and diffusion mechanism. Their observations clearly indicate that the most important mechanism that operates in the interplanetary medium is the convective expulsion of these particles by radially blowing solar wind. Based on these observations, Gleeson (1969), Forman and Gleeson (1970, 1974) proposed an elegant theoretical formulation for describing the cosmic ray particle streaming in the interplanetary medium in terms of convection and diffusion mechanism. The observed anisotropies at low energies during different phases of solar flare events namely the field aligned anisotropy during the initial phase followed by a radial convective anisotropy and easterly anisotropy at late times in a flare have been successfully explained in terms of simple convection and diffusion of particles in the interplanetary medium. The theoretical formulation by Forman and Gleeson (1970, 1974) and the experimental observations of Rao et al (1972) and Hashim et al (1972) showed very clearly that, this physical concept could be extended to explain the diurnal variation of galactic cosmic radiation ($\geq$1 GeV) observed at neutron monitors. In the next section we describe in detail the physical concept of this theory and procede to demonstrate that, the observed average characteristics as well as the day to day variability of diurnal

variation can be successfully explained using this concept. The detailed presentation of the theory however has been already described in the I chapter.

3.8 The unified convection-diffusion theory:

Fig. 3.6(a) summarizes the manner in which the convection-diffusion concept operates in the interplanetary medium resulting in the observed anisotropies of the low energy solar flare particles. It has been shown (McCracken et al, 1967, 1968; McCracken and Rao, 1970; Rao et al, 1971; Allum et al, 1974) that there are three distinct phases in a solar flare event. The early phase, that is during the rise of the flare, the observed cosmic ray anisotropy is predominantly field aligned. In the second phase after the intensity has reached its maximum value and is in equilibrium condition, the anisotropy is purely radial type and is not associated with the IPMF. This is followed by an easterly anisotropy from a direction perpendicular to the nominal Archimedean spiral field at late times in a flare. During the early phase due to the presence of large negative density gradients the cosmic ray particles of solar origin dominates the small convective component (δ_c) resulting in a practically field aligned anisotropy (δ) (case 1). After the intensity has reached its maximum value, when an equilibrium has been established in the interplanetary medium the only mechanism that can operate is the convection term (δ_c) due to the radial expulsion of particles by the

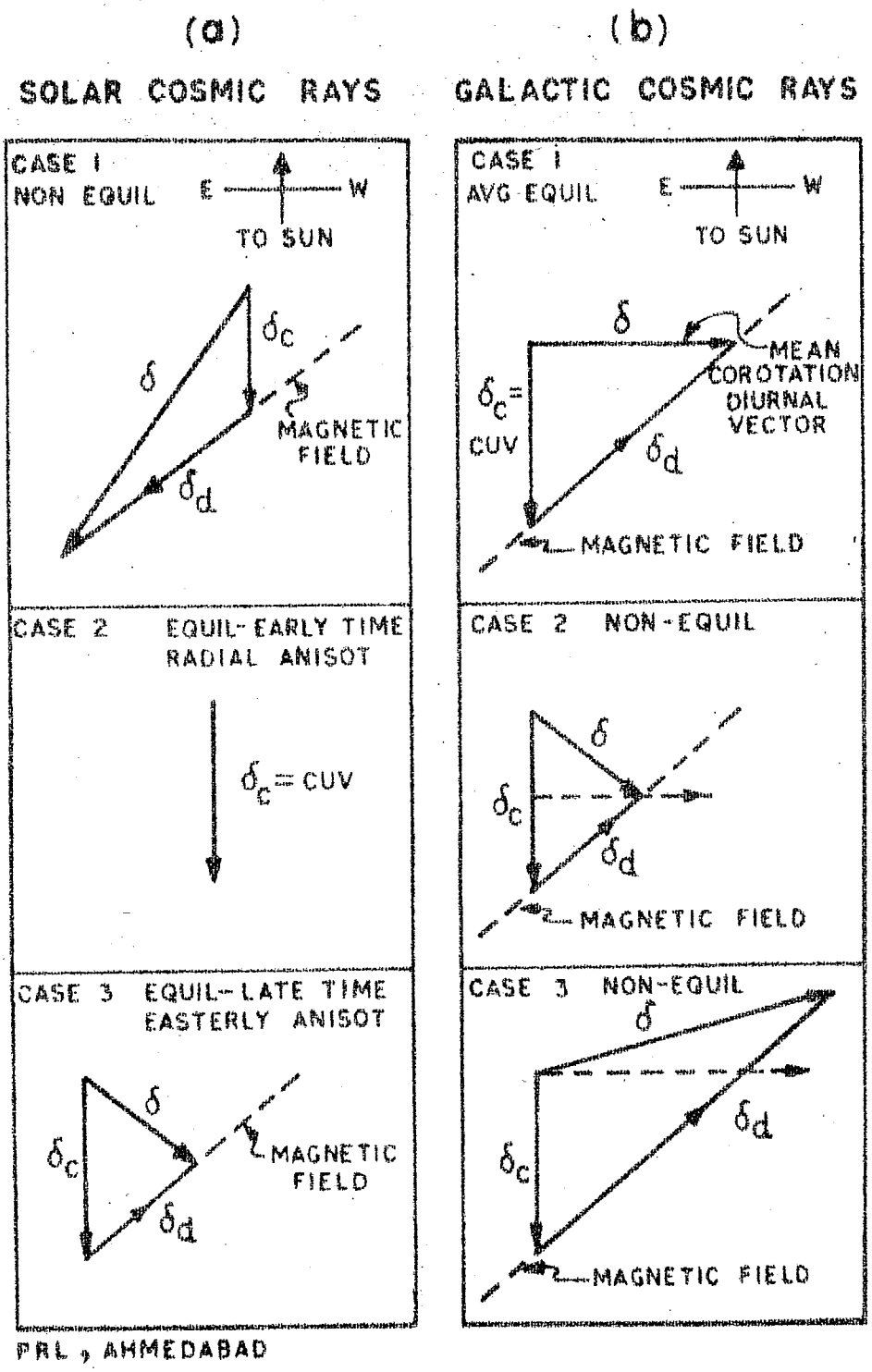

Figure 3.6 - The proposed unified convection-diffusion model explaining the cosmic ray anisotropies observed at (a) low energies (≈10 MeV) and (b) high energies (>1 GeV).

solar wind (case 2). At late times this very radial convection produces an enhanced positive density gradient which when combined with convection term yields a resultant in a direction perpendicular to the IPMF azimuth (case 3). The basic concept of azimuthal streaming of particles can be extended to explain the diurnal anisotropy of cosmic radiation observed at high energies ($\geqslant$1 GeV). In this case the observed average diurnal anisotropy essentially pertains to the equilibrium condition. As can be seen from Fig. 3.6(b) under equilibrium condition (case 1), the radial convection of particles is exactly balanced by the inward diffusion of particles due to the normal positive density gradient existing in the interplanetary medium resulting in an azimuthal (corotational) anisotropy given by

$$\xi = \delta = CUV_p \tan\psi \qquad (3.3)$$

The extension of this concept to explain the diurnal variation observed on a day to day basis becomes extremely interesting. On a day to day basis significant variations in the solar wind velocity, density gradient and the IPMF characteristics can occur, which will essentially disturb the equilibrium. That is on such days, the convection current need not balance exactly the inward diffusion current and consequently as shown in Fig. 3.6(b) results in a large deviation from average condition. In Fig.3.6(b) two typical cases of non-equilibrium condition are depicted. In the first case (case 2) a reduction

in the radial density gradient is assumed, which when combined with a normal convective component will yield a resultant along 1500 hours direction with a substantial reduction in the diurnal amplitude. Case (3) depicts the situation when the assumed condition is opposite that is, when the radial density gradient is larger than normal will yield a resultant along 2100 hours direction with an enhanced amplitude for diurnal variation. It is obvious that similar variations in amplitude and time of maximum of the diurnal variation can be achieved by changing the convection vector due to a change in the solar wind velocity or by changing IPMF direction. In view of the large amount of experimental data available which indicates the presence of considerable variability both in solar wind velocity as well as in IPMF azimuth, the physical concept derived above provide a very natural explanation for the observed variability in the diurnal variation.

For an experimental verification of the validity of the convection-diffusion concept, it is necessary to derive the convection and diffusion vectors both on an average as well as on a day to day basis. Recalling our earlier arguments, we may express the diurnal vector $\bar{\delta}$ as

$$\bar{\delta} = \bar{\delta}_c + \bar{\delta}_d \qquad (3.4)$$

Where $\bar{\delta}_c$ is the convection component and $\bar{\delta}_d$ is the diffusion component. By knowing the solar wind velocity it is

possible to estimate the convection component $\vec{\delta}_c$ accurately, the diffusion vector can be uniquely determined by subtracting the convection vector ($\vec{\delta}_c$) from the observed diurnal vector ($\vec{\delta}$). It is then only necessary to show that the diffusion vector $\vec{\delta}_d = (\vec{\delta} - \vec{\delta}_c)$ so determined is in fact field aligned. In other words the validity of the theory can be established if we can show that, the phase difference $\Delta\Phi = \Phi_d - \Phi_B \approx 0$. Where Φ_d is the phase of the diffusion vector and Φ_B is the magnetic field azimuth, that is the diffusion vector is either parallel or anti-parallel to the observed IPMF direction. In this chapter we demonstrate the validity of the theory to explain the average diurnal variation. In the next chapter, we extend this concept to explain the diurnal variation on a day to day basis.

3.9 Estimation of convection vector ($\vec{\delta}_c$):

The convective anisotropy due to the expulsion of cosmic ray particles by the radially blowing solar wind in the interplanetary medium can be estimated using the simple relation

$$\vec{\delta}_c = \frac{3\,CV_p}{v} \qquad (3.5)$$

Where C is the Compton-Getting factor, V_p is the solar wind velocity and v is the particle velocity. For a normal wind velocity of $\sim$ 400 kms/sec and C $\sim$ 1.5 the convective anisotropy ($\vec{\delta}_c$) at neutron monitor energies ($\sim$ 10 GeV) turns out to be of $\sim$ 0.6%. The anisotropy amplitude $\sim$ 0.4% observed at a ground

based monitor, when due allowance is made for the dependence of C on energy and for the detector response (Subramanian, 1971) will correspond to the free space convective anisotropy of $\sim$ 0.6%. Since the observed amplitude of $\sim$ 0.4% at the detector end and the free space amplitude of the anisotropy ($\sim$ 0.6%) are related to each other by a constant factor, we have used the observed amplitude of $\sim$ 0.4% in all our discussions as this will not affect any of our conclusions. The estimation of the convection vectors both on an average as well as on a day to day basis has been done as far as possible using 'in situ' space-craft observations of the solar wind velocity in the interplanetary medium. The details of the space-crafts whose measurements of the solar wind plasma and IPMF parameters has been used in our analysis along with the corresponding periods of observations are listed in table 3.4. Alternate methods have been used to estimate $\bar{\delta}_c$ wherever the actual measurements of solar wind velocity is not available, which has been described at the appropriate place.

3.10 Determination of the interplanetary magnetic field azimuth (ϕ_B):

Having estimated the convection vector, in order to examine the diurnal anisotropy in the light of the new concept, it is only necessary to determine the magnetic field azimuth (ϕ_B) and compare it with the phase of the diffusion vector (ϕ_d). The average IPMF vector for each day

Table 3.4

Space-craft	Solar wind velocity	Interplanetary magnetic field
Pioneer VI	18 December 1965 - 15 May 1966	16 December 1965 - 15 May 1966
Vela - 3	26 July 1965 - 06 December 1967	—
Vela - 4, Vela - 5	01 January 1969 - 12 June 1972	—
Explorer - 33	01 January 1968 - 03 July 1968	01 January 1967 - 14 December 1968
Explorer - 35		23 July 1967 - 14 December 1968

Table 3.4 - The periods of observation and the corresponding space-crafts whose measurements of the interplanetary plasma and magnetic field parameters are used in this thesis.

during 1967-68 has been obtained from the direct space-craft observations of the hourly average components of the IPMF in the earth centred ecliptic coordinate system. Table 3.4 gives the details of the space-crafts along with the periods of observation, whose measurements of the IPMF parameters are used in this analysis. The ecliptic component of the 27-day average, daily average and hourly average IPMF vectors are obtained by reversing the magnetic field vectors lying between 135° west and 45° east of the sun-earth line, since the cosmic ray streaming does not depend on the sense of the field.

For periods when space-craft measurements of the IPMF are not available, the field azimuth is obtained using the known values of solar wind velocity and assuming that the field is consistent with it being stretched in the form of an Archimedean spiral. The garden-hose angle ψ between the IPMF and the radial direction is then given by

$$\tan \psi = V_p / \Omega r \qquad (3.6)$$

Where V_p is the solar wind velocity and Ω is the angular velocity of the sun and r is the radial distance from the sun. Extensive observation by Ness et al (1966)& McCracken and Ness (1966) indicate that on an average basis, the observed field is completely consistent with the above picture. The recent Pioneer-10 and Pioneer-11 space-craft measurements clearly show that the IPMF measured near the orbit of the Jupiter (4.3 AU) is also in good agreement with the Archimedean spiral configuration. Further we have also verified that on an average basis

the values of the field azimuth derived from the observed solar wind velocity under the assumption of Archimedean spiral configuration are consistent with the direct measurements of the field azimuth for $\sim$14 solar rotations during 1967-68, for which simultaneous measurements of both solar wind and magnetic field parameters are available.

3.11 Examination of the yearly average diurnal variation:

Table 3.5 lists the observed yearly average diurnal anisotropy vector $\bar{\delta}$, yearly average solar wind velocity obtained from direct space-craft measurements and convection vector $\bar{\delta}_c$ estimated using these. The average diffusion vector $\bar{\delta}_d$ obtained from the equation 3.4 ($\bar{\delta}_d = \bar{\delta} - \bar{\delta}_c$) is listed for each year. The IPMF azimuth and the phase difference $\Delta\Phi$ between the field azimuth and the diffusion vector computed for each year during 1965-72 are also included in the same table. It is clearly evident from the table that the average diffusion vector ($\bar{\delta}_d$) is always field aligned within the practical observational error of $\sim \pm 15^{\circ}$ (3σ limit). Even during the year 1971-72, when the average diurnal time of maximum is shifted to earlier hours, the agreement between the field azimuth and diffusion vector is very good. A completely field aligned nature of the diffusion vectors is pictorially shown in Fig. 3.7, where the average diffusion vectors for each year are plotted end to end in the form of a vector diagram on which the field azimuth for each

Table 3.5

Sr. No.	Year	DIURNAL ANISOTROPY VECTOR (δ) Amplitude (%)	DIURNAL ANISOTROPY VECTOR (δ) Phase (Deg)	SOLAR WIND VELOCITY (kms/sec)	CONVECTION VECTOR(δ_c) Amplitude (%)	DIFFUSION VECTOR (δ_d) Amplitude (%)	DIFFUSION VECTOR (δ_d) Phase (Deg)	FIELD AZIMUTH (Φ_B) Phase (Deg)	PHASE DIFFERENCE ($\Delta\Phi$) ($\Phi_d - \Phi_B$) (Deg)
1.	1965	0.27±.01	270±3	395	0.40	0.48	326	315	11±3
2.	1966	0.37±.01	275±2	399	0.40	0.56	320	315	5±2
3.	1967	0.35±.01	275±3	382	0.38	0.54	320	314	6±3
4.	1968	0.41±.01	273±2	464	0.46	0.64	320	319	1±2
5.	1969	0.35±.01	277±3	398	0.40	0.56	322	315	7±3
6.	1970	0.38±.02	267±3	389	0.39	0.53	314	314	-0±3
7.	1971	0.37±.03	250±4	404	0.40	0.45	309	315	-6±4
8.	1972	0.28±.02	256±3	377	0.38	0.41	319	313	6±3
Mean (1965-1972)		0.34±.01	268±1	401	0.40	0.52	319	315	4±1

Table 3.5 - Shows the amplitude and phase of the yearly average diurnal anisotropy vector derived using a number of stations, the observed average solar wind velocity, convection vector, diffusion vector, field azimuth and the phase difference $\Delta\Phi$ for each year during 1965-72.

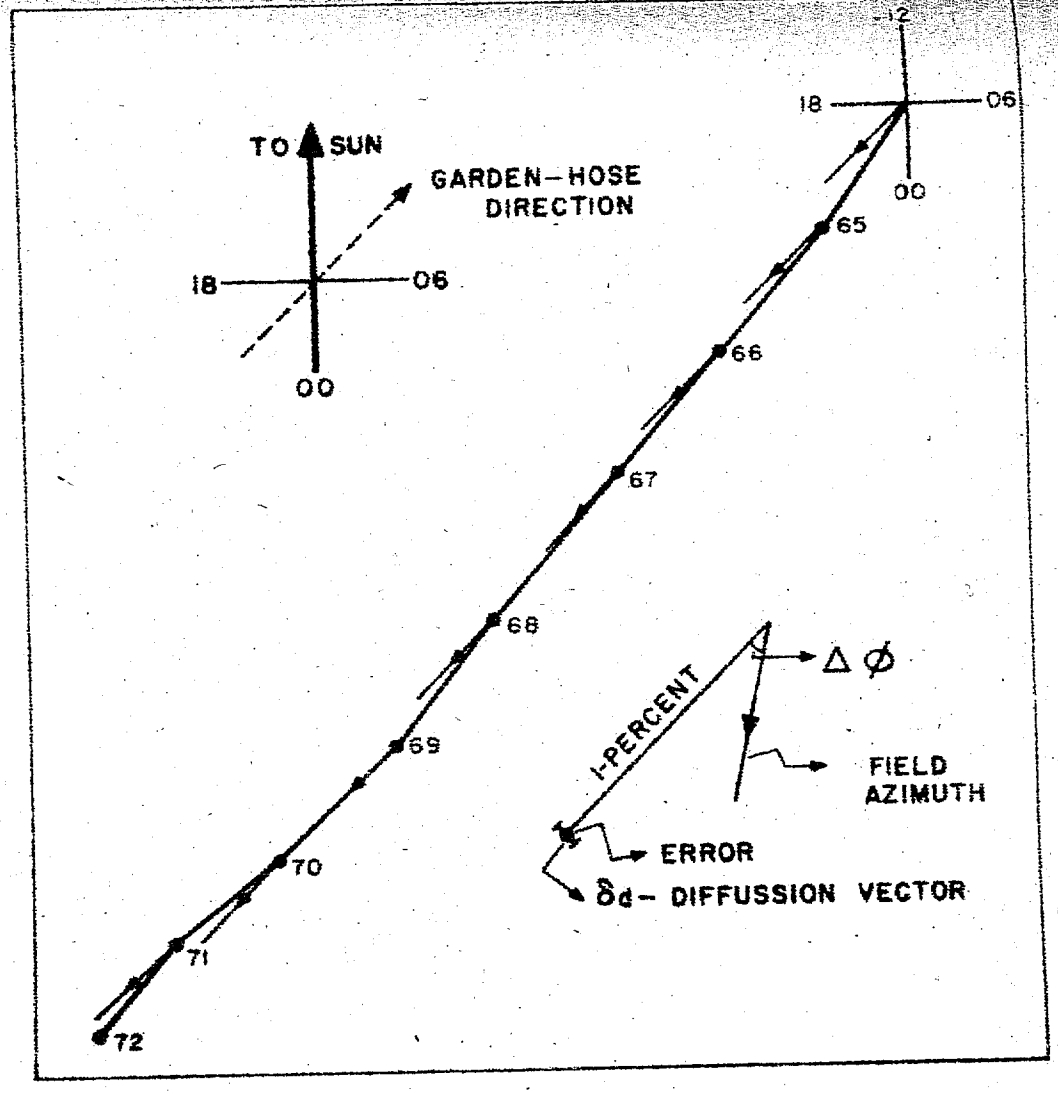

Figure 3.7 - Illustrates the field aligned nature of the yearly mean diffusion vectors during 1965-72. The field azimuth for each year is indicated by the arrow.

year is superimposed (arrows). The results presented above clearly demonstrate that the diurnal variation on an yearly average basis during the year 1965-72 is consistent with it being composed of purely a radial convection current and a field aligned diffusion current.

3.12 Examination of the 27-day average diurnal variation:

The analysis described in the earlier section has been extended to critically examine the 27-day average diurnal variation in the light of the convection and diffusion concept. Table 3.6 lists the observed 27-day average diurnal anisotropy vectors and the solar wind velocity obtained from space-craft measurements and the convection vectors derived using them. The computed average diffusion vectors along with the 'in situ' observation of the IPMF vectors are also listed in the same table. The phase difference $\Delta\Phi$ between the two for nearly 14 solar rotations during 1967-68 again indicate that the diffusion vectors ($\bar{\delta}_d$) are completely field aligned within the observational errors of $\sim \pm 15^{\circ}$. Fig. 3.8 again brings out the field aligned nature of the diffusion vectors dramatically thus confirming that even on a 27-day average basis, the diurnal variation is consistent with the simple convection and field aligned diffusion concept.

The above analysis has been extended to cover $\sim$ 73 solar rotations during 1965-72, for which the measurement of

Table 3.6

Sr. No.	Solar Rotation No.	DIURNAL ANISOTROPY VECTOR (δ) Amplitude (%)	DIURNAL ANISOTROPY VECTOR (δ) Phase (Deg)	SOLAR WIND VELOCITY (kms/sec)	CONVECTION VECTOR (δ_c) Amplitude (%)	DIFFUSION VECTOR (δ_d) Amplitude (%)	DIFFUSION VECTOR (δ_d) Phase (Deg)	MAGNETIC FIELD VECTOR ($\bar{B}$) Amplitude (Gamma)	MAGNETIC FIELD VECTOR ($\bar{B}$) Phase (Deg)	PHASE DIFFERENCE $(\Delta\phi)$ $(\phi_d - \phi_B)$ (Deg)
1.	1826	0.53±.03	272±4	338	0.34	0.64	304	2.94±0.5	303±5	1 ± 4
2.	1827	0.57±.03	270±2	394	0.39	0.69	304	3.70	312	-8 ± 2
3.	1828	0.32±.02	285±5	339	0.34	0.52	324	3.46	307	17 ± 5
4.	1829	0.62±.03	289±3	348	0.35	0.81	314	2.87	319	-5 ± 3
5.	1830	0.45±.02	262±3	393	0.39	0.55	306	3.18	324	-18 ± 3
6.	1833	0.28±.01	282±9	375	0.37	0.51	328	3.38	325	3 ± 9
7.	1834	0.27±.01	273±5	437	0.44	0.53	329	3.56	321	8 ± 5
8.	1839	0.51±.02	271±3	424	0.42	0.67	310	3.98	305	5 ± 3
9.	1840	0.30±.02	282±7	468	0.47	0.61	331	3.86	312	19 ± 7
10.	1841	0.50±.05	278±3	455	0.45	0.72	317	4.13	306	11 ± 3
11.	1842	0.49±.02	276±5	505	0.51	0.74	319	3.61	314	-5 ± 5
12.	1843	0.62±.02	283±2	463	0.46	0.85	315	3.63	316	-1 ± 2
13.	1844	0.43±.02	272±3	460	0.46	0.64	318	3.88	319	-1 ± 3
14.	1845	0.34±.03	262±3	461	0.46	0.54	321	3.34	312	9 ± 3
Mean (1826-1845)		0.45±.01	276±1	418	0.42	0.63	316	3.52	315	1 ± 1

Table 3.6 - The 27-day average diurnal anisotropy vector, wind velocity, convection vector, diffusion vector, the observed IPMF vector and the phase difference $\Delta\phi$ are shown for ~ 14 solar rotations during 1967-68.

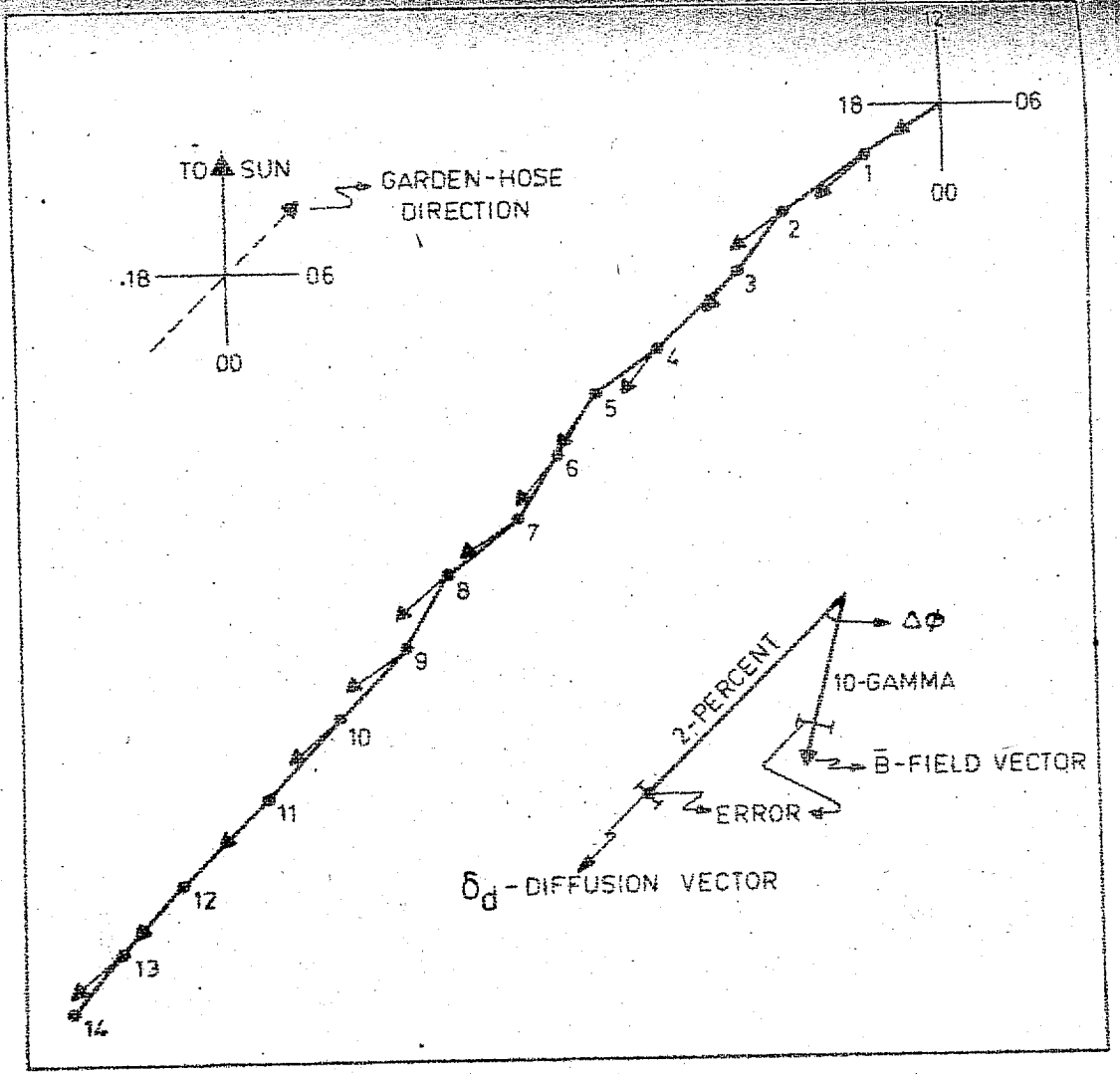

Figure 3.8 - An illustration of the field aligned nature of 27-day mean diffusion vectors on ~ 14 solar rotations during 1967-68. The observed average IPMF vector for each solar rotation is also shown (arrow).

the solar wind velocity are available. Since direct observations of the field azimuth for all the 73 solar rotations are not available, they have been derived using the solar wind velocity observations and assuming Archimedean spiral configuration (equation 3.6). The diffusion vectors $\bar{\delta}_d$ computed for each solar rotation are then resolved into two components one parallel ($\delta^{\parallel}_d$) and another perpendicular ($\delta^{\perp}_d$) to the magnetic field as shown in Fig. 3.9. The figure clearly shows that the cosmic ray diffusion parallel to the magnetic field ($\delta^{\parallel}_d$) is in general predominant and the perpendicular diffusion is quite negligible, that is in most of the cases ($\sim$80%) the parallel diffusion coefficient ($K_{\parallel}$) is much larger than the perpendicular diffusion coefficient ($K_{\perp}$) and the ratio $K_{\perp} / K_{\parallel} \sim 0$. It is also observed that on nearly 80% of the solar rotations the diffusion vectors are completely field aligned within the observational errors during 1965-72.

The analysis was limited to only 73 solar rotations out of 108 solar rotations during 1965-72, due to the non-availability of solar wind velocity observations. In order to cover the entire period even at times when the solar wind velocity observations are not available, we have estimated the solar wind velocity by taking advantage of the existence of a close empirical relationship between the solar wind velocity (V_p) and ΣK_p index, the index of geomagnetic disturbance. The empirical relationship for this period has been derived using the limited data on solar wind velocity observations from Vela-3 satellite during 1965-67. Fig. 3.10 shows the daily average wind

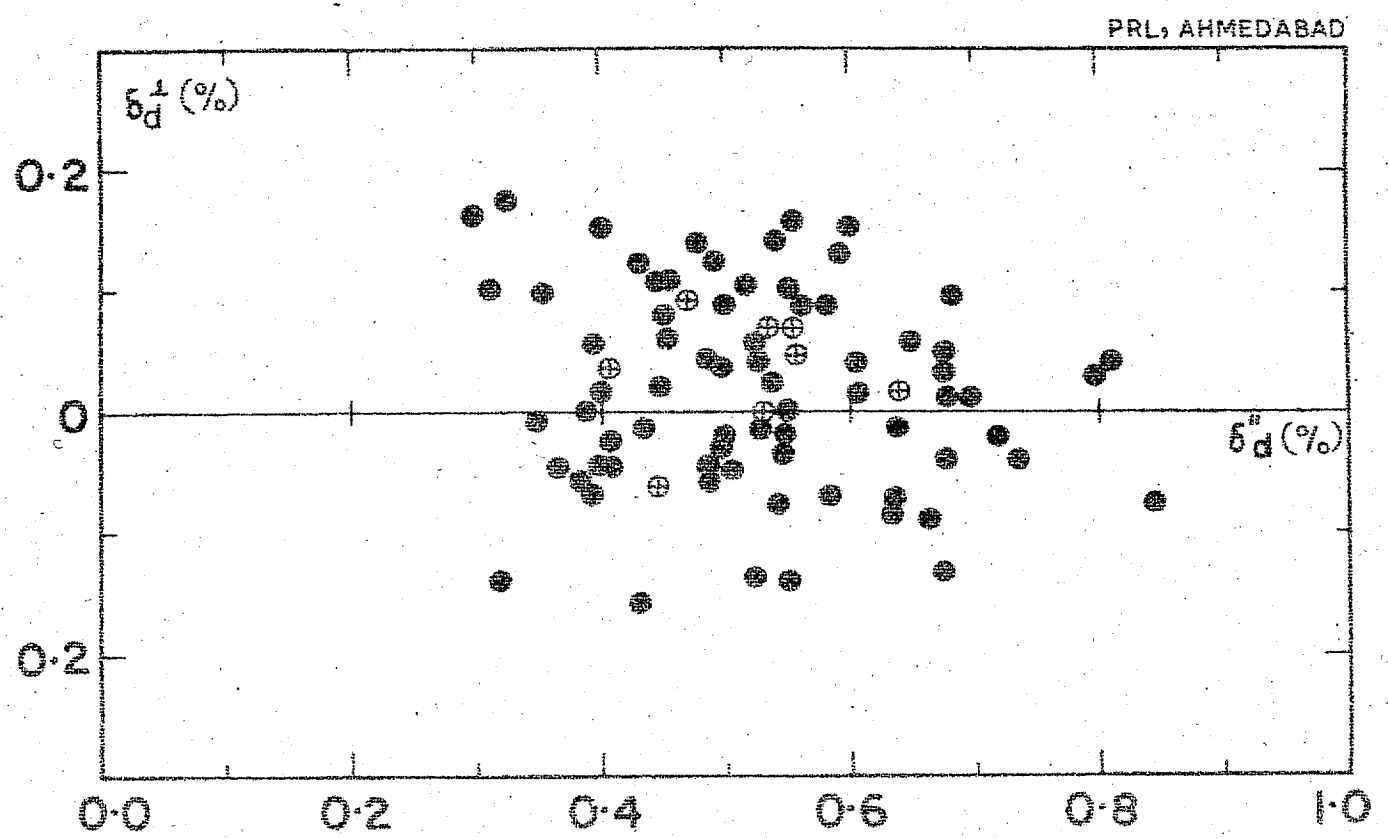

Figure 3.9 - The distribution of parallel ($\delta_d^{\parallel}$) and perpendicular ($\delta_d^{\perp}$) components of the 27-day mean diffusion vectors for ~73 solar rotations during 1965-72 (dots). The components of the yearly mean diffusion vectors for the same period are also shown (crossed open circles).

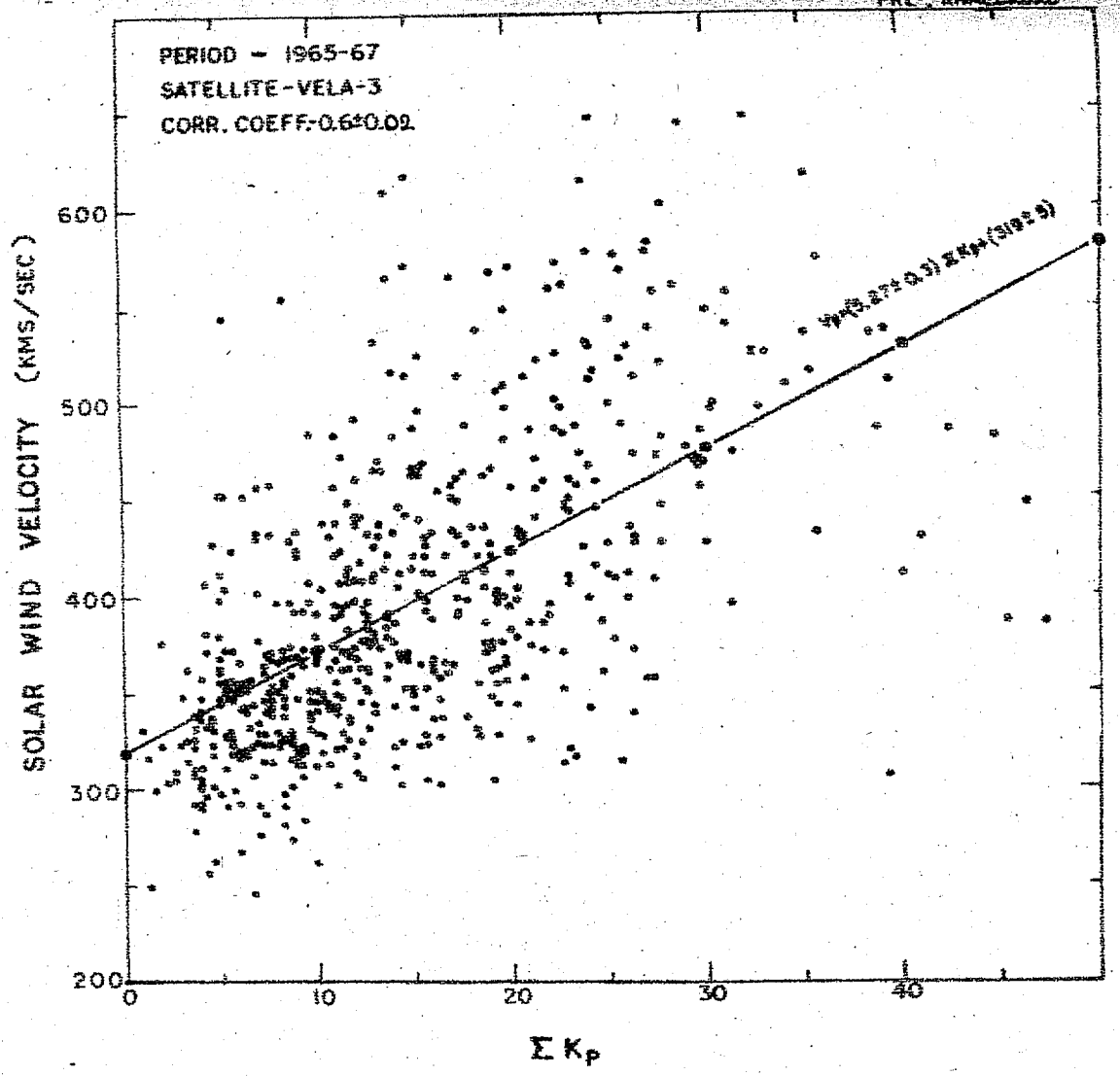

Figure 3.10 - Demonstrates the correlation between the observed solar wind velocity (V_p) and $\sum K_p$ index, the index of geomagnetic disturbance during the period 1965-67.

velocity (V_p) as observed at Vela-3 satellite plotted against ΣK_p for the above period, which indicates a good correlation between the two ($r \sim 0.6 \pm 0.02$). The observation shown in the figure are consistent with the relationship

$$V_p = (5.27 \pm 0.3) \Sigma K_p + (319 \pm 5) \text{ kms/sec} \quad (3.7)$$

Prior to the usage of this relationship for the estimation of convection vectors, it is essential to show that the results obtained using this relationship (equation 3.7) are in agreement with the results obtained using the observed solar wind velocity. Therefore for 73 solar rotations during 1965-72 for which solar wind velocity observations are available, we have computed the convection vector using the actual observations as well as using V_p derived from ΣK_p (equation 3.7). The phase difference $\Delta\phi$ between the computed diffusion vectors and the field azimuth obtained using both the above methods are compared in Fig. 3.11. The frequency distribution of the occurrence of $\Delta\phi$ computed using actual wind velocity (dotted lines) and that computed using estimated V_p from ΣK_p index (solid lines) are in good agreement, thus confirming that for all practical purposes, when actual solar wind velocity observations are not available one could use the empirical relation between wind velocity and ΣK_p index for deriving convection vectors.

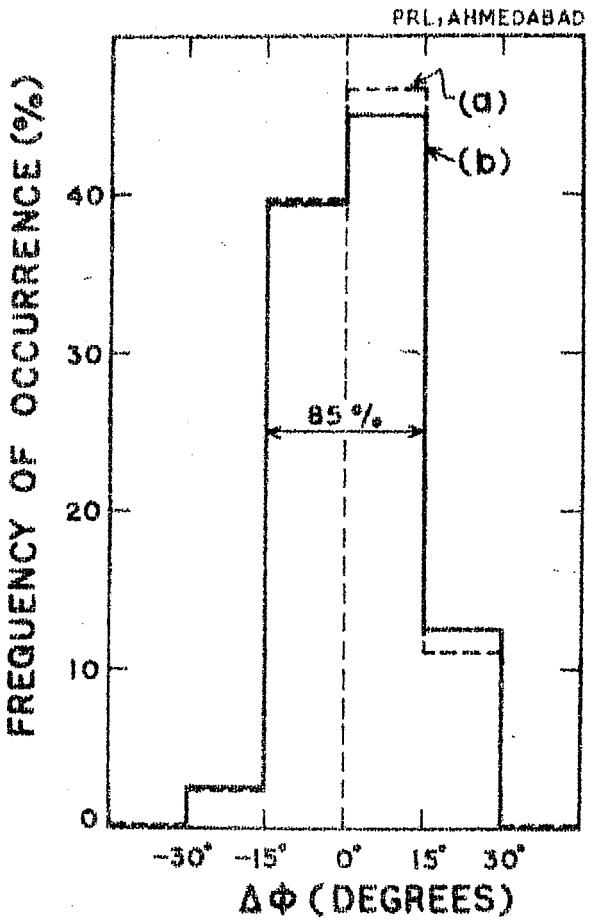

Figure 3.11 - Histograms showing the frequency of occurrence of the phase difference $\Delta\phi$ derived using convection vectors estimated from (a) observed solar wind velocity (dotted lines) (b) using ΣK_p index and the empirical relations (equation 3.7) for nearly 73 solar rotations (solid lines) during 1965-72.

In Fig. 3.12 is shown the frequency distribution of $\Delta\phi$ plotted in the form of a histogram for all the 108 solar rotations during 1965-72. It is clearly evident from the figure that on $\sim$ 82% of the solar rotations the diffusion vectors are completely field aligned within the errors and only on less than 18 solar rotations the diffusion vectors show significant departures from the field azimuth.

3.13 Discussion:

From the results presented so far it is clear that the average diurnal anisotropy observed at relativistic energies, both on an yearly as well as on a 27-day basis can be essentially explained as a resultant of the convective expulsion of these particles by the radially blowing solar wind and inward field aligned diffusion of these particles along the interplanetary field lines. Using the computed value of the diffusion vectors it is possible to estimate the radial gradient of cosmic ray particles, which is responsible for the inward diffusion. Following Gleeson (1969) and Forman and Gleeson (1970, 1974) the net diffusion current in the interplanetary medium is determined by (equation 1.16)

$$\bar{\delta}_d = K_{\parallel} \left(\frac{\partial U}{\partial r}\right)_{\parallel} + K_{\perp} \left(\frac{\partial U}{\partial r}\right)_{\perp} \qquad (3.8)$$

Since our observations of average diffusion vectors during 1965-72 clearly indicate that on an average basis the cosmic ray diffusion in the interplanetary medium is completely

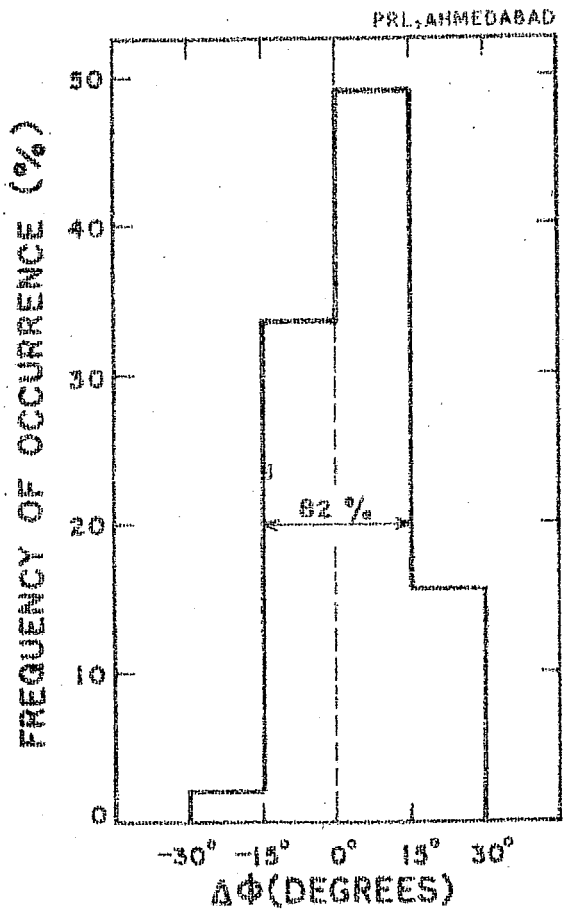

Figure 3.12 - The $\Delta\phi$ distribution is plotted in the form of a histogram for all the 108 solar rotations during 1965-72. Note that on ~ 82% of the solar rotations the diffusion vectors are field aligned.

field aligned and the diffusion perpendicular to the field is almost negligible, i.e. $K_{\perp} \sim 0$, then we have

$$S_d = K_{\parallel} \left(\frac{\partial U}{\partial r}\right)_{\parallel} \quad , \quad \bar{\delta}_d = \frac{3S_d}{Uv} \qquad (3.9)$$

the radial density gradient $G = \frac{1}{U} \left| \left(\frac{\partial U}{\partial r}\right) \right| / \cos\psi$

For a yearly mean diffusion component $\bar{\delta}_d \sim 0.52 \pm 0.01\%$ (Table 3.5) observed during 1965-72, the corresponding free space anisotropy will be $\sim 0.8\%$. Using a $K_{\parallel} \sim 5 \times 10^{21} P\beta$ where P is rigidity and $\beta = v/c$ (Jokipii and Coleman, 1968; Bercovitch, 1971a) the radial gradient (G) at neutron monitor energies ($\sim$10 GeV) turns out to be (equation 3.9) of $\sim 4.5\%$ / AU which is in good agreement with many other independent observations of the radial density gradient at these energies (Bercovitch, 1971b). We can also estimate the ratio of $K_{\perp} / K_{\parallel}$ using the mean phase difference $\Delta\phi \sim 4^{\circ} \pm 1^{\circ}$ during 1965-72 (Table 3.5) is found to be $\frac{K_{\perp}}{K_{\parallel}} \leq 0.05$ indicating that on an average basis, the transverse diffusion current is almost negligible at neutron monitor energies and $K_{\perp} \sim 0$.

3.14 Enhanced diurnal variation:

In this section, we examine the special cases of diurnal variation when the amplitude is large and the time of maximum shows considerable departure from the normal

corotational (18 hours) direction. The existence of trains of consecutive days having consistently large diurnal amplitude ($\geq$ 0.6%) and a time of maximum shifted to later hours ($\sim$ 20 hours) has been reported by a number of workers (Patel et al, 1968; Mathews et al, 1969; Hashim and Thambyahpillai, 1969; Ananth et al, 1971; Rao et al, 1972). The explanation of such large diurnal amplitude days using the well known corotation theory has not been very satisfactory. In this section we demonstrate that the convection-diffusion theory can fully explain the observed diurnal variation on such days as a result of an non-equilibrium condition created by the varying diffusion and convection currents in the interplanetary medium.

3.15 Characteristics of enhanced diurnal wave trains:

The enhanced diurnal wave trains which has been selected for this analysis consists of atleast 5 or more consecutive days on which the observed diurnal amplitude is consistently $\geq$ 0.6%. Out of a total of about 50 such events available during 1965-72, we have selected 10 prominent events, which are not associated with large intensity variations such as Forbush decreases. Table 3.7 lists the particulars of the selected enhanced diurnal wave trains during 1965-72. Fig. 3.13 shows the temporal variation of cosmic ray intensity observed at Deep River for a few typical events listed in the table 3.7.

Table 3.7

ENHANCED DIURNAL WAVE TRAIN EVENT	DIURNAL ANISOTROPY VECTOR (δ) Amp. (%)	DIURNAL ANISOTROPY VECTOR (δ) Pha. (Deg)	SOLAR WIND VELOCITY (kms/sec)	CONVECTION VECTOR (δ_c) Amp. (%)	DIFFUSION VECTOR (δ_d) Amp. (%)	DIFFUSION VECTOR (δ_d) Pha. (Deg)	FIELD AZIMUTH (Φ_B) Pha. (Deg)	PHASE DIFF. ($\Delta\Phi$) ($\Phi_d - \Phi_B$) (Deg)	SPECTRAL EXPONENT (β)
31 Dec.1965-07 Jan.1966	1.08±.03	297±3	355	0.35	1.28	312	312	0 ± 3	-0.2
02 May 1966-11 May 1966	0.92±.02	297±1	343	0.34	1.12	313	311	2 ± 1	-0.2
31 Jan.1967-07 Feb.1967	1.04±.03	284±3	350	0.35	1.17	301	311	-10 ± 3	0.0
08 Apr.1967-15 Apr.1967	1.05±.03	288±1	300	0.30	1.18	302	307	-5 ± 1	0.0
23 Feb.1968-28 Feb.1968	0.91±.03	289±2	388	0.39	1.10	308	314	-6 ± 2	0.0
16 Mar.1968-20 Mar.1968	0.97±.04	265±2	586	0.59	1.09	298	326	-28 ± 2	0.4
23 Apr.1968-01 May 1968	0.84±.06	295±2	459	0.46	1.12	317	319	-2 ± 2	0.4
11 Feb.1970-15 Feb.1970	0.53±.05	267±3	330	0.33	0.61	300	310	-10 ± 3	0.2
11 Jul.1970-17 Jul.1970	0.69±.02	272±4	424	0.42	0.82	303	317	-14 ± 4	-1.0
05 Mar.1971-09 Mar.1971	0.67±.03	275±1	352	0.35	0.78	301	311	-10 ± 1	-0.4
Mean (10 events)	0.86±.01	285±1	388	0.39	1.06	306	314	-8 ± 1	0.1

Table 3.7 - The selected enhanced diurnal amplitude wave trains along with the observed average diurnal anisotropy vector, convection vector, diffusion vector, field azimuth and the phase difference $\Delta\Phi$ for each event during 1965-72. The energy spectrum of variation (β) derived for each event is also given.

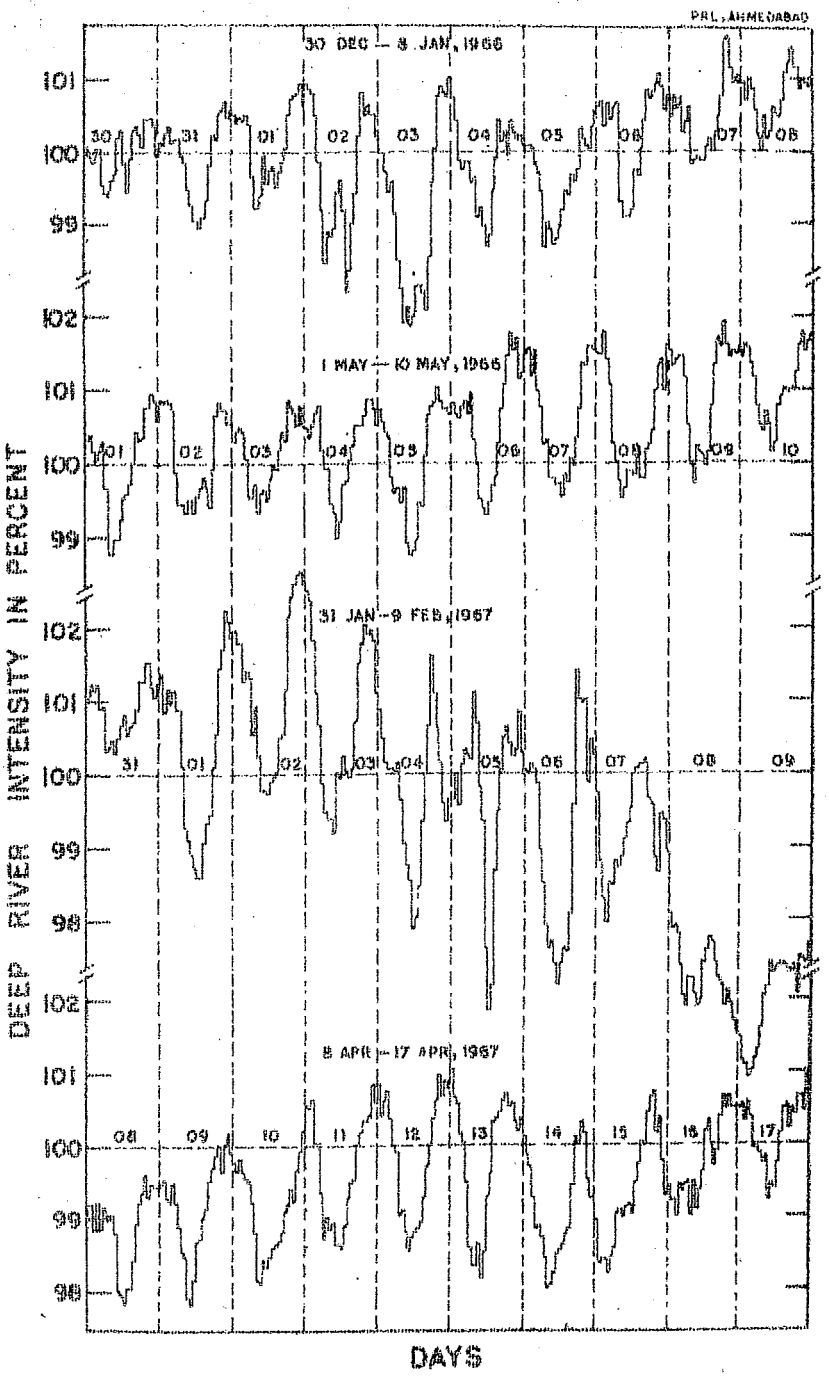

Figure 3.13 - The hourly cosmic ray intensity deviations observed at Deep River for a few selected enhanced diurnal amplitude wave trains.

Since the determination of the anisotropy characteristics during enhanced diurnal variation days requires an apriori knowledge of the energy spectrum, the energy spectrum of variation (β) for each event has been calculated using the known method (Rao et al, 1963) of deriving the direction of the anisotropy from the data from a number of stations, for different values of the spectral exponent and then computing the variance between these values. The spectral exponent corresponding to the minimum variance is taken as the appropriate spectral exponent applicable for the diurnal anisotropy for this period. Fig. 3.14 shows the variance between different values of the estimates of diurnal time of maximum as a function of the spectral exponent for a few typical enhanced wave trains, all of which indicate that the spectral exponent corresponding to the minimum variance $\beta \sim 0 \pm 0.4$. In Table 3.7 are listed the applicable spectral exponents (β) for each of the event selected for the present analysis. It is clear from the table that the diurnal anisotropy observed during the selected enhanced diurnal wave trains are consistent with their being energy independent.

3.16 Examination of enhanced diurnal variation days:

The diurnal anisotropy vector for each day for each of the event has been calculated using a energy independent spectrum ($\beta = 0$). Table 3.7 lists the mean diurnal anisotropy vector for each event along with the observed solar

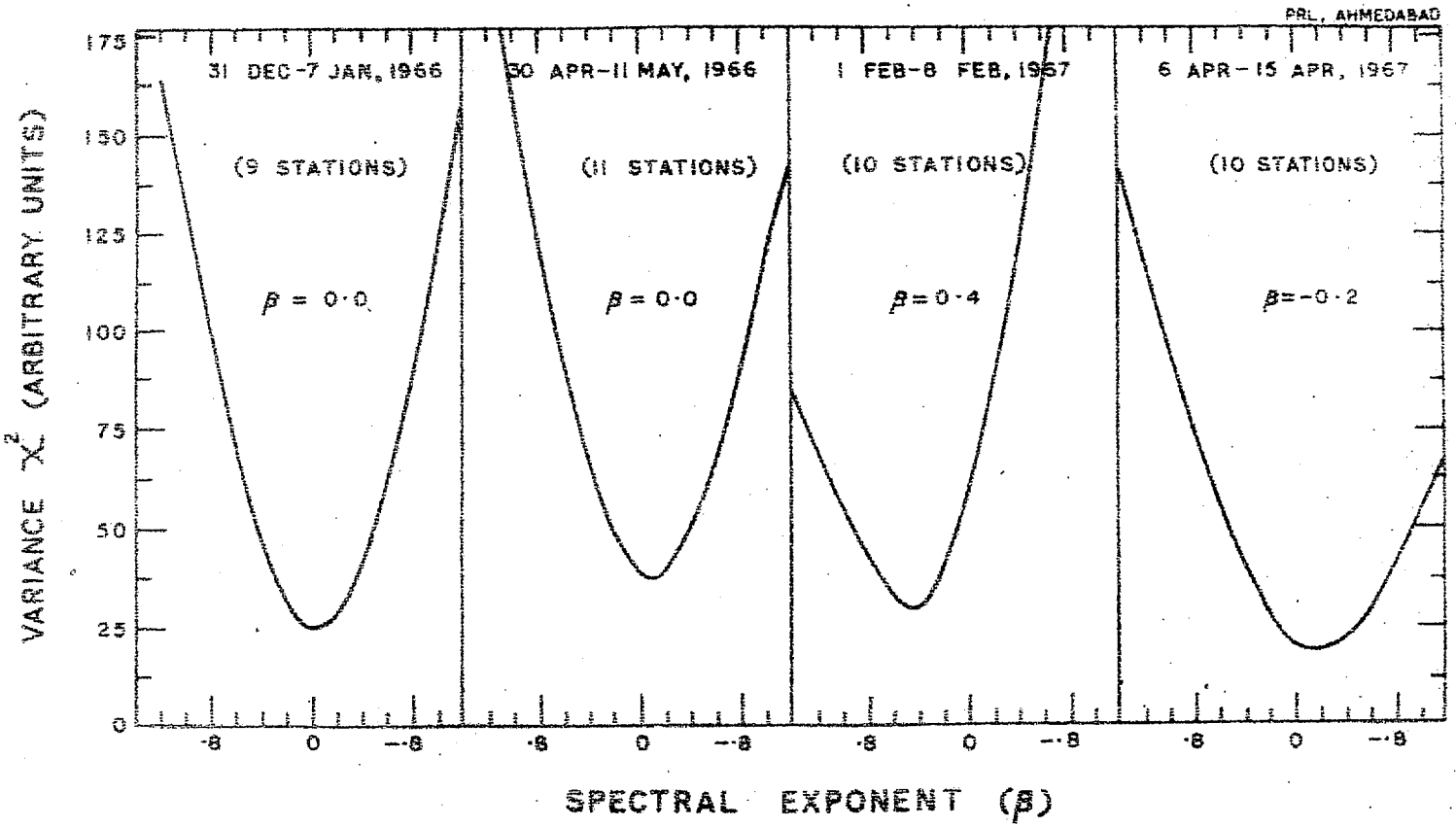

Figure 3.14 - The χ^2 distribution of the diurnal phase as a function of the spectral exponent (β) is shown for a few selected enhanced diurnal wave trains. The best fitting spectral exponent is determined from the minimum variance observed.

wind velocity and the convection vector derived using the solar wind velocity. The mean diffusion vector ($\bar{\delta}_d$) for each event as well as the IPMF azimuth are also given in the same table. The phase difference $\Delta\Phi$ between the diffusion vector (Φ_d) and field azimuth (Φ_B) listed for each event shows that except for the event of 16 - 20 March 1968, the difference is negligible and are within the observational errors, indicating that the diffusion vectors are completely field aligned. The diffusion vectors as well as the observed IPMF vectors for a few of the events are shown in Fig. 3.15 for which the direct IPMF observations are available. Fig. 3.16 shows a comparison between diffusion vectors and the field azimuth for all the events with the mean diffusion vector for each event plotted in the form of vector diagram. A close examination of the table 3.7 indicates that the average diurnal amplitude during the enhanced diurnal wave train is of $\cup$ 1% and the time of maximum for some of the events deviates as much as 30° from the corotation vector. We observe that even when the sample of days selected do not confirm to the normal pattern of diurnal variation, the observed diurnal anisotropy is consistent with it being composed of purely convection and field aligned diffusion current. Practically in all the cases it is seen that the diffusion vector is very much enhanced.

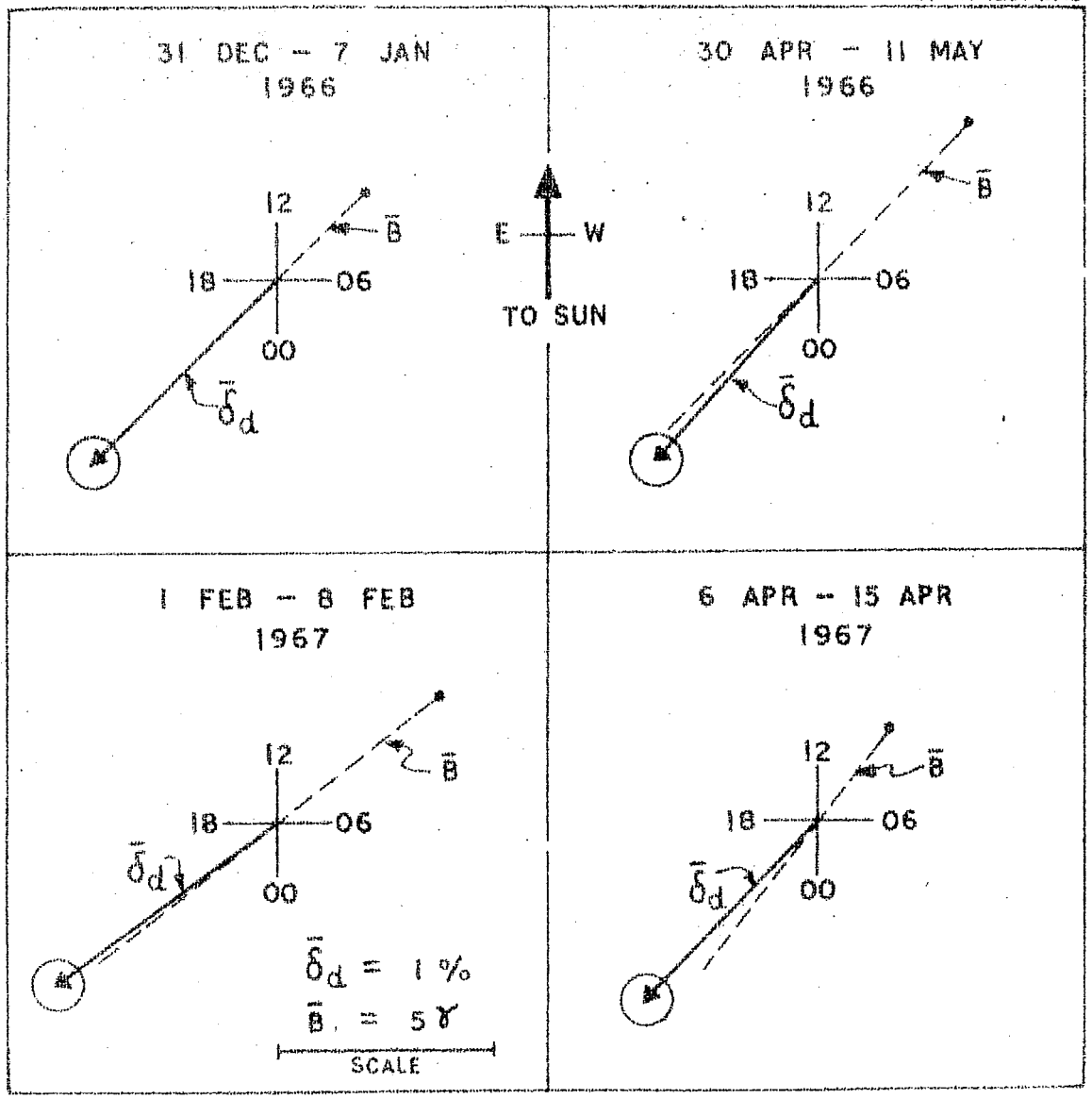

Figure 3.15 - The field aligned diffusion vectors during enhanced diurnal wave trains for which the "in situ" space-craft IPMF observations are available.

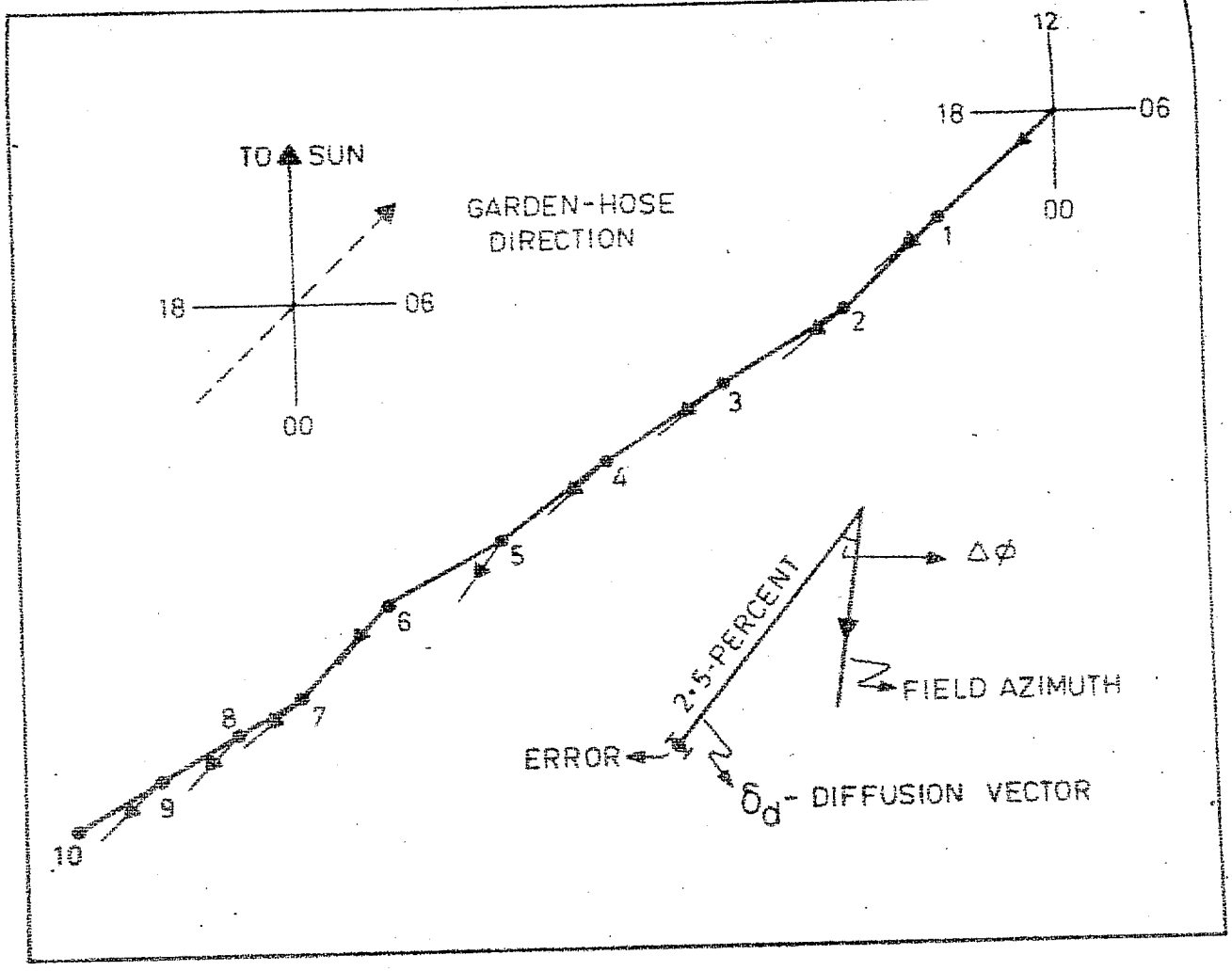

Figure 3.16 - The field aligned nature of diffusion vectors derived for all the enhanced diurnal wave trains observed during 1965-72. The arrow indicates the field azimuth in each case.

The enhanced field aligned diffusion can only result from an enhanced positive radial density gradient which is the driving force for the field aligned diffusion. An estimate of the enhanced radial gradient on these days has been made using the observed amplitude of the average diffusion anisotropy vector (Table 3.7). Substituting appropriate values in equation 3.9 we observe that the positive radial gradient existing on these days is about $\sim$ 10%/AU, which is significantly different from the normal $\sim$ 5%/AU radial gradient observed during normal conditions.

The significant positive density gradient $\sim$ 10%/AU can result as a consequence of the establishment of (a) regions of decreased cosmic ray density (sink) along the garden-hose direction or (b) regions of enhanced cosmic ray density (source) along the anti-garden-hose direction. Since the presence of a sink in the garden-hose direction or a source along the anti-garden-hose direction will essentially show the same diurnal time of maximum, the observed diurnal anisotropy vector will not reveal in any way the exact physical nature of the mechanism causing enhanced diurnal variation. In order to identify the sinks and sources of cosmic ray particles established in the interplanetary medium, we have constructed three dimensional space-time diagrams for each day for the enhanced diurnal wave trains listed in table 3.7, using the well developed technique described in chapter II. The space-time diagrams essentially define the

cosmic ray flux distribution in different asymptotic directions as a function of time and provide an instantaneous three dimensional view of the cosmic ray demography in space.

The average cosmic ray intensity deviations in all the 8 sectors each covering a longitude width of $\sim 45^{\circ}$ (3 hours) has been obtained by combining the data from a number of high latitude neutron monitoring stations. Further for each event we have computed the net cosmic ray intensity deviations observed in both garden-hose hemisphere (0 - 180° west of the sun-earth line) as well as in the anti-garden-hose hemisphere (0 - 180° east of the sun-earth line). All the events listed in table 3.7 may be phenomenologically classified broadly under three groups.

Class-1. Enhanced wave trains showing a large depression of cosmic ray intensity (sink) in the garden-hose hemisphere.

Class-2. Enhanced wave trains showing an enhanced cosmic ray flux (source) in the anti-garden-hose hemisphere.

Class-3. Enhanced wave trains showing both a depression in the garden-hose hemisphere and also an enhanced cosmic ray flux in the anti-garden-hose hemisphere.

3.17 Sink in the garden-hose hemisphere:

Table 3.8 lists all the enhanced diurnal wave trains (class-1) during which a sink of cosmic ray particles along garden-hose hemisphere was established in the interplanetary medium. The table also lists for each event the observed diurnal anisotropy characteristics, direction of minimum cosmic ray intensity and ratio between the intensities along garden-hose and anti-garden-hose hemisphere. The table clearly shows that during all the events listed in the table, a predominant sink of cosmic ray particles ($\geq$ - 1%) established in the garden-hose hemisphere.

Fig. 3.17 pictorially demonstrates the sink established in the garden-hose hemisphere during one of the major enhanced diurnal wave train occurring on 23 April to 01 May 1968 (Table 3.8), where the cosmic ray intensity deviation observed in each sector averaged over the whole event is plotted in the form of a histogram. For the same event the cosmic ray intensity deviations observed on a day to day basis is plotted separately for each sector and shown in Fig. 3.18. Both the figures clearly shows that, whereas the intensity in all other directions remain almost normal, the cosmic ray intensity along 6 - 9 and 9 - 12 hrs. direction remained significantly depressed and the establishment of a sink in the garden-hose hemisphere.

The space and time evolution of the anisotropic depression of cosmic ray intensity (sink) along the garden-hose

Table 3.8

Sr. No.	Enhanced diurnal amplitude wave train event	No. of days	Diurnal anisotropy		Average increase in 6 - 9 hours direction (%)	Ratio of average intensity (G.H/A.G.H)
			Amplitude (%)	Phase (Deg)		
1.	31 Dec. 1965 - 07 Jan. 1966	8	1.08 ± .03	297 ± 3	- 1.4	3.8
2.	31 Jan. 1967 - 07 Feb. 1967	8	1.04 ± .03	284 ± 3	- 1.9	18.5
3.	23 Apr. 1968 - 01 May 1968	9	0.84 ± .06	295 ± 2	- 1.6	4.6
4.	11 Feb. 1970 - 15 Feb. 1970	5	0.53 ± .05	267 ± 3	- 0.8	7.2

Table 3.8 - The enhanced diurnal wave trains (class 1) which shows a predominant depression (sink) established along the garden-hose hemisphere. The ratio of garden-hose to anti-garden-hose average cosmic ray flux observed is also given.

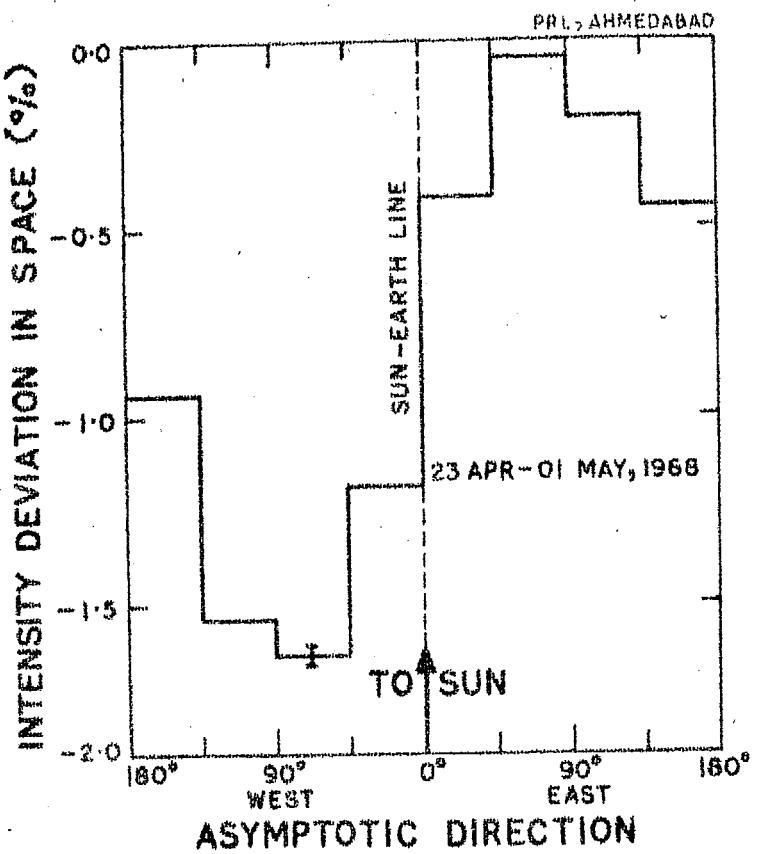

Figure 3.17 - The average cosmic ray intensity deviations as a function of asymptotic direction is plotted in the form of a histogram for a typical enhanced diurnal wave train event occurring on 23 April - 01 May 1968, which showed a predominant depression (sink) of cosmic ray flux along the garden-hose hemisphere.

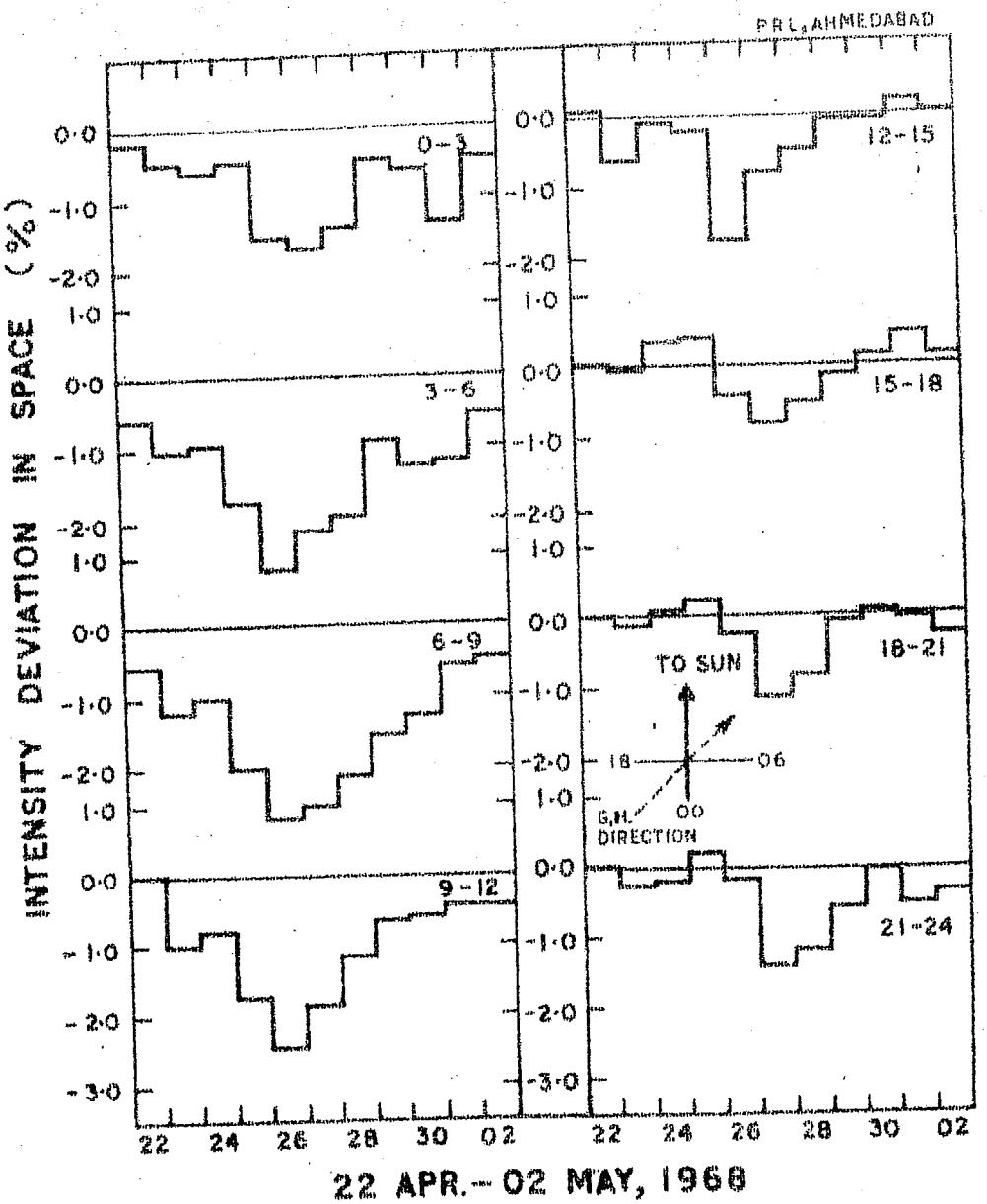

Figure 3.18 - The cosmic ray intensity deviations in each sector, separated by a longitude of $\sim 45^{\circ}$ (3 hours) is shown in the form of a histogram for the enhanced diurnal wave train event occurring on 23 April - 01 May 1968. Note the presence of a large depression (sink) in the garden-hose hemisphere.

hemisphere has been studied by constructing space-time diagrams on a day to day basis. Fig. 3.19 shows the cosmic ray intensity deviation in all the 8 sectors plotted in the form of a polar histogram for each day during the enhanced diurnal wave train event occurring on 23 April - 01 May 1968 (table 3.8). In the same figure the intensity deviations observed one day earlier and one day later to the event are also shown for the purpose of comparison. The figure clearly shows that the cosmic ray intensity which was quite normal in all the directions one day earlier to the event (22 April) started showing a small depression ($\sim$ - 1%) in the garden-hose hemisphere on 23 and 24 April. The cosmic ray depression in the garden-hose hemisphere developed further on 25 April and reached its maximum intensity level ($\sim$ - 2.5%) on 26 April along 6 - 9 and 9 - 12 hours direction. The large cosmic ray depression (sink) established in the garden- hose hemisphere started recovering on 28 April, reaching the normal flux distribution in space on 2 May, five days after the maximum depression. In spite of the cosmic ray intensity in the anti-garden-hose hemisphere remaining unaffected, a large sink of cosmic ray particles established along the garden-hose hemisphere persisted for nearly 9 days, causing enhanced diurnal variation during 23 April to 01 May 1968. The observations of Mathews et al (1969) and Hashim and Thambyahpillai (1969) for some of this class of events also support our conclusions.

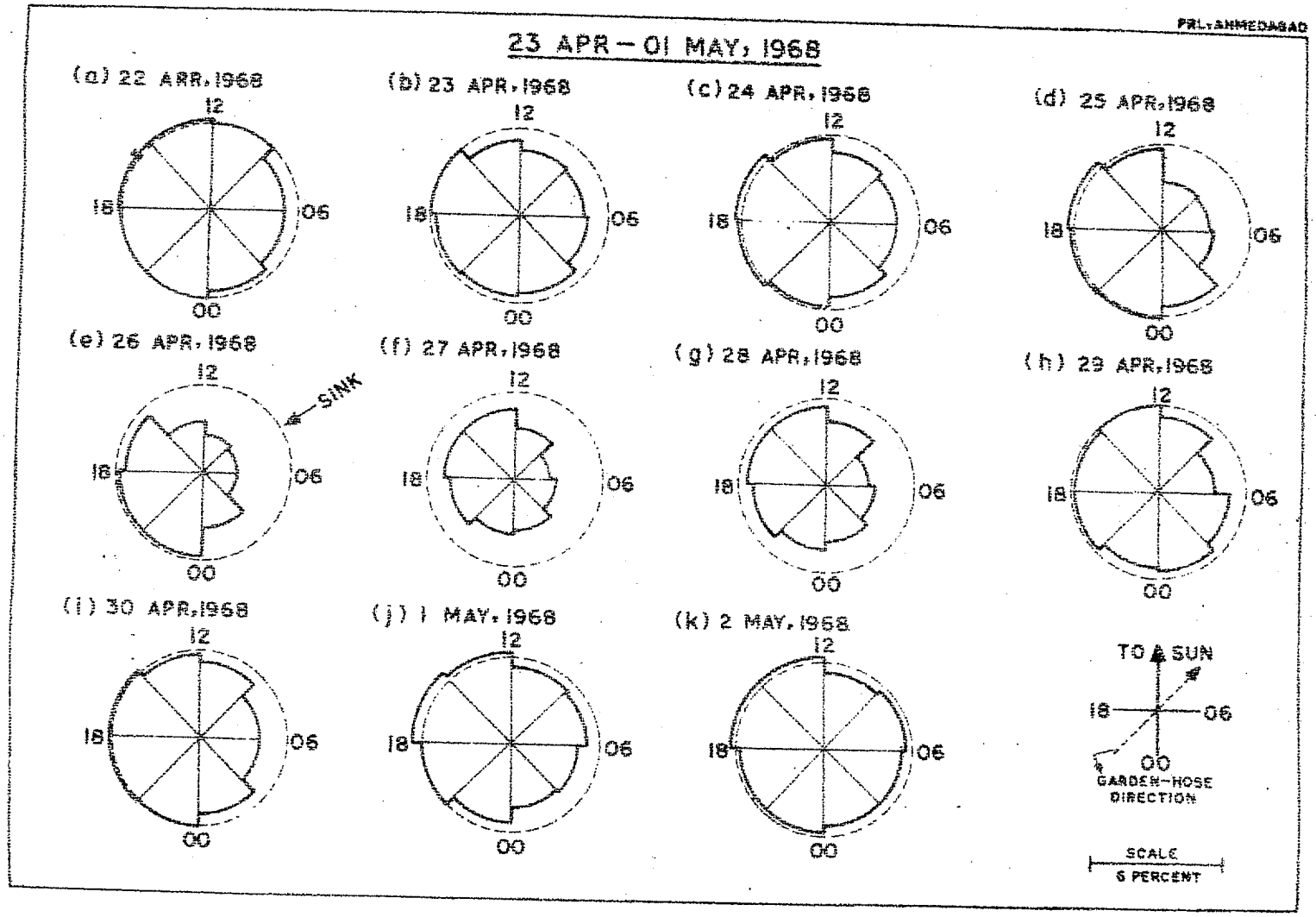

Figure 3.19 - Space-time diagrams showing the cosmic ray intensity deviations in all the 8 sectors plotted in the form of a polar histogram for each day during the enhanced diurnal wave train event occurring on 23 April - 01 May 1968. The predominant sink of cosmic ray particles established in the garden-hose hemisphere is shown by an arrow on 26 April 1968.

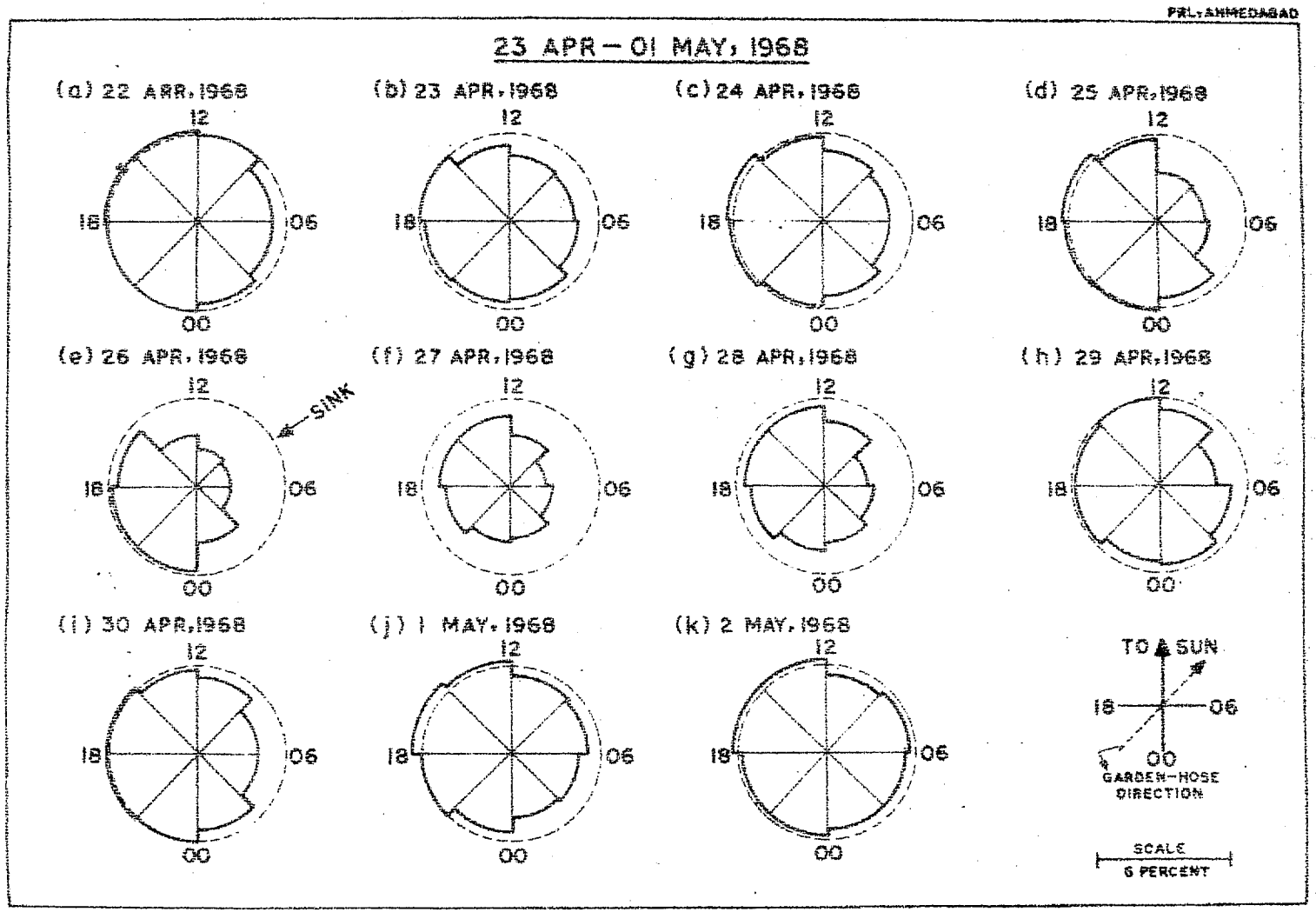

Figure 3.19 - Space-time diagrams showing the cosmic ray intensity deviations in all the 8 sectors plotted in the form of a polar histogram for each day during the enhanced diurnal wave train event occurring on 23 April - 01 May 1968. The predominant sink of cosmic ray particles established in the garden-hose hemisphere is shown by an arrow on 26 April 1968.

McCracken et al (1966b) suggested that the corotating Forbush decreases observed at low energies ($\sim$ 10 MeV) can manifest itself as an enhanced diurnal variation at relativistic energies ($\geq$1 GeV) causing a depressed cosmic ray intensity along the garden-hose direction. The enhanced wave train occurring on 31 Dec. 1965 - 7 Jan. 1966 (Table 3.8) coincides with the corotating Forbush decrease identified by McCracken et al (1966b). In the case of the enhanced wave train event occurring on 31 Jan. - 07 Feb. 1967 (table 3.8) a large solar proton increase was observed at high latitude neutron monitors four days prior to the event, which could not be attributed to any intense flare occurring on the visible disc of the sun. Hashim and Thambyahpillai (1969) have suggested that the prolonged rise time of the solar proton increase and the absence of a significant Forbush decrease at earth within few days following the solar proton event indicates that, an intense flare occurring on the reverse side of the sun caused the proton increase and the reconnection of the IPMF lines to the regions of depleted cosmic ray intensity behind the sun could result in a large depression of cosmic ray intensity (sink) along the garden-hose hemisphere.

3.18 Source in the anti-garden-hose hemisphere:

Table 3.9 lists all the enhanced diurnal wave trains which belong to the second class of events during which a predominant source of cosmic ray flux was observed in the anti-

Table 3.9

Sr. No.	Enhanced diurnal amplitude wave train event	No. of days	Diurnal anisotropy		Average increase in 15 - 18 hours direction (%)	Ratio of average intensity (G.H/A.G.H)
			Amplitude (%)	Phase (Deg)		
1.	08 Apr.1967 - 15 Apr. 1967	8	1.05 ± .03	288 ± 1	2.1	0.3
2.	23 Feb.1968 - 28 Feb. 1968	6	0.91 ± .03	289 ± 2	1.1	0.3
3.	16 Mar.1968 - 20 Mar. 1968	5	0.97 ± .04	265 ± 2	1.4	0.3
4.	11 Jul. 1970 - 17 Jul. 1970	7	0.69 ± .02	272 ± 4	1.4	0.6
5.	05 Mar.1971 - 09 Mar. 1971	5	0.67 ± .03	275 ± 1	1.4	0.7

Table 3.9 - The enhanced wave trains (class 2) during which an enhanced cosmic ray flux (source) was observed along the anti-garden-hose hemisphere.

garden-hose hemisphere. It is clear from the table that even though the diurnal time of maximum for the events listed in the table 3.9 are almost same as the one observed in the case of events belonging to class-1 unlike the latter events class-2 events shows consistently an enhanced cosmic ray flux ($\geq$ + 1%) from the anti-garden-hose hemisphere. Fig. 3.20 and 3.21 shows the source of cosmic ray flux established in the anti-garden-hose hemisphere during one of the enhanced diurnal wave train event occurring on 8 - 15 April 1967 (table 3.9). The figure clearly shows that the average cosmic ray intensity deviations in 15 - 18 and 18 - 21 hours direction is in excess of $\sim$ + 3% as compared to the intensity along other directions.

Space-time diagrams constructed for each day during the above event is shown in Fig. 3.22, where the cosmic ray intensity deviations in each sector is plotted for each day during the entire event. It is evident from the figure that the cosmic ray intensity distribution in space was normal on 7th April one day earlier to the event, shows a definitive increase along the anti-garden-hose hemisphere on 9 April. This enhancement (source) along the anti-garden-hose hemisphere developed further and on 12 April reached its maximum level ($\sim$ 3%) in 15-18 and 18 - 21 hrs. direction. This source continued till 15 April, on which date the cosmic ray flux distribution in space again became normal.

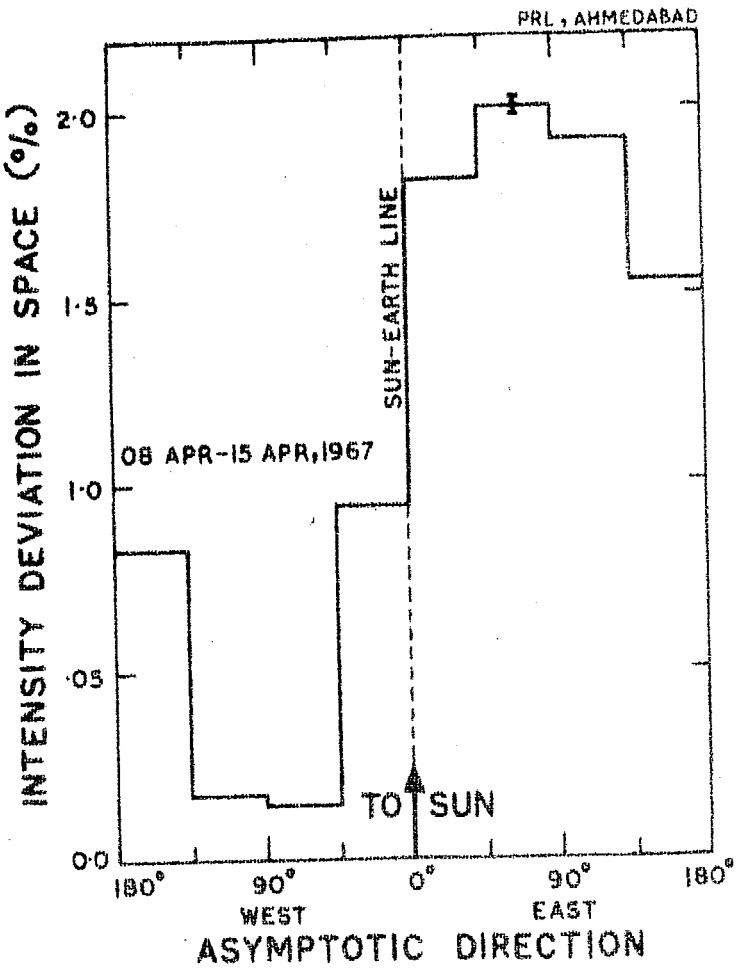

Figure 3.20 - Average cosmic ray intensity deviations in different sectors during the enhanced diurnal wave train event which indicated an enhanced cosmic ray flux (source) along the anti-garden-hose hemisphere occurring on 8 April - 15 April 1967.

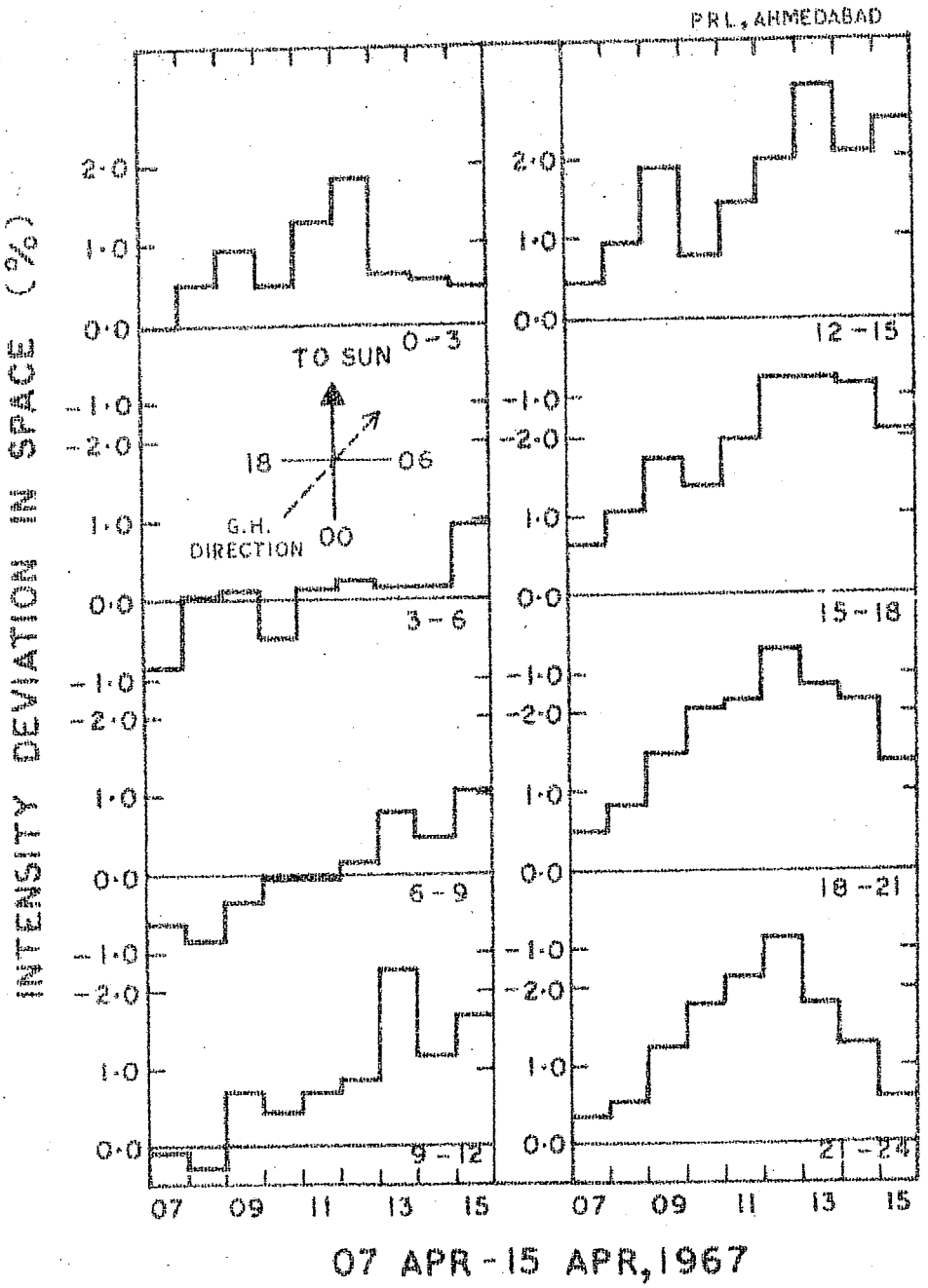

Figure 3.21 - The cosmic ray intensity deviations in each sector are shown in the form of a histogram for the enhanced diurnal wave train event occurring on 08 April - 15 April 1968. Note the presence of an enhanced cosmic ray flux (source) along the anti-garden-hose hemisphere.

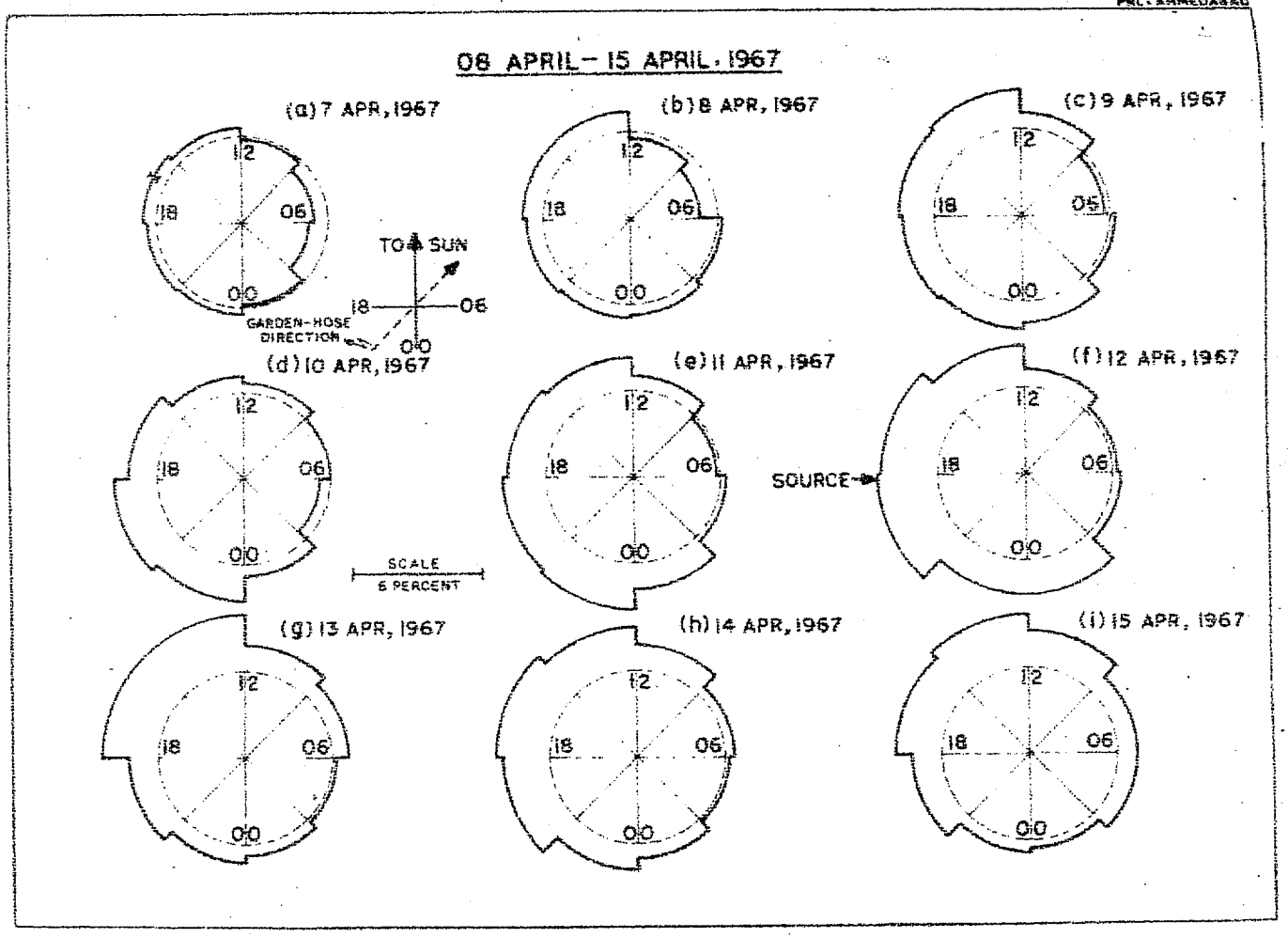

Figure 3.22 Space-time diagrams showing the cosmic ray flux distribution in space during the enhanced diurnal wave train occurring on 08 April - 15 April 1967. The predominant source of cosmic ray particles established in the anti-garden-hose hemisphere is indicated by an arrow on 12 April 1968.

3.19 Sink in the garden-hose hemisphere followed by a source in the anti-garden-hose hemisphere:

In contrast to the above simple picture the enhanced diurnal wave train occurring on 02 May - 11 May 1966 (Table 3.7) showed a complex behaviour. Fig. 3.23 shows the cosmic ray intensity deviations observed in different directions for the above event with the relevant details tabulated in table 3.7. This event was characterized by a significant depression ($\sim$ — 1%) in the garden-hose hemisphere as well as an enhanced cosmic ray flux ($\sim$ 1%) from the anti-garden-hose hemisphere. Fig. 3.24 shows the observed cosmic ray intensity deviations in different sectors plotted in the form of a histogram for all the 11 days during 02 May - 11 May 1966. A very interesting point that emerges out of fig. 3.24 is that the depression along the garden-hose hemisphere starts very early in the event reaching a maximum level around 4 - 6 May. The increase along the anti-garden-hose hemisphere starts only during later part of the event reaching its maximum intensity level around 9 - 10 May.

Following the observations and the explanation given by McCracken et al (1971) and Rao et al (1971) for the observed easterly anisotropy late in the decay of solar flare events, the complex picture presented by this type of events could be physically understood, if we assume that

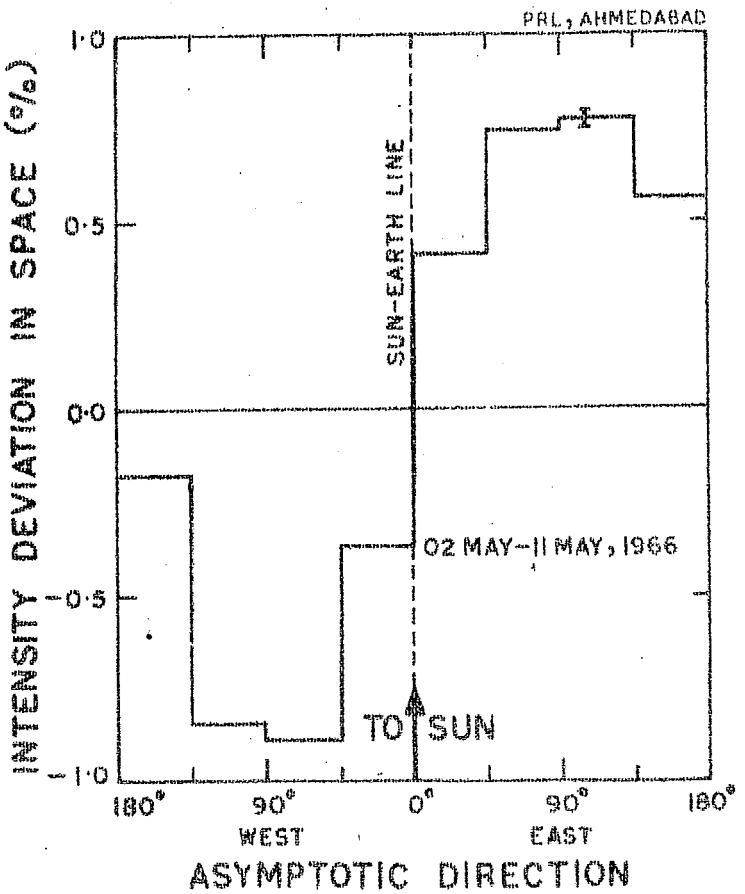

Figure 3.23 - Average cosmic ray intensity deviations as a function of asymptotic direction during a long lived enhanced diurnal wave train event occurring on 02 May - 11 May 1966, which showed the presence of both a sink in the garden-hose hemisphere and a source along the anti-garden-hose hemisphere.

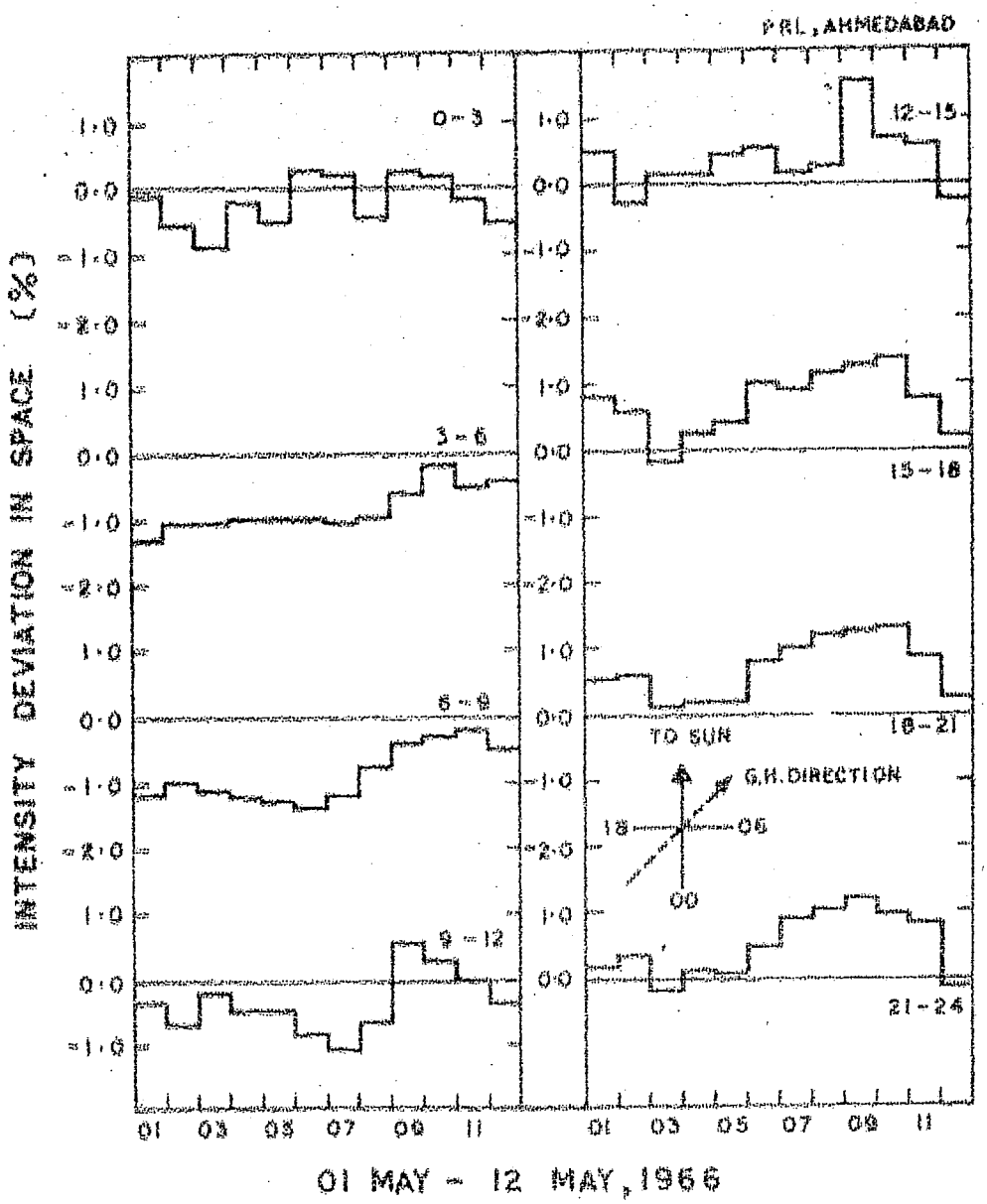

Figure 3.24 - The cosmic ray intensity deviations in each sector is shown in the form of a histogram during the enhanced diurnal wave train event occurring on 02 May - 11 May 1966. Note the establishment of a sink in the garden-hose hemisphere during earlier part of the event followed by a source along the anti-garden-hose hemisphere during later part of the event.

the enhanced convection in the early part of the event causing an enhanced positive density gradient giving rise to an increase of cosmic ray flux from the anti-garden-hose hemisphere late in the event (Ananth and Agrawal, 1971; Ananth et al, 1971). The change over from garden-hose sink to anti-garden-hose source occurring over a period of 4 - 5 days suggests that the relaxation time of the interplanetary medium to follow the changes in the density gradient in the entire modulating region is of $\sim$ 4 - 5 days. For a normal solar wind velocity of $\sim$ 400 kms/sec, this gives the dimensions of the modulating region of $\sim$ 2 AU, thus providing an independent experimental evidence for the location of boundary sometimes assumed in cosmic ray transport.

.....

C H A P T E R - IV

DIURNAL VARIATION ON A DAY TO DAY BASIS

4.1 Introduction:

Recalling our discussion on Fig. 3.3a in the III chapter, we note that there exists a large variability in both amplitude and time of maximum of the diurnal anisotropy on a day to day basis. The fact that such variability is observed at all the stations clearly demonstrates that the observed variability is truly an interplanetary phenomena and therefore can be effectively utilized for monitoring the electromagnetic state of the interplanetary medium on a day to day basis. The existence of such a large variability on a day to day basis in the diurnal anisotropy characteristics and their importance has been already emphasized by several investigators (Rao and Sarabhai, 1961; 1964; Patel et al, 1968; Pomerantz and Duggal, 1971; Rao, 1972). Efforts have also been made to explain these in terms of the existence of sources and sinks in the interplanetary medium (Rao and Sarabhai, 1964). However an unified theory to explain the detailed nature of the diurnal variation on a day to day basis does not exist. A detailed examination of the average diurnal variation during 1965-72 (chapter III) has clearly shown that the proposed convection and diffusion theory is able to explain satisfactorily all the observed characteristics of average diurnal anisotropy both on a yearly as well as on a 27-day basis. It has also

been shown that the theory can be extended to explain enhanced diurnal variation observed on several days as a consequence of an enhanced diffusion current arising out of a significant positive density gradient ($\sim$10%/AU) established due to the presence of sinks and sources of cosmic ray particles in the interplanetary medium. The large day to day variability observed in both the solar wind and IPMF parameters would create an imbalance between the convection and diffusion currents, should result in a large variability of both amplitude and direction of the diurnal anisotropy observed on a day to day basis. In this chapter we examine in the light of the above concept, the diurnal anisotropy observed on each day during 1967-68, for which the 'in situ' space-craft observations of both solar wind velocity and IPMF parameters are available.

4.2 Determination of diurnal anisotropy vectors on a day to day basis:

It is well known that the derivation of the diurnal anisotropy vectors on a daily basis is often contaminated by large world wide variations, such as Forbush decreases and transient cosmic ray variations in the interplanetary medium. Such world wide variations are found often highly anisotropic and in addition to the curvature effects (Kane, 1966) will introduce errors due to transient anisotropies which are not a part of the normal diurnal variation process. The only way to ensure that one is dealing with diurnal anisotropies

is through a comparison of diurnal anisotropy vectors observed at different stations and making sure that they agree with each other within the allowable statistical limits.

The diurnal variation observed at each station appropriately corrected for the width and declination of the asymptotic cone of acceptance (Rao et al, 1963) of the detector and geomagnetic bending assuming an energy independent spectrum ($\gamma = 0$), has been used to determine the diurnal anisotropy vectors on each day during 1967-68. After rejecting days on which large world wide variations and Forbush decrease occurred, only those days on which there is a good interstation agreement ($\sigma_{Amp} < 0.1\%$, and $\sigma_{Pha} \leq 30^{\circ}$) in the diurnal anisotropy vectors observed have been selected for further analysis. Fig. 4.1 shows the frequency of occurrence of the phase and amplitude of diurnal anisotropy vectors derived using a number of neutron monitoring stations for nearly $\sim$ 400 days during 1967-68 (solid lines). For the purpose of comparison the observation from a single station namely Deep River is also shown in the same figure (dashed lines). The figure clearly shows that the two histograms are similar and the day to day diurnal anisotropy vectors determined using a number of stations represents the true energy independent diurnal anisotropy in space.

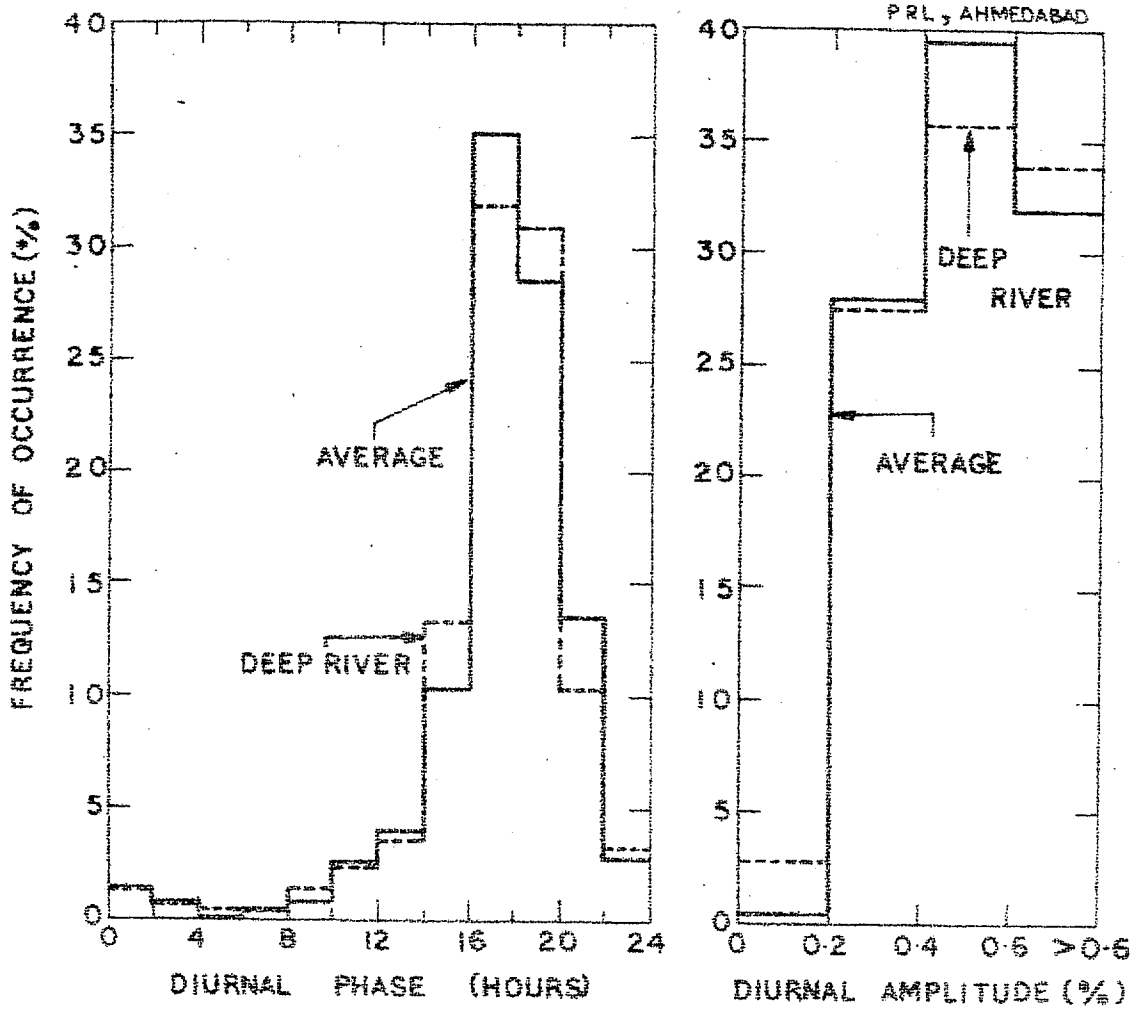

Figure 4.1 - The frequency distribution of diurnal phase and diurnal amplitude derived on a day to day basis using a number of stations (solid lines) and observed at Deep River (dashed lines) for nearly 400 days during 1967-68.

4.3 Examination of diurnal anisotropy vectors on a day to day basis:

Following similar arguments as in chapter III, the diurnal anisotropy vector ($\bar{\delta}$) for each day can be expressed as a summation of a convection vector ($\bar{\delta}_c$) and a diffusion vector ($\bar{\delta}_d$) given by

$$\bar{\delta} = \bar{\delta}_c + \bar{\delta}_d \qquad (4.1)$$

The convection vector ($\bar{\delta}_c$) for each day is estimated directly from the 'in situ' space-craft observations of the solar wind velocity and the diffusion vector ($\bar{\delta}_d$) is then derived by subtracting convection vector from the observed diurnal anisotropy vector (equation 4.1). The phase difference $\Delta\phi$ between the diffusion vector (ϕ_d) and the observed IPMF vector (ϕ_B) has been computed for each day during 1967-68.

Fig. 4.2 shows the frequency distribution of the phase difference $\Delta\phi$ computed for nearly $\sim$ 200 days during 1967-68, for which both the wind velocity and IPMF observations are available. The figure clearly shows that on $\sim$ 73% of days the diffusion vectors are field aligned ($\Delta\phi < 30^\circ$) within the allowable observational errors. If we further restrict our analysis to only those days which shows a good inter-station agreement ($\sigma_{Pha} < 30^\circ$), the percentage of days on which diffusion vectors are field aligned increases to $\sim$ 80%, that is even on a day to day basis the observations

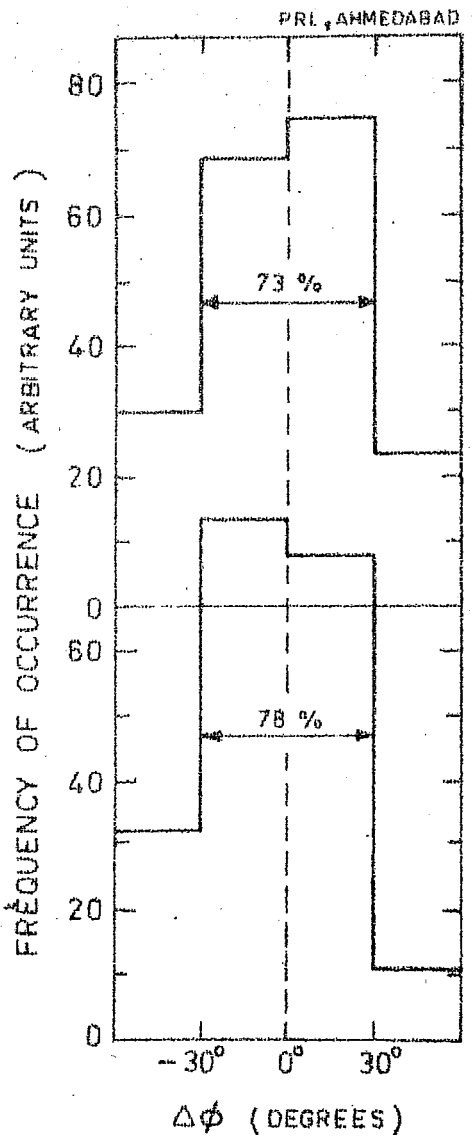

Figure 4.2 - Histograms showing the frequency distribution of the phase difference $\Delta\phi$ derived on a day to day basis for (a) nearly 200 days (b) for days on which there is a good interstation agreement in the diurnal anisotropy observed ($\sigma_{Pha} < 30^{0}$) during 1967-68.

clearly indicate that on nearly 80% of the days, the observed diurnal anisotropy can be understood in terms of a simple radial convection and a field aligned diffusion component in the interplanetary medium.

In the following examples, we apply the theory selectively for a few individual days, when the observed wind velocity is considerably higher ($\geq$ 600 kms/sec) than normal and when the observed IPMF vectors shows large departures from the average Archimedean spiral pattern. Fig. 4.3 shows few typical cases when the convection vectors are very much enhanced due to an increase in the solar wind velocity. The figure clearly shows that in all the four cases the diffusion vectors are completely field aligned. Similarly Fig. 4.4 and Fig. 4.5 shows few examples when the observed IPMF vectors are shifted to either early ($\sim$0600 hours) or later hours ($\sim$ 1200 hours) compared to the nominal garden-hose direction. In both the cases we find that the diffusion vectors are again completely field aligned indicating that in spite of the extreme conditions prevailing in the interplanetary medium the cosmic ray diffusion occurs principally along the observed IPMF direction.

The analysis has been extended to examine all the selected $\sim$ 400 days during 1967-68. Since the space-craft observations of the solar wind velocity for all the days are not available, we have used ΣK_p index and the established empirical relationship between the wind velocities and ΣK_p

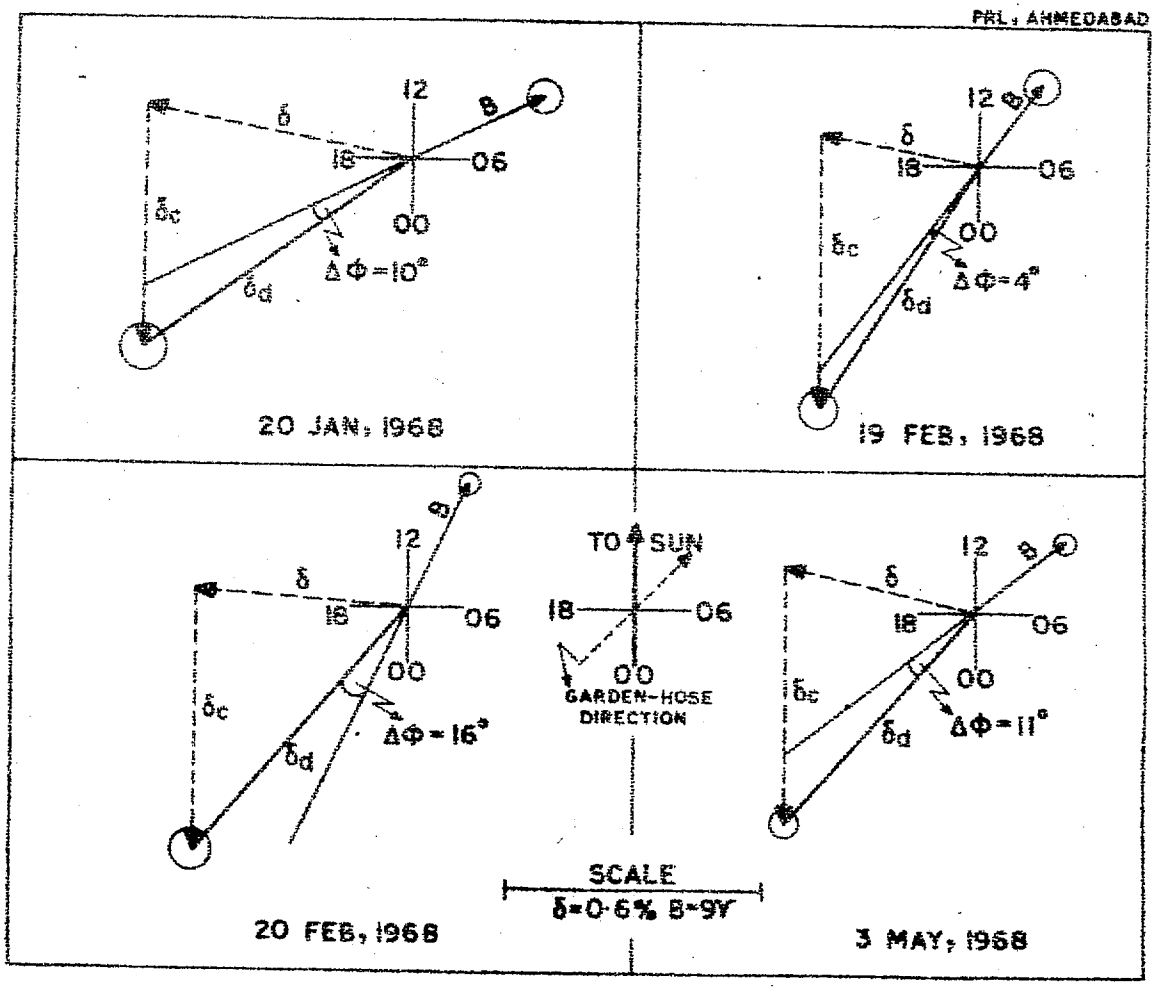

Figure 4.3 - The field aligned nature of diffusion vectors determined on a day to day basis when the observed convection vector (solar wind velocity) is very much enhanced.

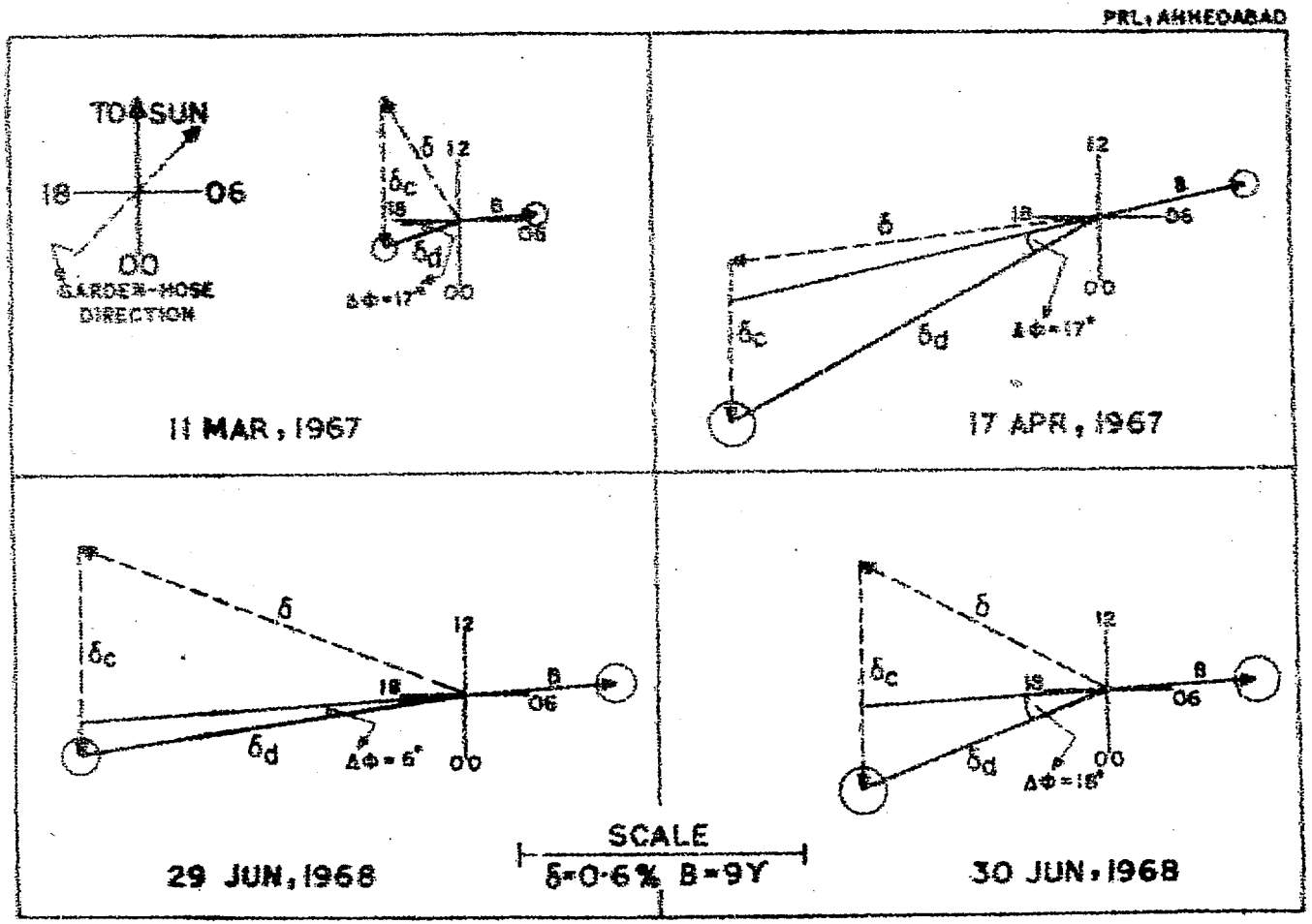

Figure 4.4 - The field aligned diffusion vectors when the direction of the observed IPMF vector is early hours (0600 hours) compared to the mean field (garden-hose) direction.

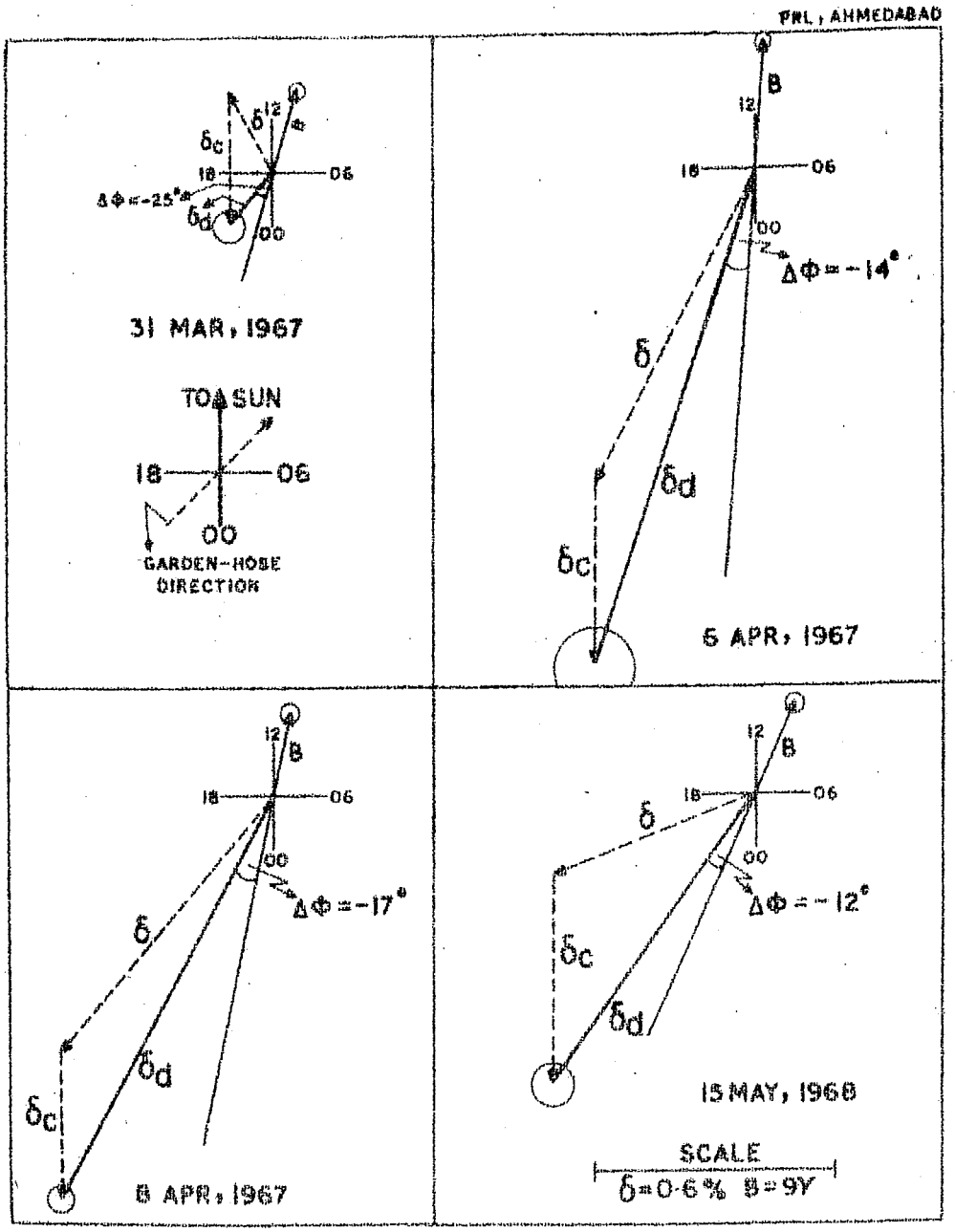

Figure 4.5 - The field aligned diffusion vectors, when the observed IPMF direction is later hours (1200 hours) compared to mean field (garden-hose) direction.

index(described in chapter III) for deriving convection vectors on a day to day basis. It is instructive to estimate the possible error that could be caused due to the non-usage of 'in situ' observations. Fig. 4.6 shows the frequency distribution of the phase difference $\Delta\Phi$ for nearly 150 days computed using convection vectors estimated from (a) observed solar wind velocity (dashed lines) (b) wind velocity derived from ΣK_p index (solid lines). A close similarity between the two histograms clearly indicates that even on a day to day basis the usage of ΣK_p index for estimating convection vectors will not significantly affect our conclusions and the maximum error introduced by this method is of$\sim \pm 5^{\circ}$, which is well within the statistical limits.

Having established the validity of using ΣK_p index for estimating convection vectors, the analysis has been extended to all the selected 400 days for which the 'in Situ' space-craft observations of the IPMF vectors are available. Fig. 4.7 shows the frequency distribution of the phase difference $\Delta\Phi$ plotted in the form of a histogram for nearly $\sim$ 400 days during 1967-68. In addition in Fig. 4.8, we have separately shown the $\Delta\Phi$ distribution for all those days on which the observed diurnal time of maximum lies between (a) 15 - 21 hours (solid lines) and (b) 0-15 and 21-24 hours (dashed lines). Fig. 4.7 clearly demonstrates that even on a day to day basis on $\sim$ 80% of the days the diffusion vectors

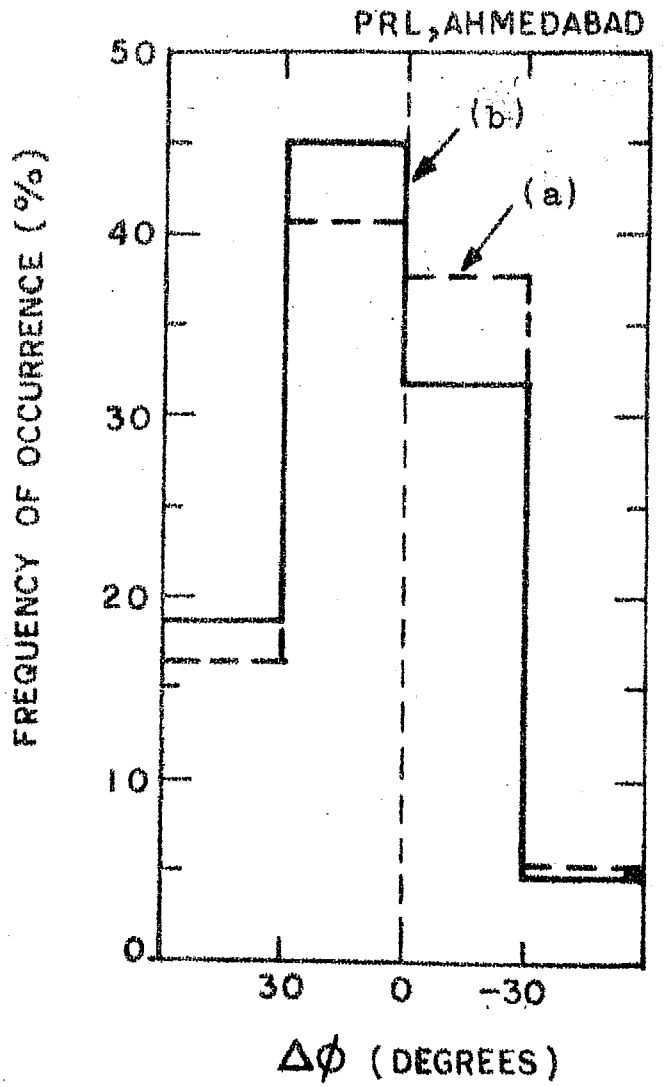

Figure 4.6 - The histograms showing the frequency distribution of the phase difference $\Delta\phi$ derived using (a) the observed solar wind velocity and (b) using ΣK_p index and the empirical relation (equation 3.7) derived in chapter III.

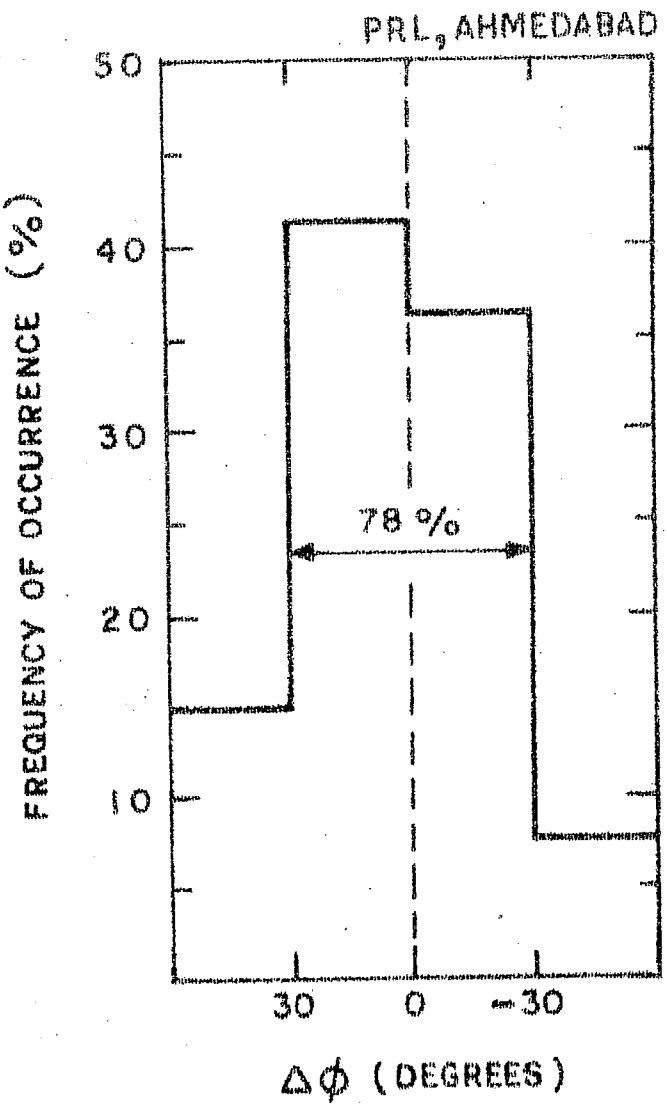

Figure 4.7 - The frequency distribution of the phase difference $\Delta\phi$ plotted in the form of a histogram for all the selected 400 days during 1967-68. Note that on $\sim$ 80% of the days the diffusion vectors are field aligned.

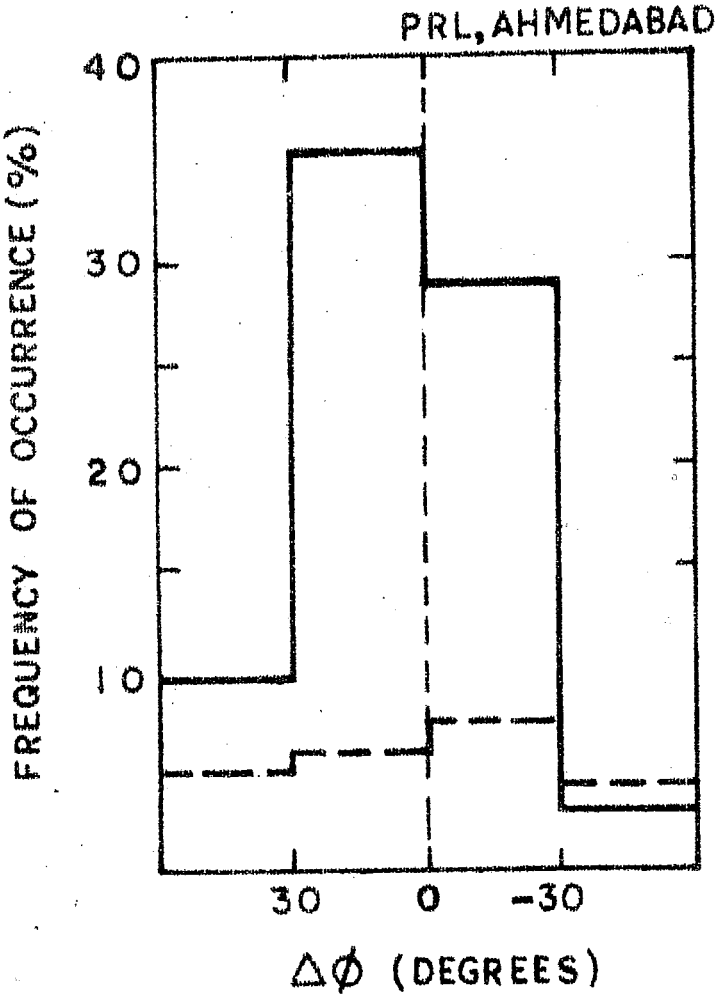

Figure 4.8 - The frequency distribution of the phase difference $\Delta\phi$ plotted in the form of a histogram separately for days on which the observed diurnal time of maximum is between 15 - 21 hours (solid lines) and 0 - 15 and 21 - 24 hours (dashed lines).

are field aligned ($\Delta\phi \leq 30^{\circ}$) and the observed diurnal anisotropy can be described in terms of a simple convection and a field aligned diffusion current of cosmic ray particles in the interplanetary medium, only on $\sim$ 20% of days the diffusion vectors are not field aligned ($\Delta\phi > 30^{\circ}$). Further a close examination of Fig. 4.8 indicates that when the observed diurnal time of maximum lies between 0 - 15 and 21 - 24 hours, that is when the observed diurnal time of maximum is far removed from the direction of corotation (1800 hours) the probability of occurrence of non-field aligned cosmic ray diffusion is considerably enhanced. On nearly 20% of the ' non-field aligned ' days on which the simple convection-diffusion concept does not hold good, have probably a significant contribution due to transverse diffusion currents in the interplanetary medium. A more detailed examination of such days is taken up in following sections.

4.4 The non-field aligned days:

In this section we try to critically examine the solar terrestrial relationship associated with nearly $\sim$ 20% of the days on which the diurnal variation characteristics show significant departure from that predicted by the simple convection-diffusion concept. These days will be termed as " non-field aligned days " in all our future discussions.

4.5 Characteristics of non-field aligned days:

Fig. 4.9 shows the frequency of occurrence of diurnal phase and diurnal amplitude plotted in the form of a histogram for all the non-field aligned days ($\sim$ 80 days) during 1967-68 (solid lines). In the same figure corresponding histograms for all the selected $\sim$ 400 days during the same period are also shown for the purpose of comparison (dashed lines). Whereas the phase distribution for $\sim$ 400 days shows a predominant peak around 1800 hours, which is consistent with the general pattern, the histograms for non-field aligned days shows almost a random phase distribution. The figure also shows that most of the days ($\sim$ 70%) on which the diurnal time of maximum lies between 0 - 12 hours, belongs to the category of non-field aligned days.

All the non-field aligned days are individually marked on a Bartel's chart and shown in Fig. 4.10. The figure shows that even though there exists a few stray individual days, most of the non-field aligned days ($\sim$ 60%) occur in trains of two or more consecutive days, suggesting that the mechanism causing non-field aligned days is not a transient phenomena but persists over a period of time. We have listed in table 4.1 all the non-field aligned trains of days observed during 1967-68, along with other relevant parameters such as diurnal and semi-diurnal variation vectors, the solar wind velocity, ΣK_p index the index of geomagnetic disturbance, and the observed

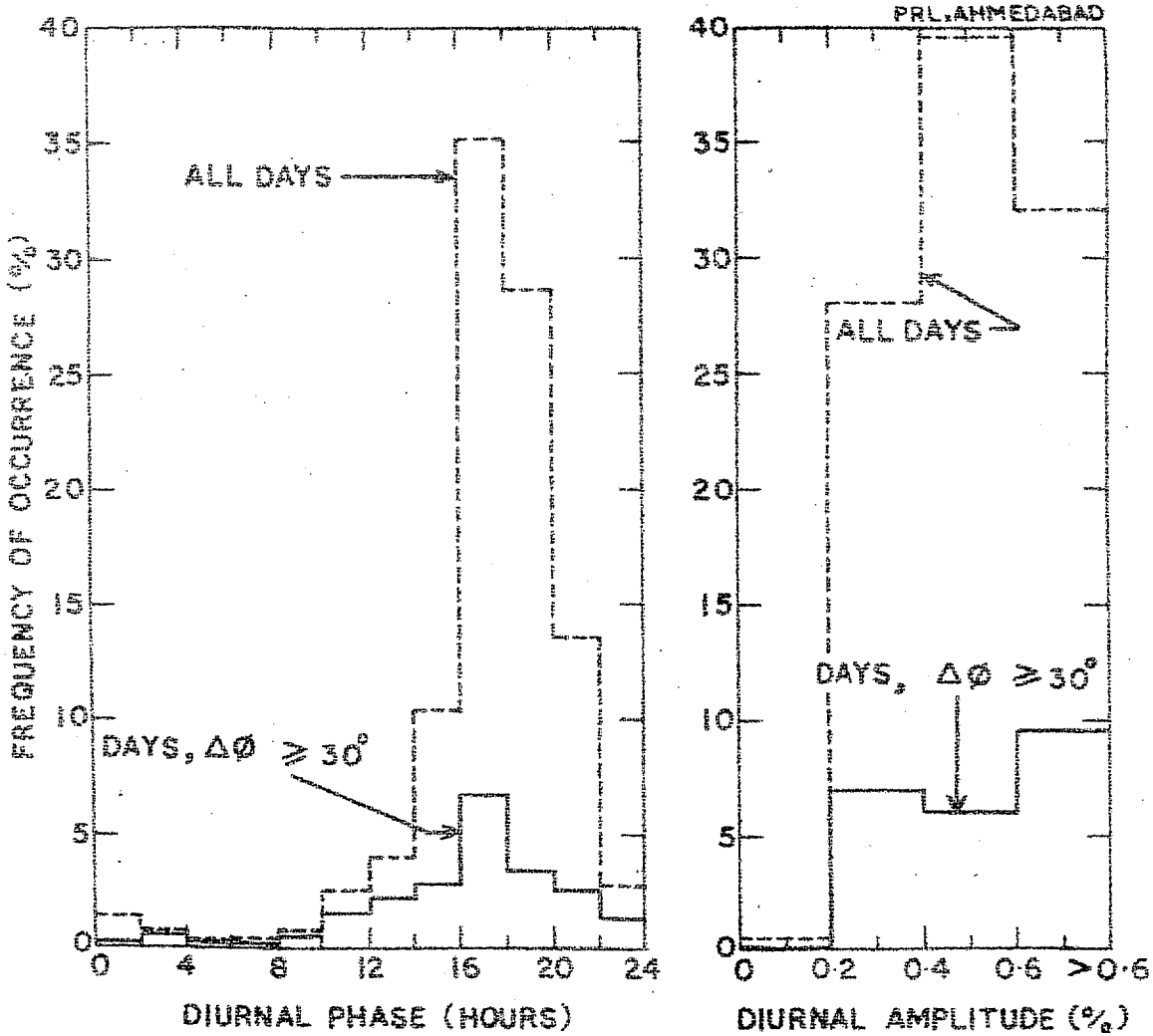

Figure 4.9 - Histograms showing the frequency of occurrence of the diurnal phase and diurnal amplitude observed during non-field aligned days (solid lines) and for all the 400 days (dashed lines) during 1967-68.

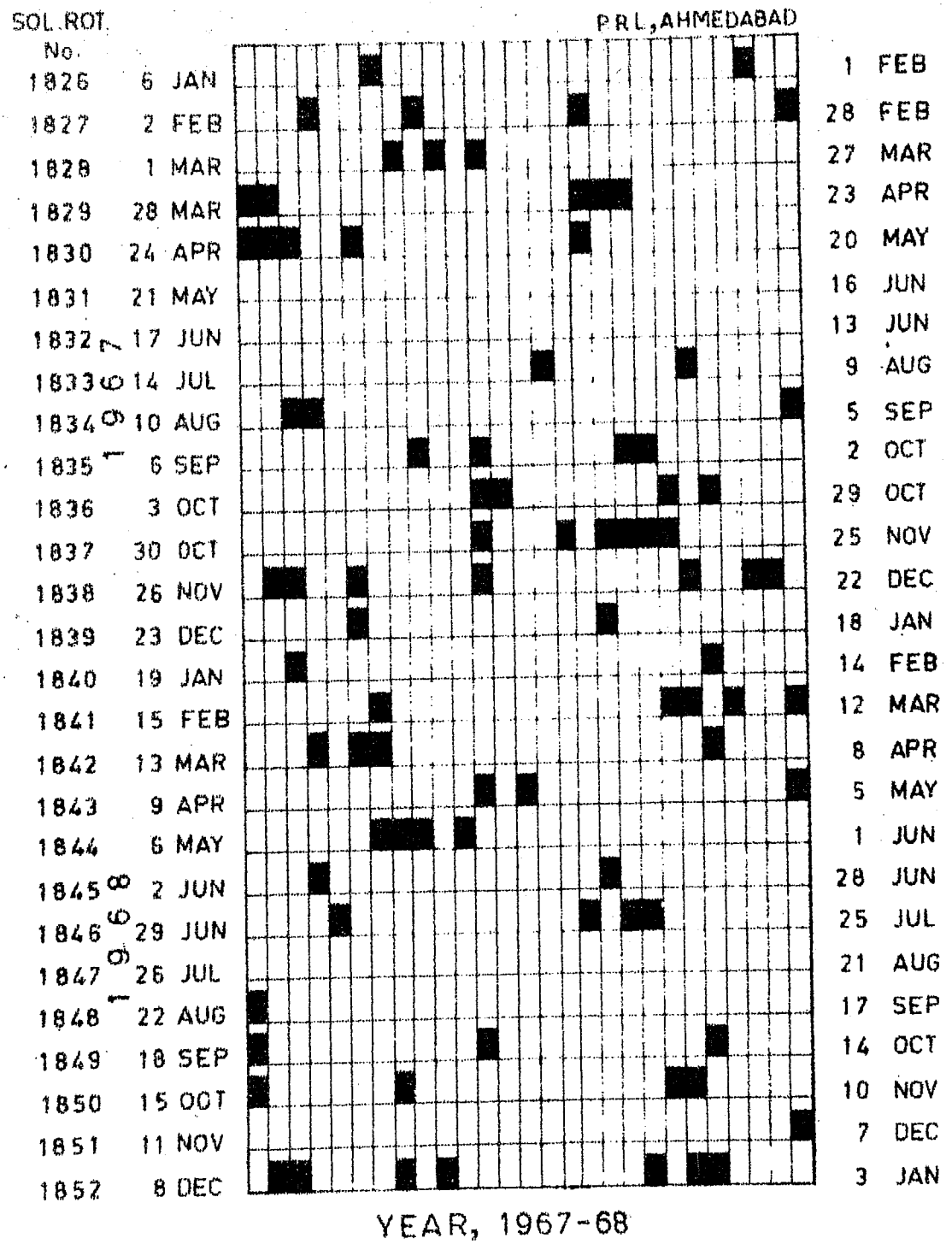

Figure 4.10 - The occurrence of all the non-field aligned days during 1967-68 are shown in a Bartel diagram.

Table 4.1

NON-FIELD ALIGNED TRAINS	DIURNAL ANISOTROPY VECTOR		SEMI-DIURNAL VECTOR		PHASE DIFFERENCE ($\Delta\Phi$) ($\Phi_d - \Phi_B$) (Deg)	ΣK_p Index	SOLAR WIND VELOCITY (kms/sec)	MAGNETIC FIELD VECTOR ($\bar{B}$)	
	Amp. (%)	Pha. (Deg)	Amp. (%)	Pha. (Deg)				Amplitude (Gamma)	Phase (Deg)
28 - 29 Mar. 1967	0.56	275	0.17	53	40	13.5	436	3.3	165
13 - 15 Apr. 1967	1.10	252	0.16	90	44	5.8	270	3.1	129
24 - 26 Apr. 1967	0.64	267	0.04	34	38	16.8	560	2.5	159
12 - 13 Aug. 1967	0.64	158	0.24	50	41	13.0	-	2.5	121
24 - 25 Sep. 1967	0.76	248	0.05	127	60	12.2	-	2.9	154
14 - 15 Oct. 1967	0.32	282	0.11	157	47	16.8	513	4.8	163
16 - 19 Nov. 1967	0.38	355	0.17	137	42	7.8	-	3.1	135
27 - 28 Nov. 1967	0.52	203	0.15	117	33	20.5	400	4.2	103
20 - 21 Dec. 1967	0.38	209	0.18	140	62	28.3	-	3.5	123
6 - 7 Mar. 1968	0.34	10	0.13	132	70	12.0	418	3.9	114
18 - 19 Mar. 1968	0.86	257	0.05	72	41	19.7	595	4.1	145
12 - 14 May 1968	0.82	271	0.10	120	45	24.1	488	3.4	160
4 - 5 Nov. 1968	0.80	266	0.05	37	42	21.6	-	4.3	153
9 - 10 Dec. 1968	0.36	155	0.09	57	77	16.2	-	3.7	146
29 - 30 Dec. 1968	0.58	317	0.21	74	51	16.2	-	4.7	95

Table 4.1 - Shows all the non-field aligned trains of days along with the observed diurnal and semi-diurnal variation vectors and other associated solar terrestrial parameters listed for each event during 1967-68.

IPMF vectors. It is seen from the table that in general no one to one correlation exists between the occurrence of non-field aligned days and other parameters described in the table. In other words such days do not seem to be associated with any abnormal solar terrestrial features such as enhanced diurnal or semi-diurnal variation, high $\sum K_p$ index or large solar wind velocity. Likewise no large cosmic ray daily mean intensity variations, Forbush decreases or 27-day recurrences are observed during non-field aligned trains of days. Since the cosmic ray propagation in the interplanetary space is essentially dictated by the characteristics of solar system magnetic fields and its configuration, we have examined the observed IPMF parameters both on a daily as well as on a hourly basis for all the non-field aligned days. For further analysis we have selected only trains of non-field aligned days occurring in two or more consecutive days, which essentially indicate a quasi-permanent anomalous condition causing a significant transverse diffusion current in the interplanetary medium.

4.6 Interplanetary magnetic field characteristics on a day to day basis:

Fig. 4.11 shows the observed daily mean IPMF vectors for a number of non-field aligned trains of days. In the same figure the IPMF vectors for a completely field aligned train of days are also shown for the purpose of comparison. It is clearly

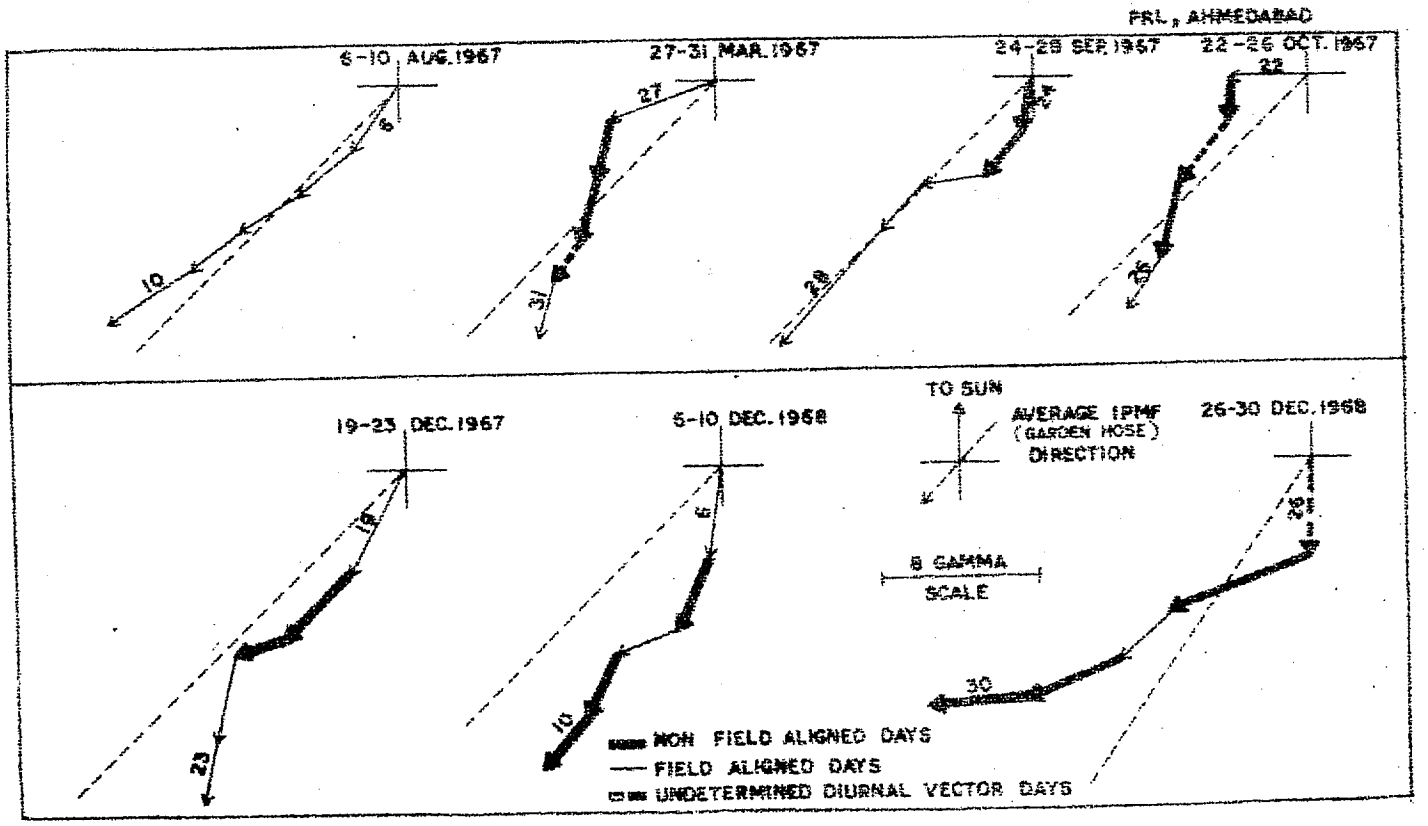

Figure 4.11 - The daily mean IPMF vectors observed during some of the non-field aligned trains of days. The IPMF vectors for a completely field aligned train of days (6 - 10 August 1967) are also shown. Note the large day to day changes ($> 50^{0}$) in the IPMF vectors during non-field aligned days.

evident from the figure that, on trains of days when the diffusion vectors are completely field aligned, the day to day changes in the IPMF azimuth are negligible and the observed IPMF do not show any significant departure from the Archimedean spiral magnetic field configuration. In the case of non-field aligned trains of days presented in Fig. 4.11, the picture is completely different. The observed IPMF azimuth on each day not only shows large deviations from Archimedean spiral direction ($\sim$ 0900 hours) but also a large change from one day to the next, the field azimuth changing by as much as 50 - 90 degrees. This clearly suggests that during the non-field aligned days, the Archimedean spiral IPMF configuration at the orbit of the earth is considerably disturbed, due to the presence of large scale magnetic field irregularities in the interplanetary medium. A closer examination of all the non-field aligned trains of days shows that they can be classified essentially into two groups.

1. Non-field aligned trains of days, on which large change in the IPMF azimuth occurs from one day to the next and which indicate the presence of irregularities of scale sizes $\geqslant$ 1 day.

2. Non-field aligned trains of days which are associated with irregularities of scale sizes less than a day.

4.7 Interplanetary magnetic field characteristics on an hourly basis:

Fig. 4.12 shows the hourly IPMF vectors observed on each day along with the daily mean vectors plotted for a number of completely field aligned trains of days. The figure brings out two important characteristics of hourly IPMF vectors observed on field aligned days.

1. There is no significant hour to hour change in the IPMF vectors observed on the same day.

2. The day to day changes in the IPMF azimuth during field aligned days are quite negligible.

Fig. 4.13 and Fig. 4.14 shows the hourly IPMF vectors plotted for a number of non-field aligned trains of days (Table 4.1) which fall into two different categories. The daily mean field vectors for each day is also shown in the same figure. On non-field aligned trains of days which fall into the first category, the IPMF azimuth changes drastically from one day to the next by as much as 50° - 90° as seen from Fig. 4.13. On non-field aligned trains of days which fall into the second category even though the daily mean field vector does not show significant deviations from one day to the next, the hourly field vectors exhibit violent disturbance due to the presence of irregularities with typical scale sizes between 4 - 6 hours. From the data presented above it is quite clear that the most significant characteristics

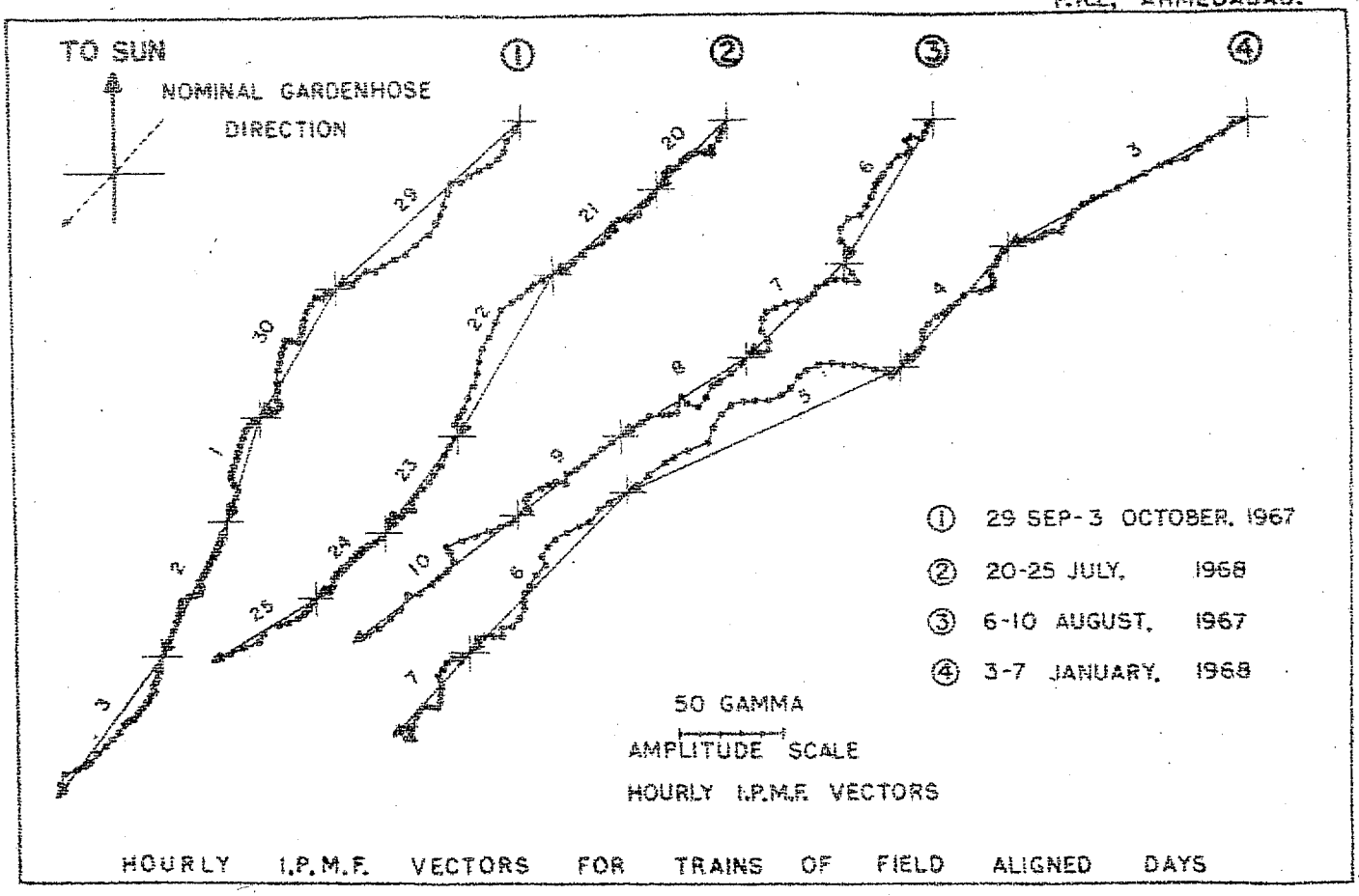

Figure 4.12 - The hourly IPMF vectors observed on a few field aligned trains of days on which the diffusion vectors are completely field aligned. The daily mean field vectors are also shown.

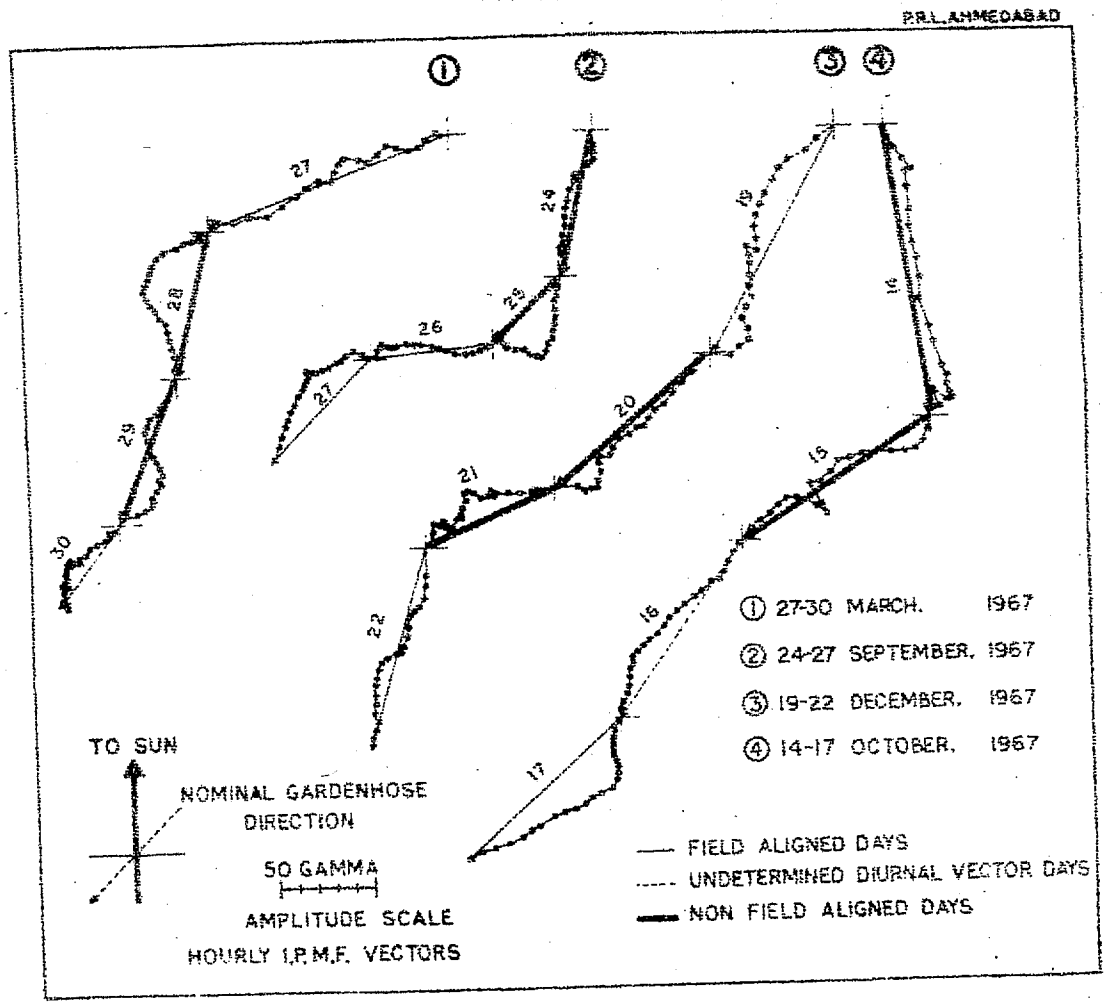

Figure 4.13 - The hourly IPMF vectors observed during a few typical non-field aligned trains of days which shows large day to day changes in the IPMF azimuth indicating the presence of irregularities of scale sizes $\geq$ 1 day.

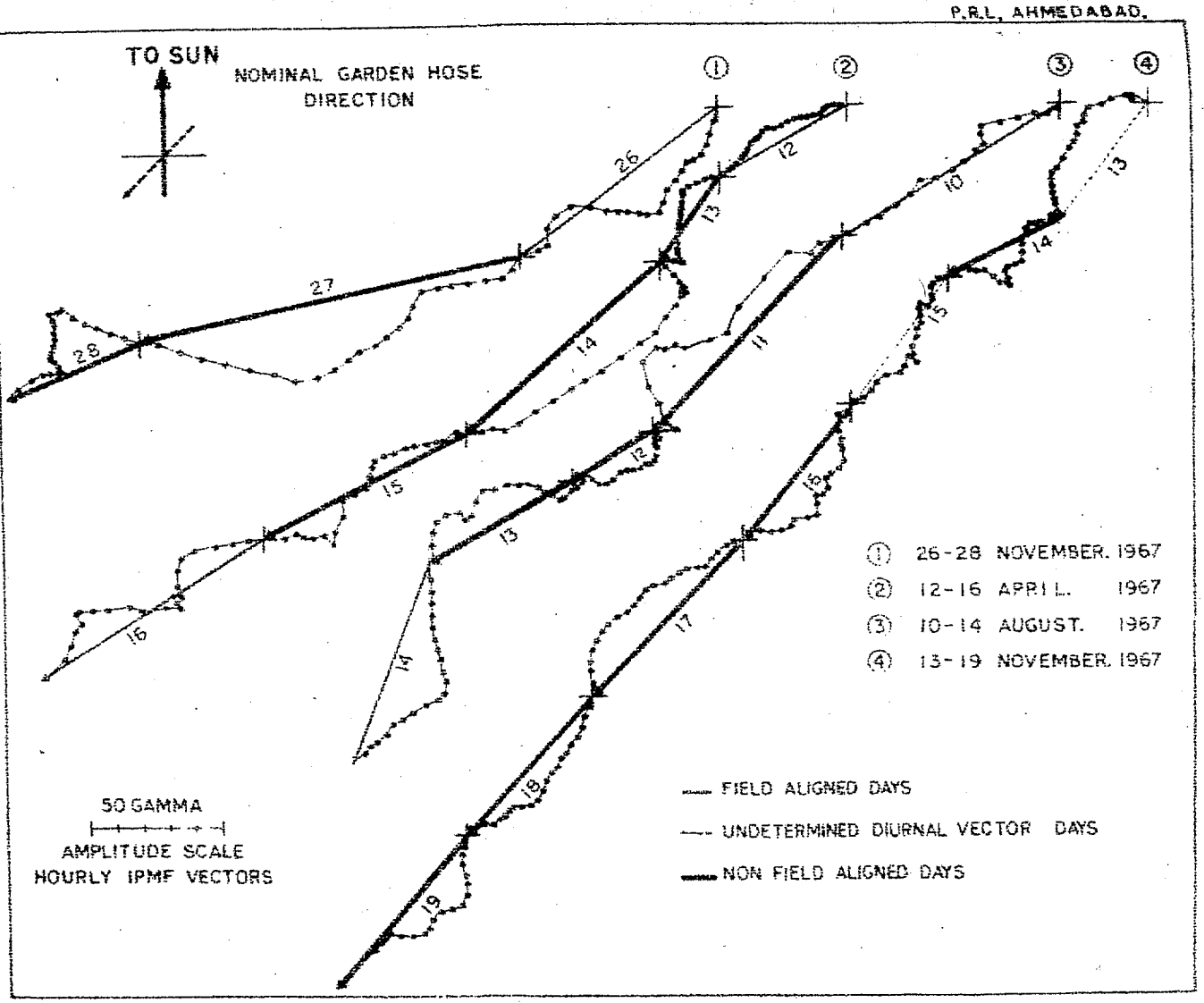

Figure 4.14 - The hourly IPMF vectors observed during non-field aligned trains of days which did not show large day to day changes in the IPMF azimuth. Note the continual presence of small scale irregularities of scale sizes > 4 hours on these days.

of non-field aligned days is the continual presence of field irregularities with scale sizes ranging from 4 hours to 1 day, in the interplanetary magnetic field observed at the orbit of the earth.

4.8 Power spectrum :

For a more quantitative estimation of the scale sizes of magnetic field irregularities, the hourly IPMF data during some of the non-field aligned trains of days have been subjected to power spectrum analysis (described in chapter II). Due to the statistical limitation of the data available, out of 8 events shown in Fig. 4.13 and 4.14, we have selected only two events occurring on 27 - 30 March 1967 and 13 - 19 November 1967 for which continuous hourly IPMF data is available for atleast a period of 5 days. The results of the power spectrum analysis for the two events are shown (dots) in Fig. 4.15 and 4.16 respectively. For purposes of comparison the power spectral density distribution for a typical completely field aligned train of days is also shown in the same figure (open circles) It is clearly seen from the figure 4.15 that inspite of the large statistical errors due to the usage of limited data, during the event 27 - 30 March 1967, a prominent spectral peak is observed corresponding to a scale size of $\sim$ 4.6 hours. Likewise as seen from figure 4.16 the power spectral density distribution during the event occurring on 13-19 November 1967 shows

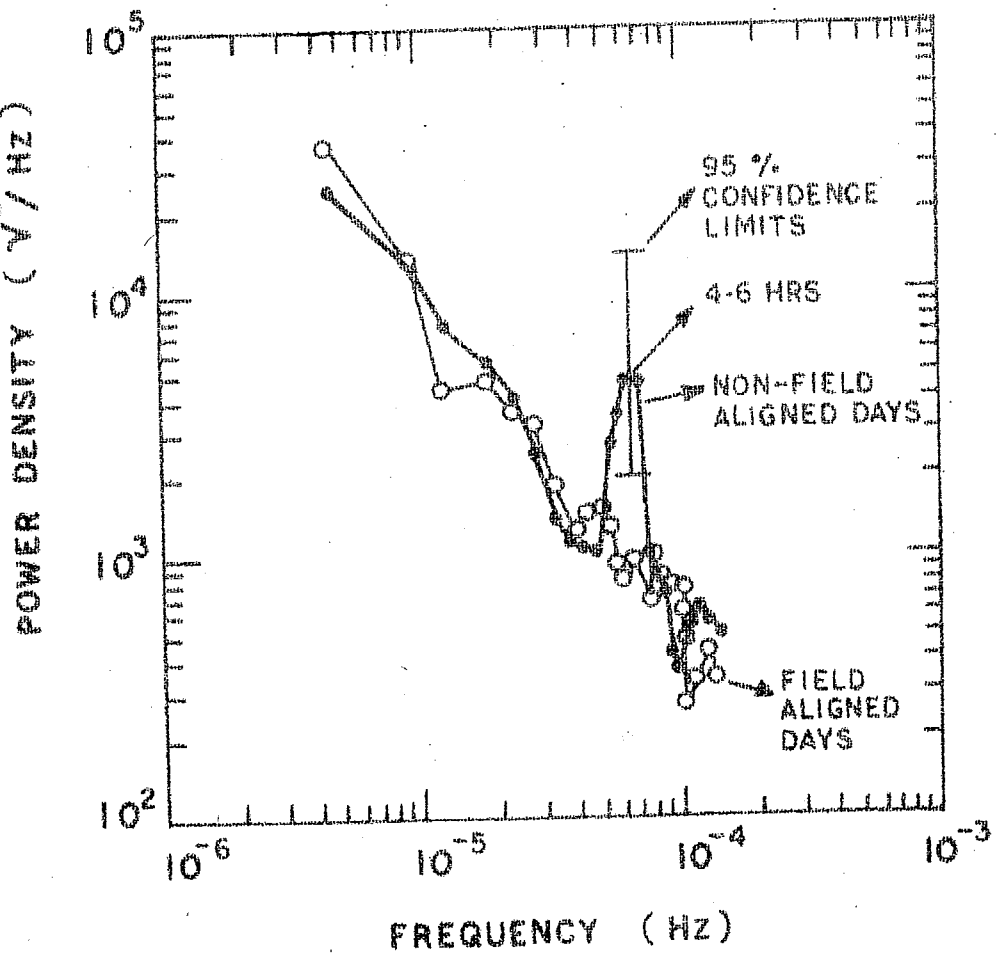

Figure 4.15 - The power density distribution of the radial component of the IPMF as a function of frequency during the non-field aligned train occurring on 27 - 30 March 1967 (dots). The power spectrum for a completely field aligned train of days occurring on 29 September - 3 October 1967 (open circles) is also shown. Note the presence of a spectral peak around 4.6 hours during non-field aligned train of days.

significant peaks corresponding to 4.3 hours and 6.6 hours. Whereas we notice the complete absence of such peaks in case of completely field aligned train of days.

4.9 Discussion:

It is well known that the irregularities present in the IPMF act as scattering centres and produce random changes in the pitch angle of the cosmic ray particles as they diffuse along the magnetic fields present in the interplanetary medium. The integrated effect of a large number of such irregularities is to produce a three dimensional random walk of cosmic ray particles. The resonant scattering is found to be maximum when the irregularities present have scale sizes of $\sim 2\pi\rho$, where ρ is the particle gyro-radius. In other words to produce an appreciable scattering of particles of energy ≥ 1 GeV the minimum scale size of the irregularities should be $>$ 4 hours, for a mean solar wind velocity of $\sim$400 kms/sec and in a magnetic field of $\sim 5\gamma$. Recently Owens (1973) and Owens and Jokipii (1973, 1974), from a power spectrum analysis of the IPMF observations demonstrated that the cosmic ray scintillations observed at ground based monitors at low frequencies ($< 5 \times 10^{-5}$ Hz $>$ 6 hours) are caused mainly by the fluctuating component of the IPMF. They have also suggested that the most likely mechanism for high energy cosmic ray scintillation observed at low frequencies is the strong interaction of cosmic ray particles with the irregularities present in the IPMF, during their propagation in the interplanetary space. Their results are consistent with our findings that non-field aligned trains

of days are characterised by strong magnetic field irregularities of scale sizes $>$ 4 hours.

Following Gleeson (1969) and Forman and Gleeson (1970, 1974), we represent the net streaming of cosmic ray particles in the interplanetary medium by the complete expression.

$$S = S_c - K_{||} \left(\frac{\partial U}{\partial r}\right)_{||} - K_{\perp} \left(\frac{\partial U}{\partial r}\right)_{\perp} - A \left(\frac{\partial U}{\partial r} \times \frac{\bar{B}}{B}\right) \qquad (4.2)$$

If we consider that the transverse diffusion and transverse gradient currents are in general negligible then the III and IV term of the equation 4.2 can be neglected. In other words the equation 4.2 can be written as

$$S = S_c - K_{||} \left(\frac{\partial U}{\partial r}\right)_{||} \quad , \; S_c = CUV_p \qquad (4.3)$$

Interpreting in terms of physical parameters, the net streaming is essentially a result of radial convection and a field aligned diffusion current. The data presented in preceding sections shows that this indeed is the case both on an average as well as on a day to day basis for most of the days ($\sim$80%). By vectorially separating the average diffusion vectors into parallel and perpendicular components, we have estimated an upper limit for the ratio of $K_{\perp}/K_{||}$ as 0.05 for all these days. However a detailed examination of diurnal anisotropy on a day to day basis presented in this chapter shows that on approximately $\sim$ 20% of the days the diurnal variation cannot be fully explained in terms of only the

I and II term of the equation 4.2. In other words on such days the III and IV term do play a significant role indicating the presence of a significant transverse diffusion current in the interplanetary medium. From the observed mean phase difference $\Delta\phi \sim 45^{\circ}$ on non-field aligned days (Table 4.2), we can estimate the ratio of $K_{\perp}/K_{\parallel}$ on these days which works out to be of $\sim$ 1. A critical examination of the interplanetary field parameters shows that, such transverse diffusion currents are caused by magnetic field irregularities of scale sizes $>$ 4 hours which is in qualitative agreement with other observations. The existence of one to one correlation between the interplanetary field irregularities and anomalous diurnal variation vectors observed by ground based neutron monitors establishes the possibility of using ground based cosmic ray observations for inferring the detailed characteristics of magnetic field structure in the interplanetary medium.

4.10 Low amplitude diurnal variation:

Finally we deal with an interesting class of days on which the diurnal vectors show extremely negligible amplitudes ($\leq$ 0.2%). Examples of occurrence of such days was first established by Fisk and Vanhollebeke (1971) and Ananth et al (1971), even though it has been noted by many other workers. It is well known that the presence of cosmic ray density gradient perpendicular to the ecliptic plane will essentially result in an additional

streaming of cosmic ray particles in the ecliptic plane, cancelling the diurnal variation vector on such days (Parker, 1964, 1965, 1967; Subramanian and Sarabhai, 1967; Quenby and Hashim, 1969; Hashim and Bercovitch, 1971; Swinson, 1971). Referring back to equation 4.2 we observe that the derivatives arising out of the III and IV term of the equation 4.2 which refer to transverse diffusion and transverse gradient currents can often effectively cancel the corotational diurnal vector resulting in either a cancellation or a significant reduction of the observed diurnal amplitude. Hence, it is of considerable importance to examine the characteristics of low amplitude days.

The low amplitude of the diurnal vectors and consequently the large statistical errors associated, however make it extremely difficult for a critical examination of diurnal variation observed on such days. Since quite often days having low amplitude diurnal variation occur in trains of two or more consecutive days, we have selected a few trains of days (Ananth et al, 1971) which essentially represent a quasi-permanent anomalous condition in the interplanetary medium. By selection of such trains of days, we are able to improve the statistical significance and then able to make a qualitative study of the characteristics of low amplitude trains of days.

4.11 Characteristics of low amplitude trains of days:

The main criteria for the selection of low amplitude days is that atleast 4 or more consecutive days must exhibit a diurnal amplitude of less than 0.2%. Out of 25 such events which occurred during the period 1965-72, we have selected only 5 events for our study, which are not associated with large cosmic ray intensity variations or Forbush decreases. Fig. 4.17 shows the hourly cosmic ray intensity deviations observed at Deep River for a few typical low amplitude diurnal wave trains. It is clearly evident from the figure that on these days the normal diurnal variation is completely absent and the cosmic ray intensity remained almost isotropic during this period.

Table 4.2 lists the five low amplitude wave trains along with the observed mean diurnal anisotropy vectors obtained using the data from a number of neutron monitoring stations and the convection vectors estimated from ΣK_p index (chapter III). The field azimuth listed in the table is also derived using wind velocities estimated from ΣK_p index as the 'in situ' space-craft observations are not available during these events. Table 4.2 also shows the phase difference $\Delta\phi$ between the diffusion vectors (ϕ_d) and the field azimuth (ϕ_B) computed for each event. A significant point to be noted in the table is that the phase difference $\Delta\phi \geq 30^\circ$ in all the cases indicate that the diurnal variation observed

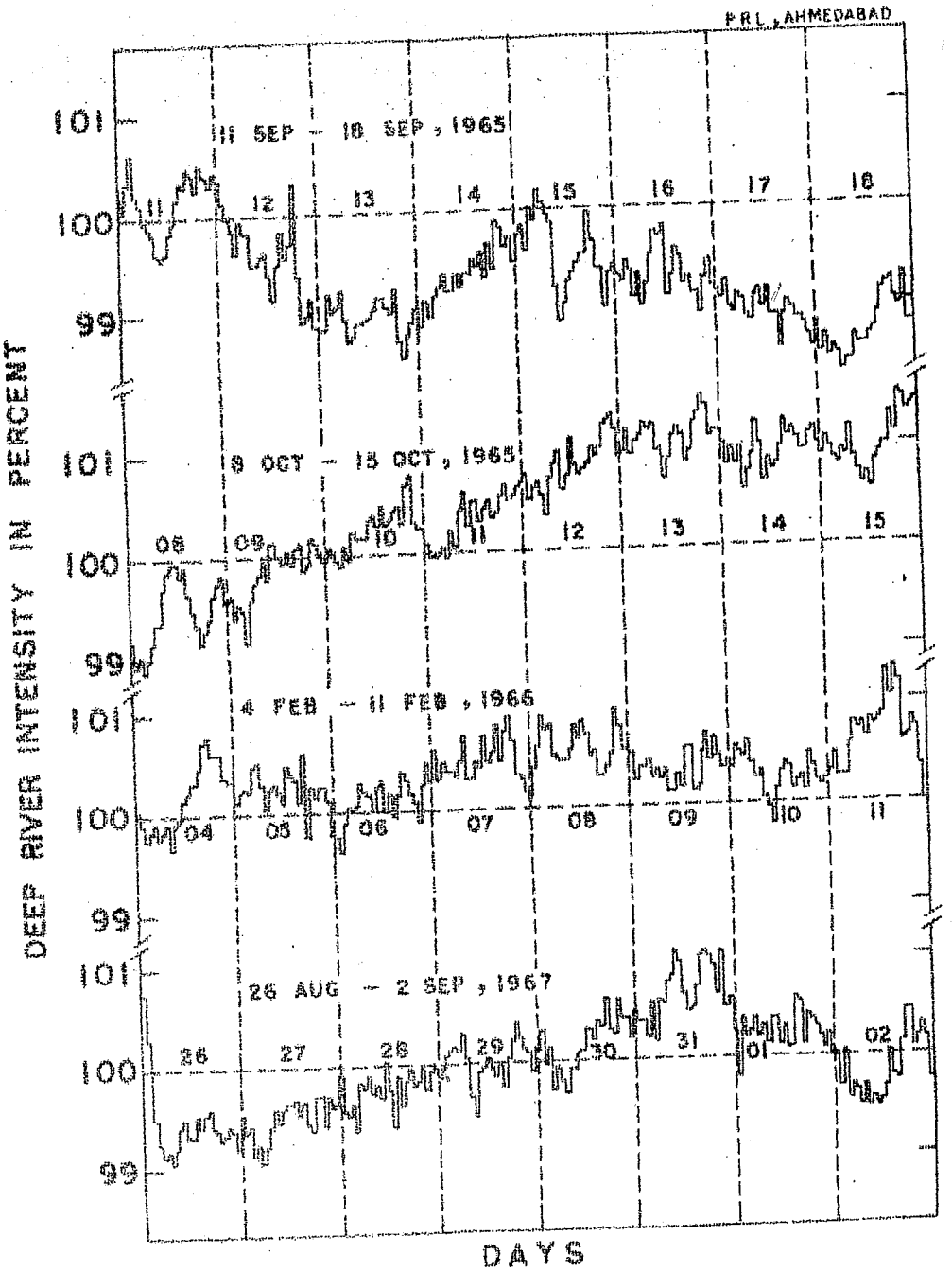

Figure 4.17 - The hourly cosmic ray intensity deviations observed at Deep River is shown for a few typical low diurnal amplitude wave trains. Note the absence of normal diurnal variation during these days.

Table 4.2

Sr. No.	Low diurnal amplitude wave train event	DIURNAL ANISOTROPY VECTOR (δ)		CONVECTION VECTOR (δ_c)	DIFFUSION VECTOR (δ_d)		FIELD AZIMUTH (Φ_B)	PHASE DIFFERENCE ($\Delta\Phi$)
		Amplitude (%)	Phase (Deg)	Amp. (%)	Amp. (%)	Pha. (Deg)	Phase (Deg)	($\Phi_d - \Phi_B$) (Deg)
1.	08 Apr. - 13 Apr. 1965	0.16± .04	262± 6	0.38	0.39	336	314	22 ± 6
2.	11 Oct. - 14 Oct. 1965	0.10± .03	288±15	0.38	0.42	347	313	34 ±15
3.	05 Feb. - 10 Feb. 1966	0.08± .03	267±17	0.39	0.39	348	314	34 ±17
4.	12 Jun. - 15 Jun. 1967	0.09± .05	334±23	0.40	0.48	6	315	51 ±23
5.	26 Jul. - 30 Jul. 1972	0.10± .02	285±14	0.39	0.43	347	314	33 ±14
	Mean	0.10± .02	285± 8	0.39	0.41	350	314	36 ± 8

Table 4.2 - Selected low diurnal amplitude wave trains along with the observed average diurnal anisotropy vector, convection vector, diffusion vector, field azimuth and the phase difference $\Delta\Phi$ for each event during 1965-72.

on these days has a significant component due to transverse gradient current in addition to simple convection and field aligned diffusion currents in the interplanetary medium.

4.12 Source in the garden-hose hemisphere:

For a more detailed examination of the days, we have constructed space-time diagrams on each day (chapter II) representing the cosmic ray flux distribution in the interplanetary space as a function of time for all the low amplitude trains listed in table 4.2. Fig. 4.18 shows the average cosmic ray intensity deviations observed in different asymptotic directions in space for one of the low amplitude wave trains occurring on 5 - 10 Feb. 1966 (Table 4.2). The figure shows that the cosmic ray intensity deviations in the garden-hose hemisphere is almost equal to that of the anti-garden-hose hemisphere, indicating that on these days cosmic ray flux distribution in the interplanetary space is almost isotropic. Such an observation is quite contrary to the cosmic ray flux distribution observed when the normal equilibrium (corotational) diurnal anisotropy is present, during which one normally observes a small depression ($\sim$ - 0.4%) in the garden-hose hemisphere and also a small enhancement of cosmic ray flux ($\sim$ + 0.4%) in the anti-garden-hose hemisphere. The absence of a depression ($\sim$ -0.4%) in the garden-hose hemisphere during the event (Fig. 4.18) clearly indicate the presence of a source of cosmic ray particles established in

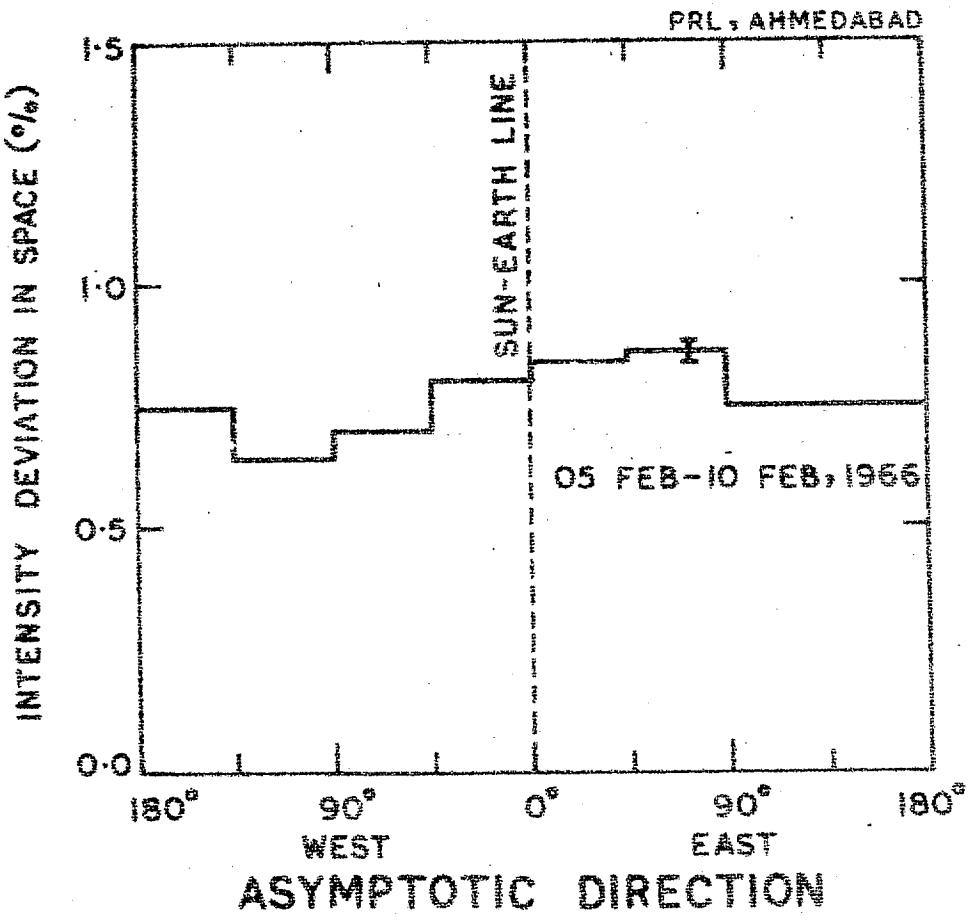

Figure 4.18 - The average cosmic ray intensity deviation in different asymptotic directions plotted in the form of a histogram for the low amplitude wave train event occurring on 5 - 10 February 1966.

the garden-hose hemisphere. However a clear picture of the cosmic ray source established in the garden-hose hemisphere and its time evolution in space can be obtained only by constructing space-time diagrams on each day during the event. Fig. 4.19 shows the observed cosmic ray intensity deviation in each sector, plotted in the form of a histogram, on a day to day basis during 4 - 11 Feb. 1966. It is quite evident from the figure that the cosmic ray intensity in the 6 - 9 and 9 - 12 hours direction which was normal on 4 Feb. suddenly increased to about $\sim$ 1% on 7 and 8 Feb. and remained at that level continuously for few days, that is upto 11 Feb. Further we observe that during these days the normal garden-hose depression ($\sim -0.4\%$) is not only absent but a source ($\sim +1\%$) of cosmic ray flux established in the garden-hose hemisphere. The enhanced cosmic ray flux from the garden-hose hemisphere will effectively cancel or reduce the equilibrium corotational diurnal anisotropy which exhibits a streaming along 1800 hours direction.

Discussion:

If we suppose that on these days the normal positive radial cosmic ray density gradient of $\sim$ 5%/AU (chapter III) has a significant component perpendicular to the ecliptic plane, then in addition to a reduced field aligned diffusion component ($\bar{\delta}_d$) a significant transverse gradient current is also established in the interplanetary medium. In such a case

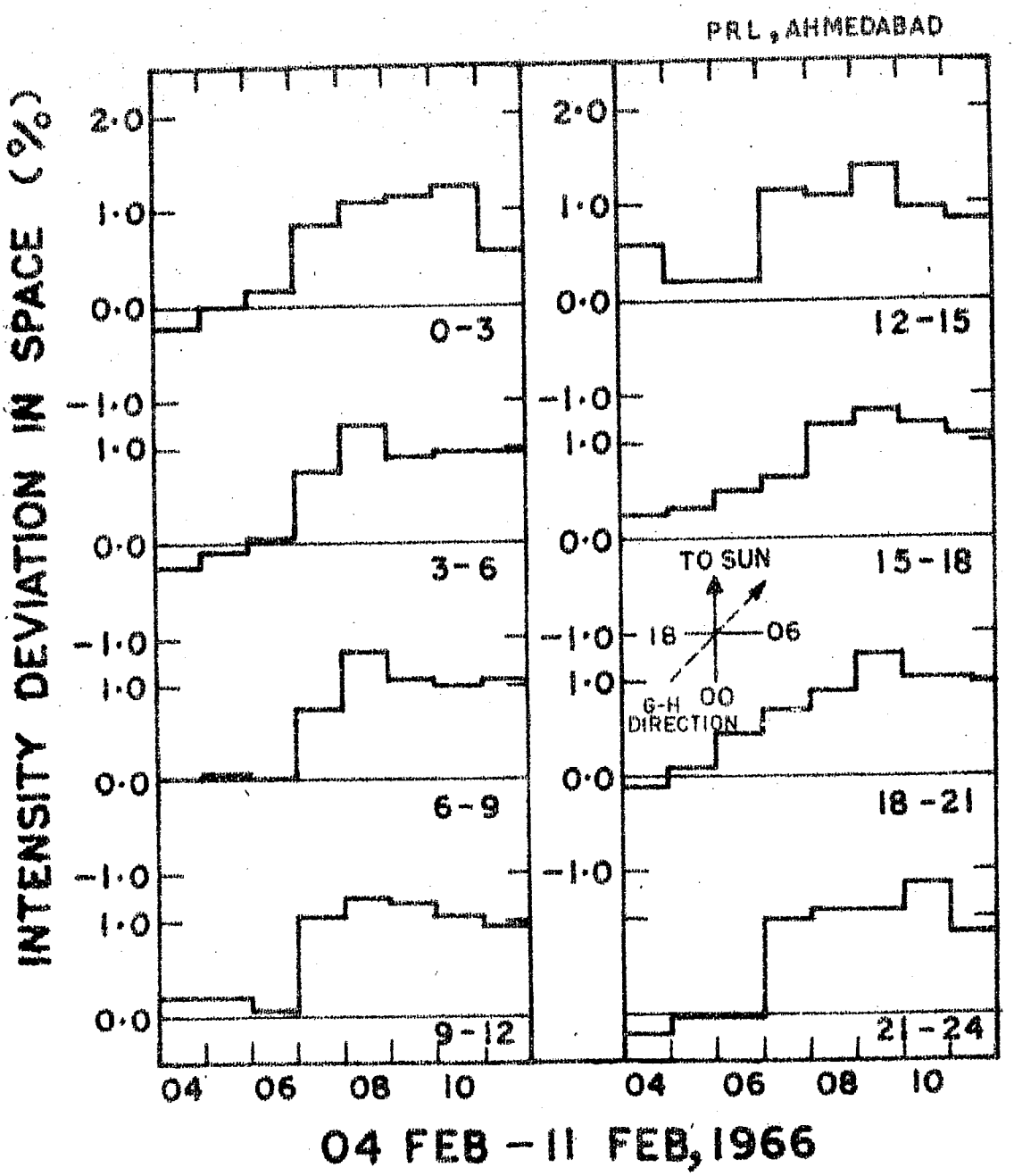

Figure 4.19 - Histograms showing the cosmic ray intensity deviation in each sector during the low amplitude wave train event occurring on 5 - 10 February 1966. Note the establishment of a source of cosmic ray flux in the garden-hose hemisphere.

one can easily show that an additional component caused by the transverse gradient current when superimposed upon normal convection and diffusion will result in an excess of cosmic ray flux either in the sun-ward direction or in the garden-hose hemisphere which ultimately cause a large reduction in the amplitude of diurnal variation. Indeed our observations of low amplitude days indicate the presence of a cosmic ray source established in the garden-hose hemisphere, thus supporting the existence of a significant transverse gradient current in the interplanetary medium. The results presented in preceding sections clearly shows that only on a day to day basis in addition to a normal convection and diffusion currents, transverse diffusion and transverse gradient currents also contribute significantly to the observed diurnal variation.

.....

REFERENCES

Ables, J.G., Barouch, E., and McCracken, K.G.	1967	Planet. Space Sci., 15, 547.
Agrawal, S.P., Ananth, A.G., and Rao, U.R.	1972	Can. J. Phys., 50, 1323.
Ahluwalia, H.S. and Dessler, A.J.	1962	Planet. Space Sci., 9, 195.
Ahluwalia, H.S. and Ericksen, J.H.	1970	Acta. Phys. Hung., 29, Supp. 2, 139.
Alfven, H.	1950	Cosmical Electrodynamics Oxford Press, (London).
Alfven, H.	1954	Tellus, 6, 232.
Allum, F.R., Palmeira, R.A.R., McCracken, K.G., Rao, U.R., Fairfield, D.H., and Gleeson, L.J.	1974	Solar Phys., 38, 227.
Ananth, A.G. and Agrawal, S.P.	1971	Ind. J. Pure and Applied Phys., 9, 498.
Ananth, A.G., Agrawal, S.P., and Rao, U.R.	1971	Proc. 12th Int. Conf. Cosmic Rays, Hobart, 2, 651.
Axford, W.I.	1965a	Planet. Space Sci., 13, 115.
Axford, W.I.	1965b	Planet. Space Sci., 13, 1301.
Axford, W.I.	1968	Space Sci. Rev., 8, 331.

Bachelet, F., Balata, P., Dyring, E., and Iucci, N.	1965	Nuovo Cimento, 35, 23.
Bachelet, F., Iucci, N., Villoresi, G., and Zongrilli, N.	1972	Nuovo Cimento, 11B, 1.
Bame, S.J., Asbridge, J.R., Hundhausen, A.J., and Strong, I.B.	1967	Trans. Amer. Geophys. Union, Abstract, 48, 190.
Bercovitch, M.	1963	Proc. Int. Conf. Cosmic Rays, Jaipur (India), 332.
Bercovitch, M.	1971a	Proc. Int. Conf. Cosmic Rays (Hobart), Rapporteur Report.
Bercovitch, M.	1971b	Proc. Int. Conf. Cosmic Rays (Hobart) 2, 579.
Bland, C.J.	1962	Phil. Mag. 7, 1487.
Brunberg, E.A. and Dattner, A.	1954	Tellus, VI 1, 73.
Bukata, R.P., McCracken, K.G., and Rao, U.R.	1968	Can. J. Phys., 46, 994.
Burlaga, L.F.	1971	Space Sci. Rev., 12, 600.
Burlaga, L.F. and Ness, N.F.	1968	Can. J. Phys., 46, S962.
Carmichael, H.	1964	Cosmic rays, IQSY Instruction Manual No.7 (London).

Carmichael, H. and Bercovitch, M.	1969	Can. J. Phys., 47, 2073.
Carmichael, H. and Steljes, J.F.	1969	World Data Centre A, Rep., UAG-5.
Carmichael, H., Bercovitch, M., Shea, M.A., Magidin, M., and Peterson, R.W.	1968	Can. J. Phys., 46, S1006.
Carmichael, H., Shea, M.A., and Peterson, R.W.	1969	Can. J. Phys., 47, 2057.
Chapman, S. and Bartels, J.	1940	Geomagnetism, II Oxford University Press.
Coleman, P.J., Jr.	1966	J. Geophys. Res., 71, 5509.
Compton, A.H. and Getting, I.A.	1935	Phys. Rev., 47, 817.
Debrunner, H. and Fluckiger, E.	1971	Proc. Int. Conf. Cosmic Rays (Hobart), 3, 911.
Dessler, A.J.	1967	Rev. Geophys., 5, 1.
Dorman, L.I.	1957	Cosmic Ray Variations, State Pub. House, Moscow.
Duggal, S.P., and Pomerantz, M.A.	1962	Phys. Rev. Letters, 8, 215.
Duggal, S.P., Forbush, S.E., and Pomerantz, M.A.	1967	Nature, 214, 154.

Duggal, S.P., Forbush, S.E., and Pomerantz, M.A.	1970	J. Geophys. Res., 75, 1150.
Faller, A.M. and Marsden, P.L.	1965	Proc. Int. Conf. Cosmic Rays (London) 1, 231.
Fenton, A.G., McCracken, K.G., Rose, D.C., and Wilson, B.G.	1959	Can. J. Phys., 37, 970.
Fermi, E. and Rossi, B.	1933	Atti Accad. Nazl. Lincei, Rend. 17, 346.
Fisk, L.A. and Vanhollebeke, M.	1971	Proc. 12th Int. Conf. Cosmic Rays (Hobart), 2, 542.
Fisk, L.A. and Axford, W.I.	1968	J. Geophys. Res., 73, 4396.
Fisk, L.A. and Axford, W.I.	1969	J. Geophys. Res., 74, 4973.
Forbush, S.E.	1938	Phys. Rev., 54, 975.
Forbush, S.E.	1958	J. Geophys. Res., 63, 651.
Forbush, S.E.	1967	J. Geophys. Res., 72, 4937.
Forbush, S.E.	1969	J. Geophys. Res., 74, 3451.
Forbush, S.E.	1973	J. Geophys. Res., 78, 7933.
Forman, M.A.	1968	Can. J. Phys., 46, S1087.

Forman, M.A. and Gleeson, L.J.	1970	Preprint, Monash University.
Forman, M.A. and Gleeson, L.J.	1974	Astrophys. and Space Sci., (under publication).
Gleeson, L.J.	1969	Planet. Space Sci., 17, 31.
Gleeson, L.J.	1971	Proc. Int. Conf. Cosmic Rays, (Hobart), Rapporteur Report .
Gleeson, L.J. and Axford, W.I.	1967	Astrophys. J., 149, L115.
Gleeson, L.J. and Axford, W.I.	1968a	Astrophys. Space Sci., 2, 431 .
Gleeson, L.J. and Axford, W.I.	1968b	Astrophys. J., 154, 1011 .
Gold, T.	1960	Astrophys. J. Supp 4, 406.
Gosling, J.T., Hansen, R.T., and Bame, S.J.	1971	J. Geophys. Res., 76, 1811 .
Gringauz, K.I., Kurt, V.G., Moroz, V.I., and Shklovsky, I.S.	1960	Dokl. Akad. Nauk USSR, 132, 1062 .
Harman, C.V. and Hatton, C.J.	1968	Can. J. Phys., 46, S1052 .
Hashim, A. and Thambyahpillai, T.	1969	Planet. Space Sci., 17, 1879 .

Hashim, A. and Bercovitch, M.	1971	Proc. 12th Int. Conf. Cosmic Rays (Hobart), 2, 596.
Hashim, A., Bercovitch, M., and Steljes, J.F.	1972	Solar Phys., 22, 220.
Hasselmann, K. and Wibberentz, G.	1968	Z. Geophys., 34, 353.
Hatton, C.J.	1971	Prog. Elementary Particle and Cosmic Ray Physics, X, North-Holland Pub. Co., Amsterdam, 1.
Hatton, C.J. and Carmichael, H.	1964	Can. J. Phys., 42, 2443.
Hatton, C.J., Marsden, P.L., and Willetts, A.C.	1968	Can. J. Phys. 46, S915.
Hedgecock, P.C.	1963	Int. Conf. on Cosmic Rays, Jaipur (India).
Hedgecock, P.C., Quenby, J.J., and Webb, S.	1972	Nature, 240, 173.
Hughes, E.B. and Marsden, P.L.	1966	J. Geophys. Res., 71, 1435.
Hughes, E.B., Marsden, P.L., Brooke, G., Meyer, M.A., and Wolfendale, A.W.	1964	Proc. Phys. Soc. London, A83, 239.
Hundhausen, A.J.	1968	Space Sci. Rev., 8, 690.

Hundhausen, A.J.	1970	Rev. Geophys. and Space Phys., 8, 729.
Jacklyn, R.M. and Humble, J.E.	1965	Australian J. Phys., 18, 451.
Jacklyn, R.M., Duggal, S.P., and Pomerantz, M.A.	1970	Acta. Phys. Hung., 29, Supp. 2, 47.
Jokipii, J.R.	1966	Astrophys. J., 146, 480.
Jokipii, J.R.	1967	Astrophys. J., 149, 405.
Jokipii, J.R. and Coleman, P.J., Jr.	1968	J. Geophys. Res., 73, 5495.
Jokipii, J.R. and Parker, E.N.	1967	Planet. Space Sci. 15, 1375.
Jokipii, J.R. and Parker, E.N.	1968	Phys. Rev. Letters, 21, 44.
Jokipii, J.R. and Parker, E.N.	1969	Astrophys. J., 155, 777.
Kane, R.P.	1964	Nuovo Cimento, 32, 273.
Kane, R.P.	1966	Nuovo Cimento, 45, 8.
Krymskiy, G.F.	1964	Geomag. and Aeronomy, 4, 763.
Lapointe, S.M. and Rose, D.C.	1962	Can. J. Phys., 40, 687.

Lemaitre, G. and Vallarta, M.S.	1933	Phys. Rev., 43, 87.
Lockwood, J.A.	1971	Space Sci. Rev., 12, 658.
Lockwood, J.A. and Webber, W.R.	1967	J. Geophys. Res., 72, 3395.
Mathews, T., Venkatesan, D., and Wilson, B.G.	1969	J. Geophys. Res., 74, 1218.
Mathews, T., Quenby, J.J., and Sear, J.	1971	Nature, 229, 246.
McCracken, K.G.	1962	J. Geophys. Res., 67, 447.
McCracken, K.G. and Rao, U.R.	1965	Proc. Int. Conf. Cosmic Rays (London), 1, 213.
McCracken, K.G. and Ness, N.F.	1966	J. Geophys. Res., 71, 3315.
McCracken, K.G. and Rao, U.R.	1966	Planet. Space Sci., 14, 649.
McCracken, K.G. and Rao, U.R.	1970	Space Sci. Rev., 11, 155.
McCracken, K.G., Rao, U.R., and Shea, M.A.	1962	M.I.T. Tech. Rep. No.77.
McCracken, K.G., Rao, U.R., and Lefan, B.W.	1966a	Preprint South West Centre for Advanced Studies, Dallas, Texas No. DASS-66-1.

McCracken, K.G., Rao, U.R., and Bukata, R.P.	1966b	Phys. Rev. Letters, 17, 928.
McCracken, K.G., Rao, U.R., and Bukata, R.P.	1967	J. Geophys. Res., 72, 4293.
McCracken, K.G., Rao, U.R., and Ness, N.F.	1968	J. Geophys. Res., 73, 4159.
McCracken, K.G., Rao, U.R., Bukata, R.P., and Keath, E.P.	1971	Solar Phys., 18, 100.
McCracken, K.G., Rao, U.R., Fowler, B.C., Shea, M.A., and Smart, D.F.	1965	IQSY Instruction Manual No.10.
Mercer, J.B. and Wilson, B.G.	1968	Can. J. Phys., 46, S849.
Michel, F.C.	1967	J. Geophys. Res., 72, 1917.
Morrison, P.	1956	Phys. Rev., 101, 1397.
Neher, H.V.	1952	Prog. in Cosmic Ray Physics, I, Interscience Pub.
Ness, N.F. and Wilcox, J.M.	1966	Astrophys. J., 143, 13.
Ness, N.F., Scearce, C.S., and Cantarano, S.	1966	J. Geophys. Res., 71, 3305.
Ness, N.F., Scearce, C.S., and Seek, J.B.	1964	J. Geophys. Res., 69, 3531.
O'Gallagher, J.J.	1972	Rev. Geophys. and Space Phys., 10, 821.

Ostman, Bo. and Awadalla, E.	1970	Preprint Cosmic Ray Group Institute of Phys., Uppsala.
Owens, A.J.	1973	Ph.D. Thesis, Calif. Inst. of Tech., Pasadena.
Owens, A.J. and Jokipii, J.R.	1973	Astrophys. J., 181, L147.
Owens, A.J. and Jokipii, J.R.	1974	J. Geophys. Res., 79, 907.
Pai, L.G., Bridge, H.S., Lynn, E.F., and Egidi, A.	1967	Trans. Amer. Geophys. Union, 48, 176.
Parker, E.N.	1958a	Phys. Rev., 110, 1445.
Parker, E.N.	1958b	Astrophys. J., 128, 664.
Parker, E.N.	1960	Astrophys. J., 132, 175.
Parker, E.N.	1963	Interplanetary Dynamical Processes, Interscience, New York.
Parker, E.N.	1964	Planet. Space Sci., 12, 735.
Parker, E.N.	1965	Planet. Space Sci., 13, 9.
Parker, E.N.	1966	Planet. Space Sci., 14, 371.

Parker, E.N.	1967	Planet. Space Sci., 15, 1723.
Parker, E.N.	1969	Space Sci. Rev., 9, 325.
Patel, D., Sarabhai, V., and Subramanian, G.	1968	Planet. Space Sci., 16, 1131.
Pathak, P.N. and Sarabhai, V.	1970	Planet. Space Sci., 18, 81.
Peacock, D.S.	1970	Acta. Phys. Hung., 29, Supp.2, 189.
Phillips, J. and Parsons, N.R.	1962	J. Phys. Soc. Japan (Supp. AII) 17, 519.
Pomerantz, M.A. and Duggal, S.P.	1971	Space Sci. Rev., 12, 75.
Pomerantz, M.A., Duggal, S.P., and Nagashima, K.	1962	J. Phys. Soc. Japan (Supp. AII) 17, 464.
Quenby, J.J.	1967	Handbuch der Physik, 46, 2, 310.
Quenby, J.J. and Hashim, A.	1969	Planet. Space Sci., 17, 1121.
Rao, U.R.	1972	Space Sci. Rev., 12, 719.
Rao, U.R. and Agrawal, S.P.	1970	J. Geophys. Res., 75, 2391.
Rao, U.R. and Sarabhai, V.	1961	Proc. Roy. Soc., A263, 101.

Rao, U.R. and Sarabhai, V.	1964	Planet. Space Sci., 12, 1055.
Rao, U.R., McCracken, K.G., and Venkatesan, D.	1963	J. Geophys. Res., 68, 345.
Rao, U.R., McCracken, K.G., and Bartley, W.C.	1967	J. Geophys. Res., 72, 4343.
Rao, U.R., McCracken, K.G., Allum, F.R., Palmeira, R.A.R., Bartley, W.C., and Palmer, I.	1971	Solar Phys., 19, 209.
Rao, U.R., Ananth, A.G., and Agrawal, S.P.	1972	Planet. Space Sci., 20, 1799.
Roelof, E.C.	1968	Can. J. Phys., 46, S990.
Sarabhai, V., Desai, U.D., and Venkatesan, D.	1954	Phys. Rev., 96, 2213.
Sari, J.W. and Ness, N.F.	1969	Solar Phys., 8, 155.
Schwartz, M.	1959	Nuovo Cimento, 11, Supp. 1, 27.
Severney, A., Wilcox, J.M., Scherrer, P.H., and Colburn, D.S.	1970	Solar Phys., 15, 3.
Shea, M.A., Smart, D.F., and McCracken, K.G.	1965	J. Geophys. Res., 70, 4117.
Shea, M.A., Smart, D.F., McCracken, K.G., and Rao, U.R.	1968	Supp. IQSY Instruction Manual No. 10, Cosmic Ray Tables AFCRL-68-0030.

Shen, M.L.	1968	Supp. Nuovo Cimento, 4, 1177.
Simpson, J.A.	1948	Phys. Rev., 73, 1389.
Simpson, J.A.	1949	Echo Lake Conf. on Cosmic Rays, P. 175 and 252.
Simpson, J.A.	1954	Phys. Rev., 94, 426.
Simpson, J.A. and Wang, J.R.	1967	Astrophys. J. Letters, 149, 73.
Simpson, J.A., Fonger, W., and Treiman, S.B.	1953	Phys. Rev., 90, 934.
Skadron, G.	1967	Preprint, Tech. Report No. 678, University of Maryland.
Singer, S.F., Laster, H., and Lencheck, A.M.	1962	J. Phys. Soc., Japan, (Supp. AII), 17, 583.
Siscoe, G.L., Davis, L., Jr., Coleman, P.J., Jr., Smith, E.J., and Jones, D.E.	1968	J. Geophys. Res., 73, 61.
Snyder, C.W., Neugebauer, M., and Rao, U.R.	1963	J. Geophys. Res., 68, 6361.

Stern, D.	1964	Planet. Space Sci., 12, 973.
Stormer, C.	1955	The Polar Aurora, Oxford, Clarendon Press.
Strong, I.B., Asbridge, J.R., Barne, S.J., and Hundhausen, A.J.	1967	Zodiacal Light and the Interplanetary Medium NASA SP-150. (ed. by J. Weinberg)
Subramanian, G.	1971	J. Geophys. Res., 76, 1093.
Subramanian, G. and Sarabhai, V.	1967	Astrophys. J., 149, 417.
Summer, D.J. and Thompson, D.	1970	Acta. Phys. Hung., 29, Supp. 2, 69.
Swann, W.F.G.	1933	Phys. Rev., 44, 224.
Swinson, D.B.	1971	Proc. Int. Conf. Cosmic Rays (Hobart), 2, 588.
Tanskanen, P.J.	1968	Can. J. Phys., 46, S819.

Thambyahpillai, T. and Elliot, H.	1953	Nature, 171, 918.
Treiman, S.B.	1952	Phys. Rev., 86, 917.
Vallarta, M.S.	1961	Handbuch der Physik, Bd.XLVI/1, S88.
Wainio, K.M., Colvin, T.H., More, K.A., and Tiffany, O.L.	1968	Can. J. Phys., 46, S1048.
Webber, W.R.	1962	Prog. in Elementary Particle and Cosmic Ray Physics, 6, 224.
Webber, W.R.	1967	Proc. Int. Conf. Cosmic Rays (Calgary) Part A, 146.
Webber, W.R. and Quenby, J.J.	1959	Phil. Mag., 4, 654.
Wilcox, J.M. and Ness, N.F.	1965	J. Geophys. Res., 70, 5793.
Wilcox, J.M. and Colburn, D.S.	1972	J. Geophys. Res., 77, 751.
Willetts, A.C., Griffiths, W,K., Hatton, C.J., and Marsden, P.L.	1970	Acta. Phys. Hung., 29, Supp. 2, 61.
Wolfe, J.H., Silva, R.W., McKibbin, D.D., and Mason, R.H.	1966	J. Geophys. Res., 71, 3329.

.....

Reprinted from
Planet. Space Sci. 1972, Vol. 20, pp. 1799 to 1816. Pergamon Press. Printed in Northern Ireland

CHARACTERISTICS OF QUIET AS WELL AS ENHANCED DIURNAL ANISOTROPY OF COSMIC RADIATION

U. R. RAO, A. G. ANANTH and S. P. AGRAWAL
Physical Research Laboratory, Ahmedabad, India

(*Received in final form* 5 *April* 1972)

Abstract—It is shown that the model which has been successful in explaining the anisotropy of low energy cosmic radiation of solar origin in terms of simple convection and field aligned diffusion can also be extended to explain both the quiet and enhanced diurnal variation of cosmic radiation at higher energies. The enhanced diurnal variation which shows a maximum around $\sim$2000 hr is shown to be caused by the superposition of normal convection and enhanced field aligned diffusion due to an enhanced positive density gradient of approximately $\sim$10 per cent/AU. The enhanced gradient in the early part of the event is caused by a depletion of cosmic ray intensity along the garden-hose direction and later in the event ($T \geqslant 4$ days) is caused by an excess flux from the anti-garden-hose direction. The quiet day average diurnal anisotropy of cosmic radiation can be understood as due to an equilibrium between the convective and diffusive flow, resulting in a corotation vector along the 1800 hr direction.

PERGAMON PRESS
OXFORD NEW YORK LONDON PARIS

Planet. Space Sci. 1972, Vol. 20, pp. 1799 to 1816. Pergamon Press. Printed in Northern Ireland

CHARACTERISTICS OF QUIET AS WELL AS ENHANCED DIURNAL ANISOTROPY OF COSMIC RADIATION

U. R. RAO, A. G. ANANTH and S. P. AGRAWAL
Physical Research Laboratory, Ahmedabad, India

(*Received in final form* 5 *April* 1972)

Abstract—It is shown that the model which has been successful in explaining the anisotropy of low energy cosmic radiation of solar origin in terms of simple convection and field aligned diffusion can also be extended to explain both the quiet and enhanced diurnal variation of cosmic radiation at higher energies. The enhanced diurnal variation which shows a maximum around $\sim$2000 hr is shown to be caused by the superposition of normal convection and enhanced field aligned diffusion due to an enhanced positive density gradient of approximately $\sim$10 per cent/AU. The enhanced gradient in the early part of the event is caused by a depletion of cosmic ray intensity along the garden-hose direction and later in the event ($T \geqslant 4$ days) is caused by an excess flux from the anti-garden-hose direction. The quiet day average diurnal anisotropy of cosmic radiation can be understood as due to an equilibrium between the convective and diffusive flow, resulting in a corotation vector along the 1800 hr direction. The observed amplitude of the annual mean diffusive vector is consistent with a positive radial density gradient of $\sim$4·5 per cent/AU, which agrees with other radial gradient measurements. The diffusive vector during both quiet and enhanced anisotropy periods is shown to be along the interplanetary field direction. The ratio of perpendicular to parallel diffusion coefficient under normal conditions is derived to be $\leqslant$0·05 indicating that the transverse gradients, in general, are negligible.

1. INTRODUCTION

The diurnal anisotropy of cosmic radiation has generally been explained in terms of azimuthal corotation (Parker, 1964; Axford, 1965), the magnitude of the corotation itself being subject to modification by transverse diffusion and transverse gradient currents. The experimental observation of 0·4 per cent mean diurnal amplitude along the 1800 hr direction (Rao *et al.*, 1963; McCracken and Rao, 1965; Rao, 1972) using the world wide neutron monitor data has been considered as supporting this concept. The reduction in the observed average amplitude from the expected full corotation vector of $\sim$0·6 per cent has been generally attributed to the transverse diffusion. Recently, however, Subramanian (1971), has made a careful estimation of the various cumulative errors that should be considered, from which he concludes that the observed amplitude during most of the period is in reasonably good agreement with the expected amplitude indicating that the transverse diffusion, on an average basis, is negligible even at relativistic energies. Such an inference is essentially in agreement with the solar flare particle data.

Even though the explanation of the average daily variation in terms of corotation has been considered generally satisfactory, considerable deviations from the above average picture (Rao and Sarabhai, 1964; Patel *et al.*, 1968) exist, on a day to day basis. The existence of consecutive days having abnormally large amplitudes ($\geqslant$ 1 per cent) has been reported by several workers (Mathews *et al.*, 1969; Hashim and Thambyahpillai, 1969), who have concluded that the diurnal variation on such days is generally caused by a depletion of the cosmic ray intensity along the garden-hose direction. Likewise trains of days having abnormally low amplitudes have also been observed in the data (Ananth *et al.*, 1971). Explanation of such abnormal amplitudes using the concept of corotation has not been satisfactory.

In this communication we present detailed data in support of a new concept for the interpretation of the diurnal variation. This concept is that the diurnal variation is completely

explainable in terms of radial convection together with diffusion which is principally along the magnetic field line. The notion that these components might be relevant to the diurnal variation was first mentioned by McCracken *et al.* (1968) as an extension of their studies of the anisotropies of solar cosmic rays. As specific formulation for both solar cosmic-ray events and the diurnal variation, together with a full theoretical basis, was given by Forman and Gleeson (1970), following earlier work on solar event anisotropies by Forman (1970). The important steps taken in this paper are the application of this convection–diffusion concept to explain diurnal variation at high energies and the demonstration that the diffusion component is mainly field aligned. According to this concept the corotational diurnal vector observed, on an average basis, is merely a special case when equilibrium exists between convection and diffusion and there is no net flow of cosmic ray flux into or out of the solar system. On a day-to-day basis, however, the fluctuation in the interplanetary parameters such as solar wind properties and the interplanetary field must necessarily cause an imbalance between convection and diffusion through the introduction of density gradients resulting in abnormal amplitudes for diurnal variation. Brief preliminary reports of observational data, at neutron monitor energies, which support this concept were presented at the 12th International Conference on Cosmic Rays at Hobart, in August 1971 by us (Ananth *et al.*, 1971); Tolba and Lindgren (1971) and Hashim *et al.* (1972) have also reported on this topic. The concept is particularly attractive because the same ideas have been used to explain anisotropy changes throughout solar cosmic-ray burst events (McCracken *et al.*, 1971) and in models which reproduce these (Ng and Gleeson, 1971).

Study of the anisotropy of low energy cosmic radiation of solar origin has clearly indicated that convection is the most important mechanism during the decay of the flare events. During the initial phase of the decay, the observed equilibrium anisotropy is from the sunward direction (McCracken *et al.*, 1967, 1968; McCracken and Rao, 1970; Rao *et al.*, 1971) suggestive of the convective removal of these particles by the solar wind. The equilibrium anisotropy during this period is given by the expression

$$\delta_e = 3C\frac{V_p}{V} \tag{1}$$

where C is the Compton–Getting factor, V_p the solar plasma velocity and V is the particle velocity.

At low energies (~10 MeV), the convective anisotropy is ~10–15 per cent while at relativistic energies, the convective anisotropy is only ~0·6 per cent. During late times in the decay, the anisotropy of low energy solar flare particles is observed to be from 45°E direction (McCracken *et al.*, 1971; Rao *et al.*, 1971) which has been interpreted as due to an equilibrium between the outward convective flow and the inward diffusion, the latter being caused by a positive density gradient set up in the interplanetary medium by the earlier enhanced convection. We believe that similar mechanism must also operate on galactic particles over short periods of time when equilibrium conditions are not established.

Separating the anisotropy vector into its two components, namely the convective and the diffusive vectors, Hashim *et al.* (1972) have recently shown that the diffusive vector is aligned along the interplanetary field direction. The field aligned inward diffusion caused by the establishment of a significant positive density gradient can result from either or both the processes (a) through the establishment of regions of decreased density (sink) in the garden-hose direction (b) through the establishment of regions of enhanced density

(source) in the anti-garden-hose direction, the physical processes responsible for the two mechanisms being possibly different.

In this communication, we show that the enhanced diurnal variation can be simply understood as due to a resultant between convection and enhanced field aligned diffusion by comparing the cosmic ray diurnal variation data with the interplanetary field data. We further show that the field aligned diffusion at early times during enhanced wave trains is caused by a sink in the garden-hose direction and at late times due to a source in the anti-garden-hose direction as a result of the establishment of a strong positive density gradient. Finally we show that even the average quiet day diurnal variation is explainable in terms of this new concept.

2. DATA MANIPULATION

The cosmic ray anisotropy characteristics have been determined from the data from a number of high and middle latitude neutron monitor stations well distributed in longitude and having narrow asymptotic cones of acceptance (See Table 1). As the Earth spins on

TABLE 1. PARTICULARS OF NEUTRON MONITORING STATIONS WHOSE DATA HAVE BEEN USED IN THE ANALYSIS

No.	Stations	Geographic co-ordinates Latitude (Deg)	Geographic co-ordinates Longitude (Deg)	Cut-off rigidity (GV)	Mean asymptotic co-ordinates Latitude (Deg)	Mean asymptotic co-ordinates Longitude (Deg)
1.	Ahmedabad	23·0	72·6	15·94	19	125
2.	Alert	82·5	297·7	<0·05	77	331
3.	Alma-Ata	43·2	76·9	6·69	25	143
4.	Calgary	51·1	245·9	1·09	28	269
5.	Churchill	58·8	265·9	0·21	40	286
6.	Dallas	32·8	263·2	4·35	25	316
7.	Deep River	46·1	282·5	1·02	27	319
8.	Durham	43·1	289·2	1·41	25	332
9.	Goose Bay	53·3	299·6	0·52	35	339
10.	Hermanus	−34·4	19·2	4·90	24	67
11.	Inuvik	68·4	226·3	<0·18	47	233
12.	Kiel	54·3	10·1	2·29	31	63
13.	Lindau	51·6	10·1	3·00	29	67
14.	Mawson	−67·6	62·9	0·22	−42	55
15.	Mt. Norikura	36·1	137·6	11·39	26	195
16.	Mt. Washington	44·3	288·7	1·14	25	331
17.	Mt. Wellington	−42·9	147·2	1·89	−25	193
18.	Pic-du-Midi	42·9	0·3	5·36	26	73
19.	Sulphur Mt.	51·2	244·4	1·14	27	270
20.	Wilkes	−66·4	110·5	<0·05	−56	107

its axis, each of these monitors scan a narrow region of the celestial sky. Combining the data from all the stations, three dimensional space time maps of cosmic ray intensity time profile in the interplanetary medium have been constructed using the method developed by Fenton *et al.* (1959), Ables *et al.* (1967), Mercer and Wilson (1968) and Carmichael and Steljes (1969). Such maps define the cosmic ray flux as a function of direction at any given time and thus provide an integrated view of the cosmic ray demography in space and therefore are ideally suited to study the characteristics of a rapidly evolving anisotropy and to identify the sources and sinks. During the period 1965–1969, there are about 25 such wave trains having enhanced diurnal amplitudes. For an unambiguous identification of sinks and sources, we have selected only four of these which are not accompanied by

large changes in the daily mean intensity. Figure 1 shows the selected abnormally high amplitude wave trains as observed at the Deep River neutron monitoring station.

The mean intensity three days prior to the commencement of the enhanced diurnal wave train, when not accompanied by large changes in flux, has been used for normalization purposes. Due to the inadequate coverage of certain longitudes because of the non-availability of neutron monitoring stations, we have been able to represent the intensity in only eight directions in space at any time, each directional belt covering a width of 3 hr in longitude. The mean of the observed amplitude in different directions have been obtained taking care to normalize the amplitude at each station to the width and declination of its asymptotic cone of acceptance. Three dimensional space–time diagrams are drawn for each three hourly interval on each day.

Besides the use of three dimensional space–time intensity profile maps, the data at various stations have also been utilised to derive the diurnal and semi-diurnal anisotropy

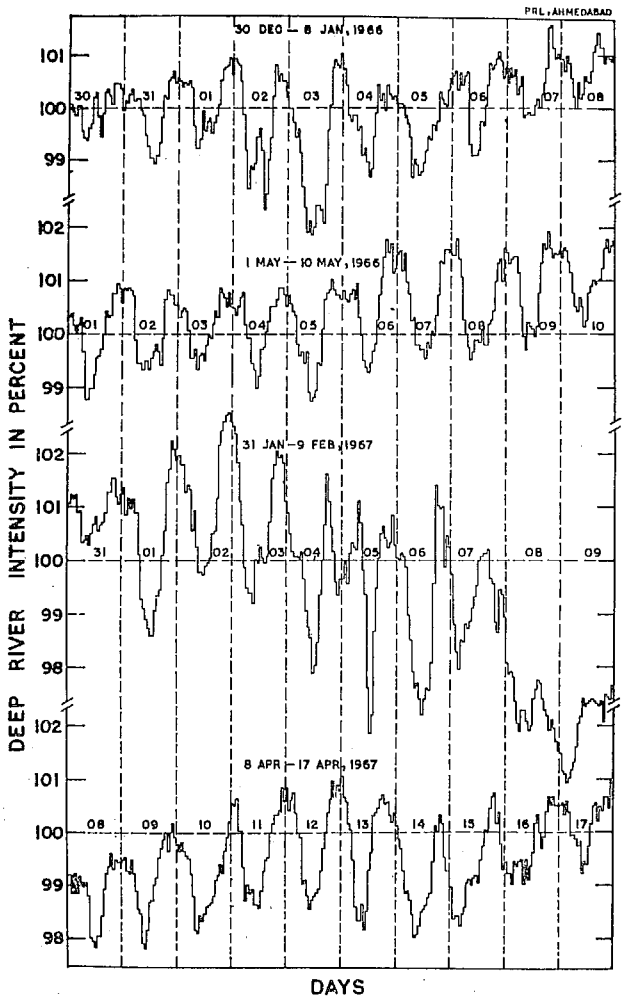

FIG. 1. SHOWING TYPICAL ENHANCED DIURNAL WAVE TRAINS AS OBSERVED BY THE DEEP RIVER NEUTRON MONITOR.

amplitudes and phases in space along with their energy spectral characteristics using the variational coefficient techniques developed by Rao *et al.* (1963) and McCracken *et al.* (1965). The interplanetary field parameters for each of these days have also been obtained from Pioneer 6, Explorer 33 and 35 measurements for comparison with the diurnal anisotropy vectors.

3. LOCATION OF SOURCES AND SINKS DURING DAYS OF ENHANCED DIURNAL VARIATION

McCracken *et al.* (1966) have suggested that the corotating Forbush decreases often observed in the low energy cosmic radiation (~10 Mev) will essentially manifest themselves as enhanced diurnal variation at relativistic energies, the depressed intensity along the garden-hose direction causing the diurnal maxima to occur along the anti-garden-hose direction. The enhanced diurnal wave train which occurred during 30 December, 1965–7 January, 1966 coincides with the corotating Forbush decrease event identified by McCracken *et al.* (1966) and we use it to test the above suggestion. Figure 2 presents the intensity profile in different directions (1200 corresponding to sunward direction)

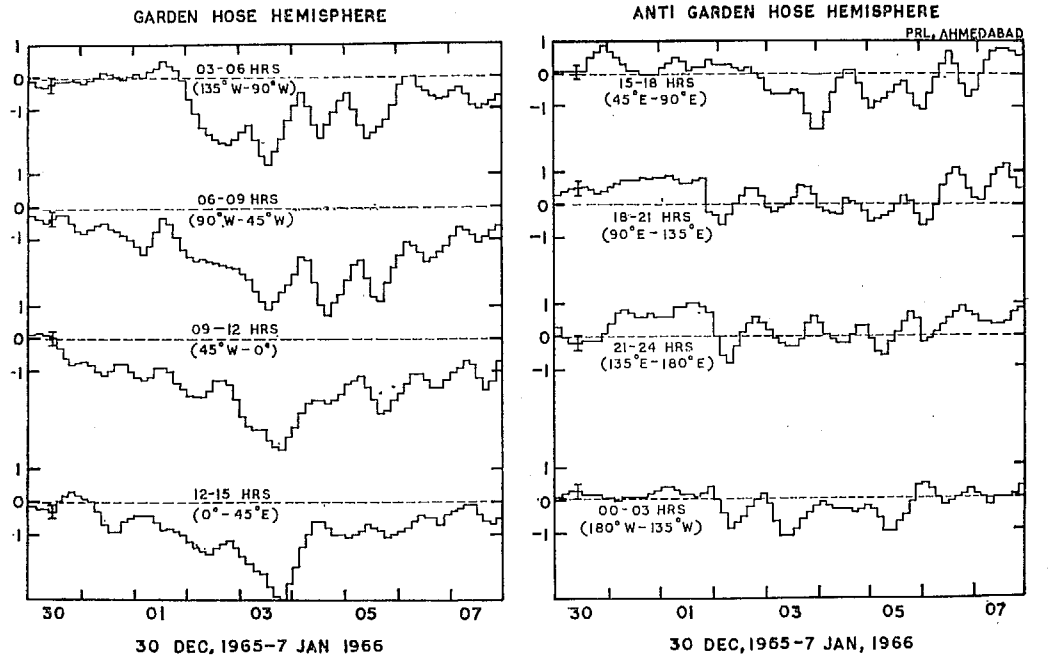

FIG. 2. COSMIC RAY SPACE TIME INTENSITY DIAGRAM DURING THE PERIOD 30 DECEMBER, 1965–7 JANUARY, 1966, DURING WHICH THE COSMIC RAY NEUTRON MONITORING STATIONS RECORDED ENHANCED DIURNAL ANISOTROPY.

during 30 December, 1965–7 January, 1966 in which period enhanced diurnal amplitude was recorded by various neutron monitors. During this period, a large depression of intensity (~2 per cent) is observed in the garden-hose hemisphere, whereas the intensity in the anti-garden-hose hemisphere is practically unaffected. In Fig. 3 the average intensity for five days (2 January–6 January, 1966) during which the garden-hose depression was predominant, is plotted as a function of direction which dramatically brings out the large depression centred around the garden-hose direction. Earlier analysis of Mathews *et al.*

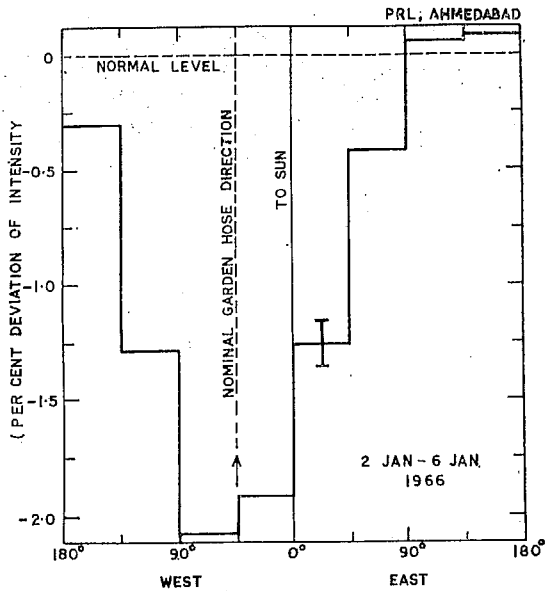

FIG. 3. MEAN COSMIC RAY INTENSITY AS A FUNCTION OF DIRECTION IN SPACE DURING 2–6 JANUARY, 1966, WHEN ENHANCED DIURNAL VARIATION DUE TO A PREDOMINANT GARDEN-HOSE DEPRESSION WAS OBSERVED BY THE NEUTRON MONITORING STATIONS.

(1969) and of Hashim and Thambyahpillai (1969) of a few events also confirm the presence of such an enhanced depression along the garden-hose direction causing enhanced diurnal variation.

In contrast to the above simple picture the long lived enhanced diurnal variation event of 30 April–11 May, 1966 shows a complex behaviour. Figure 4 shows the evolution of the cosmic ray flux distribution in space at various times during 30 April–11 May, 1966. On 29 April, 1966, prior to the commencement of the enhanced wave train, the cosmic ray flux distribution in space was found to be practically isotropic (Fig. 4a) showing a normal diurnal variation. During the early part of the enhanced diurnal variation event, i.e. 1–7 May, 1966, the cosmic ray intensity in the garden-hose direction is found to be well depressed below the normal level (Fig. 4b, 4c). By 9 May, the cosmic ray flux along the garden-hose direction seems to be just recovering to its normal value (Fig. 4e). However, the cosmic ray intensity in the anti-garden-hose direction is now found to show a large excess above the normal intensity (Fig. 4f, 4g). Thus during the later part of the event, i.e. 8–11 May, 1966, the enhanced diurnal amplitude seems to be caused by a source in the anti-garden-hose direction. We note that such a behaviour is to be expected in terms of the explanation offered by McCracken *et al.* (1971) and Rao *et al.* (1971) for the observed easterly anisotropy late in the decay of low energy solar flare events. Using similar arguments, we can expect during such times the enhanced convection by the high velocity solar wind associated with the initial shock wave which causes depressed intensity along the garden-hose-direction, to eventually establish a positive density gradient and thus a source along the anti-garden-hose direction during the later part of such enhanced diurnal wave train events.

We wish to emphasise that the simple harmonic analysis of the data would not have

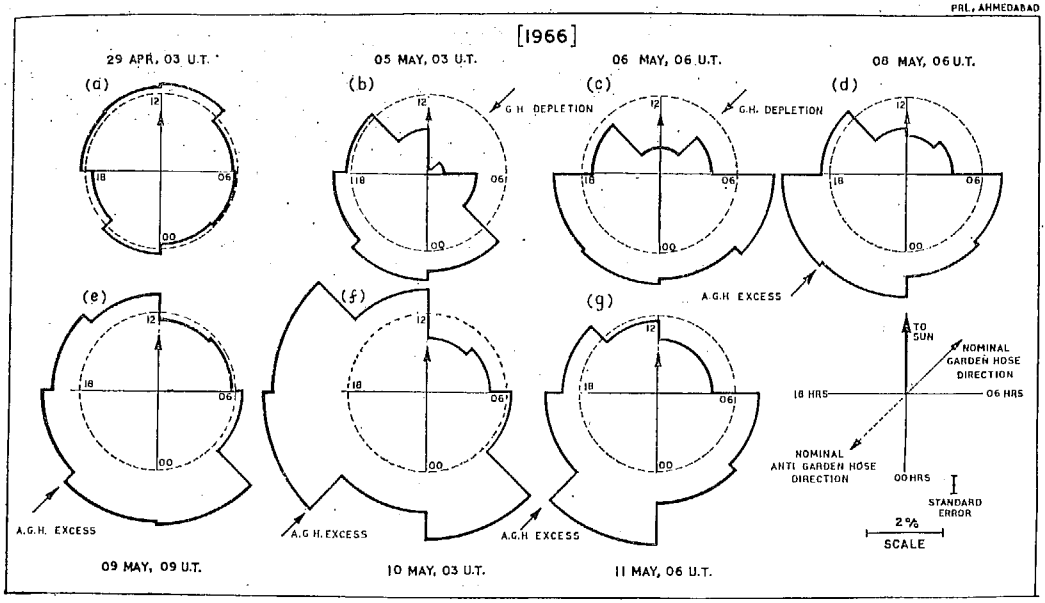

FIG. 4. SHOWING THE EVOLUTION OF ANISOTROPY DURING THE ENHANCED DIURNAL VARIATION EVENT OF 30 APRIL–11 MAY, 1966.

Note that during the early part of the event, the cosmic ray intensity is depleted along the garden-hose direction and during late in the event the cosmic ray flux in the garden-hose recovers to the normal value (shown by thin circle) whereas the flux in the anti-garden-hose direction shows a large excess.

revealed the complete physical nature of the mechanism. Both a source in the anti-garden-hose and a sink in the garden-hose directions essentially give the same time of maxima, i.e. around ~2000 hr. It is only through the type of analysis presented in this paper that the existence of sources and sinks in space can be identified. In the next section, we show that the enhanced diurnal variation whether caused by a sink in the garden-hose or a source in the anti-garden-hose direction can be explained as a resultant of normal convection and enhanced field aligned diffusion.

Referring to Fig. 4, we see that the change over from a sink in the garden-hose direction to a source in the anti-garden-hose direction occurs in a period of 4–5 days suggesting that the relaxation time of the interplanetary medium to follow the changes in the density gradient in the entire modulating region is of the order of 4–5 days. For the normal solar wind velocity observed during such periods, this would indicate that the dimension of the modulating region is of the order of 2 AU thus providing an independent experimental evidence for the location of a boundary sometimes assumed in dealing with the cosmic ray transport.

4. CHARACTERISTICS OF ENHANCED DIURNAL VARIATION

The enhanced diurnal variation amplitude and phase on each day has been obtained for each of these events. The diurnal variation during such events is observed to show a maximum at about 2000 hr during the entire period of enhanced diurnal variation in contrast with the 1800 hr maximum observed for corotational anisotropy. Figure 5 shows the diurnal anisotropy amplitude and the time of maximum for each day for two of the events along with the average value of these parameters for each of the events.

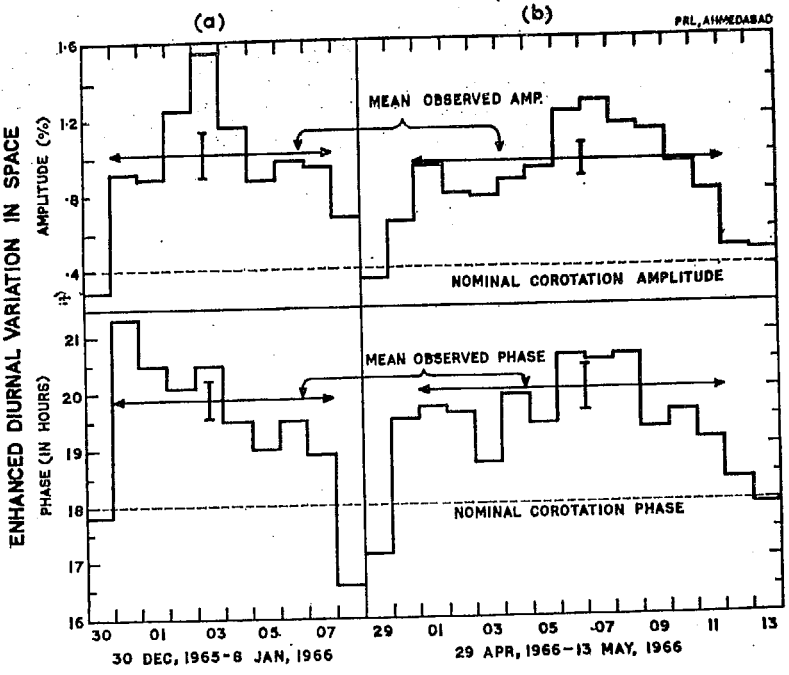

FIG. 5. THE AMPLITUDE AND PHASE OF THE DIURNAL ANISOTROPY IN SPACE ON EACH DAY DURING (a) 30 DECEMBER 1965–8 JANUARY, 1966 AND (b) 29 APRIL–13 MAY, 1966 DERIVED FROM THE DATA FROM A NUMBER OF NEUTRON MONITOR STATIONS.

The figure includes some observations both prior and later to the actual enhanced diurnal event. The mean phase and amplitude during the event is marked by an arrow.

The energy spectrum of variation for each of the enhanced diurnal variation events has been calculated using the well known method given by Rao *et al.* (1963). Computing the direction of anisotropy in space as observed by different stations for different values of the spectral exponent, the variance between the different values has been calculated. The spectral exponent corresponding to the minimum variance represents the true spectral exponent of the diurnal anisotropy. Figure 6 shows the plot of the variance in the diurnal time of maximum as a function of the spectral exponent along with the number of neutron monitoring stations whose data have been utilised for the spectral determination. The figure clearly shows that the spectral exponent in each case is consistent with it being energy independent ($0 \pm 0{\cdot}2$).

The mean amplitude and phase of the semi-diurnal component during the periods of enhanced diurnal variation generally do not exhibit any significant departure from the average picture of the semi-diurnal component given by Rao and Agrawal (1970). We, therefore, have neglected the semi-diurnal component from our discussion.

5. ENHANCED FIELD ALIGNED DIFFUSION DURING DAYS OF ENHANCED DIURNAL VARIATION

In order to establish the field aligned nature of the diffusive flow due to either a sink in the garden-hose or a source in the anti-garden-hose direction, we resolve the observed diurnal vector into two components.

$$\delta = \delta_c + \delta_d \tag{2}$$

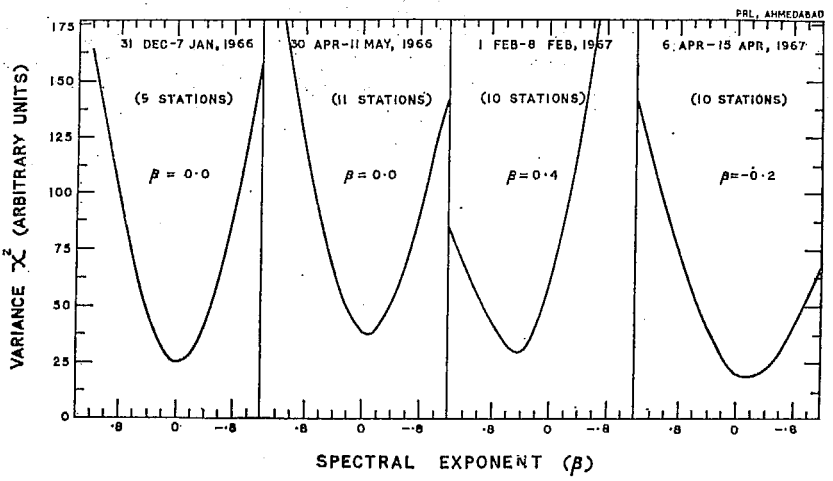

FIG. 6. VARIANCE IN THE OBSERVATIONAL VALUES OF THE DIURNAL TIME OF MAXIMUM AS A FUNCTION OF THE SPECTRAL EXPONENT FOR EACH EVENT. THE MINIMUM VARIANCE IN ALL CASES IS CONSISTENT WITH AN ENERGY INDEPENDENT SPECTRAL EXPONENT ($\beta = 0 \pm 0{\cdot}2$).

where δ_c is the anisotropy vector due to convective flow, and δ_d is the anisotropy vector due to diffusive flow. The amplitude of δ_c is $\approx 0{\cdot}6$ per cent when determined according to Equation (1) with a solar wind speed ≈ 400 km/sec and $C = 1{\cdot}5$, which is appropriate to the mean energy of response (~ 8 GeV). The space anisotropy amplitude obtained from neutron monitor observations, using the correction factors for the geomagnetic bending and width of the asymptotic cones of acceptances as given in IQSY manual (McCracken *et al.*, 1965) is $\sim 0{\cdot}4$ per cent. When this is corrected for the changes in C with energy, the upper cut off rigidity and the detector response (Subramanian, 1971), the free space amplitude would be $\sim 0{\cdot}6$ per cent. In all our treatment however, we shall deal only with the uncorrected space amplitude of 0·4 per cent, since the correction as suggested by Subramanian will only increase the true amplitude by a constant factor and will not change any of our conclusions. Using a value of 0·4 per cent in the 1200 hr direction for the convective vector, the magnitude and direction of the diffusive vector δ_d for each day for each of the four events has been calculated. Similarly the magnitude and the direction of the interplanetary field vector for each day has also been calculated from the direct spacecraft observations (Pioneer 6, Explorer 33 or Explorer 35). In Fig. 7, the diffusive flow vectors for each day is plotted end to end separately for each of the four events along with the interplanetary field vector to demonstrate the field aligned nature of the diffusive flow even on a day to day basis.

The mean diffusive vector and the corresponding mean interplanetary field vector are plotted for each of the four events in Fig. 8 (see also Table 2). Both Figs. 7 and 8 clearly demonstrate that the enhanced diurnal variation is caused by a superposition of the enhanced field aligned diffusion over the normal convective flow.

6. QUIET DAY DIURNAL VARIATION

In this section we extend the analysis of the role of convection and diffusion to the quiet day diurnal variation to show that the present concept of diurnal variation being due to convection and parallel diffusion applies most of the time. For this purpose, we have

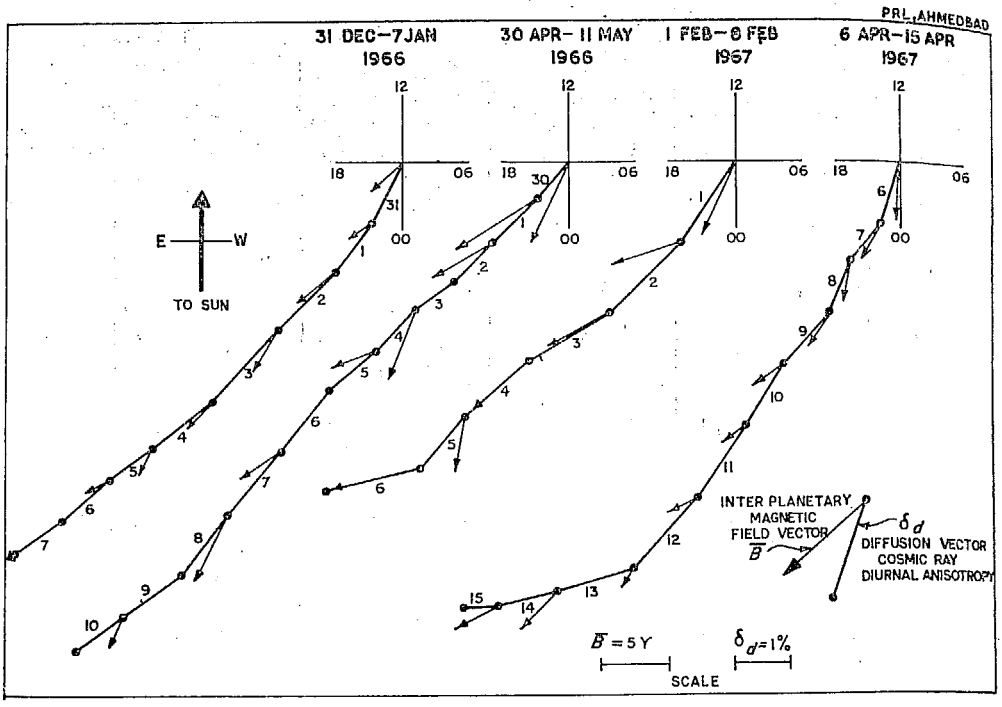

FIG. 7. SHOWING THE COSMIC RAY ANISOTROPY DIFFUSION VECTOR FOR EACH DAY PLOTTED END TO END FOR EACH OF THE FOUR ENHANCED DIURNAL VARIATION EVENTS.

The interplanetary magnetic field vector for each day is also plotted alongside the diffusive vector for each day. Note the good agreement between the field azimuth and the direction of the diffusive vector confirming the field aligned nature of the diffusive vector.

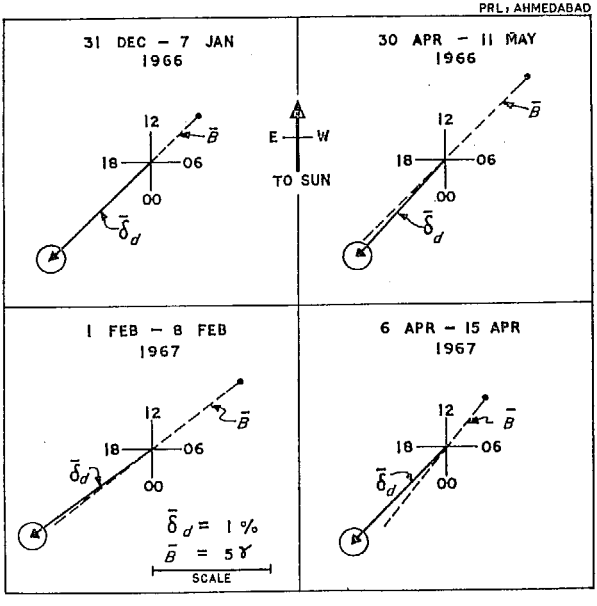

FIG. 8. SHOWING THAT THE AVERAGE DIFFUSIVE ANISOTROPY VECTOR FOR EACH EVENT IS ALIGNED PARALLEL OR ANTI-PARALLEL TO THE AVERAGE INTERPLANETARY MAGNETIC FIELD VECTOR DURING THE EVENTS EXHIBITING ENHANCED DIURNAL VARIATION.

TABLE 2. MEAN DIURNAL ANISOTROPY VECTOR, MEAN DIFFUSIVE VECTOR AND THE MEAN INTERPLANETARY MAGNETIC FIELD VECTOR DURING THE SELECTED ENHANCED DIURNAL VARIATION EVENTS

No.	Events	Mean diurnal anisotropy vector amp (%)	phase ϕ (Deg)	Mean diffusion vector amp (%)	phase ϕ_d (Deg)	Mean magnetic field vector amp (γ)	phase ϕ_B (Deg)	Phase diff. $\phi_d - \phi_B$ (Deg)
1.	31 *Dec.*– 7 *Jan.* 1966	1·02 ± 0·12	298 ± 5	1·26	314	3·0	314	0 ± 5
2.	30 *Apr.*–11 *May* 1966	0·91 ± 0·08	301 ± 6	1·17	318	5·1	315	3 ± 6
3.	1 *Feb.*– 8 *Feb.* 1967	1·10 ± 0·10	289 ± 7	1·29	306	4·9	308	−2 ± 7
4.	6 *Apr.*–15 *Apr.* 1967	0·92 ± 0·07	299 ± 4	1·17	316	2·8	322	−6 ± 4

(Derived using correction factors given in IQSY manual)

utilised the neutron monitor data for the entire period of January 1967–December, 1968, for which the interplanetary field data is available. We have utilised the data on all days excepting the days of Forbush decrease onset when large intensity gradients are observed. The average diurnal variation parameters for each of the 27 day solar rotation periods, and the average interplanetary field parameters for each of these rotations have been calculated separately. Table 3 lists the parameters along with the average diffusion vectors derived from the cosmic ray diurnal vectors using Equation (2) and the computed difference

TABLE 3. THE 27 DAY AVERAGE COSMIC RAY DIURNAL VECTOR, COSMIC RAY DIFFUSIVE VECTOR (SEE TEXT) AND INTERPLANETARY FIELD VECTOR FOR DIFFERENT SOLAR ROTATIONS DURING 1967–1968. THE COMPUTED PHASE DIFFERENCE BETWEEN THE DIFFUSIVE VECTOR AND THE FIELD VECTOR IS ALSO LISTED

No.	Solar rotation no.	No. of days used	Mean diurnal anisotropy vector amp (%)	phase ϕ (Deg)	Mean diffusion* vector amp (%)	phase ϕ_d (Deg)	Mean magnetic field vector amp (γ)	phase ϕ_B (Deg)	Phase diff. $\phi_d - \phi_B$ (Deg)
1.	1826	15	0·43 ± 0·06	255 ± 7	0·51	305	3·2	306	−1 ± 7
2.	1827	20	0·63 ± 0·02	270 ± 5	0·74	303	3·9	308	−5 ± 5
3.	1828	19	0·30 ± 0·05	279 ± 5	0·54	326	3·5	307	19 ± 5
4.	1829	16	0·81 ± 0·07	288 ± 6	1·00	310	2·9	321	−11 ± 6
5.	1830	10	0·51 ± 0·07	263 ± 5	0·61	304	3·2	324	−20 ± 5
6.	1833	13	0·20 ± 0·06	266 ± 8	0·45	333	3·3	325	8 ± 8
7.	1834	16	0·20 ± 0·03	239 ± 10	0·34	330	3·5	321	9 ± 10
8.	1835	21	0·45 ± 0·07	254 ± 9	0·51	303	3·7	308	−5 ± 9
9.	1836	19	0·34 ± 0·02	274 ± 5	0·54	321	3·7	312	9 ± 5
10.	1837	16	0·26 ± 0·06	313 ± 4	0·60	342	3·6	312	30 ± 4
11.	1838	24	0·39 ± 0·04	270 ± 2	0·56	315	4·2	311	4 ± 2
12.	1939	20	0·52 ± 0·07	263 ± 10	0·62	303	4·1	301	2 ± 10
13.	1840	17	0·33 ± 0·05	274 ± 10	0·53	322	3·7	312	10 ± 10
14.	1841	13	0·42 ± 0·06	267 ± 5	0·56	312	4·2	309	3 ± 5
15.	1842	19	0·52 ± 0·09	268 ± 10	0·65	306	3·5	314	−8 ± 10
16.	1843	22	0·64 ± 0·05	281 ± 6	0·82	310	3·6	316	−6 ± 6
17.	1844	21	0·49 ± 0·05	272 ± 8	0·64	311	3·8	320	−9 ± 8
18.	1845	19	0·35 ± 0·02	264 ± 8	0·50	317	3·3	313	4 ± 8
19.	1846	16	0·40 ± 0·06	235 ± 10	0·36	299	3·1	312	−13 ± 10
20.	1847	17	0·36 ± 0·02	278 ± 9	0·57	322	3·4	313	9 ± 9
21.	1848	16	0·47 ± 0·05	267 ± 4	0·60	309	4·0	304	5 ± 4
22.	1849	18	0·30 ± 0·07	268 ± 11	0·49	322	3·0	318	4 ± 11
23.	1850	18	0·46 ± 0·05	280 ± 6	0·66	317	3·9	312	5 ± 6
24.	1851	13	0·42 ± 0·04	294 ± 6	0·69	326	4·1	321	5 ± 6
25.	1852	23	0·33 ± 0·03	250 ± 11	0·42	313	3·6	311	2 ± 11

(Derived using correction factors given IQSY manual)

* The errors in the mean diffusive vector are of the same order as the errors in mean anisotropy vector.

between the diffusive vector and the field vector. Figure 9 shows the histogram of the phase difference between the average diffusive vector and the average interplanetary field vector. Both Table 3 and Fig. 9 show that in nearly 80 per cent of the cases, the phase difference between the diffusive vector and interplanetary field vector even on a 27 day average basis is $\leqslant 10°$, which is of the same order as the standard error of the observations thus indicating that the average quiet day diffusive vector is also field aligned.

The diffusive vector can be resolved into two components, one parallel to **B** vector and another perpendicular to it, the amplitude of the perpendicular component being a measure of the non-field aligned component. From Fig. 10 which shows the plot of the parallel and perpendicular components of the average diffusive vectors for different solar rotations, it is evident that the parallel component corresponding to the field aligned component dominates and the perpendicular component is usually less than a tenth of the parallel component.

The annual mean diurnal anisotropy has an amplitude of $\approx 0{\cdot}35$ per cent and a direction of maximum around 1800 hr (Rao, 1972) during the period 1964–1970. The annual mean diffusive vector for each year during this period has been calculated using Equation (2). The yearly average interplanetary field direction has been derived from the observed yearly average solar wind velocity (Gosling *et al.*, 1971) and assuming Archimedean spiral structure for the field. Comparison of the field azimuths for the period 1967–1968 computed from solar wind observations with actual interplanetary magnetic field observations show that these agree within 2–3°. Table 4 lists the yearly average diurnal variation parameters and the deduced interplanetary field parameters along with the computed phase difference between the yearly average diffusive vector and the corresponding field vector. The average diffusive vectors calculated for each year during 1964–1970 is also plotted in Fig. 10 along with the mean diffusive vector for the entire period 1964–1970.

The yearly mean diffusive vector for the entire period has an amplitude of $0{\cdot}53 \pm 0{\cdot}01$ per cent and makes an angle of $3 \pm 2°$ with the interplanetary field vector, the phase difference being of the same order as the observational error. In other words, the figure clearly indicates that within the observational errors, the yearly average diurnal variation is also completely explainable in terms of summation of a normal convective vector and a field aligned diffusive vector. Except during 1965 when the diffusive vector makes an angle of 11°, the diffusive vector during other years is practically aligned with the field direction. In addition to the average picture, we have also examined, in great detail, the diurnal variation on a day-to-day basis and we observe that during 1967–1968, on more than ~ 60 per cent of the days, the diffusive vector is essentially field aligned and $k_\perp$ is negligible even on a day-to-day basis. The detailed results of the analysis on a day-to-day basis will be published later.

7. DISCUSSION AND CONCLUSIONS

We now examine whether an unified model can be proposed to explain the diurnal variation, both quiet and enhanced as well as anisotropy of low energy solar flare cosmic radiation. Figure 11 depicts such a model. Referring to Fig. 11 (a), we observe that at early times in a flare event, the diffusive current driven by a negative cosmic ray density gradient due to solar produced particles dominates over the small convective vector resulting in a predominantly field aligned anisotropic flux. During late times the solar cosmic ray flow is in equilibrium and is consistent with it being simply convected out by the solar wind. At very late times, the positive density gradient created by the earlier convection provides a

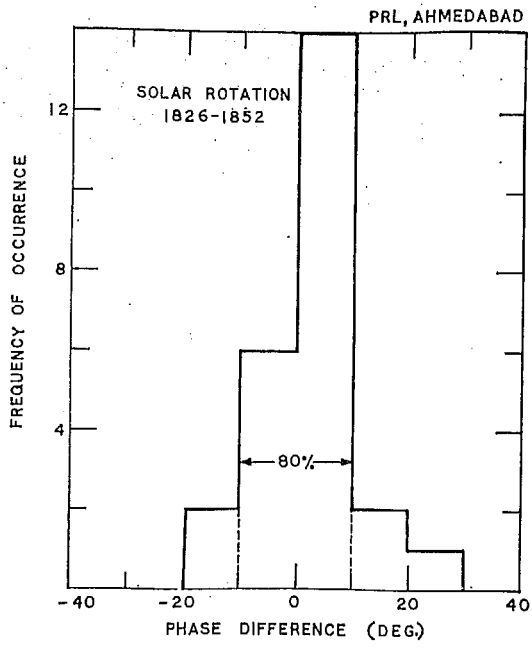

FIG. 9. HISTOGRAM SHOWING THE DISTRIBUTION OF PHASE DIFFERENCE BETWEEN THE AVERAGE COSMIC RAY DIFFUSIVE VECTOR AND THE AVERAGE MAGNETIC FIELD VECTOR FOR A NUMBER OF SOLAR ROTATIONS 1826–1852.

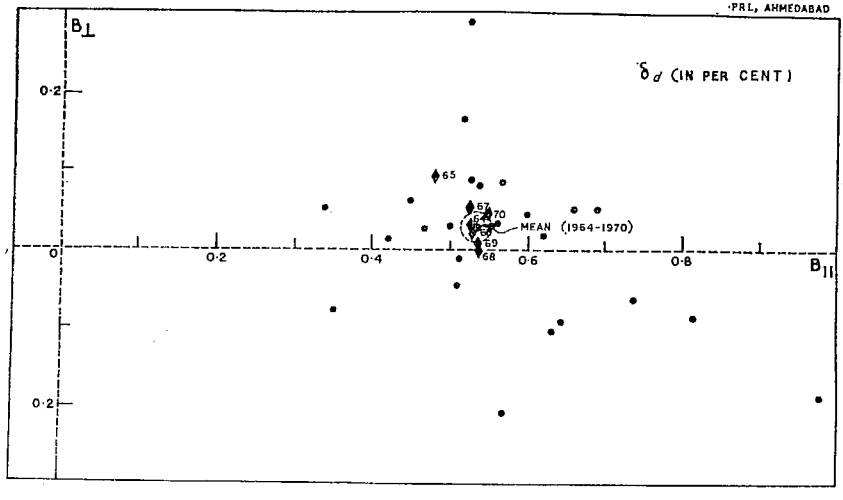

FIG. 10. SHOWING THE TWO COMPONENTS OF THE AVERAGE DIFFUSIVE VECTOR, ONE PARALLEL AND THE OTHER PERPENDICULAR TO THE AVERAGE INTERPLANETARY FIELD VECTOR FOR DIFFERENT SOLAR ROTATIONS (1826–1852) DURING JANUARY, 1967–DECEMBER, 1968. The two components of the annual mean diffusive vector for the entire period during 1964–1970 are also shown in the figure.

TABLE 4. SHOWING THE PHASE DIFFERENCE BETWEEN THE YEARLY COSMIC RAY DIFFUSIVE VECTOR AND THE MEAN FIELD VECTOR. THE FIELD AZIMUTH HAS BEEN CALCULATED FROM SOLAR WIND VELOCITY ASSUMING ARCHIMEDEAN SPIRAL CONFIGURATION. THE COSMIC RAY DIFFUSIVE VECTOR IS COMPUTED FROM THE OBSERVED AVERAGE DIURNAL VECTOR USING EQUATION (2)

Year	Mean diurnal anisotropy vector amp (%)	Mean diurnal anisotropy vector phase ϕ (Deg)	Mean diffusion vector amp (%)	Mean diffusion vector phase ϕ_a (Deg)	Mean solar wind velocity (km/sec)	Mean magnetic field direction ϕ_B (Deg)	Phase diff. $\phi_a - \phi_B$ (Deg)
1964	0·35 ± 0·03	272 ± 3	0·53	321	431	317	4 ± 3
1965	0·28 ± 0·02	270 ± 4	0·49	326	407	315	11 ± 4
1966	0·36 ± 0·02	271 ± 3	0·53	319	413	316	3 ± 3
1967	0·35 ± 0·01	272 ± 5	0·53	321	394	315	6 ± 5
1968	0·37 ± 0·01	270 ± 3	0·54	318	453	318	0 ± 3
1969	0·36 ± 0·01	270 ± 2	0·54	318	422	317	1 ± 2
1970	0·37 ± 0·02	271 ± 2	0·55	319	390	314	5 ± 2
Mean (1964–1970)	0·35 ± 0·01	271 ± 2	0·53	320	418	317	3 ± 2

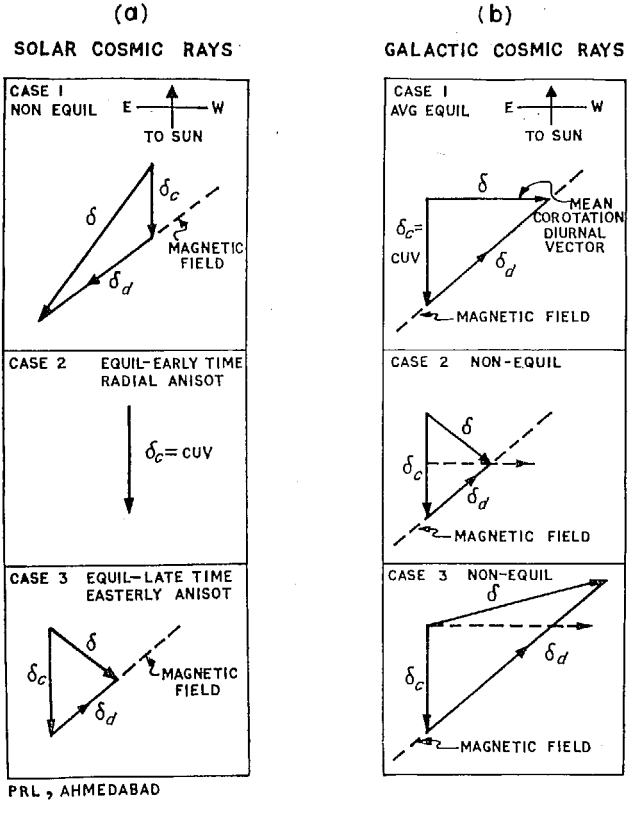

FIG. 11. A UNIFIED MODEL FOR EXPLAINING THE ANISOTROPY OF LOW ENERGY COSMIC RAY FLARE PARTICLES AND ALSO THE DIURNAL ANISOTROPY OF HIGH ENERGY PARTICLES IN TERMS OF SIMPLE CONVECTION AND FIELD ALIGNED DIFFUSION (SEE TEXT FOR EXPLANATION).

diffusive current which when superposed upon the convective vector results in an easterly anisotropy. The model embodying the extension of the same ideas to the galactic anisotropy is depicted in Fig. 11(b). Under equilibrium condition, when there is no net flow of cosmic radiation either into or from the solar system, the radial convection current $\mathbf{S}_c = \mathrm{CUV}$ is exactly balanced by the radial component of inward diffusion $k_{\parallel}\,(\partial U/\partial \mathbf{r})_{\parallel}$ resulting in an average observed corotation anisotropy of $\approx 0{\cdot}4$ per cent along 1800 hr direction. On a day-to-day basis, the diffusion vector need not exactly balance the convective vector. In the case when the diffusion vector is smaller, the resulting observed anisotropy would show a maximum earlier than 1800 hr and in the case of enhanced diurnal variation when the diffusive vector is very much greater than the convective vector, the time of maximum of the resulting diurnal variation will shift towards $\sim$ 2100 hr, the mean direction of the interplanetary magnetic field. The diffusive vector, in all cases, is aligned parallel or antiparallel to the magnetic field.

The diffusion current (Gleeson, 1969; Forman and Gleeson, 1970) can be written

$$\mathbf{S}_d = k_{\parallel}\left(\frac{\partial U}{\partial \mathbf{r}}\right)_{\parallel} + k_{\perp}\left(\frac{\partial U}{\partial \mathbf{r}}\right)_{\perp} \tag{3}$$

and since the average co-rotational anisotropy is obtained assuming the radial current $\mathbf{S}_r = 0$ and $k_{\perp}$ to be negligible we may use this together with

$$\delta_d = 3\mathbf{S}_d/VU \tag{4}$$

and the observed free space anisotropy to calculate first the density gradient along the magnetic field $(1/U)\,|\,(\partial U/\partial \mathbf{r})_{\parallel}|$ and from this the radial gradient

$$G = \frac{1}{U}\left|\left(\frac{\partial U}{\partial \mathbf{r}}\right)_{\parallel}\right| \Big/ \cos\psi \tag{5}$$

with ψ the angle between the magnetic field and the radial direction.

The magnetic power spectra of Jokipii and Coleman (1968) and Bercovitch (1971a) indicate that at neutron monitor energies $k_{\parallel} \approx 5 \times 10^{21}\, p\,\beta\ \mathrm{cm^2\ sec^{-1}}$ (p = rigidity, $\beta = V/c$) and, from the observed mean diffusive anisotropy of $0{\cdot}53 \pm 0{\cdot}01$ per cent the corresponding free space anisotropy is $\approx 0{\cdot}8$ per cent. These values lead to a radial gradient $\approx$4·5 per cent AU which is in good agreement with those from many other independent observations and summarised by Bercovitch (1971b). During the period of enhanced diurnal variation the observed average diffusive vector (Table 2) is seen to be about $1{\cdot}2 \pm 0{\cdot}1$ per cent which corresponds to an enhanced positive radial density gradient of $\approx$10 per cent/A.U. These gradients are sensitive to the value assumed for the diffusion coefficient.

From Figs. 9 and 10, we observe that the mean diffusive vectors obtained on 27 day and annual average basis are essentially field aligned, the phase difference between the diffusive vector and the field vector being, on an average, $3^\circ \pm 2^\circ$. This indicates that on an average, the ratio $k_{\perp}/k_{\parallel} \leqslant 0{\cdot}05$ (from Equation 3) which is consistent with the low energy observations.

It must be emphasised that even though $k_{\perp}$ is negligible on an average basis, there are occasions when it can be significant and which might result in a partial or complete cancellation of the diurnal anisotropy. Figure 12 shows some representative examples of trains of days when the observed diurnal variation at Deep River was negligible over a period of days. We have examined the average diurnal as well as the diffusive vectors for two such events which occurred on 27 August–1 September, 1967 and 27 July–1 August, 1968 for

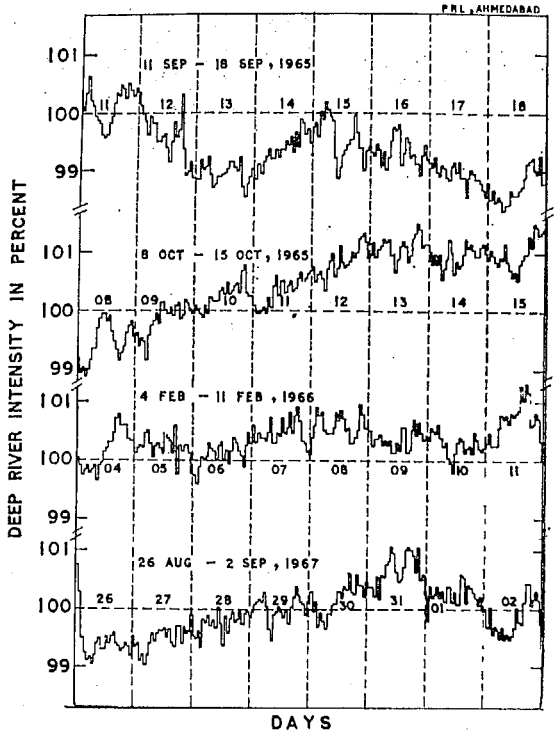

FIG. 12. TYPICAL EXAMPLES SHOWING THE COSMIC RAY INTENSITY AT DEEP RIVER DURING ABNORMALLY LOW DIURNAL AMPLITUDE DAYS.

which concurrent magnetic field data are available. For both these events, we find that the average diurnal amplitude is about 0·15 per cent and the phase difference between the average diffusive vector and the field vector is $\sim 25° \pm 8°$ indicating that for such periods $k_\perp/k_\parallel \approx 0{\cdot}5 \pm 0{\cdot}2$, which exceeds greatly the normal value of $\sim 0{\cdot}05$ observed during other days. Similarly the slight reduction in the observed average amplitude of diurnal variation in 1965 can be attributed (Fig. 11) to the increased value of $k_\perp$, $k_\perp/k_\parallel$ for 1965 being about $0{\cdot}19 \pm 0{\cdot}04$ almost a factor of three greater than the values observed during other periods.

From the data presented earlier and the discussion, we draw the following conclusions:

(1) The diurnal variation during both quiet and disturbed periods can be understood in terms of convection and field aligned diffusion. On an average basis, the net radial convection current is zero, i.e. the convection and diffusion vectors balance each other resulting in corotational anisotropy. On a day-to-day basis, the two vectors do not balance each other resulting in varying amplitudes and times of maxima for the observed diurnal anisotropy. The proposed mechanism can also explain the observed anisotropies of low energy cosmic ray flux during solar flare events. In other words, the changes in the diurnal anisotropy of cosmic radiation is explainable in terms of redistribution of cosmic ray flux following transient changes in the interplanetary medium.

(2) The diffusion vector, at most times is field aligned.

(3) On an annual or 27 day average basis, the phase difference between the diffusion vector and the interplanetary field vector is $\approx 3° \pm 2°$ which indicates that the ratio of

the perpendicular diffusion coefficient to parallel diffusion coefficient is $\leqslant 0{\cdot}05$. In other words, the transverse gradients, on an average basis, are negligible.

(4) The quiet day diffusion vector has an amplitude of $0{\cdot}53 \pm 0{\cdot}01$ per cent on an average basis, which corresponds to a positive radial density gradient of $\approx 4{\cdot}5$ per cent/AU.

(5) The spectral characteristics and observed time of maxima during periods of enhanced diurnal variation are consistent with their being caused by a superposition of convective flow with enhanced field aligned diffusive flow.

(6) During the early part of the enhanced diurnal wave train, the abnormal variation is caused by a depletion (sink) of cosmic ray particle population from the garden-hose direction. At late times, the earlier enhanced convection eventually sets up a source along the anti-garden-hose direction. Thus during the later part of the enhanced diurnal wave train, the abnormal variation is caused by a source along the anti-garden-hose direction. In both cases, the density gradient is positive.

(7) The change over from garden-hose sink to anti-garden-hose source requires about 4–5 days which represents a relaxation time of the modulation region having a dimension of about 2–3 AU.

(8) The enhanced field aligned diffusion vector during periods of enhanced diurnal variation causes the observed time of maximum of the resultant diurnal anisotropy to shift to later hours (around 2000 hr).

(9) The enhanced diffusion vector, on an average basis, has an amplitude of $1{\cdot}2 \pm 0{\cdot}1$ per cent which corresponds to an enhanced positive radial density gradient of ≈ 10 per cent/AU.

(10) Even though the ratio $k_\perp/k_\parallel$ is, on an average, negligible, there are days on which it could be significant which causes a drastic reduction in the diurnal variation. The small reduction in the average diurnal amplitude in 1965 can be attributed to an increase in the ratio of $k_\perp/k_\parallel$ by a factor of ~ 3 as compared to other periods.

Acknowledgements—We are grateful to all the investigators and the World Data Centre who have supplied the cosmic ray data and to Drs. N. F. Ness and C. P. Sonnet for kindly supplying us with the interplanetary field data. We are indebted to Dr. L. J. Gleeson for his very valuable comments and discussions. Thanks are also due to Miss H. C. Shah and Mr. B. R. Bhatt for computational help. The research presented here was supported by funds from the Department of Atomic Energy, Government of India, and funds from Day Fund Grant No.17 from the National Academy of Sciences, U.S.A.

REFERENCES

ABLES, J. G., BAROUCH, E. and MCCRACKEN, K. G. (1967). *Planet. Space Sci.* **15**, 547.
ANANTH, A. G., AGRAWAL, S. P. and RAO, U. R. (1971). *Proc. 12th Int. Conf. on Cosmic Rays* (Hobart) **2**, 651.
AXFORD, W. I. (1965). *Planet. Space Sci.* **13**, 115.
BERCOVITCH, M. (1971a). *Proc. 12th Int. Conf. on Cosmic-rays* (Hobart) **2**, 579.
BERCOVITCH, M. (1971b). *Rapporteur Report, Intensity Gradients in the Solar System* (Hobart).
CARMICHAEL, H. and STELJES, J. F. (1969). *World Data Centre A, Rep.* UAG-5, Feb.
FENTON, A. G., MCCRACKEN, K. G., ROSE, D. C. and WILSON, B. G. (1959). *Can J. Phys.* **37**, 970.
FORMAN, M. A. (1970). *J. geophys. Res.* **75**, 3147.
FORMAN, M. A. and GLEESON, L. J. (1970). Unpublished.
GLEESON, L. J. (1969). *Planet. Space Sci.* **17**, 31.
GOSLING, J. T., HANSEN, R. T. and BAME, S. J. (1971). *J. geophys. Res.* **76**, 1811.
HASHIM, A., BERCOVITCH, M. and STELJES, J. F. (1972). *Solar Physics.* **22**, 220.
HASHIM, A. and THAMBYAPILLAI, T. (1969). *Planet. Space Sci.* **17**, 1879.
JOKIPII, J. R. and COLEMAN, P. J., JR. (1968). *J. geophys. Res.* **73**, 5495.
MATHEWS, T., VENKATESAN, D. and WILSON, B. G. (1969). *J. geophys. Res.* **74**, 1218.
MCCRACKEN, K. G. and RAO, U. R. (1965). *Proc. Cosmic Ray Conf.* (London) **1**, 213.
MCCRACKEN, K. G. and RAO, U. R. (1970). *Space Sci. Rev.* **11**, 155.
MCCRACKEN, K. G., RAO, U. R., FOWLER, B. C., SHEA, M. A. and SMART, D. C. (1965). IQSY Instruction Manual No.10.

McCracken, K. G., Rao, U. R. and Bukata, R. P. (1966). *Phys. Rev. Letters* **17**, 928.
McCracken, K. G., Rao, U. R. and Bukata, R. P. (1967). *J. geophys. Res.* **72**, 4293.
McCracken, K. G., Rao, U. R. and Ness, N. F. (1968). *J. geophys. Res.* **73**, 4159.
McCracken, K. G., Rao, U. R., Bukata, R. P. and Keath, E. P. (1971). *Solar Phys.* **18**, 100.
Mercer, J. B. and Wilson, B. G. (1968). *Can. J. Phys.* **46**, S849.
Ng, C. K. and Gleeson, L. J. (1971). *Proc. 12th Int. Conf. on Cosmic-rays* (Hobart) **2**, 498.
Parker, E. N. (1964). *Planet. Space Sci.* **12**, 735.
Patel, D., Sarabhai, V. and Subramanian, G. (1968). *Planet. Space Sci.* **16**, 1131.
Rao, U. R. (1972). *Space Sci. Rev.* **12**, 719.
Rao, U. R. and Sarabhai, V. (1964). *Planet. Space Sci.* **12**, 1055.
Rao, U. R., McCracken, K. G. and Venkatesan, D. (1963). *J. geophys. Res.* **68**, 345.
Rao, U. R., McCracken, K. G., Allum, F. R., Palmeira, R. A. R., Bartley, W. C. and Palmer, I. (1971). *Solar Phys.* **19**, 209.
Rao, U. R. and Agrawal, S. P. (1970). *J. geophys. Res.* **75**, 2391.
Subramanian, G. (1971). *J. geophys. Res.* **76**, 1093.
Tolba, M. F. and Lindgren, S. T. (1971). *Proc. 12th Int. Conf. on Cosmic Rays* (Hobart) **2**, 690.

Reprinted from

Pramāna, Vol. 3, No. 2, 1974, pp. 74–88. Printed in India.

Study of cosmic ray diurnal variation on a day-to-day basis

A G ANANTH, S P AGRAWAL[+] and U R RAO*
Physical Research Laboratory, Ahmedabad 380009
[+]Now at the Physics Department, Government Science College, Rewa 486001

*Now at the Indian Scientific Satellite Project, Peenya, Bangalore 562140

ramāṇa, Vol. 3, No. 2, 1974, pp. 74–88. © Printed in India.

Study of cosmic ray diurnal variation on a day-to-day basis

A G ANANTH, S P AGRAWAL+ and U R RAO*
Physical Research Laboratory, Ahmedabad 380009
+Now at the Physics Department, Government Science College, Rewa 486001
*Now at the Indian Scientific Satellite Project, Peenya, Bangalore 562140

MS received 25 February 1974

Abstract. From a careful examination of the diurnal variation of cosmic ray intensity at high energies and the interplanetary field characteristics, the average characteristics of diurnal variation were recently explained by us in terms of a balance between outward convection and field aligned diffusion, the latter arising out of a positive radial density gradient. In this paper, we extend this new concept to explain the large variability observed in the diurnal variation on a day-to-day basis and further demonstrate that the measurement of diurnal anisotropy characteristic of cosmic ray particles on a day-to-day basis can be used directly to infer the nature and scale sizes of interplanetary field parameters. Comparing with the magnetic field vector, we show that this simple concept holds good on more than 80% of days. On the rest 20% of days which have a predominant morning maxima, the diurnal anisotropy characteristics seem to indicate the presence of a significant component of transverse diffusion current in addition to the normal convection and diffusion flow. Such days are found to be present in the form of trains of consecutive days and are found to be associated with abrupt changes in the interplanetary field direction having scale sizes > 4 hr. The value of $K_\perp/K_\parallel$ which is normally about $\leqslant 0{\cdot}05$ is found to be $\approx 1{\cdot}0$ on non-field aligned days.

Keywords. Cosmic rays; diurnal variation; interplanetary magnetic field; solar wind.

1. Introduction

For almost a decade it has been quite apparent that the average cosmic ray diurnal variation is consistent with it being due to corotation of these particles with the solar system magnetic fields which are themselves stretched in the form of an Archimedes spiral by the radially blowing solar wind. The large amount of experimental evidence (Rao *et al* 1963, McCracken and Rao 1965, Rao 1972) obtained from superneutron monitor data have conclusively shown that the yearly average diurnal variation is energy-independent up to a maximum energy $E_{max} \approx 100$ GeV and practically invariant with the solar cycle. Till recently, however, it was widely believed that the amplitude of the observed diurnal variation was considerably less than that predicted by the usual Compton-Getting effect which was attributed to the existence of a significant perpendicular diffusion due to the presence of magnetic field irregularities. Recent low energy solar particle observations made by McCracken *et al* (1968, 1971) simultaneously at different heliolongi-

tudes with widely spaced Pioneer deep space probes have clearly indicated that the azimuthal anisotropy at energies $\lesssim 100$ MeV is quite negligible and that the particle population is largely determined by the balance between radial convection and field aligned diffusion. In other words, it has been shown that at these energies $K_\perp/K_\parallel \lesssim 0{\cdot}05$. Extending these arguments to relativistic energies, McCracken *et al* (1968), Gleeson (1969) and Forman and Gleeson (1970) suggested that the diurnal anisotropy observed in the galactic cosmic radiation can also be understood as a superposition of simple convection and diffusion. Since then the apparent discrepancy between the observed amplitude of the average diurnal variation and the theoretically predicted amplitude has been successfully accounted for (Subramanian 1971) by a number of hitherto unaccounted second order effects such as the finite value of E_{max}, improper normalisation, etc.

From a careful analysis of worldwide neutron monitor network data and their comparison with measured interplanetary field parameters, Rao *et al* (1962) and Hashim *et al* (1972) have independently demonstrated that the average diurnal anisotropy can, in fact, be explained completely in terms of simple convection and diffusion. According to this concept, the radial convective flow will be balanced by the inward diffusion on an average basis causing the net radial current to be zero and resulting in a corotational anisotropy of the right magnitude. Comparing with the interplanetary magnetic field (IPMF) data, Rao *et al* (1972) showed that the diffusion vector is field aligned both on average basis and also during days exhibiting enhanced diurnal variation, the diffusion current, on an average basis, being driven by a radial density gradient of $\approx 5\%$/A.U. which is consistent with the direct measurements (O'Gallagher 1972, Rao 1972). Since this paper (Rao 1972) forms the basis of our present investigation, it will henceforward be referred to as paper I.

Even though the average picture of the diurnal variation has now been explained quite satisfactorily in terms of a good physical model, the detailed picture of the diurnal variation, on a day-to-day basis, remains to be clearly understood. The large variability present in both amplitude and the time of maximum of the diurnal variation has been established by a number of workers (Rao and Sarabhai 1964, Patel *et al* 1968). In paper I, we pointed out that the new concept of the diurnal variation was capable of explaining the day-to-day variability in terms of varying diffusion current, there being no balance between convection and diffusion on a short term basis. A few specific examples were individually treated to demonstrate the validity of the theory showing that, even on days when the interplanetary field vector showed clear departure from the Archimedes spiral pattern the cosmic ray diffusion vector derived from observations were clearly field aligned. In this paper we present detailed analysis of diurnal anisotropy on a day-to-day basis to test the validity of the new concept and demonstrate that on most of the days the concept is valid. Further we also attempt to determine the detailed characteristics of few days on which the observed diurnal anisotropy shows departure from the simple convection and diffusion picture indicating the presence of a significant perpendicular diffusion on such days.

2. Data analysis

In order to examine the cosmic ray diurnal variation on a day-to-day basis in a statistically meaningful way, we have combined the data from six high latitude

Table 1. List of stations used to derive day-to-day diurnal anisotropy vectors

Stations	Geographic coordinates		Mean asymptotic coordinates		Cut-off rigidity (G.V.)
	Latitude (deg.)	Longitude (deg.)	Latitude (deg.)	Longitude (deg.)	
Inuvik	68·4	226	47	233	0·18
Calgary	51·1	246	28	269	1·09
Churchill	58·8	266	40	286	0·21
Deep River	46·1	283	27	319	1·02
Goose Bay	53·3	300	35	339	0·52
Kiel	54·3	10	31	63	2·29

neutron monitoring stations and having a narrow asymptotic cone of acceptance. Table 1 gives the relevant physical parameters of these stations. After taking out long term variation by moving average method, the data on each day are harmonically analysed to obtain the diurnal and semi-diurnal variation vectors for each of the selected stations. The diurnal and semi-diurnal anisotropy amplitude and phase in space as observed at each station are then derived, after correcting for the width and declination of the asymptotic cone of acceptance of the detector and geomagnetic bending using the variational coefficient techniques developed by Rao *et al* (1963) and McCracken *et al* (1965). In the present analysis, all days on which Forbush decreases take place have been rejected since on such days the sharp intensity gradients are likely to cause a large error in the determination of the diurnal vector. The anisotropy information from individual stations are then combined to derive the average diurnal anisotropy in space for each day. We have selected only those days on which there is a good interstation agreement in the observed diurnal vectors ($\sigma_{amp} \leqslant 0{\cdot}1\%$, $\sigma_{pha} \leqslant 30°$) for all our further analysis. The percentage of such days is more than 80. We wish to emphasise the necessity of following the above procedure particularly when dealing with diurnal anisotropy on a day-to-day basis to avoid erroneous conclusions.

Figure 1 shows the histograms of the frequency of occurrence of both the time of maximum and the amplitude of the diurnal anisotropy vector for each day, during 1967–68 derived using the data from six selected stations (solid lines). In the same figure, the corresponding histograms for the diurnal anisotropy vectors as derived from the data from only one station, namely Deep River, are also shown (in dashed lines) for purposes of comparison. The good correspondence between the two sets of histograms demonstrates that the method of obtaining average diurnal anisotropy vectors using data from a number of similar stations provides the true anisotropy vector in space with improved statistics.

Following paper I we represent the observed diurnal vector (δ) as a summation of convective (δ_c) and diffusive anisotropy (δ_d) vectors.

$$\delta = \delta_c + \delta_d \tag{1}$$

$\delta_c = 3CV_p/V$ can be derived from a knowledge of solar wind velocity V_p, V being particle velocity and C the Compton-Getting factor. The diffusive anisotropy

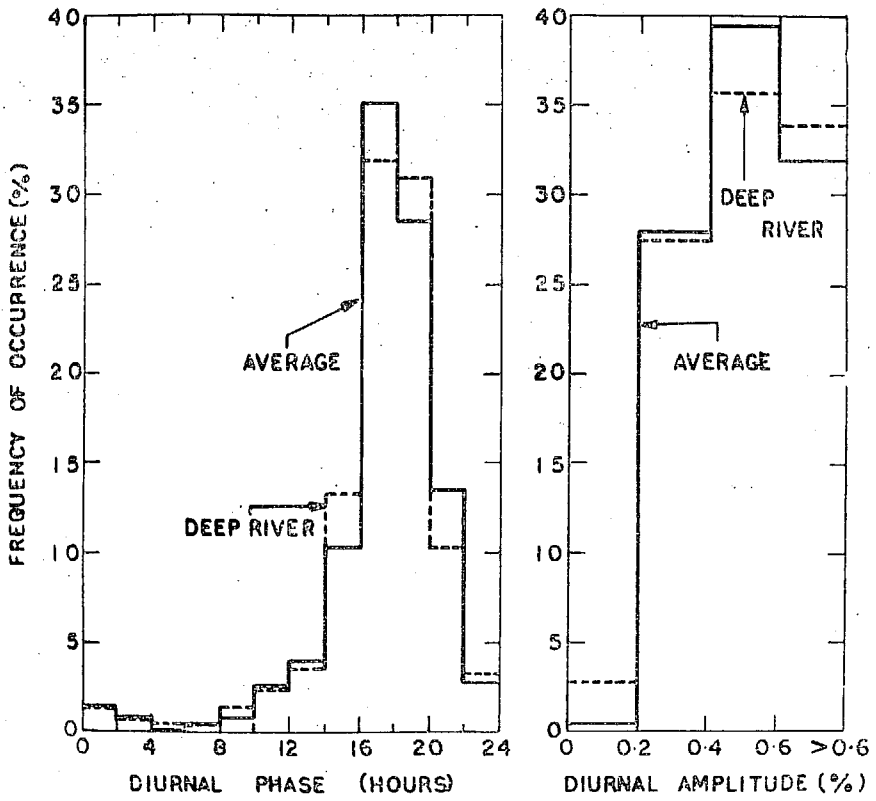

Figure 1. Histogram showing the frequency of occurrence of diurnal phase and amplitude in space obtained using average of six selected stations (solid lines) and also using only data from Deep River neutron monitor (dashed lines).

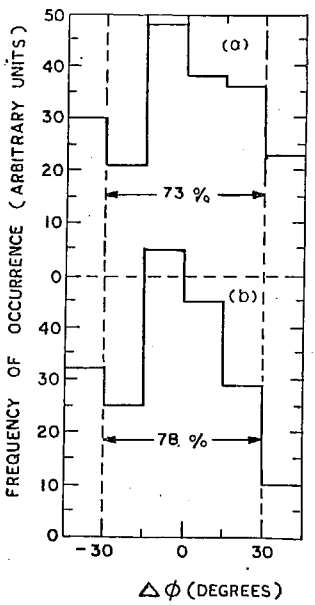

Figure 2. $\Delta\phi$ distribution is shown for a selected number of days (200 days) during 1967–68 for which both solar wind velocity and IPMF data are available. (*a*) shows the distribution for all the 200 days, and (*b*) shows the distribution for days on which there is a good interstation agreement in the determination of the diurnal phase.

vector (δ_d) for each day can be determined by subtracting the convection term δ_e from the observed diurnal anisotropy vector δ. In order to prove the field aligned nature of the diffusive vector, it is necessary to show the difference $\triangle\phi = \phi_d - \phi_n$, should be minimum ($\triangle\phi \approx 0$), *i.e.*, the phase of the diffusive vector ϕ_d is identical with the phase ϕ_n of the interplanetary magnetic field. However, due to large statistical errors, we assume that the diffusive vector is field aligned if $\triangle\phi < 30°$ which is the practical limit of statistical significance one can impose on a daily basis. Days on which diffusion vector is not field aligned, *i.e.*, $\triangle\phi \geqslant 30°$, are designated as non-field aligned days.

3. Characteristics of diurnal variation on a day-to-day basis

Figure 2 shows the histogram of the frequency of occurrence of $\triangle\phi$ for 200 days in 1967–68 for which the data on solar wind velocity are available. It is seen from figure 2 (*a*) that on nearly 73% of days $\triangle\phi < 30°$. If we restrict our analysis to only those days on which there is reasonable interstation agreement in the determination of the diurnal phase (*i.e.*, $\sigma_{pha} < 30°$), the percentage of days on which the convection diffusion concept holds good increases to about 78% (figure 2 *b*)l We may conclude that on nearly 80% of the days, the diurnal anisotropy is describable in terms of simple convection and field aligned diffusion.

Figure 3 shows some typical examples of field aligned nature of diffusion vector on a few selected days, on which either we have observed enhanced solar wind velocity (figure 3 *a*) or observed IPMF direction shows a large deviation from the mean field direction (figures 3 *b* and 3 *c*). In spite of the extreme conditions, it is evident from figure 3 that the diffusion vector is very well field aligned.

In order to extend the analysis for a larger sample of days, even when direct observations on solar wind velocity V_p are not available, we have utilised the empirical relationship between the index of geomagnetic disturbance ΣK_p and V_p for estimating V_p on such days. Existence of such a close empirical relationship between ΣK_p and V_p has been demonstrated by a number of workers (Snyder *et al* 1963, Pai *et al* 1967, Bame *et al* 1967). We have attempted to obtain such an empirical relationship between ΣK_p and V_p for 1967 using the available observations of V_p from Vela 3 satellite. Figure 4 shows the average solar wind velocity for each day for the above period plotted against ΣK_p, the correlation between V_p and ΣK_p is found to be ($0{\cdot}63 \pm 0{\cdot}03$) consistent with the relationship

$$V_p = (4{\cdot}98 \pm 0{\cdot}5) \cdot \Sigma K_p + (302 \pm 9) \qquad (2)$$

Before using the empirical relationship, it is instructive to compare the results of $\triangle\phi$ distribution derived earlier (figure 2 *b*) with results obtained, using V_p values computed from the empirical relationship, given in eq. (2). Figure 5 shows the frequency distribution of $\triangle\phi$ for 170 days during 1967–68, $\triangle\phi$ being computed using V_p values obtained from the empirical relationship using eq. (2). $\triangle\phi$ distribution obtained using observed values of V_p for the same days is also plotted for comparison. The excellent correspondence between the two distributions confirms that the method of calculating the convective vector δ_e using wind velocity values computed using eq. (2) does not affect any of our conclusions. From a close examination of the data we also confirm that the maximum error introduced by this method is less than 10°, which is well within the statistical error on a day-to-day basis.

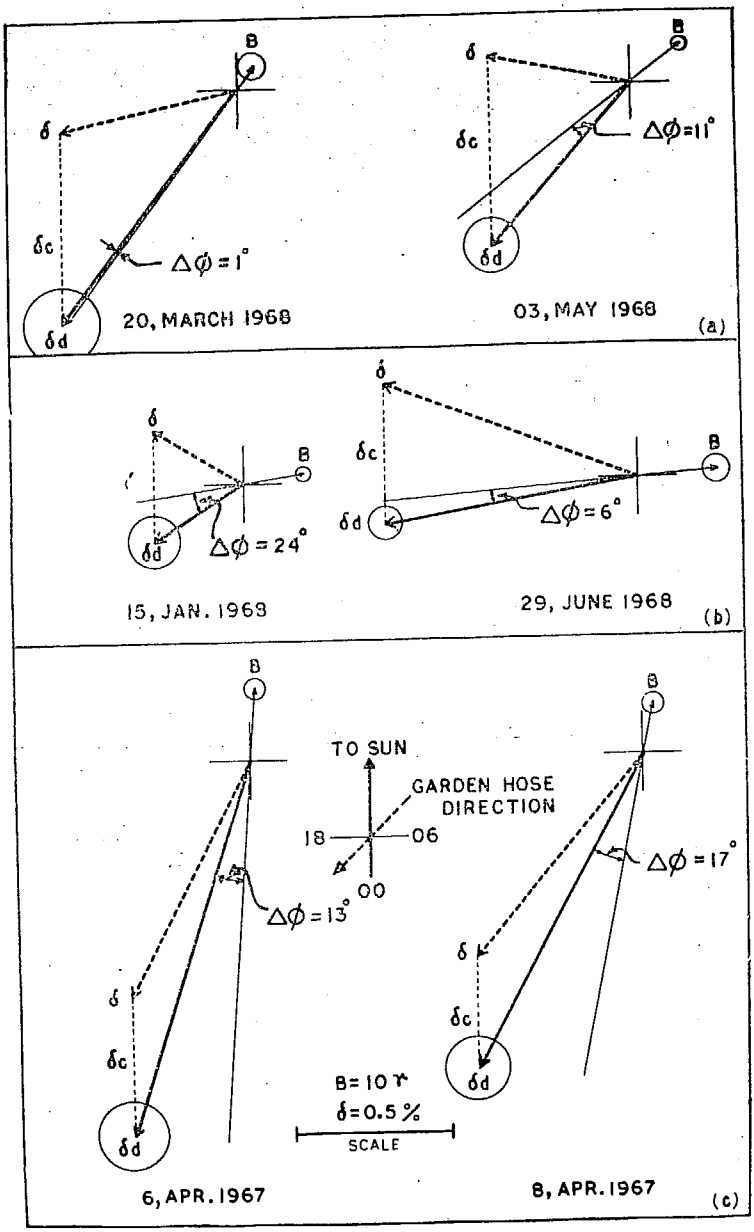

Figure 3. Typical examples showing the field aligned nature of the diffusion vector δ_d when (*a*) the convection δ_c is very much enhanced; and (*b*) and (*c*) the observed IPMF direction ϕ_B shows large departures from the mean Archimedian spiral angle.

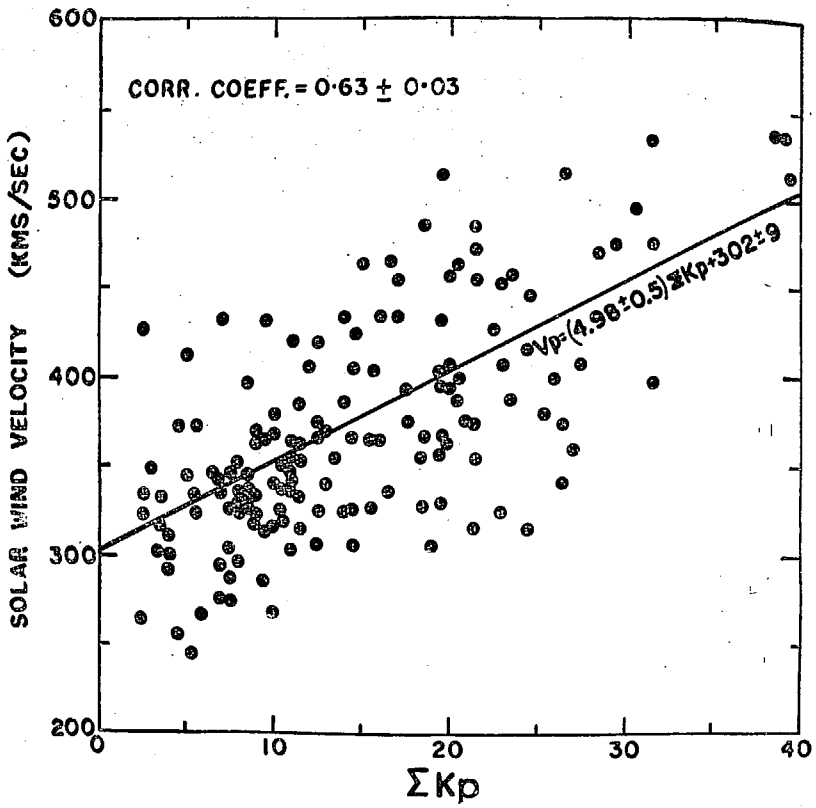

Figure 4. The correlation between observed solar wind velocity V_p and $\sum K_p$ the index of geomagnetic disturbance during 1967.

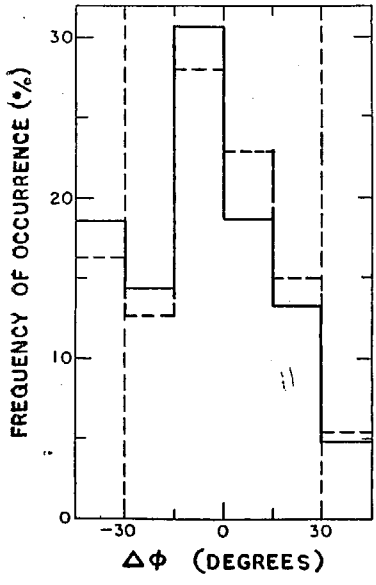

Figure 5. $\Delta\phi$ distribution for a selected number of days (solid line) during 1967-68, computed using V_p obtained from the empirical relationship shown in equation (2). The $\Delta\phi$ values obtained using actual observation of V_p for the same days is shown (dashed lines).

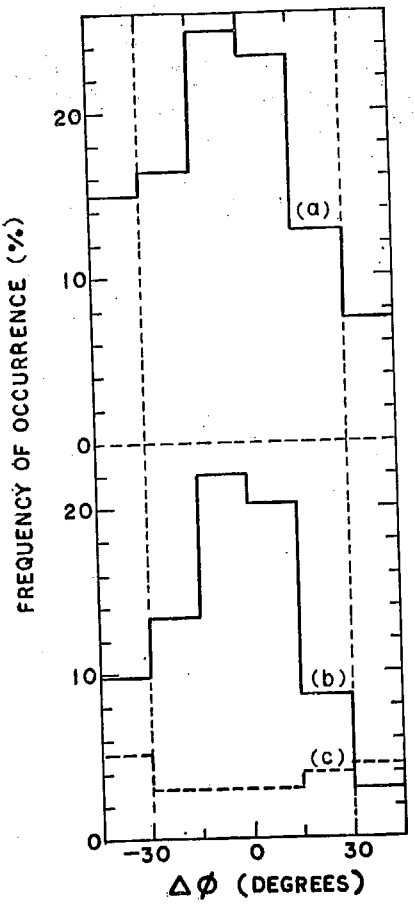

Figure 6. Histogram showing $\Delta\phi$ distribution on (*a*) nearly 400 days during 1967–68, (*b*) for days on which the observed diurnal time of maximum (α) is in between 15–21 hours, and (*c*) days on which α is in between 0–15 hours and 21–24 hours (dashed lines).

We have extended the analysis for the entire period 1967–68 by deriving convection vector on each day using the above relationship between V_p and ΣK_p. Figure 6 (*a*) shows the histograms of $\Delta\phi$ distribution for all the days (400 days) during 1967–68. We have also shown in the same figure the $\Delta\phi$ distribution separately for days on which the observed diurnal time of maximum is between (1) 15–21 hours (figure 6 *b*) and (2) 0–15, 21–24 hours (figure 6 *c*). It is evident from figures 6 (*a*) and 6 (*b*) that on more than 80% of the days the convection diffusion concept holds good. Also note that on days on which the diurnal time of maximum is between 0–15 and 21–24 hours (figure 6 *c*), the histogram of $\Delta\phi$ distribution is almost flat indicating that on those days on which the diurnal vector is far removed from the direction of corotation, the transverse diffusion currents are quite significant.

4. Characteristics of non-field aligned days

In this section, we examine the detailed characteristics and the solar terrestrial relationships of the days on which the diffusion vector is not field aligned ($\Delta\phi \geqslant 30°$), in order to understand the mechanism which causes the transverse diffusion to be significant on such days. We observe that majority of the non-field aligned days occur in trains of two or more consecutive days indicating that the mechanism

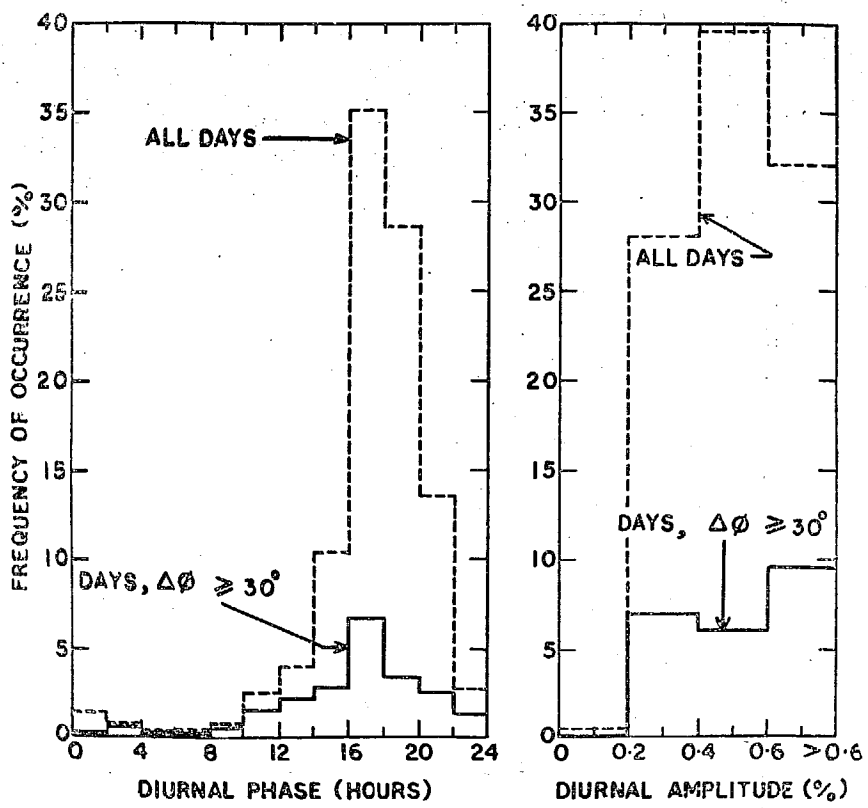

Figure 7. Histograms showing the distribution of diurnal phase and amplitude for the non-field aligned days (solid lines) during 1967–68. The corresponding histograms for all the 400 days on this period are also shown in dashed lines.

causing transverse diffusion is not a transient phenomenon, but persists over a period of time. In spite of the tendency for such days to occur on consecutive days, they do not show any characteristic features such as enhancement in the diurnal or semidiurnal components, ΣK_p index or large variability in interplanetary field parameters. Likewise no large deviation in the mean intensity or 27-day recurrence are observed during these days.

In figure 7 are plotted the frequency distribution of diurnal phase and diurnal amplitude for all the non-field aligned days (solid lines) during 1967–68. For comparison the histogram of diurnal phase and amplitude for all 400 days during 1967–68 is also shown (dashed lines). Whereas the familiar predominant peak around 18 hr direction is clearly evident from the histogram of the diurnal phase for all the days, the histogram for only non-field aligned shows a much flatter distribution. Further it is seen that practically all the days on which diurnal time of maximum is in the morning hours (0–12 hr) the diffusion vector is not field aligned.

Since the presence of trains of non-field aligned days indicate essentially quasi-permanent anomalous condition in the interplanetary space causing transverse diffusion currents we have concentrated on detailed examination of the interplanetary condition during such periods. In figure 8, we show the average IPMF vector for each day plotted end to end for a number of non-field aligned trains of days.

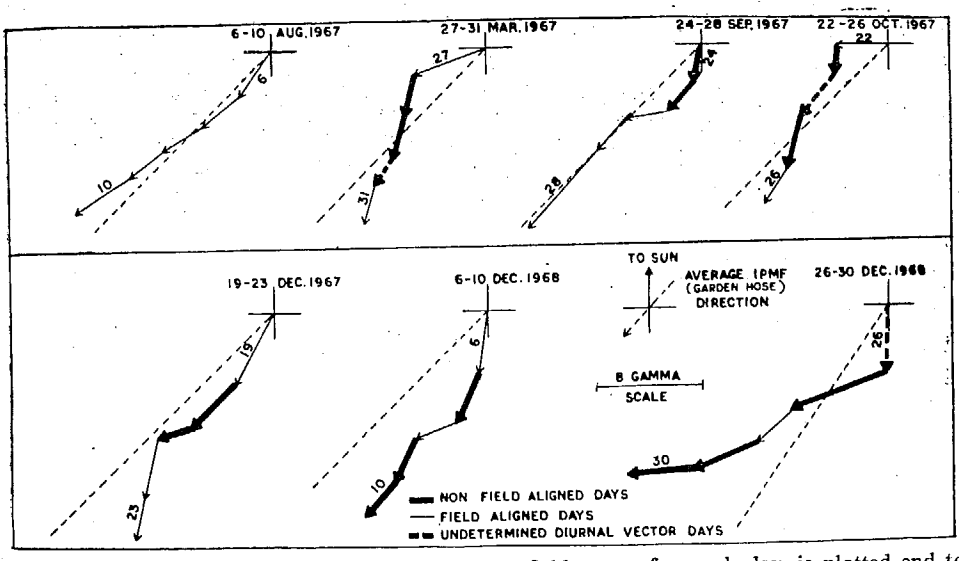

Figure 8. The interplanetary magnetic field vector for each day is plotted end to end for a few trains of consecutive non-field aligned days. For comparison the field vectors for one typical field aligned train of consecutive days (6–10 August 1967) is also shown.

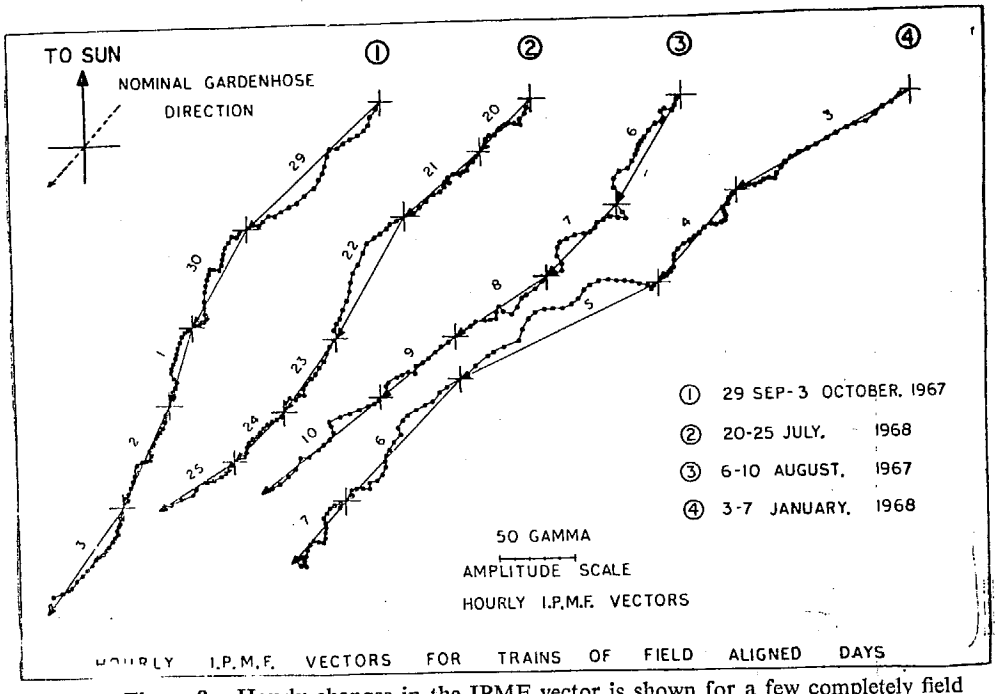

Figure 9. Hourly changes in the IPMF vector is shown for a few completely field aligned trains of days.

For comparison, the field vectors for a typical field aligned train of days is also shown. It is evident from the figure that on days on which the diffusion is field aligned the field vectors are well behaved and do not show significant departure from Archimedian spiral. On the other hand, on trains of days on which the diffusion is not field aligned, the field vectors show a large variability both in direction and in magnitude from day-to-day and often show large departures ($> 45°$) from the mean Archimedian spiral.

Before proceeding to examine in detail, the IPMF characteristics on non-field aligned days, it is instructive to examine the characteristics on field aligned days. Figure 9 shows the hourly changes in IPMF vector along with the daily mean for each day for a few typical trains of field aligned days. Examination of each of the trains shown in the figure clearly brings out the two most important characteristic features of the IPMF for these days:

(*a*) the change in the field vector from one hour to the next on the same day is relatively small, and

(*b*) the change in the field characteristics from one day to the next during each train of events is also negligible.

On the other hand, examination of trains of non-field aligned days shows that on such days large irregularities in the interplanetary field exist. In figure 10

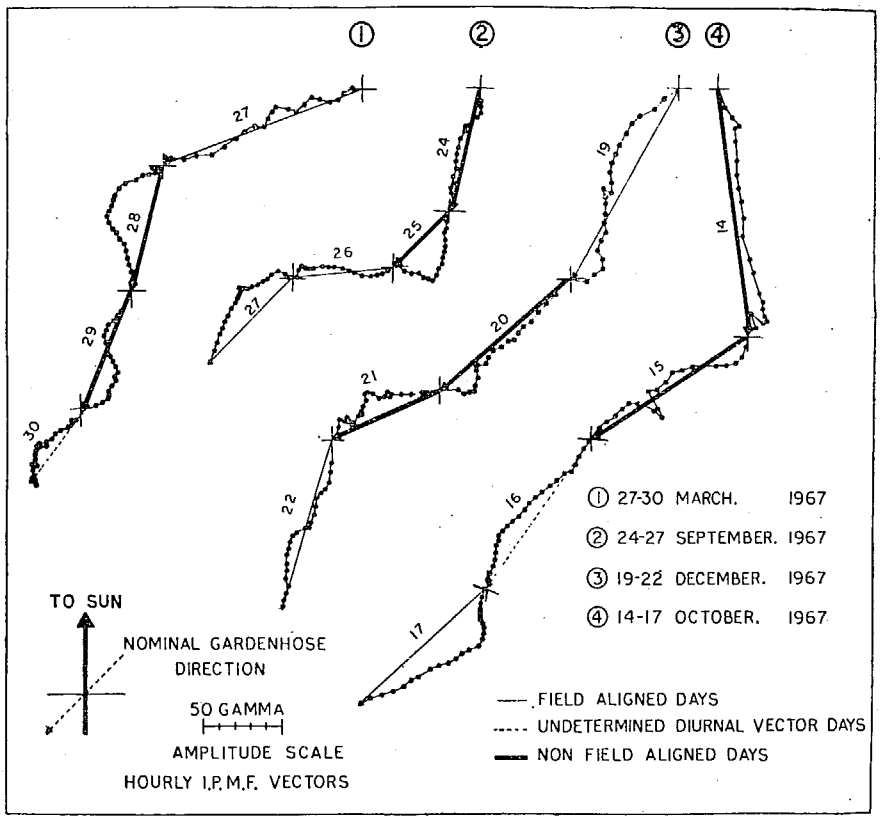

Figure 10. Hourly changes in the IPMF vector is plotted for few non-field aligned trains of days on which there is a large change in the daily mean IPMF vector from one day to the next.

are shown examples of trains of non-field aligned days when the IPMF vector exhibits large change from one day to another. The average daily field vector seems to change its direction by as much as 60–90° from one day to the next. Figure 11 shows examples of trains of non-field aligned days when the IPMF vector, even though does not show large changes from one day to the next, shows the continual presence of large irregularities having scale sizes of > 4 hr during each day.

In order to estimate the scale sizes of the irregularities present during the non-field aligned days, a power spectrum analysis of the IPMF data has been carried out and figure 12 shows the power density distribution of the radial component at various frequencies for a selected train of non-field aligned days (circles) and also for a train of completely field aligned days (dots). The figure clearly demonstrates that in spite of the large errors associated with the limited data we have used, during non-field aligned trains of days there is a tendency for irregularities having scale sizes $\approx 4{\cdot}3$ hr and $6{\cdot}6$ hr to dominate when compared with field aligned trains of days. These irregularities can effectively scatter particles > 1 GeV and thus introduce a significant transverse gradient in addition to normal convection and diffusion during non-field aligned days.

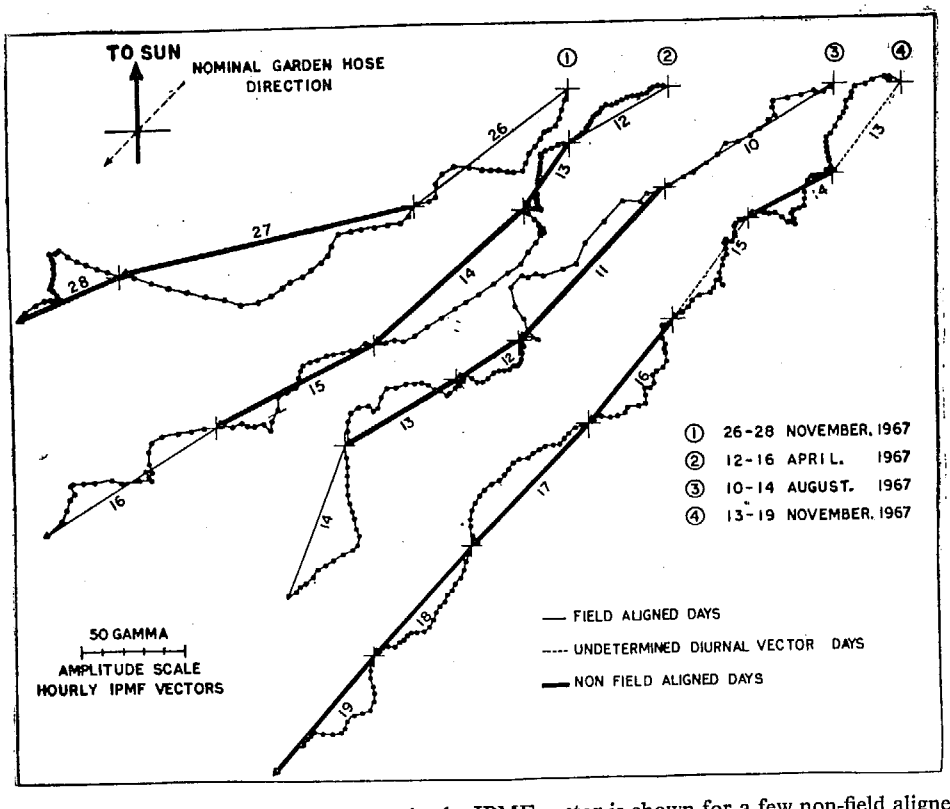

Figure 11. Hourly changes in the IPMF vector is shown for a few non-field aligned trains of days on which there is no day-to-day changes in the daily mean IPMF Note the continual presence of irregularities of scales > 4 hr on these days.

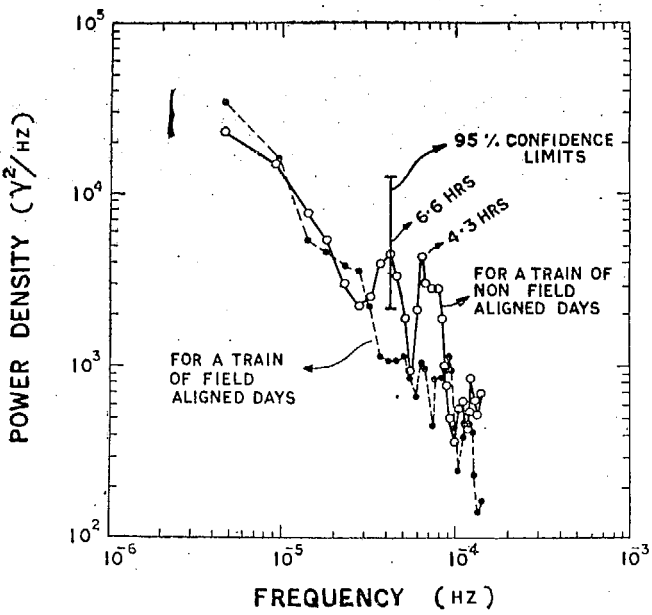

Figure 12. The power density of the radial component of IPMF is plotted against frequency for one typical train of field aligned days during 29 September to 3 October 1967 (shown by dots) and for a typical train of non-field aligned days during 14–18 November 1967 (by circles). Note the predominant peak at 4·3 hr and 6·6 hr during the train of non-field aligned days.

5. Discussion and conclusion

Following Forman and Gleeson (1970), we can write the expression for the net streaming of cosmic ray particles in the interplanetary medium as

$$S = S_c - K_{\parallel}\left(\frac{\partial U}{\partial r}\right)_{\parallel} - K_{\perp}\left(\frac{\partial U}{\partial r}\right)_{\perp} - F\left(\frac{\partial U}{\partial r}\frac{B}{B}\right) \tag{3}$$

where

$$F = \frac{V^2}{3\omega}\left[\frac{(\omega\tau)^2}{1+(\omega\tau)^2}\right],$$

$\partial U/\partial r$ is the radial density gradient and S_c is the convection current density. In paper I we showed that the diurnal variation, on an average basis, as well as enhanced diurnal variation are explainable in terms of simple convection and diffusion, *i.e.*, $K_{\perp}/K_{\parallel}$ is negligible. The diffusion current on such days was shown to be consistent with the expected radial density gradient. In this paper, we have conclusively demonstrated that this is indeed the case on more than 80% of the days even on the basis of individual days. In other words, on a majority of days $K_{\perp}/K_{\parallel}$ is negligible ($\lesssim 0{\cdot}05$) or the third and fourth terms in the right hand side of eq. (3) may be neglected. Nonetheless on a small percentage of days ($\approx 20\%$), the interplanetary conditions are such that $K_{\perp}/K_{\parallel}$ can no longer be completely neglected, *i.e.*, the daily variation on such days cannot be completely accounted only by radial convection and field aligned diffusion and the transverse currents due to perpendicular diffusion do significantly contribute to the daily variation on such days. The association of large scale interplanetary magnetic field irregularities on these

days of scale sizes ranging from a few hours ($\gtrsim$ 4 hr) to days clearly substantiates the above hypothesis. It may be noted that using power spectrum analysis Owens and Jokipii (1972) have recently demonstrated for the cosmic ray scintillations at Alert observed at low frequencies $< 5 \times 10^{-5}$ Hz (6 hr) are caused mainly by the fluctuating component of interplanetary magnetic field. They have suggested that the most likely mechanism for high energy cosmic ray scintillations at low frequencies is the strong interaction of these particles with magnetic field irregularities during their propagation in the interplanetary medium. It is interesting to note that the scale sizes which they derive for the field irregularities are consistent with our observations.

It is well known that the presence of irregularities cause random changes in the pitch angles of the particles as they move along the lines of force, the integrated effect of a large number of such irregularities being essentially to produce a three-dimensional random walk in the motion of particles. The resonant scattering due to irregularities is maximum for particles whose gyroradius (ρ) is of the same order as the scale size of the irregularities ($2\pi\rho$). In other words, to produce an appreciable scattering for particles of rigidity > 1 G.V., the scale sizes of the irregularities must be > 4 hr (assuming a mean solar wind velocity of 400 km/sec and average interplanetary field of 5 gammas) which are consistent with the observed scale sizes of the interplanetary field irregularities.

From the observed values of the diurnal variation during the trains of non-field aligned days, it is possible to estimate the value of $K_\perp/K_\parallel$. Assuming an average radial density gradient of 5%/AU, $K_\parallel$ at neutron monitor energies can be estimated to be $\approx 5 \times 10^{21}\, \rho\beta$ cm^2 sec^{-1}. On the other hand, examining a large number of trains of non-field aligned days when the average phase difference between the interplanetary field vector and diffusion vector ($\triangle\phi$) is about 42°, $K_\perp/K_\parallel$ ratio for non-field aligned days is found to be $\approx 1{\cdot}0$.

From the data and analysis presented in the foregoing sections, we draw the following conclusions:

(i) On an average basis the diurnal anisotropy of cosmic radiation is completely understood as a superposition of simple convection and field aligned diffusion. On a day-to-day basis, this concept holds good on more than 80% of the days.

(ii) On the rest of 20% of the days transverse diffusion also plays an important role. On these days, the diurnal time of maximum shows a preference to occur either during early morning (0–15) or during late evening (21–24) hours.

(iii) Days on which transverse diffusion is predominant seem to occur in trains of two or more consecutive days.

(iv) Such trains of days are usually associated with abrupt changes in the direction of interplanetary magnetic field. The non-field aligned days are associated with the presence of large irregularities in the interplanetary magnetic field of scale sizes > 4 hours.

(v) The value of perpendicular diffusion coefficient on non-field aligned days is quite significant. $K_\perp/K_\parallel \approx 1{\cdot}0$ for these days as compared to $\approx 0{\cdot}05$ observed on field aligned days.

(vi) From a careful examination of the cosmic ray anisotropy on a day-to-day basis, it is possible to infer the interplanetary field conditions and predict the nature and scale sizes of irregularities present in the magnetic field.

Acknowledgements

The research presented here was supported by funds from the Department of Space, Government of India and funds from Day Fund Grant No. 17 from National Academy of Sciences, U.S.A.

References

Bame S O, Asbridge J R, Hundhausen A J and Strong I B 1967 *Trans. Amer. Geophys. Union Abstract* **48** 190
Forman M A and Gleeson L J 1970 Preprint Manash University
Gleeson L J 1969 *Planet. Space Sci.* **17** 31
Hashim A, Bercovitch M and Steljes J F 1972 *Solar Phys.* **22** 220
McCracken K G, Rao U R, Fowler B C, Shea M A and Smart D F 1965 *IQSY Instruction Manual* No. 10.
McCracken K G and Rao U R 1965 *Proc. Cosmic Ray Conf. (London)* **1** 213
McCracken K G, Rao U R and Ness N F 1968 *J. Geophys. Res.* **73** 4159
McCracken K G, Rao U R, Bukata R P and Keath E P 1971 *Solar Phys.* **18** 100
O'Gallagher J J 1972 *Rev. Geophys. Space Phys.* **10** 821
Owens A J and Jokipii J R 1972 *J. Geophys. Res.* **77** 6639
Pai G L, Bridge H S, Lyon E F and Egidi A 1967 *Trans. Amer Geophys. Union* **48** 176
Patel D, Sarabhai V and Subramanian G 1968 *Planet. Space Sci.* **16** 1131
Rao U R, McCracken K G and Venkatesan D 1963 *J. Geophys. Res.* **68** 345
Rao U R and Sarabhai V 1964 *Planet. Space Sci.* **12** 1055
Rao U R 1972 *Space Sci. Rev.* **12** 719
Rao U R, Ananth A G and Agrawal S P 1972 *Planet. Space Sci.* **20** 1799
Snyder C W, Neugebauer M and Rao U R 1963 *J. Geophys. Res.* **68** 6361
Subramanian G 1971 *J. Geophys. Res.* **76** 1093

Pre-print

CR-74-

HIGH ENERGY COSMIC RAY INTENSITY INCREASES OF NON SOLAR ORIGIN AND THE UNUSUAL FORBUSH DECREASE OF AUGUST 1972+

S. P. AGRAWAL*, A. G. ANANTH, M. M. BEMALKHEDKAR,
L. V. KARGATHRA, U. R. RAO**
Physical Research Laboratory

PHYSICAL RESEARCH LABORATORY
AHMEDABAD-380009, INDIA.

Pre-print

CR-74-02

HIGH ENERGY COSMIC RAY INTENSITY INCREASES OF NON SOLAR ORIGIN AND THE UNUSUAL FORBUSH DECREASE OF AUGUST 1972+

S. P. AGRAWAL*, A. G. ANANTH, M. M. BEMALKHEDKAR, L. V. KARGATHRA, U. R. RAO**

Physical Research Laboratory,
Ahmedabad--380009 (India).

and

H. RAZDAN
Bhabha Atomic Research Centre
HARL, Gulmarg (India).

ABSTRACT

A series of spectacular cosmic ray events which included two relativistic solar particle enhancements and three major Forbush decreases were registered by ground based cosmic ray monitors beginning on August 4, 1972. Amongst these, the Forbush decrease which occurred on August 4–5 exhibited extremely interesting and complex behaviour, the prominent features of which are a pre-increase PI-1 prior to the largest decrease FD-2 during the recovery of which an abrupt universal time increase PI-2 occurred. Large N-S and E-W anisotropies were observed during the entire Forbush decrease event. The rigidity spectra for both FD-2 and PI-2 had practically the same exponent of -1.2 ± 0.2 with an upper cutoff rigidity of about 50–60 GV, and the anisotropy during both PI-1 and PI-2 was from the sunward direction. The paper describes the detailed observational features and presents an unified model to explain these in terms of a transient modulating region associated with the passage of a shock front. In this model, the reflection of particles from the approaching shock front accounts for the pre-increase PI-1, the early onset of FD--2 from the anti--sun direction being caused by the occultation of particle trajectories reaching the earth from that direction while the detectors looking along sunward direction are still sampling albedo particles reflected from the shock front. The main Forbush decrease occurs as the shock front containing tangled magnetic fields with large scale tangential discontinuities sweeps past the earth. The particles diffusing into the cavity, as they are swept by the Solar wind, get 'piled up' behind the tangled field region causing the abrupt increase PI--2. Evidence from interplanetary plasma, radio and field measurements are provided in support of the model wherever possible.

During the declining phase of the current solar cycle, a series of intense solar flares erupted in August 1972, from an active region (McMath plage region # 11976) on the solar disc causing severe cosmic ray disturbances on the earth (Pomerantz and Duggal, 1973a) accompained by quite spectacular visual aurorae, geomagnetic storms, radio black out and a host of other terrestrial effects. The time evolution of the active region responsible for these disturbances and the detailed description of the associated solar terrestrial effects are well documented in the reports compiled by World Data Centre-A for Solar Terrestrial Physics (Report UAG-28, Part I, II, & III, July 1973).

* Now at the Physics Department, Govt. Science College, Rewa (M. P.) --486001, India.
** Also at the Indian Scientific Satellite Project, Peenya, Bangalore--560022. India.
+ To appear in Journal of Geophysical Research 1974

Two large solar flares observed on August 2, at 1838 UT (importance 1B) and 1958 UT (importance 2B) produced sudden commencements of the geomagnetic storm (SSC) on August 4, at 0119 UT and 0220 UT respectively (Figure 1). This was followed by a third, very severe sudden commencement geomagnetic storm at 2054 UT on August 4, which if we attribute to the solar flare of importance 3B occurring at 0621 UT yields a value of $\approx$2700 km sec^{-1} for the solar wind velocity. The observation of peak solar wind velocities of $\approx$2000 km sec^{-1} by instrumentation on HEOS-2 (Gruenwaldt et al., 1972) is consistent with our assumption, if allowance is made for the deceleration of shock waves in the interplanetary medium often observed (Hundhausen 1970; Dryer et al., 1972, Dryer, 1973).

solar proton increases accompanied by three Forbush decreases. It is seen that the first of the three Forbush decreases (FD-1) had its onset at $\approx$ 02 UT on August 4, and exhibited classical features. During its recovery, a short lived anisotropic solar particle increase (SP-1) was observed with a maximum at $\approx$ 15 UT on August 4, by neutron monitors, having geomagnetic cutoff rigidity (P_c) less than 1.4 GV. Before the completion of the decay phase of SP-1 (Figure 3a), an anisotropic increase in the intensity (PI-1) was recorded in both meson and neutron monitors preceding the main Forbush decrease (FD-2). The second Forbush decrease (FD-2) had its onset between 21-22 UT on August 4, with an amplitude of about 25% at high latitude neutron monitors. This was followed by an even more rapid increase in the

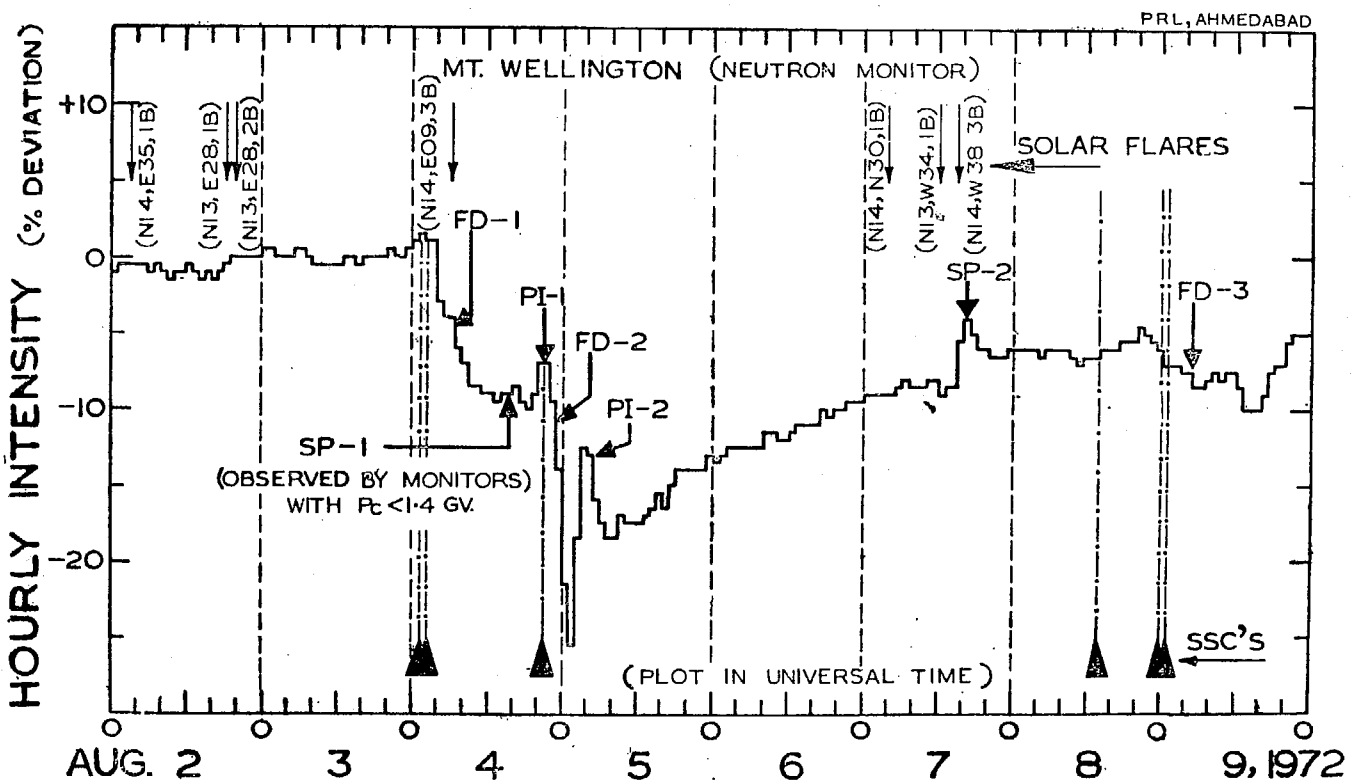

Figure 1 : The cosmic ray intensity profile during August 2-9, 1972 observed by a typical high latitude neutron monitor along with the time of SSC's and the solar flares. The prominent features in the complex intensity profile are individually marked.

Figure 1 shows the typical cosmic ray intensity rofile observed during August 2-9, 1972 by a ground ased monitor. The unusual complex features associated ith intensity changes as well as their time association ith solar and terrestrial disturbances are clearly marked n the same figure. Principally these consisted of two

intensity (PI-2), of about 10-15 % at high latitudes. Finally during the recovery of FD-2, a second solar flare particle enhancement (SP-2) occurred at $\approx$ 16 UT on August 7, which was followed a day later by the third Forbush decrease (FD-3) on August 9, 1972.

Table 1 lists the general characteristics of these individual features. The most spectacular feature of the event, in our opinion, is the main Forbush decrease (FD–2) which is accompanied by two intensity enhancements of non–solar origin, PI–1 and PI–2, all of which have not yet been fully explained for want of sufficient observations. In addition we note that longitudinal anisotropics in the equatorial plane as well as north–south (N–S) anisotropics of large amplitude exist both during FD–2 and PI–2 (Dutt et al., 1973). In the present paper, we discuss the detailed characteristics of these three features PI–1, PI–2 and FD–2 and provide only a brief summary of other features for the sake of completeness. We also describe a qualitative model based on the transient modulating region associated with the passage of the intense shock wave containing large tangled magnetic fields to provide a comprehensive understanding of the interesting and complex features mentioned above.

TABLE 1

General characteristics of various cosmic ray events (as shown in figure 1), observed during August 3–10, 1972

CHARACTERISTICS	(a) DECREASES				(b) INCREASES		
	FD–1	FD–2	FD–3	SP–1	PI–1	PI–2	SP–2
Onset time	2–4 UT	21–22 UT	01 UT	13 UT	18–19 UT	2–3 UT	16 UT
Time of Maximum	15 UT	01–02 UT	12–14 UT	15 UT	21–22 UT	5 UT	17 UT
Amplitude	7%	25%	5%	7%	2.5%	12%	5%
Spectral Exponent	-0.8 ± 0.2	-1.2 ± 0.2	–	–	0.0	-1.2 ± 0.2	–
Amplitude of anisotropy in the equatorial plane	3%	7–8%	3%	–	2%	5%	–
Direction in space	9 hrs.	5 hrs. (minimum intensity)	18 hrs.	–	12 hrs. (maximum intensity)	12 hrs.	—
Amplitude of anisotropy in the north–south direction	4%	5%	2%	—	3%	3%	—
Direction in space	South	North	North	—	North	North	—

DATA PRESENTATION AND ANALYSIS

The Physical Research Laboratory, Ahmedabad, maintains neutron and meson monitors at Ahmedabad and a neutron monitor at Gulmarg, which have high cutoff rigidities and therefore, when combined with low cutoff rigidity monitors, are most suited for studying the rigidity dependence of any cosmic ray event. The cosmic ray intensity observed by these monitors during the period August 3–10, are plotted in Figure 2. We note that the magnitude of the Forbush decrease at an equatorial station like Gulmarg during this period is $\approx 11\%$ which is largest observed todate.

Since the cosmic ray intensity is constant within statistical limits for at least three days prior to FD–1, we have taken the daily mean intensity on August 3 as the hundred percent level for all the stations given in Table 2. Figure 3 (a and b) presents the intensity profiles observed at two pairs of polar stations looking along the north and south directions. The presence of strong N–S asymmetries during FD–1, FD–2 and PI–2 is evident. Further figure 3c, which shows the percent deviations for the two stations with $P_c \approx 1.8$ GV and viewing in opposite directions in the equatorial plane, indicates likewise the presence of strong longitudinal anisotropies during FD–2 and PI–2. Even though the

TABLE–2

List of stations whose data have been utilized in the present analysis, along with their geographic coordinates, geomagnetic cutoff rigidities (P_c), mean asymptotic directions of viewing at zero Universal time (UT) and the poisson errors (in percent) derived from the hourly counting rate

No.	Station	Geog. Coordinates Lat. (DEG)	Geog. Coordinates Long. (DEG)	Altitude (Meters)	Cutoff rigidity (GV)	Asy. Coordinates Lat. (DEG)	Asy. Coordinates Long. (DEG)	Poisson error (%)
01	Ahmedabad (neutorn monitor)	23.01	72.61	40	15.94	10	130	.24
02	Ahmedabad (meson minitor)	23.01	72.61	40	15.94	10	120	.10
03	Athens	37.06	23.70	40	8.72	11	82	.35
04	Brisbane	–27.50	153.01	SL	7.0	18	245	.63
05	Calgary	51.08	245.91	1110	1.09	5	267	.12
06	Churchill	58.75	265.91	39	0.21	32	284	.12
07	Dallas	32.78	263.20	208	4.35	–28	321	.12
08	Deep River	46.10	282.50	145	1.02	5	317	.08
09	Durham	43.10	289.16	SL	1.41	–2	331	.28
10	Gulmarg	30.07	74.42	2743	11.91	1	140	.20
11	Hobart (meson monitor)	–42.92	147.24	SL	1.89	–24	186	.28
12	Huancayo	–12.03	283.12	3400	13.49	–7	353	.25

13	Itabashi	35.45	139.43	20	11.61	-1	203	.15
14	Khabarovsk	48.52	135.12	SL	5.70	-23	228	.13
15	Kiel	54.33	10.13	54	2.29	3	64	.13
16	Leeds	53.82	358.45	100	2.20	4	52	.13
17	Mawson	-67.60	62.88	SL	0.22	-39	52	.56
18	Mcmurdo	-77.85	166.62	48	0.05	-79	266	.12
19	Mexico City	19.33	260.82	2274	9.53	-11	317	.45
20	Mt. Norikura	36.12	137.56	2770	11.39	00	200	.12
21	Mt. Washington	44.30	288.70	1917	1.24	01	329	.28
22	Mt. Wellington	-42.92	147.24	725	1.89	00	196	.16
23	Oulu	65.00	25.40	15	0.81	30	63	.18
24	Pic-du-Midi	42.93	0.25	2860	5.36	-13	78	.06
25	Resolute	74.69	265.00	SL	0.00	66	273	.21
26	Rome	41.90	12.52	60	6.31	-10	87	.20
27	South Pole	-89.98	0.00	2820	0.11	-61	344	.22
28	Sulphur Mt	51.20	244.39	2283	1.14	5	265	.11
29	Swarthmore	39.90	284.65	80	1.92	-10	331	18
30	Thule	76.55	291.14	260	0.04	72	316	.16
31	Tixie Bay	71.55	128.90	SL	0.53	37	159	.13
32	Utrecht	52.08	05.13	SL	2.76	-2	62	.12
33	Yakutsk	62.02	129.72	105	1.70	10	170	.17

present paper is not intended to discuss the detailed nature of the N–S anisotropies, in view of the existence of these, the study of the longitudinal anisotropies in the equatorial plane has been made only with stations having asymptotic latitudes within ± 30°.

determining the rigidity dependence of various events listed in Table 1. Such a method overcomes the ambiguity in the determination of the spectral exponent arising from large special anisotropies.

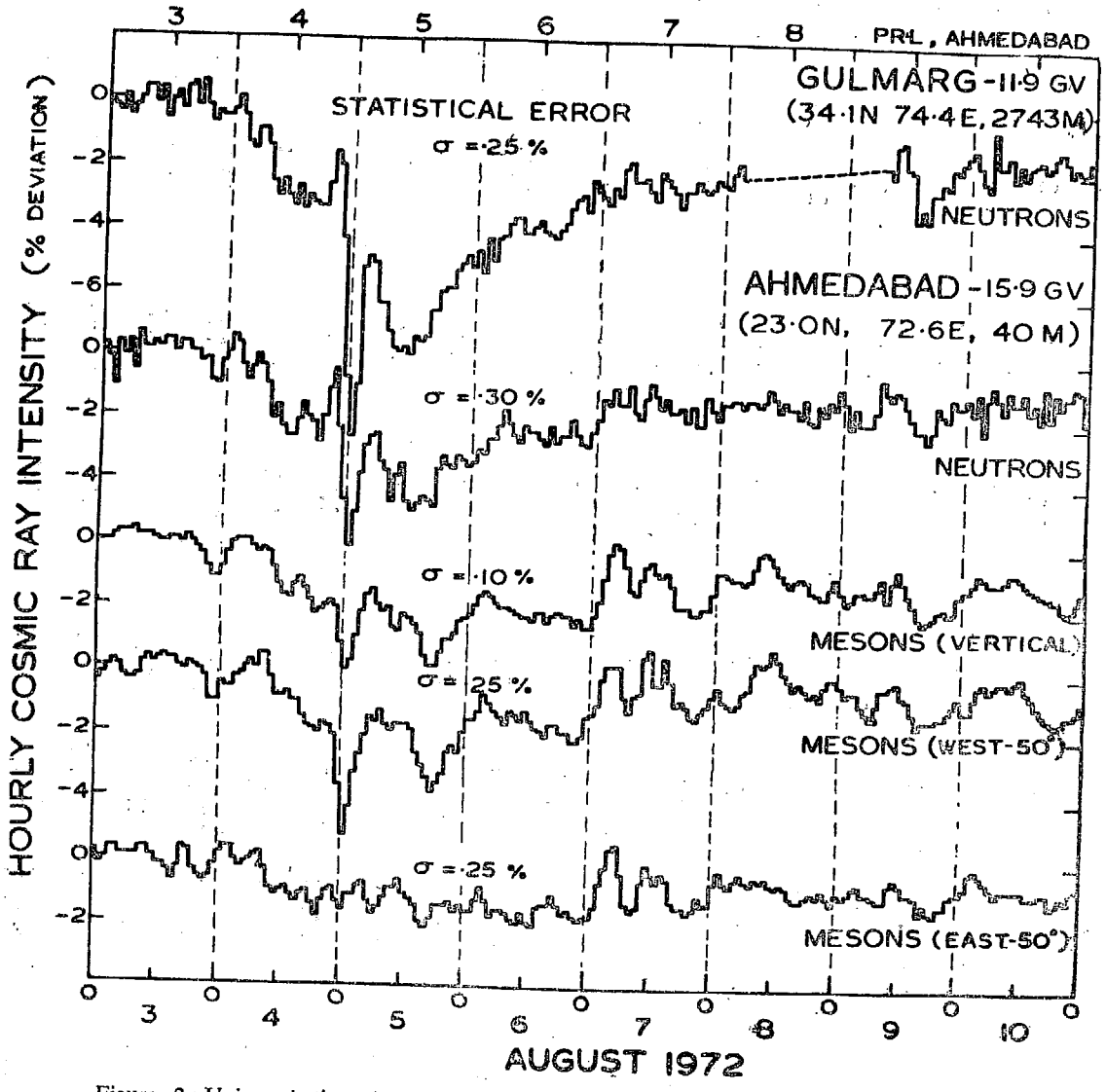

Figure 2 ; Universal time hourly cosmic ray intensity during the period August 3–10, 1972 recorded by neutron and meson monitors operated by the Physical Research Laboratory, Ahmedabad. The geographic latitude, longitude and the altitude of the station in metres above sea level are also given in the figure.

Figure 4 shows the intensity profile observed at different stations, seperately for three asymptotic longitude belts of width 120° each. Since the volume of data available in the longitude belt 120°–240° East is much larger, the monitors in this belt have been utilized for

DETAILED FEATURES OF AUGUST EVENT

Forbush Decrease FD–1 on August 4, 1972; The cosmic ray intensity started decreasing in the early hours of August 4, resulting in the first Forbush decrease FD–1. The high latitude sea level neutron monitors recorded a

present paper is not intended to discuss the detailed nature of the N–S anisotropies, in view of the existence of these, the study of the longitudinal anisotropies in the equatorial plane has been made only with stations having asymptotic latitudes within ± 30°.

determining the rigidity dependence of various events listed in Table 1. Such a method overcomes the ambiguity in the determination of the spectral exponent arising from large special anisotropies.

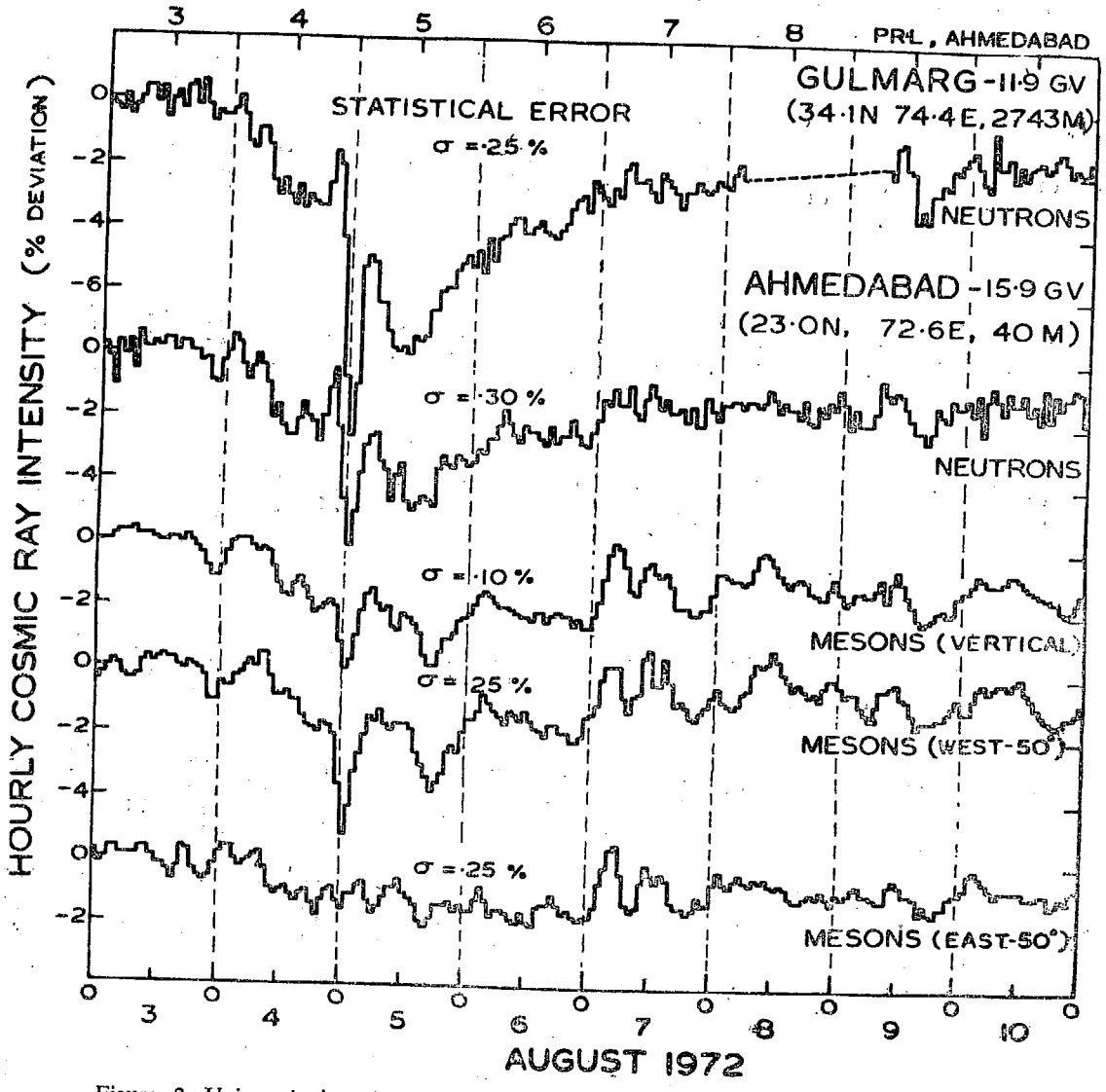

Figure 2 ; Universal time hourly cosmic ray intensity during the period August 3–10, 1972 recorded by neutron and meson monitors operated by the Physical Research Laboratory, Ahmedabad. The geographic latitude, longitude and the altitude of the station in metres above sea level are also given in the figure.

Figure 4 shows the intensity profile observed at different stations, seperately for three asymptotic longitude belts of width 120° each. Since the volume of data available in the longitude belt 120°–240° East is much larger, the monitors in this belt have been utilized for

DETAILED FEATURES OF AUGUST EVENT

Forbush Decrease FD–1 on August 4, 1972; The cosmic ray intensity started decreasing in the early hours of August 4, resulting in the first Forbush decrease FD–1. The high latitude sea level neutron monitors recorded a

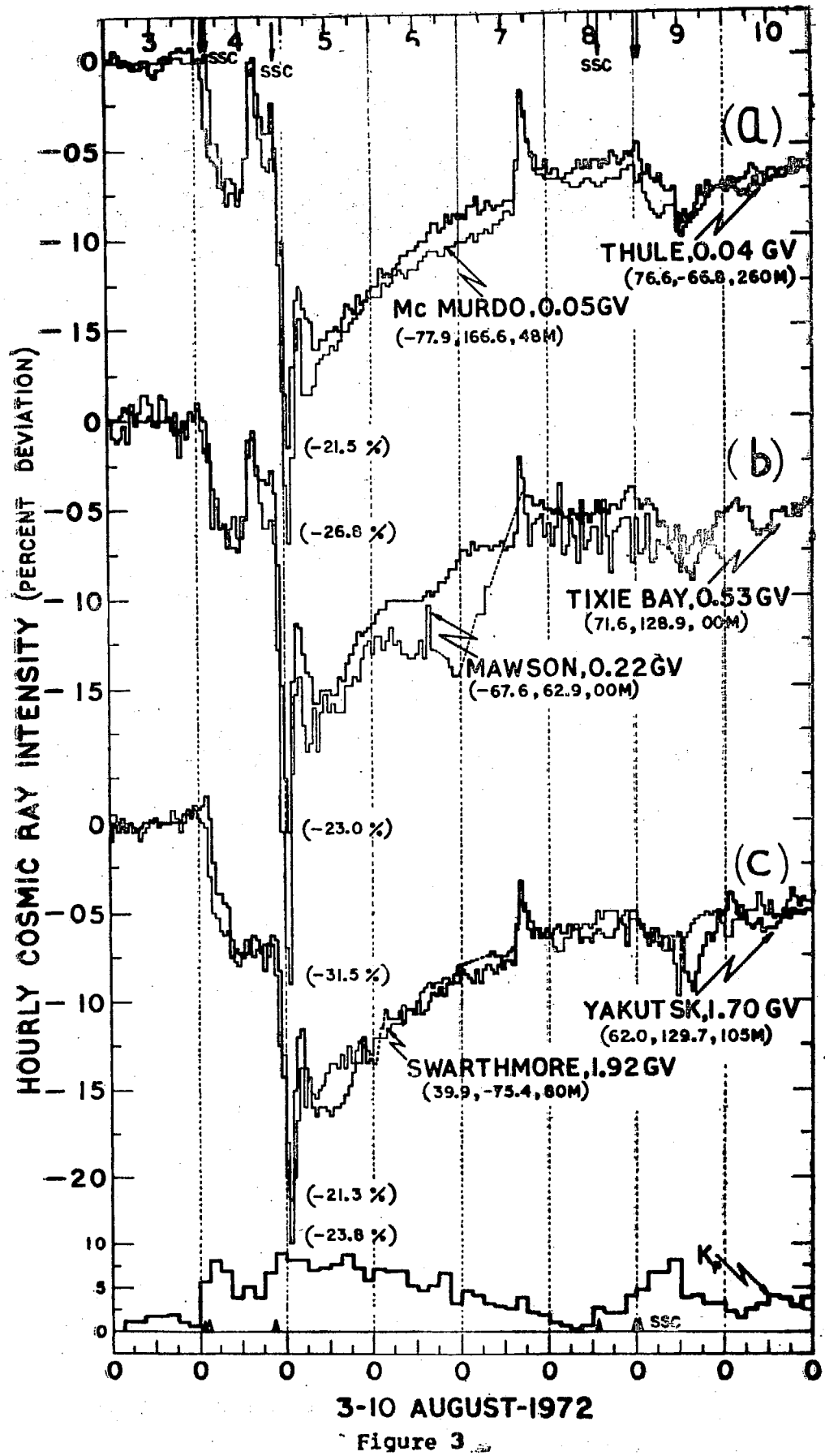

Figure 3

Figure 3: Universal time hourly cosmic ray intensity during the period August 3–10, 1972 recorded by three pairs of neutron monitors; (a) polar stations, Thule and McMurdo (Asymptotic latitude 72°N, and 79°S respectively), (b) High latitude stations, Tixie Bay and Mawson (Asymptotic latitude 37°N and 39°S), (c) Equatorial viewing stations, Yakutsk and Swarthmore (Asymptotic longitude at 00 UT, 170°E and 350°E). The geographic latitude, longitude and the altitude in metres above sea level for each station along with their geomagnetic cutoff rigidity are shown in the figure. K_p index representing the geomagnetic disturbance is also plotted in the same figure.

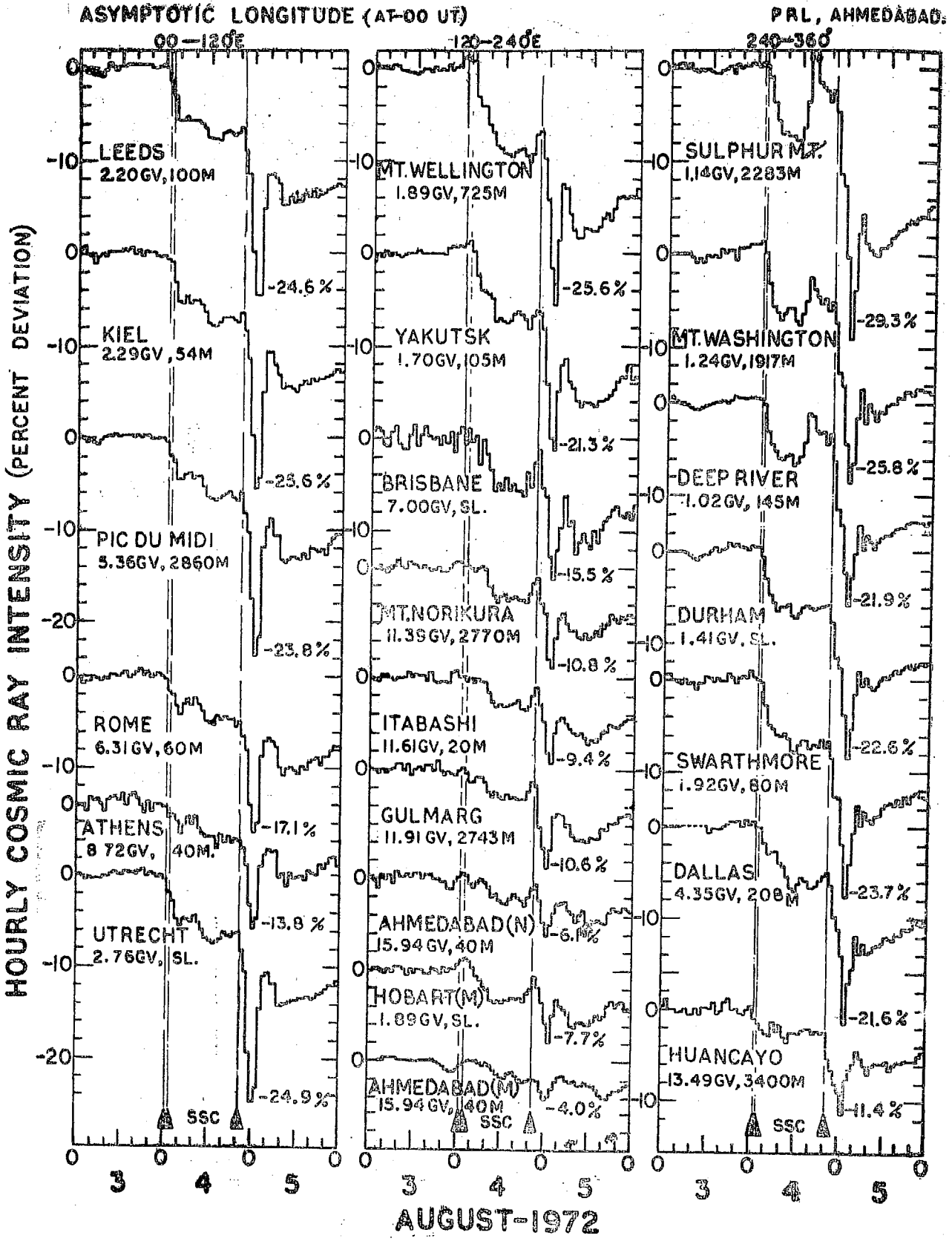

Figure 4 : Universal time hourly cosmic ray intensity during August 3–5, 1972 observed by a number of selected neutron and meson monitors. The geomagnetic cutoff rigidity of each station and its altitude in meters above sea level are marked in the figure. The stations have been grouped in three asymptotic longitude belts of width 120° each. The asymptotic directions correspond to zero Universal time.

maximum decrease of $\approx$ 7–8% at about 10–12 UT. Due to the presence of the strong equatorial anisotropy, the onset time at different stations varied widely ($\approx$ 3 hrs), the earliest being recorded by stations looking in the garden hose direction. With a power law rigidity spectrum having a spectral index of -0.8 ± 0.2, FD–1 exhibits features of a typical Forbush decrease (Lockwood, 1971).

The superimposed intensity increase or a hump like structure observed in the FD–1 profile detween 04–08 UT on August 4 (See Figure 4), is especially noticeable in stations with $P_c > 1.4$ GV and sampling particles mainly from sunward direction. During the seme period, a geomagnetic storm was recorded with a decrease of $\approx$ 200 gammas in the horizontal component of the geomagnetic field at low latitudes (Kawasaki et al., 1973). From the time association of these two events we suggest that the intensity increase during FD–1 is caused by the lowering of the geomagnetic cutoff rigidity (P_c). Quantitative calculations indicate that a change of $\approx$ 200 gammas in the horizontal component of the geomagnetic field, produces a change of $\approx$ 0.6 GV in P_c (Obayashi, 1959, Dorman, 1963) which in turn can cause $\simeq$ 4% increase in the cosmic ray intensity recorded at sea level stations having $5 \leqslant P_c \leqslant 8$ GV (Dorman, 1963, Yoshida et al., 1968), consistent with our observations.

Solar Flare increase SP—1 on August 4, 1972 : An anisotropic increase of about 7–8% in the neutron intensity which had its onset at 12–13 UT on August 4, was observed by stations with $P_c < 1.4$ GV. Inspite of the long time delay of $\approx$ 6 hours we suggest that the most likely candidate for causing SP–1 is a solar flare of importance 3B which occurred at 0621 UT (N14, E09), since this was the only major flare that could be associated with the increase (Pomerantz and Duggal, 1973b). Spacecraft observations at lower energies support this contention (McKinnon, 1972).

Solar Flare Increase SP–2 on August 7, 1972 : The second solar flare increase starting at $\approx$ 16 UT on August 7, during the recovery phase of FD–2 shows a number of peculiar characteristics : (1) the conspicuous absence of solar flare cosmic ray particles with energies $\leqslant$20 MeV per nucleon deduced from various spacecraft measurements. (2) the relativistic solar particles were observed before Hα maximum phase of the solar flare at 1509 UT on August 7 (importance 3B) but in near coincidence with the maximum phase of the white light flare (Mathews and Lanzerotti, 1973) and (3) while an increase of only 5–6% was observed at sea level stations having $P_c < 1.4$ GV, the increase was still significant at stations with $P_c \cong 2.7$ GV, which indicates that the rigidity spectrum of SP–2, is less steep compared to SP–1 and to previous solar flare increases (Obayashi, 1964; McCracken and Rao, 1970).

Forbush Decrease FD–3 on August 9, 1972 : The third Forbush decrease was observed on August 9, with its onset time varying widely (4–6 hours) for stations with different asymptotic longitudes. The Forbush decrease was highly anisotropic and short lived, the total time duration from the onset to the recovery being less than 24 hours.

Pre–increase PI–1 : A significant increase in the cosmic ray intensity PI–1 is seen at all stations sampling particles from the sunward direction (Figure 4). The maximum intensity occurs around 21–22 UT on August 4, which coincides with the passage of the shock front at the earth at 2054 UT, prior to the onset of second Forbush decrease FD–2. The increase at stations with $P_c \geqslant 1.4$ GV is not clearly identifiable due to the superposition of the solar proton event SP–1, whose decay phase persists even beyond 21 UT. Therefore, for further analysis of this pre–increase, all stations with $P_c < 1.4$ GV have been excluded.

The cosmic ray intensity at stations with $P_c \geqslant 1.4$ GV being practically constant for about 6–8 hours prior to the onset of pre–increase PI–1 at $\approx$ 18 UT, the intensity level for this period provides the requisite base level for computing the magnitude of this increase. The percent increase as observed at a number of stations is plotted in Figure 5, against their mean asymptotic longitude of viewing at 21 UT. It may be noted from the figure that in each given asymptotic direction the percent increase observed at low latitude stations ($P_c \geqslant$ 8 GV) is comparable in magnitude to the percent increase observed at high latitude stations (P_c = 1.4–4 GV), indicating a flat spectrum for the increase. In view of this, a smooth curve has been drawn in Figure 5 through all the observational points. The presence of a predominant anisotropy with a maximum increase being

egistered by stations viewing along the sunward direction s clearly evident from the figure. Referring to figure 4, t is seen that the anisotropic pre-increase continues to ɔe significant upto 22 UT in Asian longitude belt (sunward lirection) even one hour after the SSC whereas the lecrease in intensity has already commenced in the other wo longitude belts during the interval 21–22 U.T.

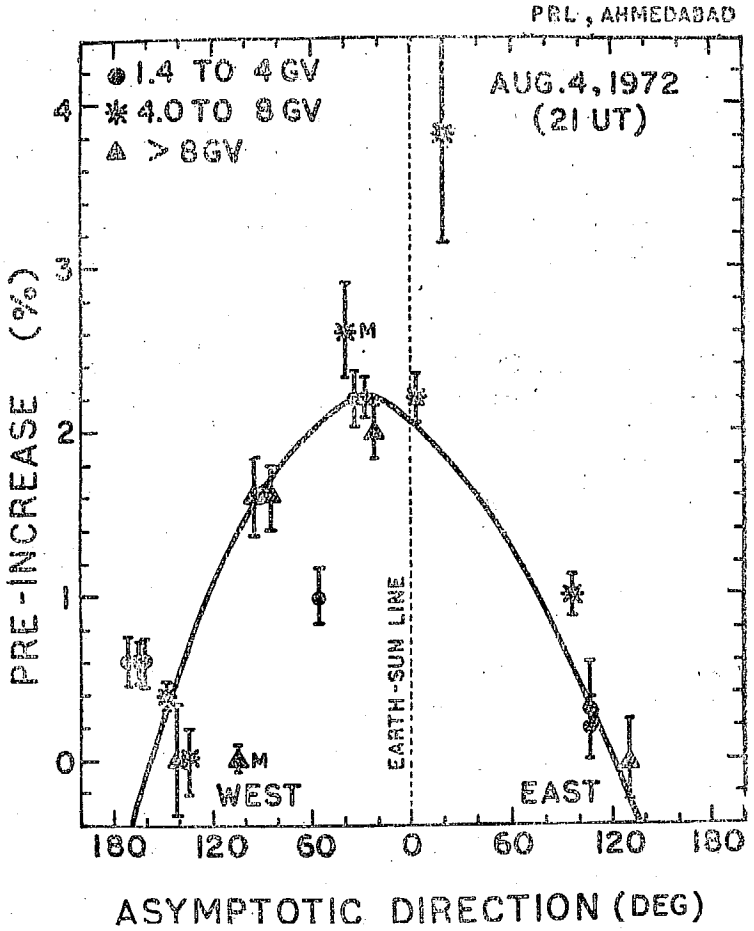

Figure 5 : Persent increase PI–1, in the cosmic ray intensity recorded by different stations plotted against their mean asymoptotic longitude at 21 UT, on August 4 1972, 'M' denotes the observed increase for the meson monitor in this figure.

ince the geomagnetic field is almost constant at least pto 21 UT, the increase PI–1 cannot be attributed to ıe lowering of the cutoff rigidity. However a small ontribution due to the geomagnetic perturbations at nd beyond 22 UT cannot be completely ruled out.

The anisotropic pre-increases of type PI–1, which ave been observed on earlier occasions have been escribed by Dorman (1963). Dorman et al. (1970). Lookwood (1971), and Kusmicheva et al, (1972). There have been generally explained as due to the reflection of particles (albedo mechanism) from the outward moving shock front from the sun (Dorman, 1963: Rao et al., 1967: Dorman et al., 1970) containing large magnetic fields. The albedo mechanism predicts an anisotropic increase from the sunward direction, the increase generally preceding SSC by a few hours. Assuming reasonable values for different parameters, Dorman (1963) has calculated the pre-increase for a number of events, and found them in qualitative agreement with the observations. For a solar wind velocity of $\simeq$ 2000 km Sec^{-1}, this model would predict a pre-increase of about 1.5–1.8% from the sunward direction and with a flat spectrum, which are in qualitative agreement with our observations.

The Sharp Forbush Decrease FD–2 : Immediately after the SSC at 2054 UT on August 4, a sudden decrease in cosmic ray intensity (Fd–2) was observed, which reached a magnitude of $\approx$ 25 % within five hours, at high latitude sea level neutron monitors. The hourly rate of decrease exceeded even 6 % per hour which is the highest recorded so far. The onset of this decrease was highly anisotropic exhibiting both N–S anisotropy and the longitudinal anisotropy in the equatorial plane. The spectral exponent of the rigidity dependence of the decrease is -1.2 ± 0.2, which is slightly higher than the normally observed values.

To study the characteristics of the rapidly evolving anisotropies and to identify the isotropic time variations, we have constructed the space–time diagram of cosmic ray intensity, by using neutron monitor data from a number of high latitude sea level stations ($P_c \leqslant 2$GV), with narrow asymptotic cone of acceptance and scanning the equatorial belt (Fenton et al., 1959, Ables et al., 1967: Mercer and Wilson, 1968), Figure 6, obtained from such a space–time diagram, describes the snapshots of the cosmic ray intensities at various longitudes in the equatorial plane at different times during FD–2 and PI–2. An examination of Figure 6 reveals that the decrease commenced at least one hour earlier at stations viewing within a cone of 120* centred around the antisun direction. The anisotropy amplitude during this period (22 UT) was about 3–4% The early onset along the anti–sun direction is also reflected in the intensity profile observed by low latitude monitors. This picture is contrary to what has been usually observed, namely the early onset of the Forbush decrease from the garden hose direction (Fenton et al., 1959: McCracken, 1962: Lookwood and Razdan, 1963a) which is understood in terms of sampling of the depressed cosmic ray intensity behind the approaching shock from the garden–hose direction.

During the main phase of FD–2, following the anisotropic depression along the anti–sun direction, a large anisotropic depression with a maximum along $\approx$ 100°–120° west of the earth–sun line is developed between 24 UT on August 4, and 02 UT on August 5. The maximum amplitude of the anisotropy is about 7–8% at 24 UT which reduces to 3–4% at 02 UT, thereafter the cosmic ray intensity profile shows an abrupt increase (PI–2) at all stations. The unusual anisotropy features exhibited both at the time of the onset of FD–2 and during its main phase and the inital recovery period, in our opinion, provide a very important clue for an understanding of the Forbush decrease mechanism. A simple unified model explaining all these features is proposed and discussed at the end.

The Rapid Universal Time Increase PI–2 : The observed rate of increase PI–2 in the cosmic ray intensity, just after the maximum decrease in FD–2, is comparable or even faster (10% per hour for some stations) than the rate of decrease. Such a fast increase of non–solar origin has been observed for the first time. Since the observations from various monitors suggest that the recovery in cosmic ray intensity continues over a long period of time ($\geqslant$ 7 days), the abrupt increase observed on August 5 (3–09 UT with maximum at 05 UT) can be considered as a short lived enhancement superimposed on the normal recovery of the Forbush decrease FD–2.

The characteristics of this increase PI–2 have been studied by estimating the magnitude of the increase for various stations by two independent methods: (a) by considering the amplitude of the increase from the minimum of FD–2 to the maximum at about 05 UT and (b) by estimating the magnitude of the increase, above a smooth recovery curve drawn through the intensity profile from the minimum of FD–2 (Figure 7). Both the methods yield a rigidity spectrum with an exponent -1.2 ± 0.2 with an upper limiting rigidity R_{max} of 50–60 GV for the increase PI–2, the same as that for the main Forbush decrease FD–2.

The spatial anisotropies during the increase PI–2 are again evident from Figure 6. The anisotropy maximum lies in the sunward direction thoughout the increase, However its amplitude changes with time, being about 5% initially at 03 UT which reduces to $\approx$2% at the time of maximum increase at 05 UT. The anisotropy increases again to $\approx$ 4 % at 06 UT. and decays thereafter till the intensity becomes nearly isotropic at about 17 UT after which the normal recovery proceeds.

A survey of the past Forbush decreases since IGY shows a number of sudden superimposed universal time increases during their recovery periods. Examples are the Forbush decreases of February 11, 1958: August 17, 1958, September 18, 1959: April 27, 1960: October 29, 1963 and

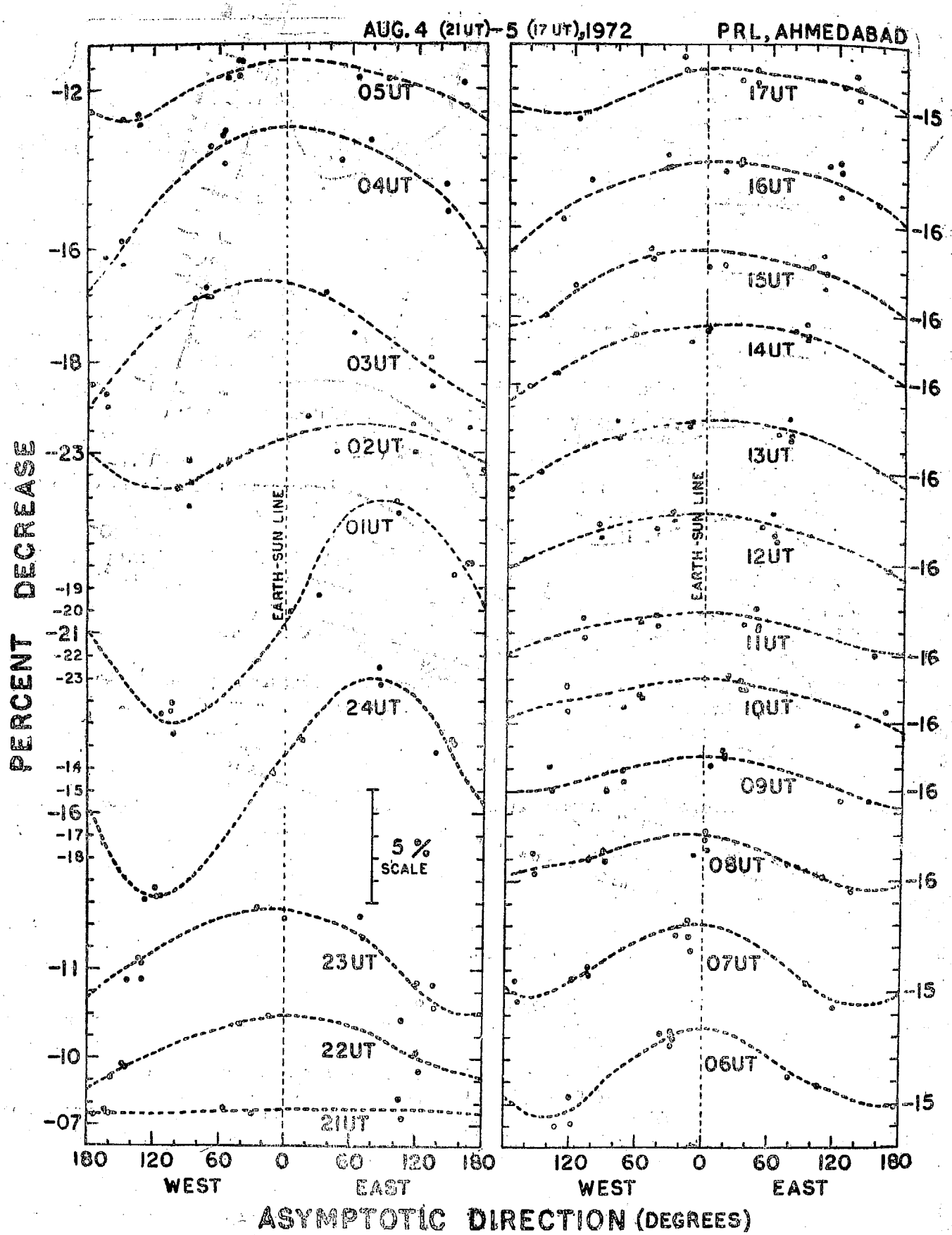

Figure 6 ; Snapshots showing percent decrease in cosmic ray intensity at different times derived from the data of a number of high latitude neutron monitors (Pc $\geq$2 GV) viewing the equatorial plane. The intensities are plotted as a function of mean asymptotic longitude from 21 UT on August 4 to 17 UT on August 5, 1972, covering the entire period of FD-2 and PI-2.

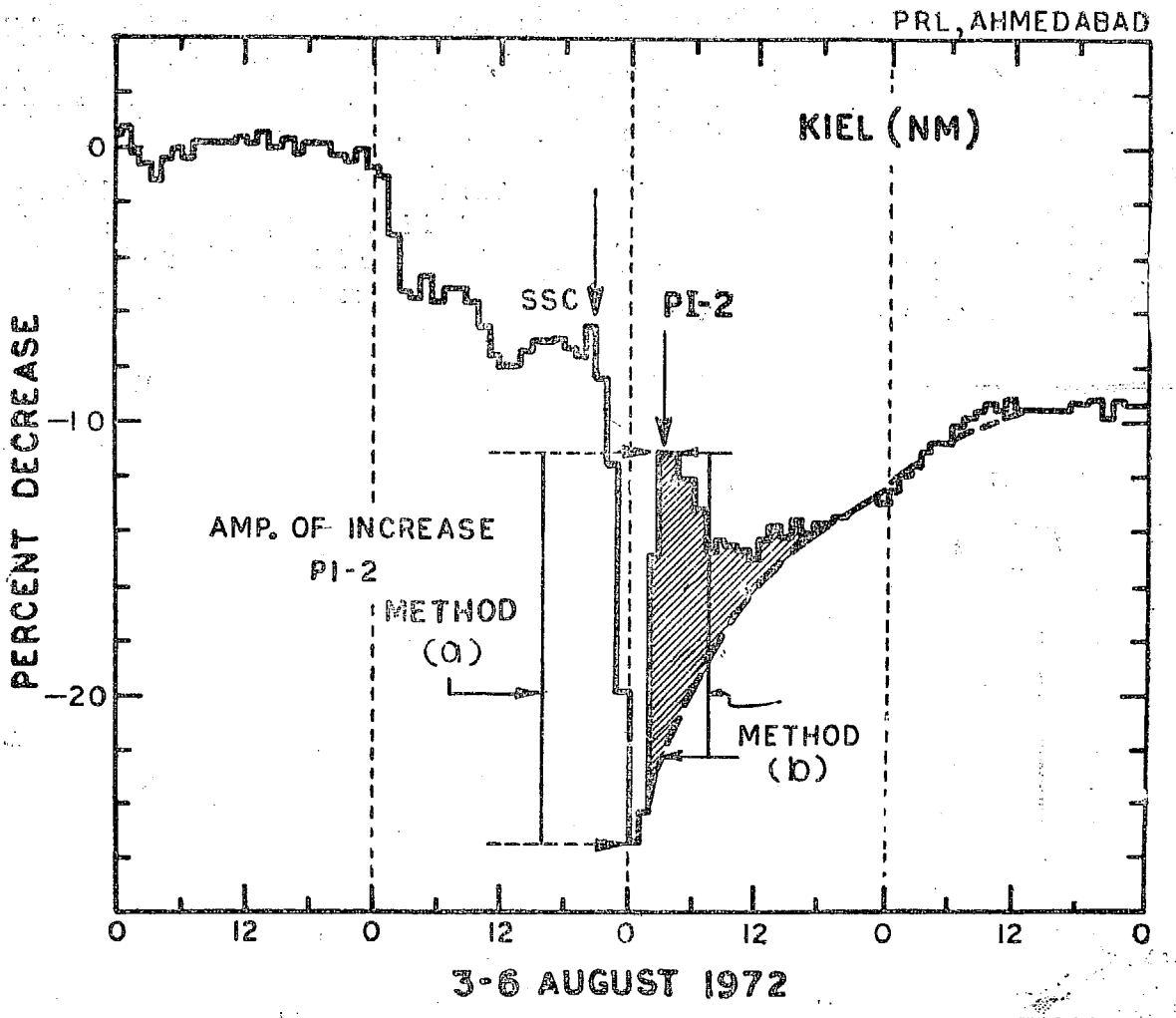

Figure 7: The cosmic ray intensity profile during August 3–6, 1972 showing the Forbush decrease FD-2 and the increase PI-2. The figure indicates two methods for estimating the increase PI-2. Method (a) defines its magnitude from the minimum intensity of FD-2, to the peak of PI-2, whereas the method (b) defines it as a superimposed increase over the smooth fit to the normal recovery phase shown by curvy dashed line.

January 13, 1967. A few of these increases have been discussed in literature (Lockwood 1960; Lockwood and Razdan, 1963b; Blokh et al., 1964; and Yoshida et al., 1968) and these have been mainly attributed to a reduction in the cutoff rigidity at the monitoring station, following a geomagnetic storm (Kondo. 1961; Dorman, 1963; Yoshida et al. 1968). However, the decrease in geomagnetic cutoff rigidity (P_c) cannot produce any increase in the cosmic ray intensity observed by the sea level neutron monitors with $P_c < 1.4$ GV (since atmospheric cutoff $\approx$ 1.4 GV). and the meson monitor with $P_c < 4$ GV(atmospheric cutoff$\approx$4 GV). We note that the abrupt universal time increase PI-2 on August 5, is observed at all stations including the neutron monitors with $P_c < 1.4$ GV and meson monitors with $P_c < 4$ GV (Figures 3 & 4). Moreover, the increase in intensity due to reduction in P_c is expected to be maximum for sea level neutron monitors with $P_c \approx 5$–8 GV, which is contrary to the present observations. From these evidences, we can exclude the reduction in P_c as the cause for the observed abrupt increase PI-2.

DISCUSSION AND CONCLUSION

The prominent features in the series of cosmic ray intensity variations during August 1972 which requires an adequate explanation are (1) the establishment and evolution of the pre-increase PI-1(2) the unusual anisotropy from anti-sun direction during the onset time of the main

Forbush decrease FD–2 coinciding with the last phase of the pre-increase PI–1, (3) the unusually large magnitude of the decrease during FD–2 which takes place in a short duration of about 5 hours and (4) an even sharper increase in intensity PI–2 with prominent anisotropy from sunward direction, We propose here a qualitative model to explain the observed characteristics of PI–1, PI–2 and FD–2, mentioned above. The model is based on the convection by a transient modulating region containing very high of intense magnetic field of 50–80 gammas following the shock, add credence to the above hypothesis. Figure 8 is a schematic sketch describing the essential features of the model.

The essential features of the model we propose are summarised in Figure 8, which shows a region of high tangled magnetic fields behind the leading edge of the shock front where the cosmic ray particulate flux is

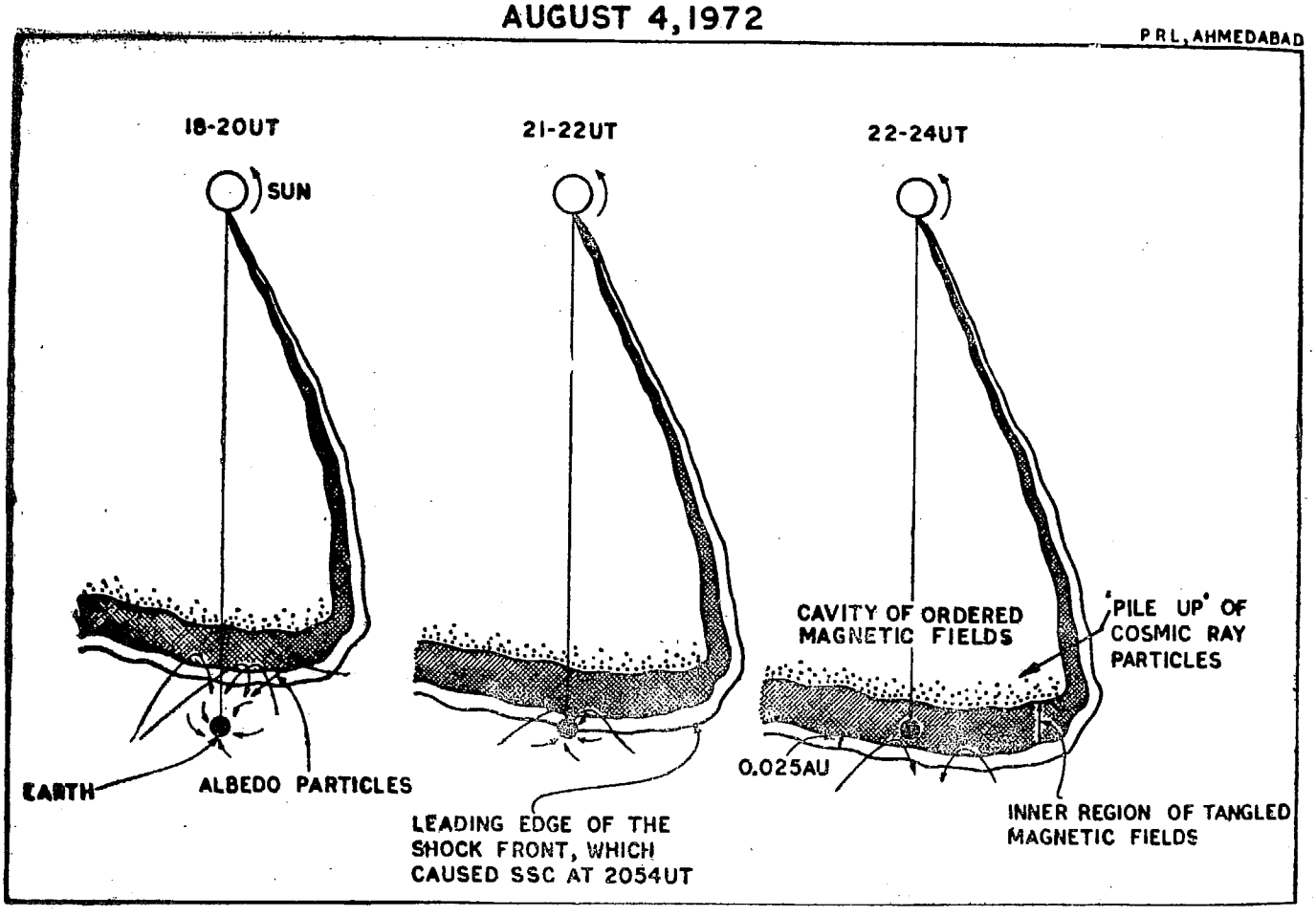

Figure 8 : Schematic diagram of the model proposed to explain the various features observed during the Forbush decrease FD–2 and the intensity increases PI–1 and PI–2. Cross-hatched area represents the region of large tangled magnetic fields. In figure 8 'a, b, c' are shown the cosmic ray effects observed by a ground based monitor as the shock front gradually approaches the earth. The dotted region at the interface between the tangled field region and the cavity, represents the 'pile up' of cosmic ray particles due to their convection by the solar wind.

tangled magnetic fields behind the shock front which is followed by a Gold/parker (Gold 1959; Parker 1963) type cavity containing fairly well ordered magnetie fields and depressed cosmic ray intensity. The spacecraft observations, highly depressed. Immediately behind this, is a region of enhanced particle intensity having sharp density gradients which is followed by the main cavity with well ordered magnetic fields and depressed intensity. The cosmic ray

intensity within the cavity recovers exponentially with time. The earth bound monitors experience different cosmic ray intensity ' states ' as the entire beam convects past the earth.

In Figure 8_a we represent the cosmic ray flux distribution in the interplanetary medium prior to the arrival of the shock front at the earth, when PI-1 has just commenced. The earth-bound cosmic ray monitors viewing along the sunward direction are able to sample, well in advance of the arrival of the shock front, enhanced cosmic ray flux resulting from the reflection of cosmic ray particles at the shock boundary. As noted earlier, the magnitude of PI-1$\approx$2-3 % and the spectral characteristics are in gross agreement with the predictions of albedo mechanism. The monitors looking along the anti-sun direction however, sample only the galactic flux and consequently do not show any pre-increase. Note that particles which reach monitors viewing along the anti-sun direction come from a large number of asymptotic directions. In Figure 8b the leading edge of the shock front has engulfed the earth, however, the albedo particles are still being received along the sunward direction from the inner region of the shock (cross hatched area in Figure 8), which contributes to the enhanced intensity above normal level from these directions even after the SSC at 2054 UT. At the same time the number of allowed directions for the particles which reach anti-sun direction has been reduced considerably resulting in the early onset of the decrease along the anti-sun direction. In other words we suggest that, even though the monitors viewing along the anti-sun direction have started sampling reduced intensity in the interval 21-22 UT, the sunward pointing monitors are still seeing the enhanced flux due to the reflection of particles from the inner region which is approaching the earth. The reduction in intensity along the anti-sun direction is due to the occultation of allowed particle trajectories by the interplanetary shock.

In Figure 8c the inner region containing large tangled magnetic field with tangential discontinuities has comptely engulfed the earth resulting in a fast decrease in all directions. Quenby (1971) has shown that such tangential discontinuities extending over large region in space can produce intense Forbush decreases. Using the values for the interplanetary field from spacecraft observations, he has been able to quantitatively account for the observed Forbush decrease during February 26, 1969, with the above model. Even though due to the non-availability of interplanetary field parameters we are not at present able to provide a quantitative estimate, we propose that the unusually high solar wind velocity and the large field magnitude in the shock region observed during this event make this hypothesis very attractive. As the transient modulating region of tangled magnetic fields with the Gold/Parker type cavity behind containing depressed cosmic ray intensity convects out from the sun, cosmic ray particles diffuse into the cavity particularly from directions away from the plane of ecliptic both from northern and southern hemispheres, However, the diffusion into the shock front with high tangled fields is minimal as a consequence of which the particle intensity within the tangled field region is lowest. In other words, immediately following PI-1 the earth bound detectors will register a very sharp fall. The sharp intenstiy decrease which continues for about 5 hours indicates that the thickness of the region had a scale size of the order of 0.2. AU.

The most unusual feature of this event is the abrupt universal time increase of cosmic ray intensity PI-2 following the main phase of FD-2, which is explained here in terms of ' pile up' of particles behind the tangled field region. Such a ' pile up ' is a consequence of the the unusual conditions present during this period and we suggest that this feature should be apparent whenever a major disturbance takes place on the sun producing unusually high velocity shock front with intense tangled magnetic fields behind. A sharp cosmic ray density gradient created at the interface between the tangled field region and the cavity behind it, causes diffusion of particles from the cavity into the region of tangled magnetic fields. Note that these particles had originally diffused into the cavity largely from directions north and south of ecliptic as the modulating depth is smaller in these directions. It is further proposed that diffusion of bulk of particles into the tangled magnetic field region would be from the sunward direction due to an outward convection of particles within the cavity and a probable field line connection between the cavity and the tangled field region. However, a smooth flow of particles is not expected due to the presence of strong magnetic field irregularities at the interface. The particles undergo multiple scattering in this region and, in the

quasi--equilibrium state, spend a certain average time in the interface region, which leads to a 'pile up' of particles causing the intensity increase PI–2. Since the particles which diffuse into the region of tangled magnetic fields are guided along the lines of force within the cavity which are relatively well ordered, the anisotropy during the entire duration of PI–2 should be from the sunward direction. Reference to Figure 6 clearly shows that this is indeed the case. During the entire period of the increase, a prominent anisotropy from the sunward direction in exhibited.

The level of intensity following PI–2 and its gradual recovery to normal represents the classical picture observed in any Forbush decrease, the depressed intensity being representative of the flux within the cavity and the recovery with time being affected due to the slow diffusion of particles into the cavity from outside (Lockwood, 1971).

The active region producing the solar flare and causing the decrease FD–2 has coordinates N 14, E 09. At the time when the shock hit the earth and produced an SSC at 2054 UT on August 4, this region moved to central meridian. However, the fact that Pioneer–9 located at $\approx$ 0.8 AU, due 45° east of the earth–sun line, recorded the arrival of the shock (with velocity $\simeq$ 1100 km sec^{-1} only), about 4 hours after its being recorded at the earth, indicates that the centroid of the cone of the transient modulating region was near the earth–sun line. Interplanetary scintillation observations by Armstrong et al., (1973) also indicate that earth was located very near to the flare normal. Such a picture gives a larger depth of the modulating region towards west which is consistent with the observed maximum depression in FD–2 along 100° west of the earth–sun line.

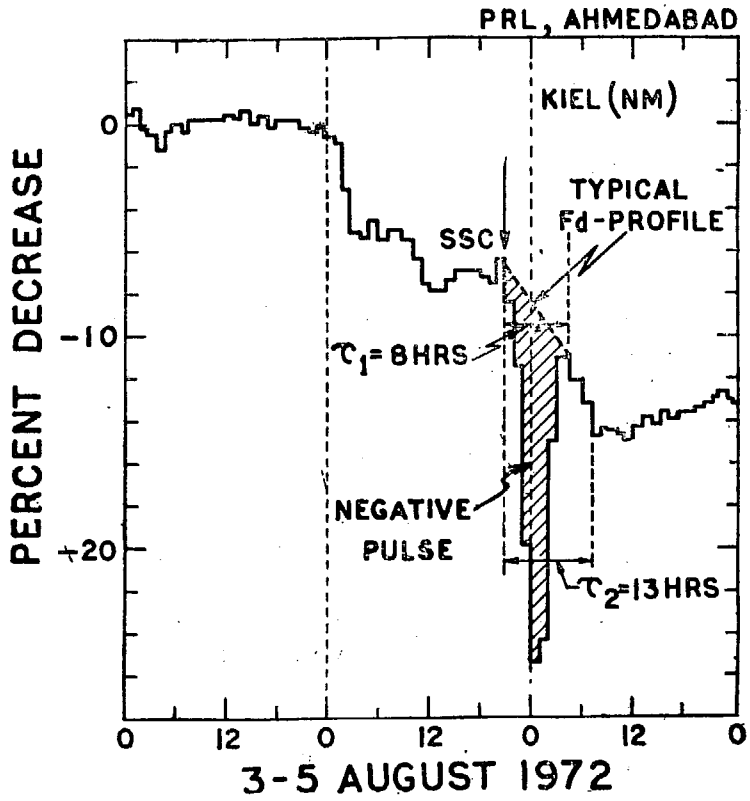

Figure 9: Pictorial representation of a negative pulse-like structure (hatched area) superimposed on the typical Forbush decrease profile of cosmic ray intensity (slant dashed line) depicting an alternate explanation for FD–2 and PI–2.

An alternative but conceptually simple explanation for the complex phenomenon is to look upon the inten-

sity profile during FD–2 and PI–2, as a negative pulse superimposed on a normal Forbush decrease, the negative pulse representing the cosmic ray intensity profile in the region of tangled magnetic fields. The intensity profile on August 3–5, 1972 plotted in Figure 9, pictorially depicts the above view point, where the slant dashed line smoothly joining the onset of FD–2 and the peak PI--2, represents a typical Forbush decrease and the hatched area shows the superimposed negative pulse like structure. The duration of the pulse (τ_1) is $\simeq$ 8 hours and the total time of decrease (τ_2) is $\simeq$ 13 hours. It has also been possible to fit a similar smooth line representing the Forbush decrease for all the stations. Neglecting the negative spike, the rigidity spectrum of the Forbush decrease (represented by slant dashed line) is found to have an exponent of $\simeq -0.6 \pm 0.2$ which is typical for Forbush decreases.

The negative pulse can be interpreted as due to a sharp cosmic ray intensity decrease in the region of tangled magnetic fields containing large scale tangential discontinuities (Quenby, 1971). It is postulated that this region is enclosed by a forward.-reverse shock ensemble similar to that discussed by Schubert and Cummings (1967, 1969) and Dryer (1973). In this model the particulate flux within the tangled field is minimal, with the maximum depression being somewhere near the centre of the tangled field configuration. The lower particle flux within this field region is a result of very slow particle diffusion. Thus, in this model, the tremendous negative spike is a special intensity structure in space which is superimposed upon the general Forbush decrease. From the foregoing presentation and discussion we conclude that—

1. The universal time pre–increase PI–1 with its maximum amplitude $\approx$ of 2–3% along the sunward direction has a flat rigidity spectrum and is in agreement with the enhancement being caused by reflection of particles from the approaching shock front.

2. The apparent early onset of FD–2 from the anti-sun direction can be explained in terms of the occultation of the particle trajectories reaching the detectors viewing along this direction as the shock front engulfs the earth. The detectors looking along the sunward direction should continue to receive enhanced albedo flux.

3. The large decrease FD–2, is mainly due to the depressed cosmic ray intensity in the region of tangled magnetic field behind the shock.

4, The Universal time intensity enhancement PI–2 is of interplanetary origin and not due to a change in geomagnetic cutoff rigidity. The sharp enhancement is a result of 'pile up' at the interface between the tangled magnetic field and the cavity behind it.

5. The depressed cosmic ray intensity inside the cavity behind the tangled magnetic field region and its exponential recovery with time due to slow diffusion of particles particularly from north and south directions, accounts for the typical recovery characteristics exhibited following PI--2.

The model presented here is somewhat qualitative. However, for arriving at a rigorous theoretical model, it is necessary to have data from both surface and underground monitors with a good time resolution as well as detailed measurements of interplanetary field and plasma parameters. A more detailed consideration of the model is therefore postponed to a later publication.

ACKNOWLEDGEMENTS

The authors express their indebtedness to various investigators and to the World Data Centre--A (Solar--Terrestrial Physics) for providing the cosmic ray data. The financial support received from the Departments of Space and Atomic Energy, Government of India and from Day Fund Grant No. 17, National Academy of Sciences, USA, are acknowledged.

REFERENCES

Ables, J. G., E.Barouch and K. C. McCracken, The Cosmic radiation anisotropy as a separable function of time and radiation, Planet. Space Sci., **15,** 547, 1967.

Armstrong, J. W., W. A, Coles. J. K. Harmon, S. maagee, B. J. Rickett und D. C. sime, Radio Scintillation measurements of the solar wind following the flares of August 1972, world Data Centre A, Report UAG-28, Part II. 371, July 1973.

Blokh, Ya. L., N. S. kaminer and L. I. Dorman, On Cosmic ray effects; the forerunners of magnetic storms, NASA tech, transl, F--127, p. 41, June 1964.

Collected Data reports on August 1972, Solar--Terrestrial events. World Data Centre–A for Solar--Terrestrial physics, Report UAG--28, part I, II and III, July 973; H. E. Coffey (Ed).

Dorman, L. I. Geophyical and Astrophysical aspects of cosmic radiation Prog. in elementary particle and osmic ray physics North--Holland Pub. Company. msterdam, **7,** 1963

Dorman, L. I., N. S. Kaminer and T. V. Kebuladze, Cosmic ray intensity increases before Forbush effects, cta. Phys. Acad. Sci. Hungarica, 29, Suppl. **2,** 227, 1970.

Dryer, M., E. J. Webber, A. Eviatar, A. L. ehlich, A. Jacobs and J. H. Joseph, EOS, Trans. GU (Abstract), **53,** 1058, 1972

Dryer, M., Interplanetary shock waves generated by lar flares. Space Sci. Rev., **15,** 403, 1974.

Dutt, J. G., J. E. Humble and T. Thambyahpillai, The nprecedented cosmic ray disturbances of early August, 972, World Data Centre A, Report UAG--28, part II, 23, July 1973.

Fenton, A.G., K. G. McCracken, D. C. Rose and . G. Wilson, The onset times of Forbush type cosmic ay intensity decrease, Can. J. Physics, **37;** 970, 1959.

Gold, T., Plasma and magnetic fields in the solar stem, J. Geophys. Res., **64,** 1665, 1959.

Gruenwaldt, H., M. D. Montgomery and H. osenbauer, Extreme solar wind conditions observed ter the activity related to McMath region, 11976 bstract) EOS. Trans. AGU, **53,** 1058; 1972

Hundhausen, A. J., Composition and dynamics of the solar wind plasma, Rev. Geophys, Space Phys., **8,** 729, 1970

Kawasaki, K., Y. Kamida, F. Yasuhara and S. I. Akasofu, Geomagnetic disturbances of August 4–9, 1972, World Data Centre A, Report UAG–28, Part III, 702, July 1973

Kondo, I., On cosmic ray intensity increase during geomagnetic storm, Rep. Ionosphere Space Res. Japan, **15,** 319, 1961.

Kusmicheva, A. Ye, L.I. Dorman and N.S. Kaminer, Statistical analysis of Forbush decreases and cosmic ray intensity increases preceding them, Geomagnetism and Aeronomy, **12,** 525, 1972

Lockwood, J. A., An investigation of the Forbush decreases in the cosmic radiation, J. Geophys. Res., **65,** 3859, 1960

Lockwood, J.A.. Forbush decreases in the cosmic radiation, Space Sci. Rev., **12,** 658, 1971

Lockwood, J. A. and H. Razdan, Asymmetries in the Forbush decreases of the cosmic radiation, 1. Differences in onset time. J. Geophys. Res., **68,** 1581, 1963a

Lookwood, J. A. and H. Razdan, Asymmetries in the Forbush decreases of the cosmic radiation, 2. Superimposed intensity variations during a Forbush decrease, J. Geophys, Res.. **68,** 1593, 1963b

Mathews, T. and L. J. Lanzerotti, Detection of relativistic solar particles before the Hα maximum of a solar flare, Nature, **241,** 335, 1973

McCracken, K. G., The cosmic ray flare effect. 3, Deductions regarding the interplanetary magnetic field, J. Geophys. Res., **67,** 447, 1962

McCracken, K. G. and U. R. Rao, Solar cosmic ray phenomena, Space Sci. Rev., **11,** 155, 1970

McKinnon, J. A., August 1972 solar activity and related geophysical effects, Tech. Memo. ERL/SEL–22, NOAA, Boulder, Colo, December 1972

Mercer, J. B. and B. G. Wilson, Morphology of the March 23, 1966 Forbush decrease, Can J. Phys., **46.** S849, 1968

Obayashi, T., Entry of high energy particles into the polar ionosphere, Rep. Ionosphere Space Res. Japan, **13**, 201, 1959

Obayashi, T., The streaming of solar flare particles and plasma in interplanetary space, Space Sci. Rev., **3**, 79, 1964

Parker, E. N., Interplanetary dynamical processes, Interscience, John Wiley and Sons, 1963

Pomerantz, M. A. and S. P. Duggal, Record Breaking Cosmic ray storm stemming from the outstanding solar activity centre in August 1972, Nature, **241**, 331, 1973a

Pomerantz, M. A. and S. P. Duggal, Remarkable cosmic ray storm and associated relativistic solar particle events of August 1972, World Data Centre A, Report UAG-28, Part I, 430, July 1973b

Quenby, J.J., The mechanism for the Forbush decraeses in particular for the event of February 26, 1969, Proc. 12th Int. Conf. Cosmic rays, Hobart, **2**, 730, 1971

Rao. U.R., K.G. McCracken and R.P. Bukata, Cosmic ray propagation process, 2. The energetic storm particle event, J. Geophys. Res., **72**, 4325, 1967

Schubert, G. and W.D. Cummings, The double shock wave structure in the solar wind, J. Geophys. Res., **72**, 5275, 1967

Schubert, G. and W.D. Cummings, Effects of high electron–proton temperature ratios on the double shock wave structure in the solar wind, J. Geophys. Res., **74**, 897, 1969

Yoshida, S., S. I. Akasofu and P.C. Kendall, Ring Current effects on cosmic rays, J., Geophys. Res. **73**, 3377, 1968